Technical Report 17-01

FEBEX-DP Synthesis Summary of the Full-Scale Engineered Barriers Experiment – Dismantling Project

September 2021

F. Kober, J.L. García-Siñeriz, M.V. Villar,
G.W. Lanyon, V. Cloet, U.Mäder,
P. Wersin, O. Leupin, P. Sellin,
A. Gens, R. Schneeberger

National Cooperative
for the Disposal of
Radioactive Waste

Hardstrasse 73
5430 Wettingen
Switzerland
Tel. +41 56 437 11 11

www.nagra.ch

nagra.

Technical Report 17-01

FEBEX-DP Synthesis Summary of the Full-Scale Engineered Barriers Experiment – Dismantling Project

September 2021

F. Kober[1], J.L. García-Siñeriz[2], M.V. Villar[3], G.W. Lanyon[4], V. Cloet[5], U.Mäder[6], P. Wersin[6], O. Leupin[1], P. Sellin[7], A. Gens[8] & R. Schneeberger[1]

[1] Nagra, Switzerland
[2] Amberg Infraestructuras, Spain
[3] CIEMAT, Spain
[4] Fartcure Systems, UK
[5] Arcadis, Switzerland
[6] University of Bern, Switzerland
[7] SKB, Sweden
[8] UPC, Spain

National Cooperative
for the Disposal of
Radioactive Waste

Hardstrasse 73
5430 Wettingen
Switzerland
Tel. +41 56 437 11 11

www.nagra.ch

ISSN 1015-2636

"Copyright © 2021 by Nagra, Wettingen (Switzerland) / All rights reserved.
All parts of this work are protected by copyright. Any utilisation outwith the remit of the copyright law is unlawful and liable to prosecution. This applies in particular to translations, storage and processing in electronic systems and programs, microfilms, reproductions, etc."

Foreword

The Grimsel Test Site

Nagra and its partners have been conducting underground research at the Grimsel Test Site (GTS) since 1984. The projects have contributed substantially to the development and confirmation of safe geological disposal concepts and to the characterisation of potential host rock formations. The GTS is reached by an access tunnel belonging to the Kraftwerke Oberhasli AG (KWO), the local hydropower company.

The tunnels of the GTS were excavated in 1983 and 1984 using both a tunnel-boring machine (TBM) and drill and blast techniques. Expansion of the site in 1995 and 1998 provided space for two large-scale demonstration tests. The branching tunnel system of more than 1 km in length is located at an elevation of 1'730 m a.s.l., about 400 metres beneath the Juchlistock in the granite and granodiorite of the Aar Massif that was formed some 300 million years ago. As part of the characterisation studies, over 5 km of cored boreholes have been drilled so far. The local geology is ideal for the investigation of a wide range of experimental concepts and scientific issues, with both tectonically overprinted and fractured areas as well as zones of homogeneous intact rock.

More than two dozen organisations and research institutes from twelve countries together with the European Union have participated in the six phases of the research programme. Each phase has focused on the key issues at the time, attempting to anticipate the next steps in national programmes for the long-term management of radioactive waste. The multi-decade Phase VI began in 2003 and is dedicated to integrative projects with: a) field experiments under repository-relevant boundary conditions, i.e. large-scale, long-term experiments with realistic hydrogeological settings; and b) projects addressing the implementation of a geological repository in terms of engineering feasibility, potential construction impacts on the surrounding rock, operational aspects, closure, and monitoring. A radiation-controlled zone of IAEA (International Atomic Energy Agency) Level B/C allows field experiments to be carried out with radioactive tracers.

The GTS has emerged from its first three decades as an internationally renowned research laboratory in the field of safe disposal of radioactive waste in deep geological repositories. It has firmly established its roles as a strong driving force for scientific and technological progress, as an effective platform for international cooperation, as a hands-on training stage for knowledge transfer to the younger generation, and as a host for transparent dialogue with decision-makers and the public.

The FEBEX project

The Full-Scale Engineered Barriers Experiment (FEBEX) was designed to demonstrate the feasibility of constructing an engineered barrier system, and to increase the understanding of coupled processes in the near-field of a geological repository for high-level waste (HLW). FEBEX comprises a full-scale in-situ test at the Grimsel Test Site, a large-scale mock-up test, a supporting laboratory test programme and modelling activities. FEBEX was dismantled in two stages: the first heater was dismantled after five years of continuous operation at 100 °C, while the second heater was dismantled after 18 years of operation – to date the longest-running heater experiment to be fully investigated, and the main focus of this report.

From its inception in 1995 to its final dismantling in 2015, FEBEX was operated under five different institutional frameworks. FEBEX I and II (1995 – 2004) focused on demonstrating feasibility and verification of the performance of the engineered barriers, while the NF-PRO (2005 – 2007) and FEBEXe projects (2008 – 2014) focused on developing a detailed understanding of near-field

processes and early-time coupled processes, respectively. Results from these four projects are also summarised in this report. From 2015 onwards, FEBEX was continued as FEBEX-DP – the final dismantling project.

Support has been provided as in-kind and financial contributions by the following FEBEX project partners: AITEMIN (Asociación para Investigación y el Desarrollo Industrial de los Recursos Naturales, Spain), Andra (Agence Nationale pour la Gestion des Déchets Radioactifs, France), BGR (Federal Institute for Geosciences and Natural Resources, Germany), CIEMAT (Centro de Investigaciones Energéticas Medioambientales y Tecnológicas, Spain), ENRESA (Empresa Nacional de Residuos Radiactivos, Spain), KAERI (Korea Atomic Energy Research Institute, Korea), Nagra (National Cooperative for the Disposal of Radioactive Waste, Switzerland), Obayashi Corporation (Japan), ONDRAF/NIRAS (Organisme National des Déchets Radioactifs et des Matières Fissiles Enrichies, Belgium), Posiva (Posiva Oy, Finland), RWM (Radioactive Waste Management, Great Britain), SKB (Swedish Nuclear Fuel and Waste Management Company, Sweden), SÚRAO (Správa Úložišť Radioaktivních Oodpadů, Czech Republic) and US DoE/LBNL (U.S. Department of Energy/Lawrence Berkeley National Laboratory, USA). The project was further supported by the E.U. Directorate General XII, Science, Research and Development, and the Swiss Federal Ministry of Science and Technology.



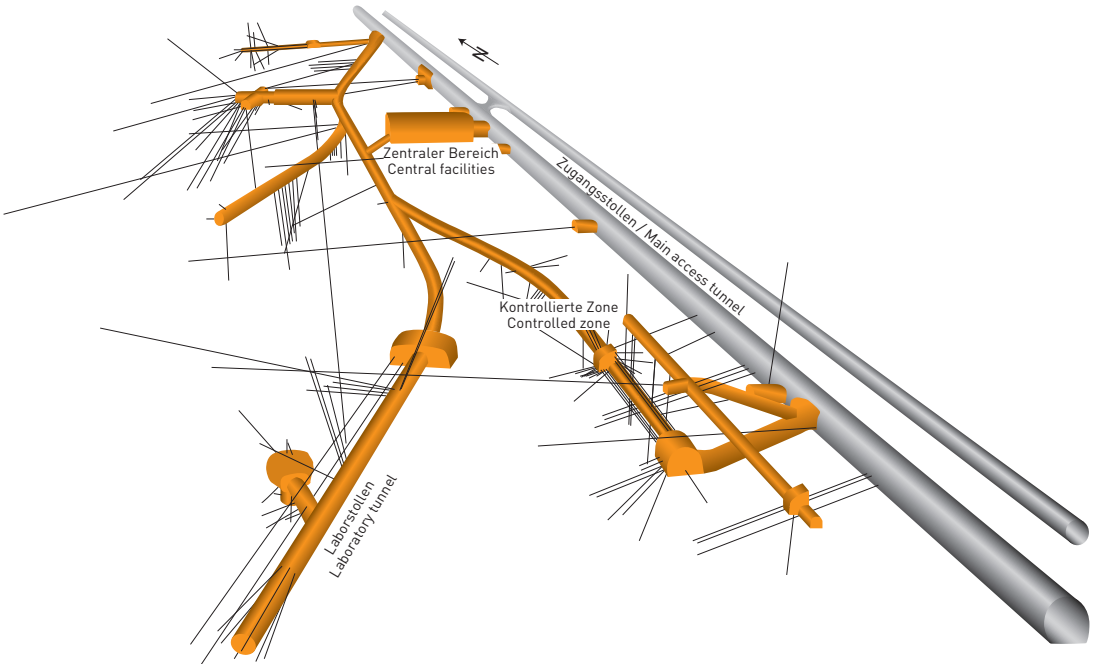
Location of Nagra's underground Grimsel Test Site on the Grimsel Pass in the Central Swiss Alps (Bernese Alps)

Grimsel area (view to the west)



1 Grimsel Test Site 2 Lake Raeterichsboden 3 Lake Grimsel 4 Juchlistock

Grimsel Test Site



Summary

This report summarises the results from the FEBEX in-situ experiment at the GTS. The full-scale heater test ran for over 18 years from the start of heating in 1997 to final dismantling ending in 2015. This report is one of the outputs from the FEBEX-DP project and culminates a series of Nagra work reports (NAB) covering different aspects of the FEBEX-DP project.

The FEBEX in-situ experiment was the longest-running in-situ full-scale heater experiment (the laboratory-based FEBEX mock-up test was started at the same time as the in-situ test and is still running, as of February 2022). Work on the project started in 1995 with the characterisation of the experimental rock volume, followed by the excavation of the FEBEX drift, further geosphere characterisation and the emplacement and instrumentation of the engineered barrier system (EBS) and plug. The initial total sealed test section comprised a total length of 14 m, which was filled with FEBEX (Serrata Clay) compacted bentonite blocks and embedding two steel heaters, each 4.5 m long and 0.9 m in diameter (11 tons weight) inserted in a liner. Heating started in 1997 and continued without interruption until 2002 when Heater #1 was removed during a partial dismantling activity, while Heater #2 was maintained at the same heating level. Heater #2 was switched off in 2015 and the section was fully dismantled and sampled. Throughout this time, the EBS and geosphere were continuously monitored and routine sampling was performed. During the partial (2002) and final (2015) dismantling, the EBS was characterised, providing a comprehensive dataset of EBS buffer properties (mineralogy, geochemistry, dry density, water content and thermo-hydro-mechanical (THM) properties), which allows a detailed evaluation of changes in the buffer during the early evolution of the EBS due to 18 years of heating and saturation.

Upon final dismantling, the buffer was close to full saturation with only a small, partially non-saturated volume remaining around Heater #2. The attainment of high saturation means that many of the most important processes associated with saturation had occurred and the buffer was close to reaching a reference state relevant to long-term safety assessment (albeit still in the thermal period). This allows assessment of safety-relevant aspects of the early evolution of such systems.

Special attention was paid to the characterisation of interfaces within the EBS and in the contact with the geosphere. These are of high importance as locations for likely alteration of material properties and were analysed in great detail.

Modelling of the in-situ experiment based on the detailed geosphere and buffer material characterisation allowed the prediction of the overall saturation progress and understanding of the key processes. Modelling performed at the start of the project was successful in predicting the observed evolution (monitoring) and final distribution of water content and dry density in the buffer and demonstrated the ability to represent the overall behaviour of a large full-scale system encompassing the ensemble of THM phenomena and their interactions. Multiple modelling approaches have been applied to the test and the dataset continues to be used as part of international modelling studies.

The monitoring and dismantling datasets from the in-situ experiment represent a unique resource for understanding the early evolution of the buffer during heating and natural saturation. This report provides an introduction and summary of the underlying reports and an initial synthesis of the results.

Zusammenfassung

Der vorliegende Bericht fasst die Ergebnisse des FEBEX-in-situ-Experiments im Felslabor Grimsel (GTS) zusammen. Der Heizversuch im Massstab 1:1 lief über 18 Jahre, vom Beginn des Heizens im Jahr 1997 bis zum endgültigen Rückbau im Jahr 2015. Dieser Bericht ist eines der Ergebnisse des FEBEX-DP-Projekts und bildet den Abschluss einer Reihe von Nagra-Arbeitsberichten (NAB) zu verschiedenen Aspekten des FEBEX-DP-Projekts.

Das FEBEX-in-situ-Experiment war das bisweilen am längsten laufende In-situ-Heizexperiment im Massstab 1:1 (der laborgestützte FEBEX-Mock-up-Test wurde zur gleichen Zeit wie der Insitu-Test gestartet und läuft weiterhin, Stand Februar 2022). Die Arbeiten an dem Projekt begannen 1995 mit einer umfassenden Charakterisierung des Gesteinsvolumens des in Frage kommenden Tunnelbereichs, gefolgt vom Auffahren des FEBEX-Stollens, der weiteren Charakterisierung der Geosphäre und schlussendlich der Einbringung und Instrumentierung der technischen Barriere (EBS) und des Verschlusses. Die anfänglich vollständig abgedichtete Teststrecke umfasste eine Gesamtlänge von 14 m. Zwei zylindrische Stahlheizelemente von je 4.5 m Länge und 0.9 m Durchmesser (11 Tonnen Gewicht) wurden in einen Liner eingebaut, welcher von verdichteten FEBEX-Bentonitblöcken (Serrata Ton) umhüllt wurden. Die Heizphase begann 1997 und lief ohne Unterbruch bis ins Jahr 2002, indem Heizelement #1 ausgebaut wurde, während Heizelement #2 weiterhin auf 100°C betrieben wurde. Heizelement #2 wurde im Jahr 2015 abgeschaltet und ebenfalls vollumfänglich ausgebaut und beprobt. Während der Heizperiode wurden die EBS und die Geosphäre kontinuierlich überwacht, und es wurden routinemässige Probenahmen durchgeführt. Daten und Analysen aus dem teilweisen (2002) und endgültigen (2015) Ausbau des Experiments bzw. der EBS erlauben eine tiefgründige Charakterisierung der Barriereneigenschaften nach einer 5-, respektive 18-jährigen Heizphase, wodurch ein umfassender Datensatz der EBS-Barriereneigenschaften (Mineralogie, Geochemie, Trockendichte, Wassergehalt und thermohydromechanische (THM) Eigenschaften) geschaffen wurde.

Beim finalen Ausbau des Experiments war die Bentonit-Barriere nahezu vollständig gesättigt, wobei nur ein kleines, nur teilweise gesättigtes Volumen um Heizelement #2 verblieb. Das Erreichen einer hohen Sättigung bedeutet, dass viele der wichtigsten mit der Sättigung verbundenen Prozesse stattgefunden haben und die Barriere nahe an einem für die Langzeitsicherheit relevanten Referenzzustand war (wenn auch noch in der thermischen Periode). Dies ermöglicht die Beurteilung sicherheitsrelevanter Aspekte der frühen Entwicklung solcher Systeme.

Ein besonderes Augenmerk wurde auf die Charakterisierung von Grenzflächen innerhalb des EBS und zur Geosphäre gelegt. Diese sind als Orte einer wahrscheinlichen Veränderung von Materialeigenschaften von grosser Bedeutung und wurden vertieft analysiert.

Die Modellierung des In-situ-Experiments auf Basis der detaillierten Charakterisierung der Geosphäre und der Barriere ermöglichte die Prognose des gesamten Sättigungsprozesses sowie Fortschritte im Verständnis der Schlüsselprozesse. Die zu Beginn des Projekts durchgeführte Prognose-Modellierung war erfolgreich bei der Vorhersage der beobachteten Entwicklung (Überwachung) und der endgültigen Verteilung des Wassergehalts und der Trockendichte in der Barriere. Sie demonstrierte des Weiteren die Fähigkeit, das Gesamtverhalten eines grossen Systems in vollem Massstab darzustellen, welche das Ensemble der THM-Phänomene und deren Wechselwirkungen umfasst. Mehrere Modellierungsansätze wurden während der Experimentlaufzeit angewendet, und der Datensatz wird weiterhin als Teil internationaler Modellierungsstudien verwendet.

Die Überwachungs- und Ausbaudatensätze aus dem In-situ-Experiment stellen eine einzigartige Ressource für das Verständnis der frühen Entwicklung einer Barriere während der Erwärmung und der natürlichen Sättigung dar. Dieser Bericht bietet dazu eine Einführung und Zusammenfassung der zugrunde liegenden Berichte sowie eine erste Synthese der Ergebnisse.

Résumé

Ce rapport résume les résultats de l'expérience in-situ FEBEX qui s'est déroulée au laboratoire souterrain du Grimsel (GTS). L'essai de chauffage à l'échelle réelle a duré plus de 18 ans, du début du chauffage en 1997 au démantèlement final qui s'est terminé en 2015. Ce rapport est l'un des résultats du projet FEBEX-DP et résume une série de rapports de travail de la Nagra (NAB) couvrant différents aspects du projet FEBEX-DP.

L'expérience in-situ FEBEX a été la plus longue expérience in-situ de chauffage à grande échelle (l'essai de maquette FEBEX en laboratoire a débuté en même temps que l'essai in-situ et est toujours en cours, état : février 2022). Le projet a débuté en 1995 par la caractérisation du volume rocheux expérimental, suivie de l'excavation de la galerie FEBEX, d'une caractérisation plus détaillée de la géosphère, puis de la mise en place et de l'instrumentation du système de barrières ouvragées (EBS) et du bouchon. La section d'essai initiale complètement scellée avait une longueur totale de 14 m. Deux éléments chauffants cylindriques en acier, de 4.5 m de long et 0.9 m en diamètre (poids 11 tonnes), ont été insérés dans un revêtement, lui-même entouré de blocs de bentonite compactée FEBEX (argile Serrata). Le chauffage a commencé en 1997 et s'est poursuivi sans interruption jusqu'en 2002, lorsqu'on a procédé à un démantèlement partiel et au retrait de l'élément chauffant n° 1, tandis que l'élément chauffant n° 2 continuait de fonctionner. L'élément chauffant n°2 a été éteint en 2015, puis on a procédé à son démantèlement complet et à un échantillonnage. Pendant toute la période de chauffage, l'EBS et la géosphère ont été surveillés en permanence et un échantillonnage de routine a été effectué. Au cours du démantèlement partiel (2002) et final (2015), on a procédé à la caractérisation de l'EBS, compilant ainsi un ensemble complet de données sur ses propriétés de confinement (minéralogie, géochimie, densité sèche, teneur en eau et propriétés thermo-hydro-mécaniques (THM). Ceci a permis d'évaluer de manière détaillée les modifications intervenues dans le remblai au cours de l'évolution précoce de l'EBS suite à 18 ans de chauffage et de saturation.

Lors du démantèlement final, le remblai était proche de la saturation complète, seul un petit volume partiellement non saturé subsistant autour de l'élément chauffant n°2. Le fait qu'un niveau de saturation élevé ait été atteint montre que bon nombre des processus les plus importants associés à la saturation ont eu lieu et que le remblai était sur le point d'atteindre un état de référence pertinent pour la sûreté à long terme (bien qu'encore pendant la période thermique). Ceci autorise une évaluation de l'évolution précoce de ces systèmes sous l'angle de la sûreté.

Une attention particulière a été accordée à la caractérisation des interfaces entre l'EBS et la géosphère. Ces interfaces sont d'une grande importance en tant que lieux d'altération probable des propriétés des matériaux et ont été analysées de manière très détaillée.

La modélisation numérique de l'expérience in-situ basée sur la caractérisation détaillée de la géosphère et du remblai a permis de prédire la progression globale de la saturation et de mieux comprendre les processus clés. La modélisation effectuée en début de projet reflète de manière adéquate l'évolution observée par le biais de la surveillance et la distribution finale de la teneur en eau et de la densité sèche dans le remblai. De plus, la modélisation a démontré sa capacité à représenter le comportement global d'un système à l'échelle réelle englobant l'ensemble des phénomènes THM et leurs interactions. De multiples approches de modélisation ont été appliquées au test et l'ensemble de données recueillies pendant l'expérience in-situ continue d'être utilisé dans le cadre d'études de modélisation internationales.

L'ensemble des données recueillies pendant la surveillance et le démantèlement de l'expérience in-situ représentent une ressource unique pour comprendre l'évolution précoce du remblai pendant le chauffage et la saturation naturelle. Le présent rapport constitue une introduction à l'expérience in-situ, un résumé des rapports de travail et une première synthèse des résultats.

Table of Contents

Foreword I

Summary V

Zusammenfassung VII

Résumé IX

List of Tables XVI

List of Figures XVII

Authors/sources for report XXIV

1 Introduction 1

1.1 The FEBEX experiment 1

1.1.1 Objectives of waste management organisations in the 1990s and safetyrelevant aspects 25 years later 2

1.1.2 FEBEX and other 1:1 in-situ tests and dismantling operations 3

1.1.3 Project history: FEBEX I – FEBEX II – NF-PRO – FEBEXe – FEBEX-DP 4

1.2 The FEBEX bentonite 5

1.3 The FEBEX gallery at the GTS: geology, structural geology, geophysical and hydrogeological characterisation 6

1.4 FEBEX I/II – test configuration, operation, partial dismantling, reconstruction and sealing 7

1.4.1 FEBEX I – test configuration and operation 7

1.4.2 Dismantling of Heater #1 and subsequent test configuration (FEBEX II) 14

1.5 FEBEX-DP aims and objectives 18

1.6 FEBEX-DP – forecast of anticipated status 19

1.7 FEBEX-DP project organisation and management 19

1.8 Milestones of the FEBEX experiment 21

1.9 Structure/organisation of report 22

2 Monitoring: evolution of the bentonite buffer and rock 1997 – 2015 25

2.1 Bentonite barrier evolution 25

2.2 Applied power 25

2.3 Temperature evolution 1997 – 2015 26

2.4 Total pressure (stress) ... 27
2.5 Pore pressure ... 29
2.6 Water content/suction ... 31
2.7 Effects of heater shutdown and dismantling ... 34
2.8 Measurements at the service area ... 35
2.9 Near-field/rock evolution ... 37
2.10 Final sensor status after Heater #2 shutdown ... 38

3 Pre-dismantling investigations ... 39
3.1 Redox state prior to dismantling ... 39
3.2 Gas-water sampling in GRS and CIEMAT pipes ... 40
3.3 Round robin of key buffer variables for materials characterisation ... 43
3.4 Colloids in radial and FUNMIG boreholes ... 44

4 Dismantling of Heater #2 and buffer sampling in 2015 ... 45
4.1 Technical pre-dismantling preparations and optimisations ... 45
4.2 Dismantling and sampling plan ... 45
4.2.1 Sample labelling ... 47
4.3 Dismantling operations ... 48
4.3.1 Preparations ... 48
4.3.2 Plug sampling and overcoring ... 49
4.3.3 Plug demolition, concrete sampling and switch-off of Heater #2 ... 51
4.3.4 Buffer/bentonite dismantling and sampling before dummy retrieval ... 53
4.3.5 Dummy retrieval ... 56
4.3.6 Removal and sampling of bentonite and liner up to the front of Heater #2 ... 56
4.3.7 Extraction of Heater #2 ... 56
4.3.8 Removal and sampling of the remaining bentonite and liner ... 58
4.3.9 Sampling and sensor dismantling ... 59
4.3.10 Sampling for corrosion and microbiology ... 59
4.4 Overall dismantling conclusions ... 59

5 Analysis and laboratory tests ... 61
5.1 Concrete and interfaces with bentonite and granite (NAB 16-18) ... 61
5.1.1 Introduction and scope ... 61
5.1.2 Methods ... 62
5.1.3 Concrete evolution ... 65

5.1.4 Alterations at the concrete-bentonite interface 66
5.1.5 Interactions at the concrete-granite interface 70
5.1.6 Impact on long-term safety – a concrete perspective 71
5.1.7 Lessons learned, remaining questions and recommendations 71
5.2 Buffer on-site analysis and laboratory tests (NAB 16-12) 72
5.2.1 Physical state of the barrier determined on site 72
5.2.2 Changes in the barrier during dismantling 74
5.2.3 Radial symmetry 74
5.2.4 Role of gaps during the course of the experiment 76
5.2.5 Longitudinal changes 77
5.2.6 Degree of saturation 80
5.3 Buffer/bentonite studies including interfaces (bentonite characterisation and assessment) (NAB 16-17) 80
5.3.1 Physical state and microstructure 81
5.3.2 Mineralogy and geochemistry 85
5.3.2.1 Mineralogy 85
5.3.2.2 Solid chemistry 87
5.3.2.3 Porewater chemistry 88
5.3.3 Thermo-hydro-mechanical properties 90
5.3.3.1 Thermal properties 91
5.3.3.2 Swelling properties 92
5.3.3.3 Compression testing 93
5.3.3.4 Hydraulic properties 95
5.4 Metal corrosion and iron-bentonite interaction studies (NAB 16-16) 98
5.4.1 Introduction and scope 98
5.4.2 Methods 98
5.4.3 Metal coupons (Cu, Ti, stainless steel): macro/micro observations and corrosion studies 100
5.4.3.1 Copper coupons 100
5.4.3.2 Titanium coupons 101
5.4.3.3 Stainless steel 101
5.4.3.4 Redox conditions 101
5.4.4 Carbon steel-related studies 102
5.4.4.1 Macroscopic observations 102
5.4.4.2 Corrosion studies 104
5.4.4.3 Interface studies 106

5.4.4.4 Other findings at the Fe/clay interface 107
5.4.4.5 Tentative model for corrosion and Fe-clay interaction process 108
5.4.5 Implications for repository conditions from a corrosion perspective..... 108
5.5 Microbiological studies (NAB 16-15)..... 110
5.5.1 Scope and objectives 110
5.5.2 Methods..... 110
5.5.3 Results 111
5.5.4 Conclusions 114

6 Sensor evaluation 115
6.1 Sensor sampling and observations 115
6.2 Post-mortem sensor evaluation 117
6.3 TDR re-scaling 121
6.4 Conclusions and lessons learned 122

7 Pre-dismantling modelling activities and synthesis of modelling activities 125
7.1 Overview of THM modelling and codes until dismantling..... 125
7.1.1 Modelling by CIMNE 125
7.1.2 Modelling by EPFL 129
7.1.3 Modelling performed within the framework of the DECOVALEX III project..... 130
7.1.4 Summary of THM modelling and codes until dismantling..... 133
7.2 Overview of THC modelling and codes until dismantling..... 133
7.3 Pre-dismantling THM modelling 136
7.3.1 Pre-dismantling modelling by CIMNE 137
7.3.2 Pre-dismantling modelling by EPFL..... 141
7.3.3 Pre-dismantling modelling by Clay Technology..... 143
7.3.4 Summary of the modelling analyses and comparison with test observations..... 145
7.4 Pre-dismantling THC modelling 149
7.4.1 Pre-dismantling modelling by UDC..... 149
7.4.2 Pre-dismantling modelling by LBNL..... 152
7.4.3 Pre-dismantling modelling by Clay Technology (CT) 153
7.4.4 Combined summary of the three modelling approaches 155
7.5 Post-dismantling modelling..... 156
7.6 Synthesis and outlook..... 158

8 Geosphere THM response 161
8.1 Introduction and scope 161
8.2 Investigations and influence of the excavation-damaged zone (EDZ) on buffer evolution 161
8.3 Geosphere thermal response 162
8.4 Geosphere hydraulic response 163
8.5 Geosphere mechanical response 167
8.6 Summary of geosphere THM response 168

9 Groundwater chemistry characterisation 171

10 Comparison of the buffer characteristics from the dismantling in 2002 versus 2015 175
10.1 Comparison results 2002 versus 2015: evolution of the barrier 175
10.1.1 Physical state of the barrier 176
10.1.2 Bentonite properties 181
10.1.3 Implications for long term performance 184

11 Assessment of the FEBEX experiment 185
11.1 Performance of the EBS in the FEBEX experiment 185
11.1.1 Limiting transport in the near-field 185
11.1.2 Resisting mineralogical transformations 187
11.1.3 Canister protection 188
11.1.4 Limiting pressure on canister and rock 188
11.1.5 Corrosion 189
11.2 Assessment of the performance of the FEBEX bentonite with regard to disposal systems 189
11.3 Assessment of the instrumentation and monitoring system 189
11.4 Assessment of modelling performance and developments 189

12 Conclusions & lessons learned 191
12.1 FEBEX – have the objectives been met? 191
12.2 FEBEX-DP – have the objectives been met? 191
12.3 Lessons learned 192
12.3.1 Lessons learned from the FEBEX partial dismantling 192
12.3.2 Lessons learned from the FEBEX-DP – final dismantling 193
12.4 Relevance of the project over the last 20 years and for the future 195
12.5 Future and outlook based on FEBEX/FEBEX-DP 196

13 References 197

Appendix A A-1

A.1 MAP 1 Geology FEBEX Gallery – Geotechnisches Institut A-1

A.2 MAP 2 Geology FEBEX Gallery – Geologisches Institut A-2

List of Tables

Tab. 1-1: Project history of FEBEX 4
Tab. 1-2: Bentonite main mineral content as percentages for FEBEX, S-2 (ENRESA 2000) and MX-80 R1 (SKB 2011) bentonites 5
Tab. 1-3: FEBEX block dimensions 10
Tab. 1-4: Sensors installed at the time of construction of the FEBEX in-situ test 14
Tab. 1-5: Sensors dismantled and newly installed in the FEBEX in-situ test during partial dismantling in 2002 15
Tab. 1-6: Dates of major activities throughout the FEBEX experiment with a continuous count of days 21
Tab. 1-7: Dedicated FEBEX-DP reports 23
Tab. 2-1: Total pressures (MPa) in the buffer on 24 April 2015, day 6'630 29
Tab. 2-2: Pore pressure (relative) values on 1 May 2014, day 6272 (MPa) 31
Tab. 2-3: Capacitive sensors on 24 April 2015 (% relative humidity) 33
Tab. 4-1: Breakdown of all the collected samples 47
Tab. 4-2: Summary of long cores obtained 49
Tab. 5-1: Concrete, concrete-bentonite and concrete-granite interfaces analysed by the different teams, sections, sample type and methods 64
Tab. 5-2: Structural formulae calculated from the chemical analyses of the < 2 µm grain size fraction of the samples (number of samples analysed in parentheses) 86
Tab. 5-3: Samples analysed for corrosion and Fe-bentonite interaction listed by the teams, sections, sample type and methods 99
Tab. 5-4: Fe phases identified on carbon steel surfaces and in the Fe/clay interface zone 105
Tab. 5-5: Most probable numbers of SRB, NRB and IRB in FEBEX bentonite core samples with lower and upper confidence limits (CL) from Micans study 112
Tab. 6-1: Breakdown of FEBEX sensors 118
Tab. 6-2: Summary of sensor failure causes 121
Tab. 7-1: Funding organisations, modelling teams and computer codes involved in the FEBEX in-situ test DECOVALEX III benchmark 131
Tab. 7-2: Couplings and phenomena considered by the various teams involved in the modelling of Part B 131
Tab. 7-3: Chemical species considered in models CGM-0, CGM-1 and CGM-2 134
Tab. 7-4: Main features of the THM analyses 145
Tab. 7-5: Main features of the analyses involving geochemistry 155
Tab. 7-6: Funding organisations, modelling teams and computer codes involved in Task 9 of the EBS Task Force 157

Tab. 7-7: Funding or10-1ganisations, modelling teams and computer codes involved in Task D (INBEB) of the DECOVALEX 2019 project 157

Tab. 10-1: Average properties for each section as computed from fitting of polynomial functions 178

Tab. 10-2: Average values computed from the longitudinal profiles 179

List of Figures

Fig. 1-1: Schematic of the Spanish disposal concept for high-level waste: AGP Granito 2
Fig. 1-2: FEBEX project timeline and the different institutional frameworks 4
Fig. 1-3: Borehole geometry 7
Fig. 1-4: General layout of the FEBEX in-situ test configuration: FEBEX I (top) and FEBEX II (bottom) 8
Fig. 1-5: FEBEX bentonite block dimensions (upper row) and vertical cross-sections of a heater and a heater-free section (lower row) 10
Fig. 1-6: Photo (Section 42/Bentonite layer 61) and cross-section through heater, liner and block assembly 11
Fig. 1-7: Heater layout and dimensions 12
Fig. 1-8: Liner segment 13
Fig. 1-9: FEBEX layout 2002 – 2015 showing additional instrumentation sections (in red) and HR (relative humidity) and CPT (cone penetration test) pipes to measure total pressure and equipped with a thermocouple 17
Fig. 1-10: FEBEX-DP project organizsation and management 20
Fig. 2-1: Power output from Heaters #1 and #2 during the entire operational phase 26
Fig. 2-2: Temperature evolution at different locations in the buffer 27
Fig. 2-3: Total pressure evolution at different locations in the buffer 28
Fig. 2-4: Pore pressure rise (relative) at different locations in the buffer during the full operational phase 30
Fig. 2-5: Evolution of relative humidity at different locations in the buffer 32
Fig. 2-6: Evolution of volumetric water content in section M2 until final dismantling 34
Fig. 2-7: Recorded relative humidity in the air of the service area, beyond section U outside the confined test section 35
Fig. 2-8: Displacements measurements obtained at the shotcrete plug in section U, colours refer to different sensors 36
Fig. 2-9: Temperature and pressure evolution in the SF12 borehole 37
Fig. 3-1: Concentration of oxygen gas (in vol.-%) in the different GRS pipes (GF) obtained during the First Operational Phase (1996 – 2002) and in the CIEMAT pipes (FP) obtained during the Second Operational Phase (2002 – 2015) 41
Fig. 4-1: General layout of the sampling sections 46
Fig. 4-2: Location of long core boreholes at the plug surface 49
Fig. 4-3: Shotcrete core C-C-32-4 and following overcore, after retrieval 50
Fig. 4-4: Robot installation in the drift (left) and in operation (right) 51

Fig. 4-5: Dismantling plan layout of Section 34 (short cores C-C-34-1 to 11 in yellow) 52
Fig. 4-6: View of the dummy canister (left) and its adhesion to the liner segment (right) 53
Fig. 4-7: Percussion hammers (left) were used to obtain bentonite core samples of 4.5 cm in diameter (right); microbiological sampling (bottom) 54
Fig. 4-8: Dummy canister secured with a steel support 55
Fig. 4-9: Dummy canister extraction (in liner section) 56
Fig. 4-10: Uncovered heater front (left) and close-up of the gap filled with bentonite (right) 57
Fig. 4-11: Extraction of Heater #2 (left) and general view of the heater at the drift entrance (right) 57
Fig. 4-12: Inner view of the liner once the heater was extracted (left) and detail of the bentonite protrusions inside the liner (right) 58
Fig. 4-13: Start (bentonite layer 60, left) and end (granitic back end showing the cemented total pressure sensor slots, right) of the dismantling of the remaining test section 58
Fig. 5-1: Design of the concrete plug installed after the dismantling of the first heater in the FEBEX in-situ experiment 61
Fig. 5-2: Pictures of sections 32 (a) and 34 (c), both sampling for concrete; (c) shows three large boreholes from interface overcoring; schematic cross-sections of sample locations in section 32 (Fig. 5-2b) and section 34 (Fig. 5-2d) 63
Fig. 5-3: Total porosity (left) and pore size distribution (right) of the samples of core C-C32-2 in both plug sections (Sections 1 and 2) 65
Fig. 5-4: Images of cut surfaces of half cores from C-C-32-6-OC-cb viewed through a liquid epoxy layer 66
Fig. 5-5: Total porosity (MIP) of the concrete and the bentonite as a function of distance to the interface in dry-drilled samples C-C-34-10 and 12, BC-C-35-1 and 2, BC-S-35-3 and B-B-36-7 68
Fig. 5-6: SEM-EDX elemental map for S (top) and Mg (bottom) 69
Fig. 5-7: SEM images of concrete scraped from the bentonite surface in the BC-S-35-3 sample (UAM) 70
Fig. 5-8: Location along the gallery of the sampling sections used for determination of bentonite water content and dry density on-site 72
Fig. 5-9: Position of sampling radii in a section and photo of the template used to locate the drillings and the crown drill bit 73
Fig. 5-10: Contour maps for water content, dry density and degree of saturation in a section around the heater (S45) and in a "cold" section (S58): water content (upper panel), dry density (middle panel) and degree of saturation (bottom panel) 75

Fig. 5-11: Radial dimension of different types of blocks measured along the gallery on dismantling 76

Fig. 5-12: Appearance of the bentonite barrier around Heater #2 during installation in 1997 and during dismantling in 2015 77

Fig. 5-13: Dry density (top) and water content (bottom); distribution in a vertical longitudinal section 78

Fig. 5-14: Average water content and dry density for the sections sampled along the barrier 78

Fig. 5-15: Bentonite adhered to granite showing striation parallel to the axis of the gallery (indicated by an arrow) 80

Fig. 5-16: Location of the sampling sections used by each organisation for bentonite characterisation 81

Fig. 5-17: Water retention curves of the reference bentonite compacted at 1.6 g/cm^3 (crosses), obtained by measuring the suction of blocks (NAB 16-17, filled symbols) and obtained in cells with the vapour transfer technique 83

Fig. 5-18: Distribution of void ratio for pore sizes greater and less than 50 nm in samples from cool sections (left) and sections around the heater (right) 84

Fig. 5-19: BET specific surface area measured by CIEMAT, ETH and UAM in bentonite samples taken from different sections 85

Fig. 5-20: Sodium and magnesium content in bulk samples from different sections analysed by BGR and CIEMAT 87

Fig. 5-21: Exchangeable sodium and magnesium determined by different laboratories in samples from sampling sections around the heater 88

Fig. 5-22: Concentration of soluble chloride and sodium in 1:4 aqueous extracts of samples from several sampling sections 89

Fig. 5-23: Concentration of soluble sulphate in 1:4 aqueous extracts (after equilibration) of samples from several sampling sections (left; each point represents the average for all the samples taken at the same distance from the heater) and in porewater obtained by squeezing (right) 90

Fig. 5-24: Thermal conductivity measured in-situ by Nagra in different sampling sections 91

Fig. 5-25: Dependence of thermal conductivity of bentonite measured in-situ (filled symbols) and in the laboratory (empty symbols) on water content and dry density, and empirical relationships for the FEBEX reference bentonite (lines) 92

Fig. 5-26: Comparison between the vertical strain measured at the end of the swelling under load tests for samples from different sampling sections and the strain for equivalent samples of the reference bentonite tested under the same conditions 93

Fig. 5-27: Apparent pre-consolidation stresses estimated from the oedometer tests for samples trimmed from blocks retrieved from different sampling sections, for a reference block (UPC) and for compacted samples of the reference bentonite (CIEMAT) 94

Fig. 5-28: Maximum deviator stress for samples trimmed along a radius of section S47 and samples recompacted from a reference block (left) and corresponding strain (right) 95

Fig. 5-29: Samples taken for gas permeability in sampling section S44 and appearance of the interface between blocks in a sample from the outer ring (barely visible, indicated by an arrow, BC-44-6) and another from the inner ring (BC-44-2) 96

Fig. 5-30: Effective gas permeability values of samples from different sampling sections for different confining pressures as a function of the position in the barrier (no samples with interface are shown) 96

Fig. 5-31: Gas permeability as a function of the accessible porosity for the FEBEX reference and for FEBEX-DP samples with and without interface 97

Fig. 5-32: Left: teams involved in Corrosion and Fe-clay interaction studies, Right: locations of corrosion and Fe/clay interface samples 98

Fig. 5-33: Metal coupons from section 48 after extraction 100

Fig. 5-34: Photograph of Cu-ETP coupon and optical micrograph of pit analyses at 0 mm depth from the surface 101

Fig. 5-35: Heater after extraction and transport to AITEMIN workshops, end of extensometer SHSD2-01, steel liner in contact with clay and corrosion halos in bentonite induced by corroding fissurometer 103

Fig. 5-36: Schematic view of the different compartments between carbon-steel-based materials and the bentonite clay (not to scale) 104

Fig. 5-37: a) Fe/Al ratio (EDX data) as a function of distance from the interface for two samples in Section 41 (blue and red curves); b) contents of elements (wt.-% oxides) (XRF data) as a function of distance from the interface for one sample in Section 42 106

Fig. 5-38: Speciation of Fe (shown as excess iron relative to natural clay) as a function of distance from the steel contact determined from Mössbauer spectrometry and XRF in Section 41 107

Fig. 5-39: Water content and dry density along the tunnel axis and with respect to the heater and location of samples for mineralogical studies 111

Fig. 5-40: Extracted cells from sample B-C-60-18 stained with DAPI (4',6-diamidino-2-phenylindole) in 1'000× magnification 111

Fig. 5-41: Numbers of aerobic and anaerobic cells cultivated by BGR at 30 °C and 70 °C as function of gravimetric water content (w) 113

Fig. 6-1: Status of a psychrometer (left), a capacitive moisture and pore pressure sensor before being retrieved (centre) and detail of a pore pressure sensor (right) 116

Fig. 6-2: TDR probes with various types of damage at the time of on-site inspection 116

Fig. 6-3: Results of the verification of different types of sensors 119

Fig. 6-4: (Slightly) deformed (bended) extensometer 120

Fig. 6-5: Evolution of sensors operating throughout the lifetime of the experiment (top) and breakdown of defective sensors (bottom) 123

Fig. 7-1: Evolution of degree of saturation with alternative retention curves for the bentonite resulting in granite desaturation (SH) and no granite desaturation (PGSH) 127

Fig. 7-2: Computed (OBC analysis) and observed evolution of degree of saturation in Section E1 (across Heater #1, Fig. 1-4) at different radial distances r from the tunnel axis 127

Fig. 7-3: Stages considered in the dismantling modelling 128

Fig. 7-4: Predicted and observed distributions of dry density and water content in a section across Heater #1 129

Fig. 7-5: Computed and experimental evolutions of relative humidity in a section across Heater #2 130

Fig. 7-6: Comparison of computed evolutions of relative humidity by the different modelling teams and observations. Experimental results are in orange and labelled UPC 132

Fig. 7-7: Comparison of computed distributions of Cl^- concentrations with recalculated experimental data after 1930 days of heating (first dismantling) 135

Fig. 7-8: Comparison of computed distributions of Cl^- concentrations with inferred aqueous extract data after 1930 days of heating (first dismantling) 136

Fig. 7-9: Location of sections F2 and G selected for checking blind predictions 137

Fig. 7-10: Stages considered in the simulation of the final dismantling (CIMNE model) 138

Fig. 7-11: Predictions of water content and dry density for the final dismantling, a) Section F2, b) Section G (CIMNE model) 139

Fig. 7-12: Range of retention curves used in the sensitivity analyses (CIMNE model) 140

Fig. 7-13: Distributions of water content and dry density with values of P0 of 7 MPa (black line) and 20 MPa (red line), Section F2 (CIMNE model) 140

Fig. 7-14: ACMEG-TS model 141

Fig. 7-15: Computed and observed distributions of dry density and water content after first (partial) dismantling of Section 27 (hot section, near instrumented section F1, ~ 6.9 m into buffer from first plug, see Fig. 1-4) (EPFL model) 142

Fig. 7-16: Computed and observed distributions of dry density and water content after first (partial) dismantling of Section 15 (cool section, ~ 3.3 m into buffer from first plug, see Fig. 1-4) (EPFL model) 142

Fig. 7-17: Predictions of water content and dry density for the final dismantling 143

Fig. 7-18: Geometry and boundary conditions of the CT analyses 144

Fig. 7-19: Computed distributions of water content and dry density at different times (CT model) 144

Fig. 7-20: Variation of the thermal conductivity of bentonite with degree of saturation for the three modelling teams (left) and variation of the intrinsic permeability of bentonite with porosity for the three modelling teams (right) 146

Fig. 7-21: Predictions of distributions of water content (a) and dry density (b) in section F2 from the three modelling teams at final dismantling 147

Fig. 7-22: Comparison between predicted distributions of water content (a) and dry density (b) in section F2 with dismantling observations 148

Fig. 7-23: Comparison between predicted distributions of water content (a) and dry density (b) in section G with dismantling observations 148

Fig. 7-24: 1D analysis domain used by the UDC team 150

Fig. 7-25: Effect of a change in the retention curve on the distribution of Cl^- concentration at first dismantling 150

Fig. 7-26: Comparison of the distribution of Cl^- concentration at first dismantling computed with the initial and updated model 151

Fig. 7-27: Comparison of the distribution of Cl^- concentration at first dismantling (2002) and final dismantling (2015) computed with the updated model 152

Fig. 7-28: Distributions of Cl^- concentration at first dismantling (5.3 years) and final dismantling (18.3 years) using the linear swelling model (LS) and the BExM model 153

Fig. 7-29: 1D (planar) analysis domain (CT model) 154

Fig. 7-30: Prediction of distributions of chemical species concentrations after 5'000 days of simulation (CT model) 154

Fig. 7-31: Comparison of predictions of the distributions of (a) chloride (Cl^-) and (b) sulphate (SO_4^{-2}) by the three modelling teams with first observations from final dismantling 156

Fig. 8-1: Temperature response in boreholes SF21 – 24 162

Fig. 8-2: Variation of temperature with radial distance from the FEBEX drift axis at key times during the in-situ experiment for sensors in the Heater #2 section of the drift 163

Fig. 8-3: Measured pore pressure in boreholes 164

Fig. 8-4: Variation of pore pressure with radial distance from the FEBEX drift axis at key times during the in-situ experiment 164

Fig. 8-5: Estimated (left) pressure at the gallery wall and b) pressure gradient slope with *ln r* based on the measurements from borehole intervals in SF21 – 24 165

Fig. 8-6: Average inflow (ml/min) estimated from increase in bentonite water content at partial and final dismantling 166

Fig. 8-7: Measured total pressure in borehole: a) SG1 (vertical up) and b) SG2 (horizontal) 167

Fig. 8-8: Measured displacements in the SB1 and SB2 boreholes (displaying slight expansions) 168

Fig. 9-1: Pie diagram of mean concentration values for major ions in groundwater from radial and parallel boreholes 172

Fig. 10-1: Schematic representation of the FEBEX gallery with indication of the sampling sections used for on-site analyses in 2002 (sections S9 to S31) and 2015 (sections S37 to S61) 175

Fig. 10-2: Appearance of the core of the barrier in cold zones after 5 years (left, slice 118) and 18 years (right, slice 17) of operation 176

Fig. 10-3: Water content and dry density of the bentonite barrier along the gallery axis in cold sections after 5 and 18 years of operation 177

Fig. 10-4: Water content and dry density of the bentonite barrier along the gallery axis in sections around the heaters after 5 and 18 years of operation 177

Fig. 10-5: Average water content and dry density for the sections sampled along the barrier in 2002 and 2015 179

Fig. 10-6: Concentration of ionic species measured in 1:4 aqueous extracts of bentonite samples taken in 2002 (S12 to S28) and 2015 (S47 to S59) 182

Fig. 10-7: Hydraulic conductivity of samples trimmed from blocks retrieved from different sampling sections in 2002 (S12 to S28) and 2015 (S47 and S53) as determined by different laboratories 183

Fig. 10-8: Apparent pre-consolidation stresses estimated from oedometer tests for samples trimmed from blocks retrieved from different sections in 2002 (S19 and S28) and 2015 (S47) 183

Authors/sources for report

Chapter 1 **F. Kober** (Nagra)

Chapter 2 **J.L. García-Siñeriz** (Amberg Infraestructuras S.A.)

Chapter 3 **F. Kober** (Nagra)

Chapter 4 **J.L. García-Siñeriz** (Amberg Infraestructuras S.A.)

Chapter 5

Section 5.1 **V. Cloet** (Arcadis), **U. Mäder** (University of Bern)

Section 5.2 **M. Villar** (CIEMAT)

Section 5.3 **P. Wersin** (University of Bern)

Section 5.4 **P. Wersin** (University of Bern)

Section 5.5 **P. Wersin** (University of Bern)

Chapter 6 **J.L. García-Siñeriz** (Amberg Infraestructuras S.A.)

Chapter 7 **A. Gens** (UPC)

Chapter 8 **G.W. Lanyon** (Fracture Systems Ltd.), **F. Kober** (Nagra)

Chapter 9 **G.W. Lanyon** (Fracture Systems Ltd.), **F. Kober** (Nagra)

Chapter 10 **M. Villar** (CIEMAT)

Chapter 11 **G.W. Lanyon** (Fracture Systems Ltd.), **O. Leupin** (Nagra), **P. Sellin** (SKB), **F. Kober** (Nagra)

Chapter 12 **G.W. Lanyon** (Fracture Systems Ltd.), **F. Kober** (Nagra)

Overall editorial contribution:

G.W. Lanyon (Fracture Systems Ltd.). **Raphael Schneeberger** (Nagra), **F. Kober** (Nagra)

1 Introduction

This report summarises the FEBEX (**F**ull-Scale **E**ngineered **B**arriers **EX**periment) in-situ experiment, with the focus on the activities and results of the final dismantling (FEBEX-DP: FEBEX – **D**ismantling **P**roject). Using information from continuous monitoring, the partial dismantling in 2002 (ENRESA 2006a) and FEBEX-DP in 2015, the FEBEX in-situ experiment is summarised herein with respect to the evolution of an engineered barrier system (EBS) under natural conditions and on realistic scales over almost two decades and the relevant understanding of performance assessment requirements.

1.1 The FEBEX experiment

The FEBEX experiment was a demonstration experiment based on the Spanish reference concept for disposal of radioactive waste in crystalline rock (AGP Granito, Fig. 1-1). The concept was developed during the 1980s and 1990s with waste canisters placed in horizontal drifts and surrounded by a clay barrier (buffer) constructed from highly compacted bentonite blocks (ENRESA 1995, 2000).

The experiment consisted of four main parts (ENRESA 2006a - PT05-0/2006):

- an in-situ test in natural conditions and at full scale (discussed in this report)
- a mock-up test at almost full scale (see Lanyon & Gaus 2016, Martín et al. 2006, Zheng & Samper 2008)
- a programme of laboratory tests to complement the information from the two large-scale tests (Villar et al. 2008, 2010); and
- the development, verification and partial validation of THM and THC (thermo-hydro-chemical) models. The models describe the THM behaviour of the buffer during the early evolution of the repository near-field (see this report and Lanyon & Gaus 2016)

With its suitable laboratory conditions, Nagra's Grimsel Test Site (GTS) was selected for the performance of the in-situ test due to the similarity between the Spanish and Swiss reference repository[1] concepts at that time. The GTS is located at an elevation of around 1'730 m a.s.l., roughly 400 to 450 metres beneath the Juchlistock mountain in the southern section of the Central Aar Massif in Central Switzerland (Schneeberger et al. 2019).

While the mock-up test at the CIEMAT facilities, Madrid, is still running, the laboratory test programme and the in-situ test have been completed. This report focuses on the summary findings of the final dismantling of the FEBEX in-situ experiment (FEBEX-DP) in 2015 and its subsequent analysis and reporting performed from 2015 to 2019.

---

[1] Nagra's programme at that time was dedicated to the *Kristallin-I* project and its predecessor, "*Projekt Gewähr*". The crystalline basement of Northern Switzerland was considered as a potential host rock for the disposal of high-level and long-lived, intermediate-level radioactive waste in a deep geological repository (Nagra 1994).

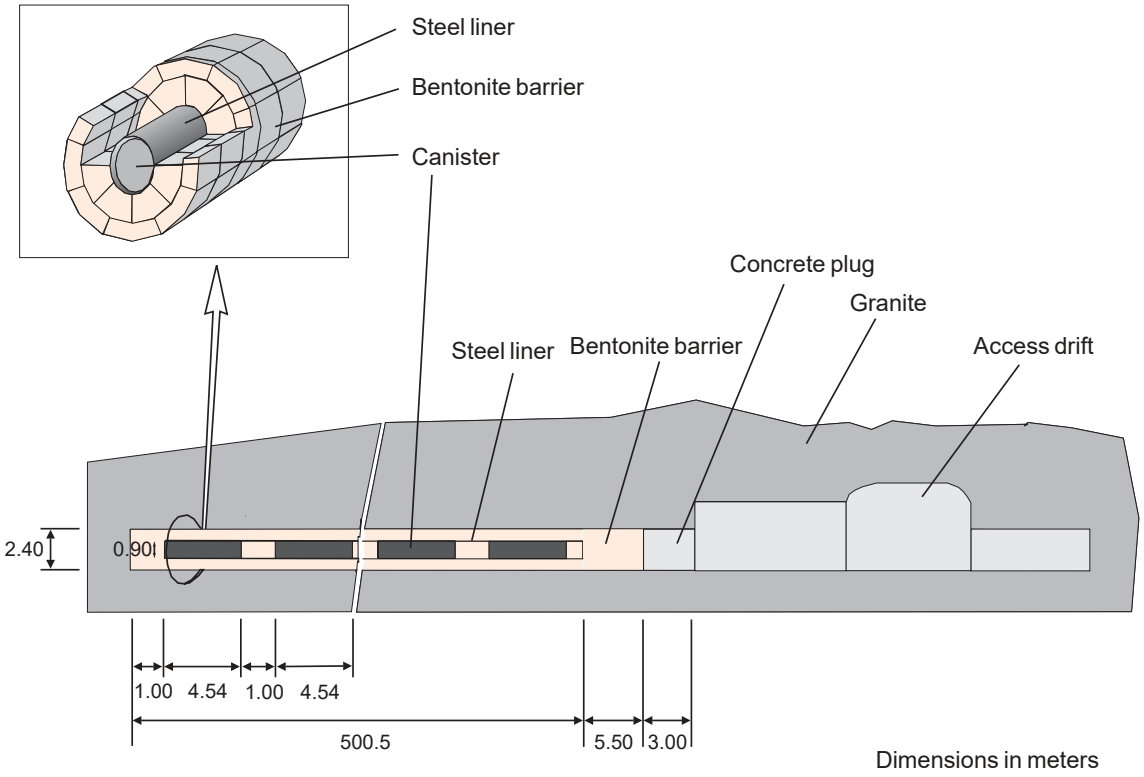


Fig. 1-1: Schematic of the Spanish disposal concept for high-level waste: AGP Granito

The in-situ test of the FEBEX experiment was designed to serve multiple objectives (ENRESA 1995):

- demonstrating the feasibility of fabricating and assembling an engineered barrier system at a 1:1 scale under natural conditions with components constructed with the actual design dimensions of a repository drift
- developing, supporting, and validating the predictive capabilities of models to evaluate the thermo-hydro-mechanical (THM) and thermo-hydro-geochemical (THG[2]) behaviour of the near-field

1.1.1 Objectives of waste management organisations in the 1990s and safety relevant aspects 25 years later

Although initiated more than 25 years ago, FEBEX still meets current needs in terms of demonstrating the functionality, safety and performance of various repository components. Nevertheless, advances in in-situ and laboratory experiments and modelling have led to refinements and further requirements. Additionally, objectives and scientific questions addressed today by experiments may diverge from those of experiments developed over 25 years ago.

The safety functions and, in particular, the requirements on the safety functions with regard to the parameters influencing them, depend on the specific repository system under consideration. For example, parameters impacting system safety include the disposal concept and its components,

[2] THG and THC have equivalent meanings, indicating thermo-hydro-geochemical and thermo-hydro-chemical processes.

emplaced waste, the host rock, the geosphere and the biosphere. In the case of high-level waste/spent fuel (HLW/SF) disposal in crystalline rock, concepts using clay-based buffer and seal materials and the respective buffer safety functions have been summarised by Sellin and Leupin (2013) as:

- limiting transport in the near-field, primarily limiting advective transport (determined by the hydraulic properties), but also retardation or attenuation (determined by the chemical retention properties)
- reducing microbial activity (to protect the canister)
- damping rock shear movements (to protect the canister)
- resisting mineralogical transformations (to retain the favourable properties on the short and long term)
- preventing canister sinking (to protect the canister)
- limiting pressure on canister and rock (to protect the canister or the overlying bedding structure in the case of sedimentary host rocks)

The final dismantling of the almost fully saturated FEBEX experiment provided very valuable data for the early buffer and near-field evolution in an EBS. The joint experimental and theoretical studies have provided a better understanding and assessment of barrier performance over the early resaturation phase and the transient phase towards partial or full saturation. These data are highly important for the comparison of model predictions with the actual behaviour (Alonso and Alcoverro 2005, Andersson 2005, www.decovalex.org). The FEBEX experiment also provides data for evaluating the impact of different types of heterogeneity (construction, early and late saturation stages, hydraulic conductivity in the buffer and the geosphere, thermal effects) on EBS evolution and safety requirements.

1.1.2 FEBEX and other 1:1 in-situ tests and dismantling operations

FEBEX was the first full-scale demonstration experiment of a HLW disposal system. Complementary to FEBEX, other organisations conducted heater experiments in various host rocks. A full-scale experiment has since been performed for the Atomic Energy of Canada Limited's (AECL) HLW concept (Buffer Container experiment, Graham et al. 1997, Dixon et al. 2002), where a sand-bentonite mixture was heated up to 85 °C for 2.5 years. SKB has conducted a KBS-3V concept-based experiment, the Prototype Repository Experiment at the Äspö Hard Rock Laboratory, where the outer section of the experiment was dismantled in 2010/2011 after 7 years of heating with heater surface temperatures of 90 °C under natural hydration conditions (Svemar et al. 2016). A demonstration of Nagra's concept for the Opalinus Clay has been investigated at a 1:2 scale in the ongoing HE-E experiment (heater surface ~140 °C) at the Mont Terri Rock Laboratory (Gaus et al. 2014, Wieczorek et al. 2017). A full-scale emplacement (FE) heater test (heater surface ~ 135 °C) was set up also at the Mont Terri Rock Laboratory and has been running since 2015 (Müller et al. 2017, Nagra 2019).

1.1.3 Project history: FEBEX I – FEBEX II – NF-PRO – FEBEXe – FEBEX-DP

Given the long duration and joint operation of the FEBEX project, it has had various funding sources, institutional frameworks and management structures (Fig. 1-2 and Tab. 1-1). The project started in 1994 with the support of the European Commission through consecutive contracts, identified as FEBEX I for the period January 1996 to June 1999, and FEBEX II from September 2000 to December 2004. Thereafter, NF-PRO (Near Field PROcesses) took place from January 2005 to December 2007. Finally, in January 2008, the in-situ test was transferred from ENRESA to the FEBEXe Consortium composed of SKB (Sweden), POSIVA (Finland), CIEMAT (Spain), Nagra (Switzerland) and more recently KAERI (South Korea). For FEBEX-DP, the FEBEXe group invited interested parties to participate and was then joined by Andra (France), BGR (Germany), Obayashi (Japan), RWM (UK), SÚRAO (Czech Republic), and the US DOE (USA).

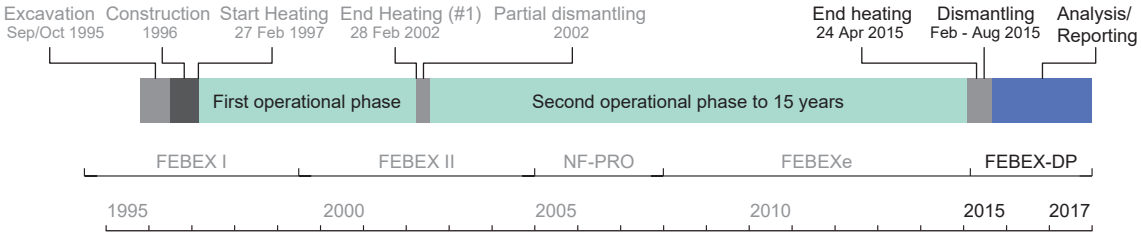


Fig. 1-2: FEBEX project timeline and the different institutional frameworks

Tab. 1-1: Project history of FEBEX

Project	Time	Activities
FEBEX I	1995 – 1999	Design, construction with heating initiated in 1997
FEBEX II	2000 – 2004	Continued saturation and partial dismantling of the in-situ test (2002)
NF–PRO	2005 – 2007	Continued saturation
FEBEXe	2008 – 2014	Ongoing saturation and planned final dismantling for the in-situ test
FEBEX–DP	2014 – 2017	Final dismantling of the in-situ test

1.2 The FEBEX bentonite

The FEBEX bentonite – also known as "Serrata" clay – was extracted from the Cortijo de Archidona deposit (Minas de Gádor, S. A., in Serrata de Níjar, Almería, Spain) (ENRESA 1998a). The deposits were formed following volcanism associated with Neogene tectonic activity, which occurred between 15 and 18 Ma ago. Subsequent episodes of emersion and immersion, together with ongoing volcanic activity, contributed to the alteration of the volcanic rocks into silica, alunite, jarisite, kaolinite or bentonite depending on to the composition of the solutes. The mineralogy of the FEBEX bentonite, Bentonite S-2 (a related bentonite from the same deposit) and MX-80 R1 (the reference bentonite for SKB's SR-Site) are given in Tab. 1-2. Extensive characterisation of the FEBEX bentonite, with special emphasis on the influence of temperature, is documented in ENRESA (1998a, 2000, 2006b, 2006c), Lloret et al. (2003), Villar & Lloret (2004), Fernández & Rivas (2005), Lloret & Villar (2007) and Villar et al. (2010). The raw material prepared for the fabrication of the blocks is a bentonite granulate with less than 5% of the grains greater than 5 mm and more than 85% of the grains less than 74 μm, with a water content of 12.5% to 15.5%.

Tab. 1-2: Bentonite main mineral content as percentages for FEBEX, S-2 (ENRESA 2000) and MX-80 R1 (SKB 2011) bentonites

Mineral [%]	FEBEX bentonite	Bentonite S-2	MX-80 R1
Smectite	92 ± 3	92 ± 4	84 ± 3
Quartz	2 ± 1	2 ± 1	3 ± 1
Plagioclase (Na, Ca)	3 ± 1	3 ± 1	–
Cristobalite	2 ± 1	2 ± 1	0 – 1
Feldspars	Traces	–	4 ± 2
Calcite	1 ± 0.5	1 ± 1	0 – 1

The decision to select the FEBEX bentonite was based on the favourable properties that characterise this clay (ENRESA 2000):

- very high montmorillonite content of 92 ± 3%
- large swelling pressure (average swelling pressure for a dry density of 1.60 g/cm^3: 5 MPa)
- low permeability (average saturated hydraulic conductivity for a dry density of 1.60 g/cm^3: 4×10^{-14} m/s)
- acceptable thermal conductivity
- good retention properties and ease of compaction for the fabrication of blocks.

The liquid limit was 102 ± 4%, while the specific weight was estimated to be 2.70 ± 0.04 g/cm^3.

A 300-tonne batch of duly homogenised and conditioned bentonite was processed in 1996 for the FEBEX project. The processing consisted of homogenisation, air-drying and manual removal of volcanic pebbles on-site and, at the factory, crumbling, drying in a rotary oven at temperatures between 50 °C and 60 °C, and sieving through a 5-mm mesh. A comprehensive characterisation programme of laboratory tests was performed (ENRESA 2006a, Villar 2002).

1.3 The FEBEX gallery at the GTS: geology, structural geology, geophysical and hydrogeological characterisation

The host rock of the FEBEX gallery is Grimsel Granodiorite. During the Alpine Orogeny (starting 40 Ma ago), the Aare Granite was subject to regional shear displacement and weak to intermediate metamorphosis. The latter caused significant foliation, whereas the shear movement resulted in the development of cataclastic and mylonitic shear zones (Keusen et al. 1989, Schneeberger et al. 2019). The major structural features are depicted in Map 1 (Appendix).

Extensive hydraulic testing in existing and new boreholes was performed as part of the FEBEX project. Tests included pressure build-up, pulse tests and longer production/injection tests (Meier et al. 1995, Guimerà et al. 1996, 1998). Larger-scale hydraulic tests were performed in boreholes BOUS 85.001, BOUS 85.002, FBX 95.001, and FBX 95.002 (see Fig. 1-3a). Extensive hydraulic testing together with monitoring of the response to the excavation were performed to identify the most important hydraulic structures and their connectivity. The inflows to the tunnels from these shear zones were approximately 60 and 23 ml/min (for K and S shear zones, respectively, NW-SE and NE-SW fault sets, Schneeberger et al. 2019) before installation (Guimerà et al. 1996, 1998). These differences in flowrate measurements are due to the heterogeneity of the fracture system and the influence of the various tunnel systems within the GTS (including the main GTS access tunnel).

The main hydraulic feature that intersects the test section of the FEBEX drift is associated with the metabasic dykes (lamprophyre dyke, Schneeberger et al. 2019) that intersect close to Heater #1. Martínez-Landa & Carrera (2005, 2006) suggest that the hydraulic conductivity of the background rock (matrix and small fractures) is ~ 10 – 11 m/s, while, locally, features such as Fr-7 (metabasic dyke channel, see Fig. 1-3b and Map 2 in the appendix) are many orders of magnitude more permeable.

Small-scale tests showed a range of transmissivity from 10^{-12} to over 10^{-7} m^2/s, with a mode ~ 10^{-11} m^2/s representing the background rock volume (Schneeberger et al. 2019). Transmissivity estimates of the identified structures from cross-hole tests varied from 10^{-10} to 3×10^{-8} m^2/s, with one feature (Fr-7, a highly conductive channel associated with the metabasic dyke margin) having a transmissivity ~ 10^{-5} m^2/s (Martínez-Landa & Carrera 2006). Inflow from this feature may have caused some problems during installation (Guimerà et al. 1998), although Svemar & Huertas (2004) suggest that there were no problems with inflow during construction of the FEBEX EBS.

In 2005, as part of the FUNMIG project (**FUN**damental Processes of Radionuclide **MIG**ration), two boreholes (FUN 05.001, FUN 05.002, see Map 2 in the appendix) were drilled below the drift from the former keyed FEBEX plug and parallel to the FEBEX drift at distances of 30 and 60 cm to investigate geochemical gradients and bentonite colloid concentrations in the near-field (Pérez-Estaún et al. 2006, Buil et al. 2010). Fracture transmissivity was typically very low with values of 10^{-12} – 10^{-11} m^2/s, with the exception of interval FU1-1 intersecting a fracture with a transmissivity of $6 – 8 \times 10^{-10}$ m^2/s close to the end of the drift (known as the "September" fracture). This feature may be related to the fracture zone containing Fr-5 intersected by boreholes J5 and B23 (Fig. 1-3b). Inflows to the FEBEX drift were measured during and after excavation using a variety of methods. The total was estimated at 7.8 mL/min (Alonso et al. 2005, Martínez-Landa & Carrera 2005), approximately half of which came from six identified inflow points.

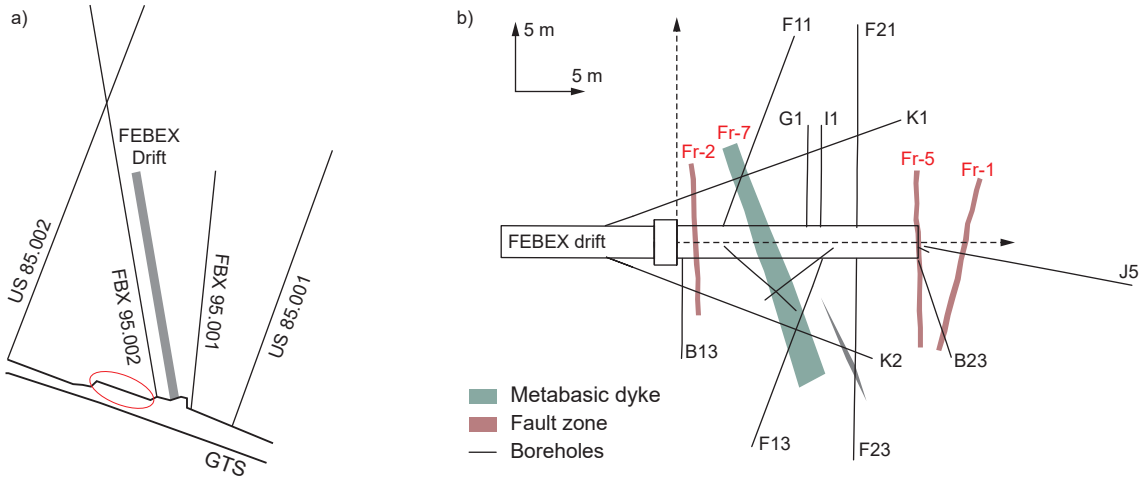


Fig. 1-3: Borehole geometry

Meier et al. (1995)

a) prior to gallery excavation with the future gallery indicated. The red ellipse indicates the on-site laboratory during the final dismantling in 2015.

b) during the FEBEX experiment (Martínez-Landa & Carrera 2006).

1.4 FEBEX I/II – test configuration, operation, partial dismantling, reconstruction and sealing

1.4.1 FEBEX I – test configuration and operation

The site for the FEBEX drift at the GTS was chosen for ease of access for the machinery based on reconnaissance data from two boreholes (BOUS 85.001,2) and geophysical surveys. Following the site selection, the seismic data were reinterpreted and two additional boreholes (FEBEX 95.001,2) were drilled and tested.

The horizontal drift with a diameter of 2.28 m and a total length of 71.4 m was excavated in 1995 in the northern part of the GTS in Grimsel Granodiorite using a TBM (tunnel-boring machine) (Fig. 1-4). The diameter differed slightly from that of the reference concept (2.4 m) but was selected on the basis of equipment availability at the time. The drift was designed with a 1% ascending slope to aid drainage. There were some minor difficulties in alignment of the TBM in the portal section, which resulted in variability in slope at the start of the tunnel.

Following excavation, the "test section", comprising the section from TM53 to the end of the tunnel, was characterised, including detailed hydrogeological investigations, profiling and further hydrogeological testing of the drift and surrounding rock. This work formed the basis of the hydrogeological model of the site (Guimerá et al. 1998).

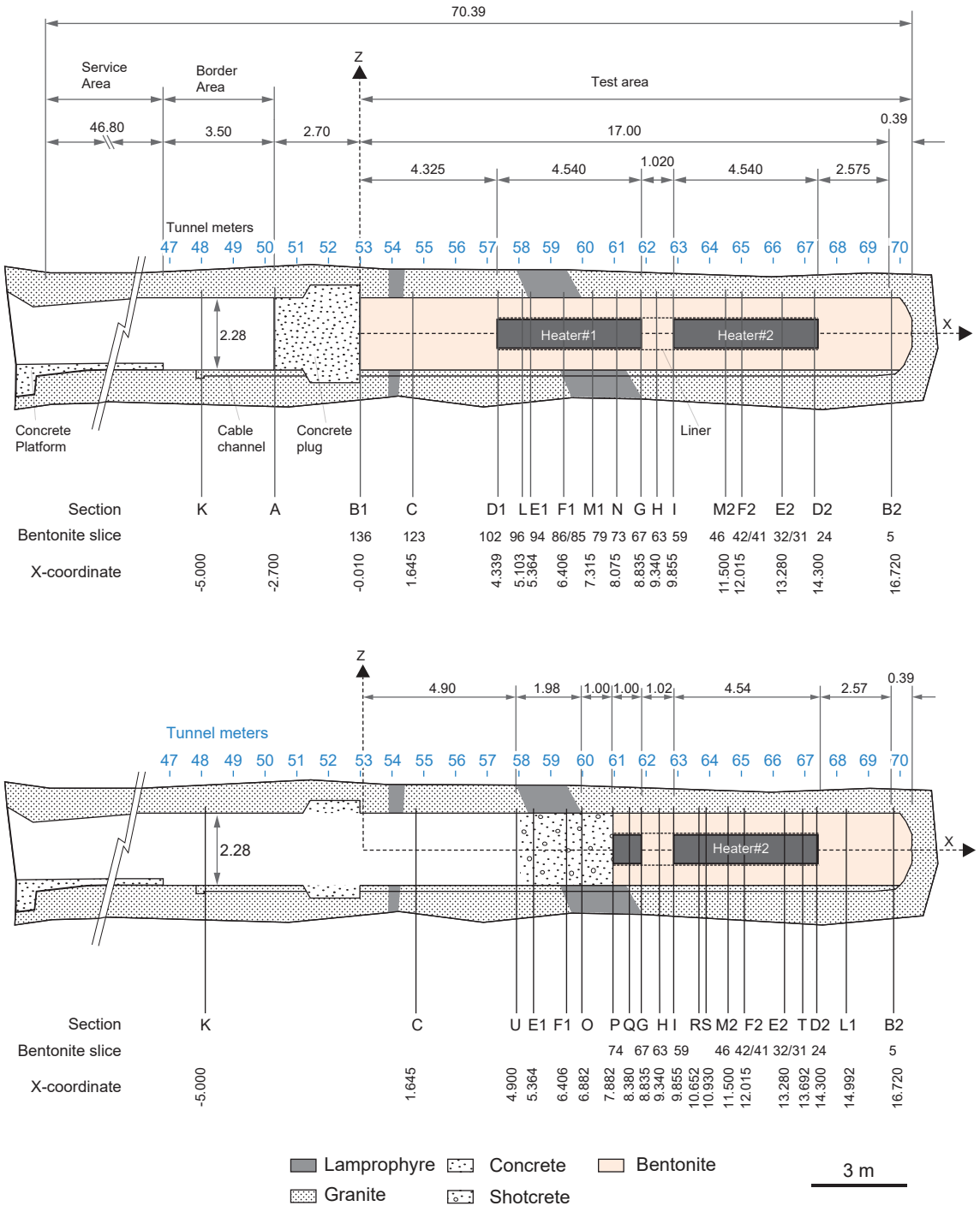


Fig. 1-4: General layout of the FEBEX in-situ test configuration: FEBEX I (top) and FEBEX II (bottom)

Note the waterproof membrane that was placed between the new shotcrete plug (1st stage) and the new shotcrete plug (2nd stage), roughly at TM 60. "Section" refers to instrument section.

The buffer – between the heaters and the rock – was backfilled with compacted FEBEX bentonite blocks. The backfilled area was sealed with a plain key-type concrete[3] plug placed in a recess excavated in the rock. The plug had a length of 2.7 m and a volume of 17.8 m^3. The plain concrete recess plug was designed to resist a swelling pressure of the bentonite of 5 MPa and was constructed without any reinforcement to facilitate subsequent dismantling. No specification was made for the water tightness or gas tightness of the concrete plug. The concrete used had a low hydration heat value, minimum shrinkage allowance and was concreted in three sections perpendicular to the axis of the drift and compacted by vibration. Fig. 1-4 schematically shows the dimensions and layout of the test components (ENRESA 1998b, 2006a) as initially emplaced in 1996 (FEBEX I) and the revised layout after partial dismantling in 2002 (FEBEX II).

The EBS consisted of 136 vertical bentonite block slices, each 12.5 cm wide and numbered sequentially (Fig. 1-4). Slices 1 – 3 were at the rear of the tunnel (17.39 – 17.0 m along the test section), and blocks were adjusted to match the concave end of the tunnel. Slice 4 was therefore the first complete vertical slice and slices 4 – 136 followed the patterns shown in Fig. 1-4. Details of the slices can be found in ENRESA (1998b). In all, the EBS was made up of a total of 5'531 blocks. Each block weighed between 20 and 25 kg and five different block shapes (named BB-G-01 to 05) were used to form the different slices (see Figs. 1-4 to 1-6, Tab. 1-3). Thus, the constructed buffer extended for a length of 17.40 m (the original FEBEX test section extended from 53 to 70 m gallery length), requiring a total of 115.7 tonnes of bentonite. The blocks were compacted to a dry density of ~ 1.7 g/cm^3 so that the average dry density achieved after emplacement was 1.6 g/cm^3. A cross-section of the block dimensions is shown together with the block layouts in Fig. 1-5.

The manual construction of the barrier included the placing of the one-meter-long steel liner segments on a provisional support followed by the construction of the barrier around the steel liner, in complete vertical slices. A strict axis alignment of the liner was required avoiding difficulties in inserting the heaters later.

---

[3] Throughout the report, shotcrete and concrete are used interchangeably. The second plug was constructed by shotcreting. Of interest are the cement interactions that are independent of the aggregates the plug was composed of.

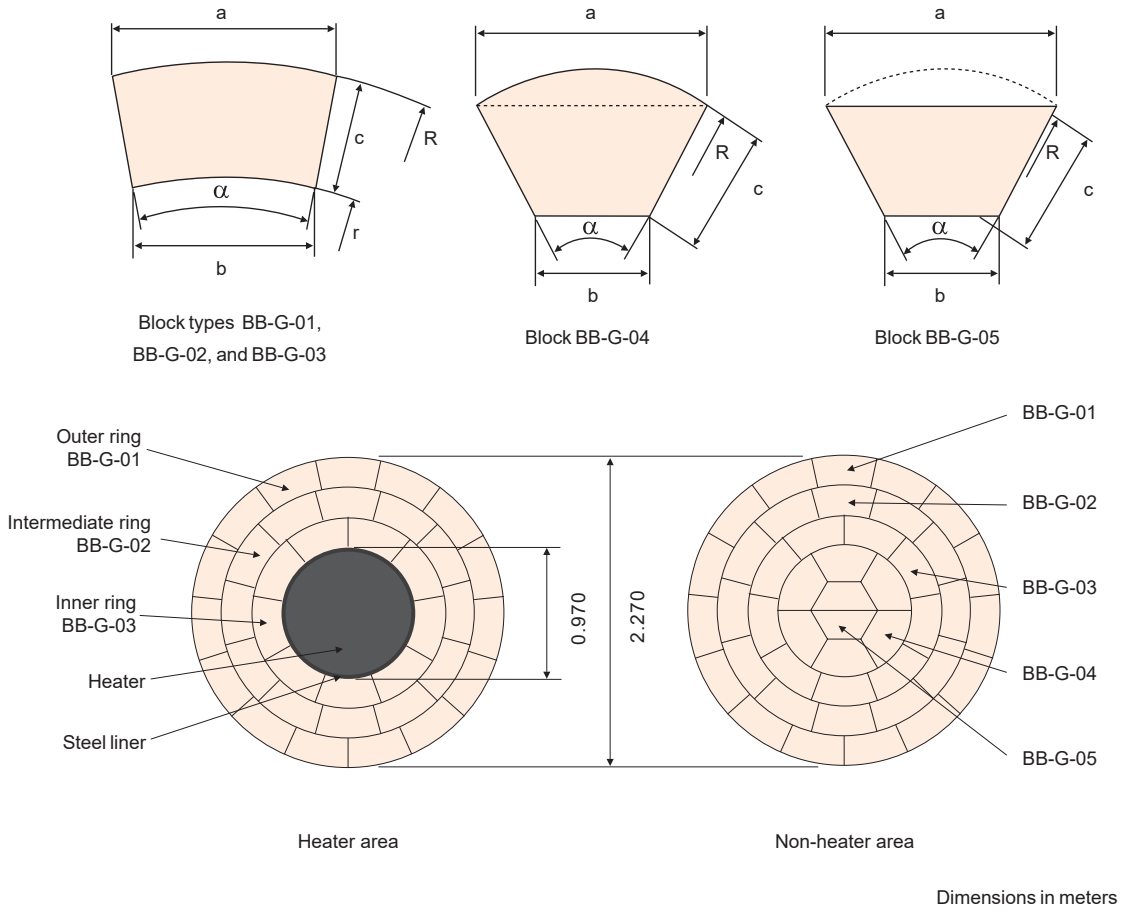


Fig. 1-5: FEBEX bentonite block dimensions (upper row) and vertical cross-sections of a heater and a heater-free section (lower row)

ENRESA (2006a)

Tab. 1-3: FEBEX block dimensions

For type and specification, see Fig. 1-5.

Type	**a** [mm]		**b** [mm]		**c** [mm]		**Thickness** [mm]		**R** [mm]	**r** [mm]	**α** [°]
BB-G-01	470.0	+2.0 –5.0	380.0	+2.0 –4.0	214.0	+2.0 –3.0	125.0	+2.0 –2.0	1'133	919	24
BB-G-02	473.0	+2.0 –5.0	361.0	+2.0 –4.0	214.0	+2.0 –3.0	125.0	+2.0 –2.0	917	703	30
BB-G-03	478.0	+2.0 –5.0	330.0	+2.0 –3.0	214.0	+2.0 –3.0	125.0	+2.0 –2.0	701	487	40
BB-G-04	483.0	+2.0 –5.0	240.0	+2.0 –3.0	240.0	+2.0 –3.0	125.0	+2.0 –2.0	485	–	60
BB-G-05	483.0	+2.0 –5.0	240.0	+2.0 –3.0	240.0	+2.0 –3.0	125.0	+2.0 –2.0	–	–	60



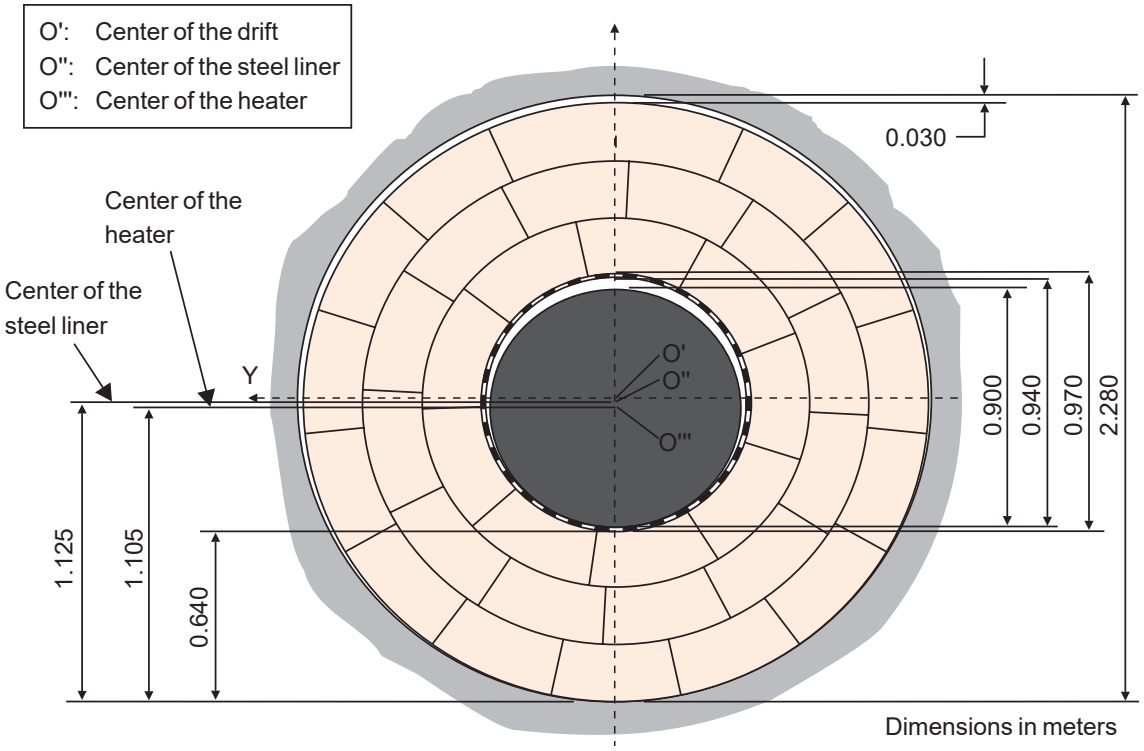


Fig. 1-6: Photo (Section 42/Bentonite layer 61) and cross-section through heater, liner and block assembly

ENRESA (2000a)

Note the gap between the top centre line of the buffer and the rock (tunnel wall) and in between blocks (photo) as well as in the perforated liner (photo).

For heating, two electrical heaters were used (heating elements – electrical resistances) of dimensions and weight equivalent to those of the canisters in the Spanish disposal concept (AGP Granito concept: 4.54 m in length, diameter of 0.90 m, Fig. 1-7) with a weight of approximately 11 tonnes. The exterior casing consisted of a forged tube with a wall thickness of 100 mm, and two welded metal plate end covers, each measuring 150 mm in thickness. The casing was carbon steel without any treatment or covering, except sandblasting of the exterior surface.

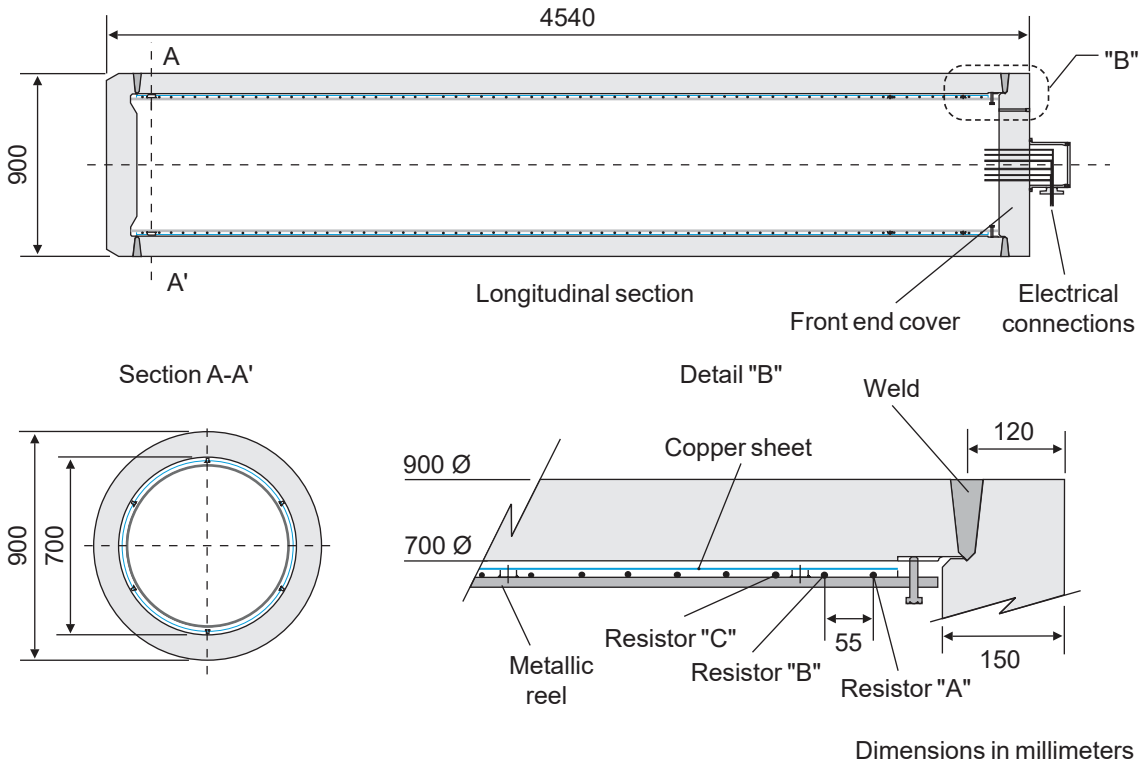


Fig. 1-7: Heater layout and dimensions
ENRESA (2000)

The heaters were placed in a central steel liner (Fig. 1-8) with a length of 11 m that extended over the EBS section containing the two heaters and the 1-metre gap between them (Fig. 1-4). The liner consists of 15-mm-thick perforated steel with an inner diameter of 940 mm, thus leaving 40 mm of margin with respect to the outer diameter of the heaters, a value that was considered sufficient for the correct insertion of the heaters, taking into account typical errors of alignment in an installation of this type. No consideration was given to a possible deformation due to swelling of the bentonite, or to bentonite swelling through the perforated liner. Since the original duration of the experiment was no more than five years, no bentonite swelling of the inner blocks into the perforated liner was expected.

In terms of thermal management, the aim was to subject the bentonite, at the point of contact with the steel liner, to a constant temperature of 100 °C. Nevertheless, in order to reach this temperature in a time period compatible with the test duration and maintain it in an isolated drift, it was necessary to increase the power of the heaters beyond the value anticipated in the AGP Granito concept for the maximum residual thermal power of the canisters, that is 1'200 W. After various analyses and modelling, the maximum rated power of the heaters was set at 4'300 W per heater.

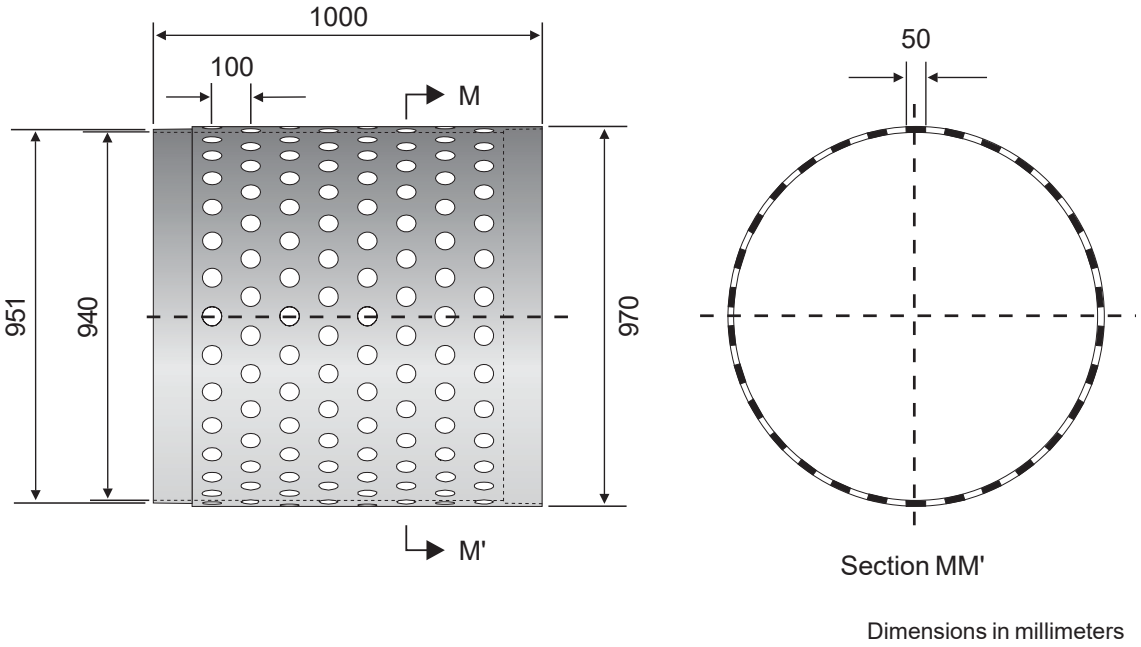


Fig. 1-8: Liner segment
ENRESA (2000a)

Sensors in the buffer were arranged in a series of vertical cross-sections (see Fig. 1-4 and Tab. 1-4). Sections with the same identifying letter (e.g. B1, B2) had identical sensor configurations. Geosphere sensors were located in boreholes BOUS 85.001, BOUS 85.002, FBX 95.001 and FBX 95.002, and in 19 boreholes drilled from the drift (see Fig. 1-3 and Martínez-Landa & Carrera 2006). Other sensors, such as psychrometers and TDR (time-domain reflectometry) probes were installed in shorter boreholes drilled from the drift (up to 2.5 m long).

A total of 636 instruments were located in several instrumented sections, both in the bentonite buffer and in the host rock, to monitor relevant parameters such as temperature, humidity, total and pore pressure, and displacements. The data acquisition and control system (DACS) was located in the service area of the FEBEX drift. This local system recorded and stored information from the sensors and controlled the power applied to the electrical heaters in order to maintain a constant temperature at the heater/bentonite interface. The DACS allowed to run the experiment in automated mode, with remote supervision from Madrid. Data stored in the local DACS were periodically downloaded in Madrid and used to construct the experimental master database (see Martínez et al. 2016).

To monitor the gas pressure generated, as well as to characterize the permeability of the barrier to this gas, six ceramic filter pipes were installed by GRS (Gesellschaft für Reaktorsicherheit) in the bentonite buffer around Heater #1. The pipes were made of sintered ceramic with Teflon couplings in a protective perforated metal cover.

Specimens of steel, titanium and copper coupons were emplaced in the bentonite close to the heaters to study corrosion. Chemical tracers were also placed in the bentonite and at the periphery (interface blocks – rock wall). Tracers included iodine, rhenium, selenium, boron, deuterium, europium, caesium, thorium, uranium and neodymium. Five glass ampoules containing deuterium were included in the outer ring of blocks close to the centre of Heater # 1 (instrumentation

Section M1, dismantling Section S29, Fig. 1-4), while other tracers were emplaced using the following methods: in sintered metallic capsules, mixed with bentonite in compacted bentonite plugs, and in impregnated filter paper (see details in ENRESA, 2006a).

Tab. 1-4: Sensors installed at the time of construction of the FEBEX in-situ test

Measurement	Type	Count
Temperature	Thermocouple	189
Total pressure	Vibrating wire	40
Water content	Capacitive, psychrometer, TDR	59, 76, 24
Hydraulic pressure	Borehole interval, packers, bentonite	62, 62, 52
Displacements	Vibrating wire, LVDT*, potentiometer	48
Heater	Resistor current and voltage	12
Gas pressure & flow	Gas & atmospheric measurements	12
Total at construction		636

* Linear variable differential transformer

The construction of the concrete plug was completed in October 1996 and the heating operation started on 27 February 1997 ("day 0"). There was therefore an approximate six-month "isothermal" saturation period from buffer emplacement to the start of heating. After the "isothermal" period, a constant temperature of 100 °C was maintained at the heater/bentonite interface for a period of five years. A complete installation report and the results gathered after two years of operation is given in ENRESA (1998b).

1.4.2 Dismantling of Heater #1 and subsequent test configuration (FEBEX II)

In 2002 (end of heating Heater #1: 28 February 2002, "day 1827"), the in-situ test was partially dismantled after five years of continuous heating (ENRESA 2006a). The dismantling consisted of removing the plug, Heater #1 and the surrounding buffer. The design and planning of the partial dismantling operation were driven by three basic objectives:

- to carry out an intensive sampling programme of the test components (bentonite, rock, metals and instruments) located in the area of the first heater
- to perform a canister retrieval exercise in such a way as to provide information on the technological problems that can potentially arise in a real operation of this kind
- to implement the necessary amendments and improvements, in order to continue the heating and hydration phase with the second heater over a long timescale.

The dismantling operation included the demolition of the concrete plug and removal of the section of the test containing the first heater, while leaving Heater #2 in operation and all remaining sensors in monitoring mode, and finally sealing the remainder of the test with a new shotcrete plug. A large number of samples from all types of materials were taken for analysis. A number of instruments were subsequently dismantled, and a small number of new instruments were installed (Fig. 1-4, see futher below).

The buffer and all components (sensors, cables, etc.) were removed up to two metres from Heater #2 to minimise disturbance of the remaining buffer. No signs of bentonite swelling through the perforated liner were visible. A dummy steel cylinder with a length of one metre was inserted in the liner void left by Heater #1 in the centre of the buffer. Some new sensors were installed, resulting in a total number of 501 sensors in the system monitoring the environment of Heater #2 (see Tab. 1-5).

The dismantled sensors and their cables were found to be in good contact with the bentonite and those close to the rock walls were pressed tightly against the rock. Some of them had been damaged due to the high pressure. No noticeable changes in sensor positions were found. One of the sensors in the bentonite were found to be severely corroded, especially at the front end of Heater #1 (ENRESA 2006a).

Tab. 1-5: Sensors dismantled and newly installed in the FEBEX in-situ test during partial dismantling in 2002

Parameter (or instrument)	**Code**	**Sensor type**	**Heater + Bentonite + Plug**			
			Initial	**Removed**	**Added**	**Total**
Temperature (bentonite)	T	Thermocouple	91	37		54
Temperature (heaters)	T	Thermocouple	36	28		18
Temperature (instrumented pipe)	T	Thermocouple			8	8
Total pressure on heaters	P	Vibrating wire	6	3	1	4
Total pressure (instrumented pipe)	P	Piezoresistive			8	8
Total pressure bentonite-plug contact	P	Vibrating wire			2	2
Total pressure inside plug	P	Piezoresistive			2	2
Pore pressure in bentonite	Q	Vibrating wire	52	24		28
Humidity (bentonite buffer)	WC	Capacitive	58	27	3	34
Humidity (instrumented pipe)	WC	Capacitive			18	18
Humidity	WP	Psychrometer	48	24		24
Humidity	WT	TDR	20	10		10
Heater displacement	SH	Vibrating wire	9	2		7
Bentonite block expansion	SB	Vibrating wire	8	4		4
Displacements in bentonite	SS	Potentiometer	6	6		0
Inclinometers	IT	LVDT	12	12		0
Plug displacements	S	LVDT	4			4
Crack meter	3S	LVDT	3			3
Gas pressure in clay buffer	GP	Piezoresistive	4	4		0
Gas flow	GF	Manual reading	6	6		0
Total			363	177	42	228

During dismantling, the zone around Heater #2 that experienced significant thermal changes extended up to Section I (Fig. 1-4) of the experiment, i.e., the front part of Heater #2. At Section I a temporary temperature drop at the heater surface was recorded from 90 °C to 80 °C after shutting off Heater #1. The temperature recovered after 7 years. At Section G (formerly the end of Heater #1), the temperatures in the inner part of the experiment dropped from around 100 °C to around 40 °C within one month (Martínez et al. 2016).

Mechanical deformation of the dismantled probes and cable defects could be observed during the excavation phase. TDR calibration measurements in air and water were performed after excavation and compared to the calibration measurements before installation. No change of the TDR signal in air could be detected, but in water an approximately 10% longer travel time was observed. Bentonite samples in the vicinity of TDRs were analysed for water content and density to calibrate the TDRs.

After removal of Heater #1, additional sensors were also added along three new plastic pipes inserted into the buffer and at the interface with the plug (see Fig. 1-9). New instrument sections were defined as O, P, Q, R, S, T and U. Section P corresponded to the new total pressure cells at the concrete/bentonite interface and S to temperature sensors (see Fig. 1-9).

Three sintered stainless-steel drainage pipes were installed around Heater #2. Each pipe contained four stainless-steel tubes for gas extraction/injection. In addition, six pipes were installed in April 2003 to collect porewater from the bentonite (see Fig. 1-9). These pipes contained sintered porous 316L stainless steel at depths corresponding to Sections G, I and F2. Humidity sensors and filters to collect porewater from the bentonite were placed within each section (G, I, F2), providing 18 sampling points.

The new concrete plug was constructed in two stages (Fig. 1-9): an initial temporary plug measuring one metre in length, which was built immediately after dismantling, and a second section to complete the plug length to the three metres planned in the design of the experiment. Unlike FEBEX I, the new plug was a parallel friction plug, without a recess excavated into the rock, and was constructed by shotcreting. The configuration of the test, after completing the partial dismantling operation and construction of the full plug length, is shown in Fig. 1-4 (ENRESA 2006a).

Evidence of significant corrosion and microbial activity after five years of heating obtained during partial dismantling is limited to one instrument section where conditions may have been aerobic and humidity influenced the instrumentation (ENRESA 2004b). No macroscopic mineralogical changes and near-constant global chemistry suggested restricted microbial activity (ENRESA 2006a). The degree of humidity and the presence of sulphate-reducing bacteria or chlorides and/or products may suggest that these conditions enhanced controlled (stress) corrosion processes as locally obeserved.

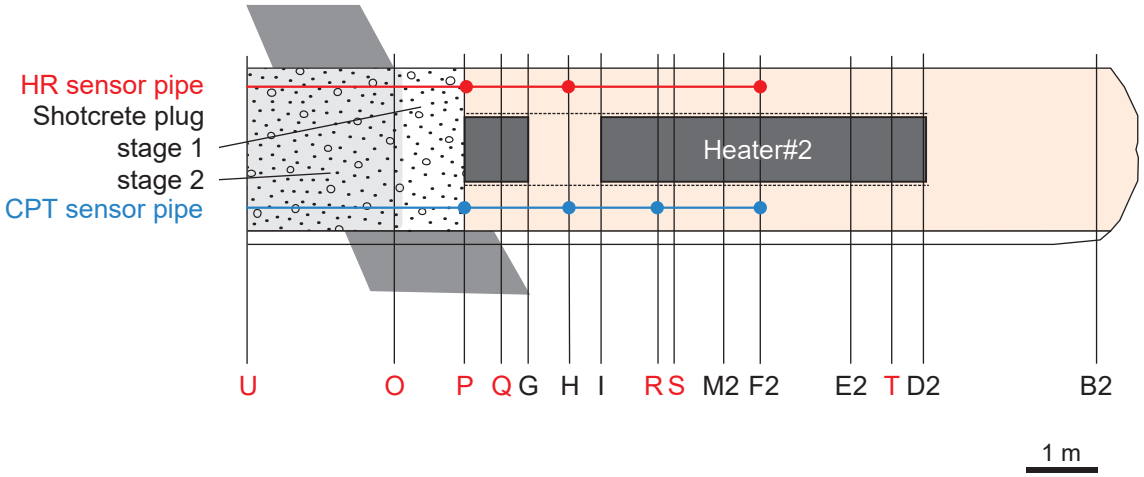


Fig. 1-9: FEBEX layout 2002 – 2015 showing additional instrumentation sections (in red) and HR (relative humidity) and CPT (cone penetration test) pipes to measure total pressure and equipped with a thermocouple

In experiment Phase 1 prior to the partial dismantling, it was observed that oxygen levels decreased rapidly after the closure of the experiment (see Chapter 3). Similar observations have subsequently been made in other full-scale experiments, such as the FE experiment at the Mont Terri Rock Laboratory (FMT) (Giroud et al. 2018). However, a measurable concentration of O_2 was still observed in the FEBEX in-situ test. While the low measured concentrations can indicate the presence of O_2 in the experiment, they can also be the consequence of a small air contamination of the samples upon sample collection or handling, and are therefore not considered conclusive. Furthermore, although the porewater is reducing (predominance of Fe^{+2} in the total iron), an increase of oxidised species was observed in the solid phase as compared to a reference sample of FEBEX bentonite. The combined study of the corrosion of metallic components and of the microbial activity in the bentonite showed a strong influence of anaerobic SRB (sulphate-reducing bacteria) in the parts of the experiment where substantial corrosion had been observed. However, in the same samples, aerobic microorganisms were also detected in similar or even greater counts.

In 2013/2014, a decision on the final dismantling of the FEBEX in-situ test was made based on the results of scoping models and the expectation that the further evolution of the buffer state would be very slow, and that no significant new information would be obtained. Under the same constant operating conditions, complete buffer saturation was unlikely to be achieved within an acceptable timeframe, whereas the likelihood of sensor failure would increase with time.

1.5 FEBEX-DP aims and objectives

After 13 additional years of heating, final dismantling of Heater #2 was scheduled for 2015. The objective of the second dismantling operation was to dismantle all the remaining parts of the in-situ test. This operation included a complete sampling of the bentonite, rock, relevant interfaces, sensors, metal components and tracers to allow the analysis of the barrier condition after 18 years of heating and natural hydration.

Analytical results were to be compared with data obtained from the partial dismantling (ENRESA 2006a), the monitoring data (Martínez et al. 2016) and the results derived from modelling activities (see summary in Lanyon & Gaus 2016). The results were expected to increase current knowledge and confidence in the bentonite performance with a focus on thermo-hydro-mechanical (THM) and thermo-hydro-chemical (THC) processes as well as on corrosion and microbial activity.

Based on this, the main objectives of the final dismantling were to:

- Analyse the physical, physico-chemical, mineralogical, chemical and textural changes that occurred in the clay due to heating and hydration and to determine the potential changes with respect to the reference bentonite (ENRESA 1998a). Additionally, the effect of joints between blocks and interactions at interfaces (concrete, granite, metal components, corrosion products) were to be taken into account. A major focus was on determining the on-site water content and dry densities.
- Analyse the chemical evolution of the bentonite porewater as a function of: a) the hydration and temperature profiles, b) the interaction with alkaline waters from the concrete plug; and c) the interaction with sensors, heater, organic compounds and corrosion products.
- Study the flow paths of the different types of chemical tracers that were placed in the clay and the clay/rock contact during the installation phase.
- Validate and check the capacity of the numerical codes (THM and THC) developed to predict the bentonite behaviour in an engineered barrier.

Secondary objectives were to:

- Recalibrate the sensors and update monitoring results and, if required, analyse sensor mechanical performance.
- Analyse corrosion products and microbially induced corrosion.
- Study the dependencies of microbial survival and the related effects of swelling pressure in clay barriers under redox conditions.
- Investigate the performance of the shotcrete at macro- and micro-level as well as potential chemical changes occurring along the interfaces (concrete/bentonite, concrete/granite and concrete/lamprophyre).
- Characterise the status of the heater and liner that were subjected to high temperatures, humidity and pressures and therefore potential corrosion, as well as changes in position and deformations.
- Investigate the granite host rock zone (as only negligible changes were identified from the partial dismantling), by considering the much longer period of the experiment of over 18 years.

1.6 FEBEX-DP – forecast of anticipated status

The anticipated status prior to dismantling was scoped in Kober & van Meir (2017) and is summarised below. Due to the specific configuration of the FEBEX in-situ test and its location, it was emphasised that several conditions might not reflect final or future repository designs. Such conditions include:

- The Grimsel host rock has only a very spatially limited EDZ.
- Shear zones and dykes are present in the emplacement gallery.
- The Grimsel groundwater is characterised by low electrical conductivity, neutral-to high pH (7 – 10), low carbonate alkalinity and content, and low dissolved oxygen.
- The bentonite used was FEBEX (Serrata clay) emplaced as highly compacted blocks.
- The temperature curve of the thermal management of the experiment chosen does not resemble the expected temperature behaviour of heat-generating waste after container emplacement.
- The composition of the initial cement plug and its overall design were not ideal for the prevention of water and gas leakage and for establishing stable redox conditions and inhibit microbial activity in a controlled way. The configuration of the second plug was optimised and less permeable (in terms of redox conditions and microbial activity).
- The experiment was not initially designed and constructed for specific corrosion and microbial investigations (see below).
- The partial dismantling in 2002 caused a perturbation of THM/THC effects for the remaining part of the experiment.

The gas analyses performed during experiment Phase 2 (2002 – 2014) revealed low O_2 concentrations. However, the variability of the data during Phase 2 is even greater than that observed in Phase 1 (Giroud 2014). This is likely attributable to air contamination before, during, or after sampling. The plug was designed with special care to make the plug water- and gas-tight during Phase 2. However, the low concentrations of oxygen in the gas phase, together with the presence of anaerobic bacteria in some parts of the bentonite and a predominance of Fe^{+2} in the total iron of the porewater suggests that the FEBEX experiment tends towards an anoxic, reducing environment. Heterogeneities in the redox state are likely due to the possible inflow of O_2 through the plug, along the sensor cables and pipes, or possibly the EDZ. The difficulty in assessing the redox conditions in general was due to the very high sensitivity of the redox potential to contamination by the atmosphere. Before dismantling started, gas and water samples were collected from the existing sampling tubes (see Section 1.4).

1.7 FEBEX-DP project organisation and management

The FEBEX-DP project organisation and management were structured as shown in Fig. 1-10 and followed the main objectives of the project. The organisation between the FEBEXe partners and the new FEBEX-DP partners was regulated in an experiment agreement.

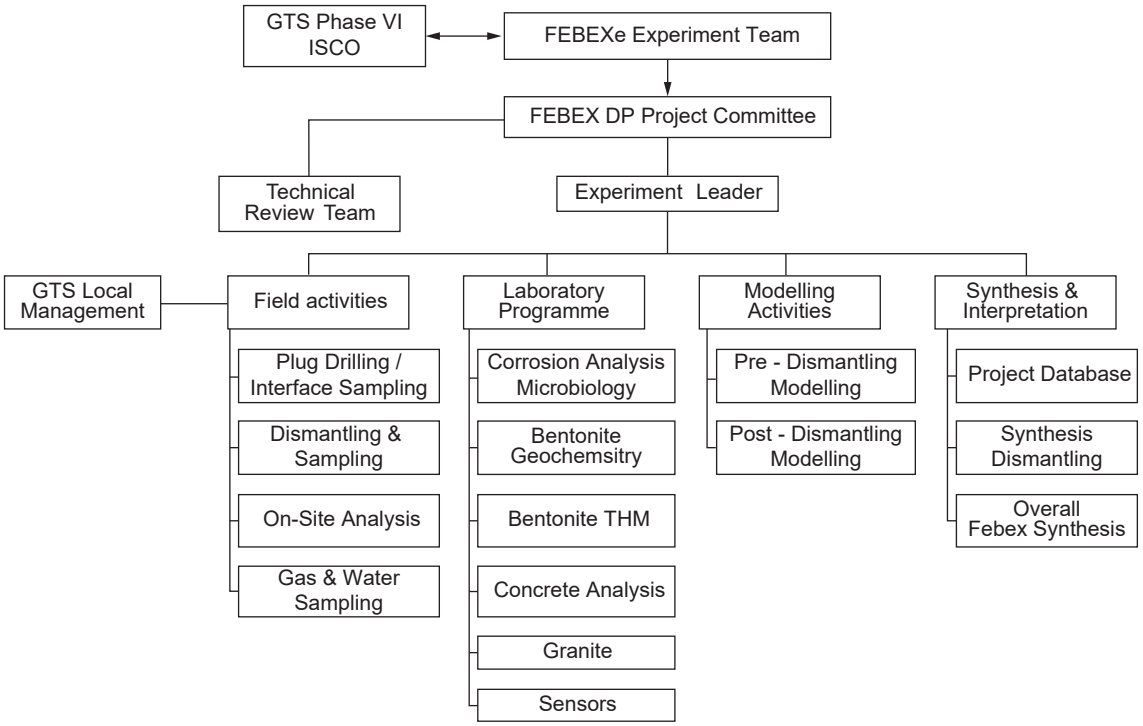


Fig. 1-10: FEBEX-DP project organizsation and management

1.8 Milestones of the FEBEX experiment

The major milestones for the FEBEX experiment are summarised in Tab. 1-6.

Tab. 1-6: Dates of major activities throughout the FEBEX experiment with a continuous count of days

Date	Day No.	Activity
25.10.1995		Start of tunnel–boring–machine excavation of the FEBEX gallery at GTS
01.07.1996		Start of FEBEX engineered barrier system (EBS) construction
15.10.1996		End of EBS construction
27.02.1997	0	Start of heating[4]
28.02.2002	1'827	Switch–off of Heater #1
02.04.2002	1'860	Start of partial dismantling
23.07.2002	1'971	Start of new shotcrete plug construction (1st stage)
26.07.2002	1'975	End of partial dismantling
17.02.2015	6'564	Start of final dismantling (plug overcoring and sampling)
08.04.2015	6'614	Start of plug demolition
24.04.2015	6'630	Switch–off of Heater #2
08.05.2015	6'644	Start of buffer sampling
04.06.2015	6'671	Heater #2 retrieval
05.08.2015	6'733	Completion of buffer dismantling

[4] The system was allowed to equilibrate after installation of the plug and prior to the start of heating.

1.9 Structure/organisation of report

This report summarises the activities performed throughout the final FEBEX Dismantling Project. Details of individual activities and analyses can be found in the dedicated reports listed in Tab. 1-7. Aside from these, the on-site dismantling activities have been documented in daily reports, extra reports and auxiliary reports that are compiled in NAB 16-68. The remaining chapters of this report are structured as:

- Chapter 2: Monitoring: evaluation of the bentonite buffer and rock 1997 – 2015
- Chapter 3: Pre-dismantling investigations
- Chapter 4: Dismantling of Heater #2 and buffer and sampling in 2015
- Chapter 5: Analysis and laboratory tests
- Chapter 6: Sensor evaluation
- Chapter 7: Pre-dismantling modelling activities and synthesis of modelling activities
- Chapter 8: Geosphere THM response
- Chapter 9: Groundwater chemistry characterisation over 18 years of FEBEX
- Chapter 10: Comparison of the buffer characteristics from the dismantling in 2002 versus 2015
- Chapter 11: Assessment of the FEBEX experiment
- Chapter 12: Conclusions & lessons learned

Tab. 1-7: Dedicated FEBEX-DP reports

NAB	Title	Author(s)
14-55	FEBEX - Assessment of Redox Conditions in Phase 2 before Dismantling	Giroud
15-14	FEBEX-DP - Full Dismantling Sampling Plan (In-situ Experiment)	Bárcena & García-Siñeriz
15-15	FEBEX-DP - Full Dismantling Test Plan (In-situ Experiment)	Bárcena & García-Siñeriz
16-09	Results of laboratory investigations in preparation of the dismantling of the FEBEX-e/FEBEX-DP in-situ test and on-site experiments during the dismantling	García-Siñeriz et al.
16-10	FEBEX-DP Plug Overcoring and Concrete-Bentonite Interface Sampling prior to Dismantling	Mäder et al.
16-11	FEBEX DP: Dismantling of Heater #2 at the FEBEX "in-situ" test Description of operations	García-Siñeriz et al.
16-12	FEBEX-DP on-site analyses report	Villar et al.
16-13	Gas and water sampling from the FEBEX in-situ test	Fernández et al.
16-14	Hydrogeochemical characterisation of the groundwater in the FEBEX gallery	Garralon et al.
16-15	FEBEX-DP: Microbiological Report	Bengtsson et al.
16-16	FEBEX-DP Metal Corrosion and Iron-Bentonite Interaction Studies	Wersin et al.
16-17	FEBEX-DP Postmortem THM/THC Analysis Report	Villar et al.
16-18	FEBEX-DP Concrete ageing, concrete/bentonite and concrete/rock interaction analysis	Turrero et al.
16-19	FEBEXe/FEBEX-DP Final Sensor Data Report	Martínez et al.
16-20	FEBEX-DP Post-mortem analysis: Sensors	Rey et al.
16-21	FEBEX-DP Bentonite TDR probe inspection and data verification report	Sakaki et al.
16-22	Pre-dismantling THM modelling of the FEBEX in-situ experiment	Papafotiou et al.
16-23	FEBEX-DP: Pre-dismantling THC Modelling	Birgersson et al.
16-24	Thermo-Hydro-Mechanical Postmortem Analysis of bentonite performed at CIEMAT	Villar et al.
16-25	Thermo-hydro-chemical (THC) behaviour of a Spanish bentonite after dismantling Heater #1 and Heater #2 of the FEBEX in-situ test at the Grimsel Test Site	Fernández et al.
16-54	Corrosion Study of FEBEX-DP Components	Madina
16-68	FEBEX-DP - Dismantling related supplementary documents	Kober & Van Meir

NTB	Title	Author(s)
15-04	Main outcomes and review of the FEBEX In-situ Test (GTS) and Mock-up after 15 years of operation	Lanyon & Gaus
17-01	FEBEX-DP Dismantling Synthesis Report	Kober et al. (this report)

2 Monitoring: evolution of the bentonite buffer and rock 1997 – 2015

The FEBEX experiment was monitored continuously over 18 years. This chapter summarises the monitoring data obtained for the entire operational phase from the start of heating (day 0) for Heater #1 and Heater #2 with a focus on Heater #2. Further detailed information on monitoring Heater #1 can be found in ENRESA (2006a).

Aside from the evolution of the bentonite buffer and the near-field/rock, the evolution of the engineered barrier system (EBS) depends heavily on the proximity to the heat source, thus the heaters (Fig. 1-4) define the so-called "cold" or "hot" sections. More specifically, the parameter values considered for the buffer discussed in this chapter will very much depend on the position of the three rings of bentonite blocks that form the buffer (Fig. 1-6), i.e., the outer (close to the rock), middle and inner (centre or closer to the heaters) bentonite block ring.

The evolution of the in-situ test has been described in various data reports (ENRESA 2000, 2006a, Bárcena et al. 2007, AITEMIN 2012, Lanyon & Gaus 2016). The report covering the entire lifetime, with a focus on the last days including the final dismantling, is the one from Martínez et al. (2016).

2.1 Bentonite barrier evolution

The main parameters that illustrate the evolution and status of the bentonite barrier are temperature, total pressure, pore pressure and water content/suction. The power applied to the heaters is directly linked to the temperature field in the bentonite barrier and the near-field (rock), therefore information about its evolution is required to understand the THM evolution of the EBS.

2.2 Applied power

Power to each heater was applied in two steps, namely, 1'200 W for the first three weeks (to calibrate the control system) and then 2'000 W for 30 more days according to the scoping calculations. Afterwards, the heating system was left to regulate the power to reach and then maintain 100 °C maximum at the liner-barrier contact. Thus, the power increased to reach values of up to 2'200 W for Heater #1 and 2'700 W for Heater #2, then decreased slowly and stabilised after the first year to about 1'940 W for Heater #1 and 2'170 W for Heater #2 (Fig. 2-1).

After one year, the power required for Heater #1 started to increase slowly until its decommissioning when it reached 2'160 W (Fig. 2-1, black line). Approximately two years after the start of the experiment, the power applied for Heater #2 also started to increase slightly and maintained this trend until the decommissioning of Heater #1, reaching a value of around 2'300 W (Fig. 2-1, red line).

A noticeable increase of about 5% (about 100 W) was clearly seen for Heater #2 during approximately two months after the disconnection of Heater #1. Afterwards, the applied power continued with a slightly increasing trend of around 40 W per year to maintain 100 °C at the bentonite contact. The power applied to Heater #2 reached 2'796 W just before it was switched off for decommissioning. The total increase in power seen from day 56 (24.04.1997) up until switch-off was around 18.5%. This is due to the change in geometry after removal of Heater #1 and the increasing thermal conductivity of the buffer as it saturated.

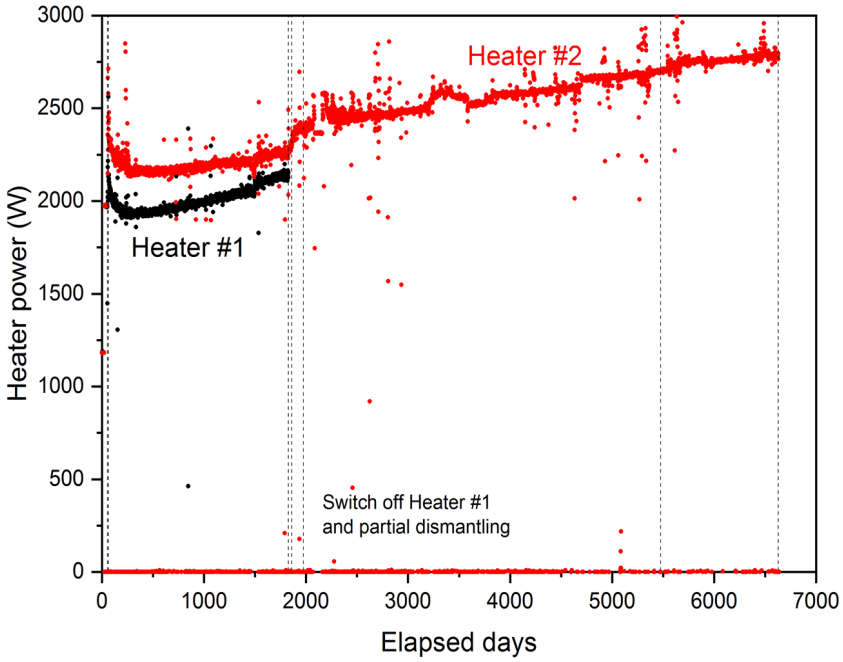


Fig. 2-1: Power output from Heaters #1 and #2 during the entire operational phase
Vertical dotted lines before day 2000 show the steps of the partial dismantling.

2.3 Temperature evolution 1997 – 2015

Temperatures in the barrier system increased very quickly once the heaters were switched on. The fastest response was in the region close to the heaters (Fig. 2-2). Maximum temperatures, up to 100 °C at the hottest point of the liner around the heaters, were reached around 61 days after the heating phase started (Fig. 2-1). After about four months of operation, temperatures in some areas of the liner surface began to decrease, while maintaining 100 °C at the hottest point (centre and bottom part). This is likely a consequence of the bentonite wetting that improves thermal conductivity (possibly gap closure due to thermal expansion). This trend did not change until three years later. Temperature differences of up to 20 °C were measured along the surface of the liner in contact with the heater.

The temperature distribution in the buffer was approximately radially symmetric with axial variations depending on the position relative to the heaters. Values were typically higher below the heater, which was probably due to the position of the heater within the steel liner. Temperatures in the middle part of the buffer reached 50 – 60 °C and either stabilised or increased slowly over the entire duration of the experiment.

At the outer part of the buffer or at the rock contact, the temperatures increased more gradually: the maximum temperature at the rock surface reached 35 °C after three months of heating and 40 °C after seven months. At the same time, the temperature was 16 °C at the inner face of the plug and 18 °C at the rear end of the test (see Fig. 1-4 top).

From then onwards, the temperature evolution shows a slight gradual temperature increase until the transient period caused by switching off Heater #1 and its subsequent dismantling. The magnitude of temperature is decreasing with distance from the heaters and with a central plane of symmetry between Heaters #1 & #2 (Fig. 2-2).

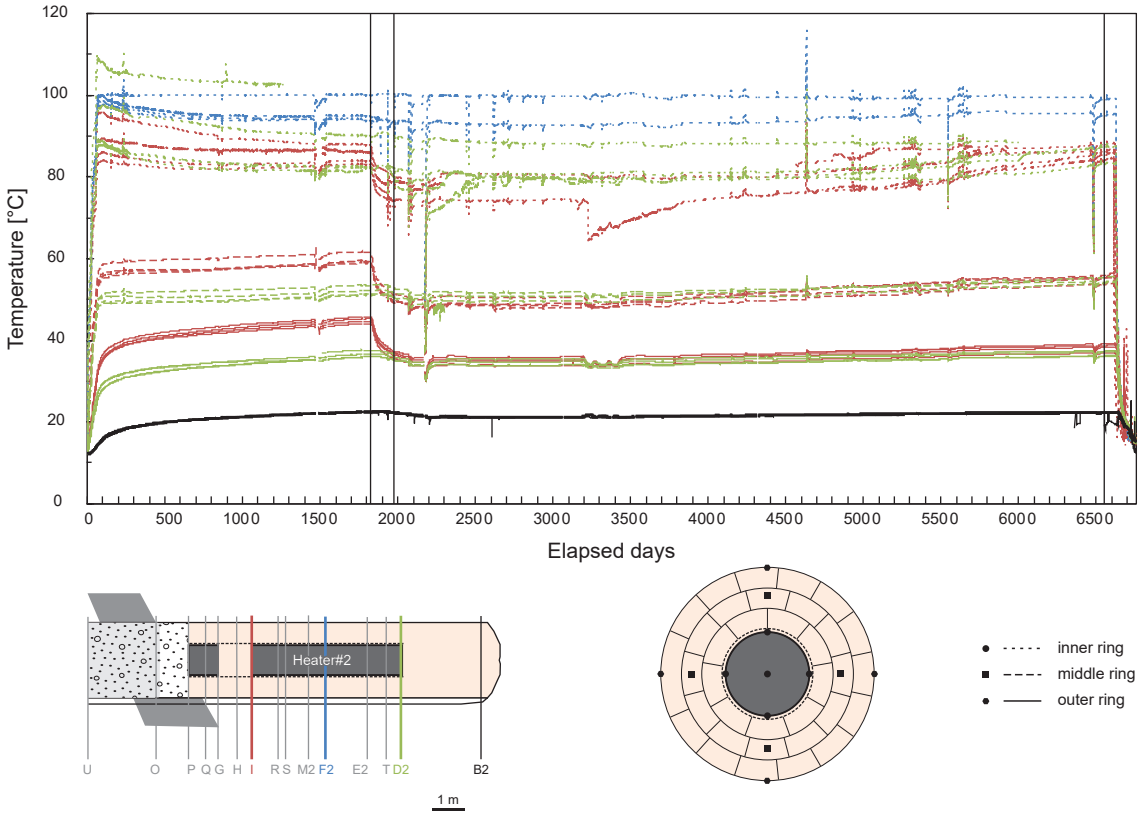


Fig. 2-2: Temperature evolution at different locations in the buffer

Vertical lines mark major events related to dismantling of the experiment. For inner, midlle and outer ring see Fig. 1-5).

Around Heater #1, an overall drop in temperature to around 25 °C occurred after the heater was switched off. The temperature then remained more or less stable or even increased slightly around Heater #2 except for Section I, located closest to Heater #1, where a drop of 8 – 10 °C was recorded for the sensors at the liner surface (Fig. 2-2). The temperatures at those points tend to equal those of their equivalent points at the other end of Heater #2 in Section D2. At the most distant points from Heater #1, the switch-off had no effect. Hence, the system tended to behave as a single-heater system with the same trends as before and with a central plane of symmetry on Heater #2.

A further observation was that the temperatures at the bottom of the buffer continued to be higher than at the sides and the upper part for each section.

2.4 Total pressure (stress)

Measured total pressure increased with ongoing saturation starting from about month 3. After one year, the values at the rock contact were in the range of 1 – 2.2 MPa and up to 0.2 MPa at the liner (Fig. 2-3). Values were always higher at the right-hand side and the bottom; this phenomenon could be linked to water inflow from the SI2 borehole during test construction (ENRESA 1998b, see Fig. 1-3). Before Heater #1 was switched off, the highest values were at the rock/buffer contact and reached over 5 MPa. Loads on the liner were below ~ 2 MPa.

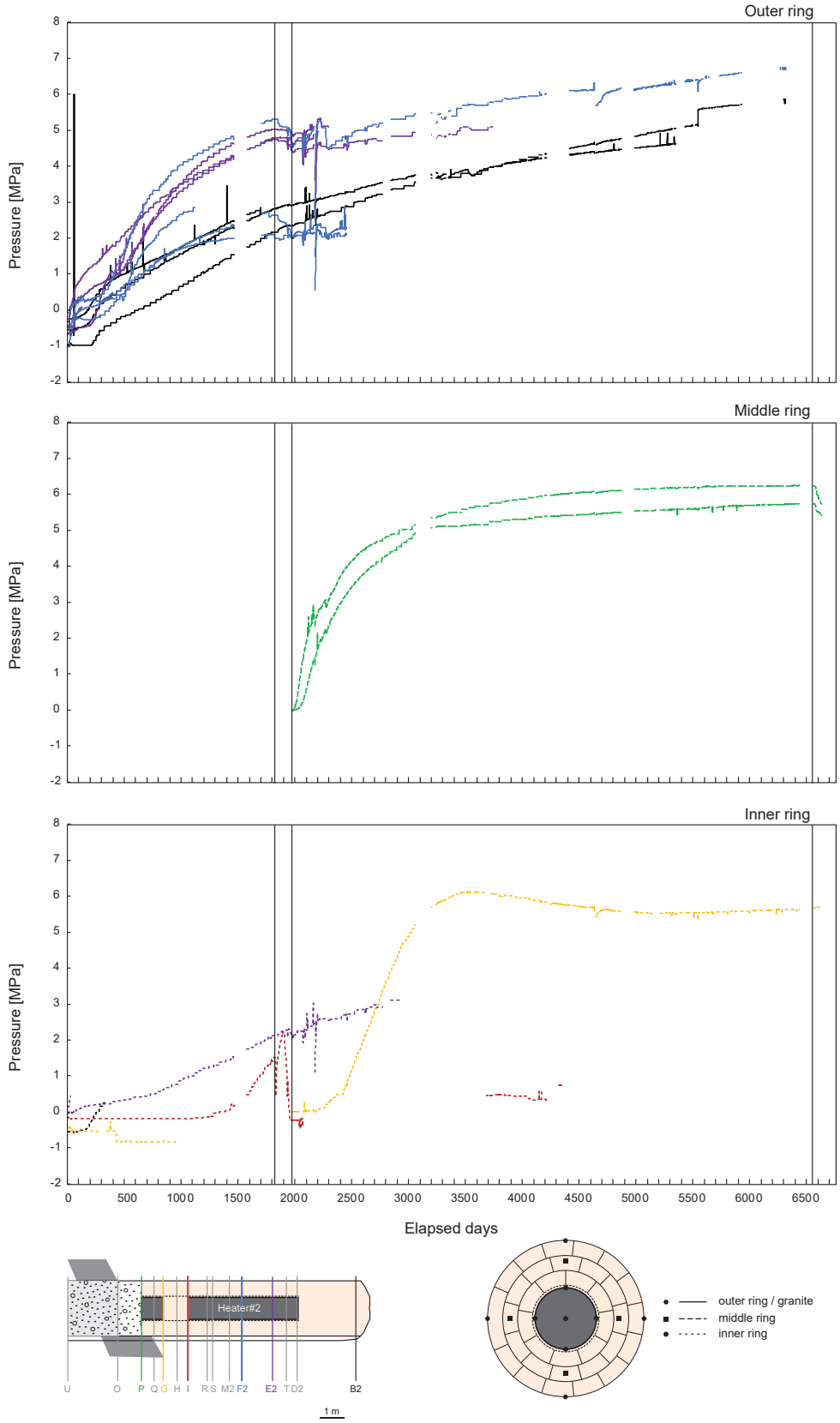


Fig. 2-3: Total pressure evolution at different locations in the buffer

Vertical lines mark major events related to the dismantling of the experiment.

Total pressure declined during partial dismantling (from day 1'827 onwards) only in sections close to the dismantled part but recovered over the next 1'000 days with a generally increasing trend. This behaviour was clearly seen in the new sensors installed during the partial dismantling as those of Section P (green and yellow lines in Fig. 2-3).

After the partial dismantling, total pressure cells located at the rock surface in Sections E1 and F1 were totally covered by the new plug. The still operating sensors registered very slightly increasing pressures related to the transmission of the loads from ongoing bentonite swelling through the concrete mass towards the rock walls.

Over the entire operational period, an increasing trend of the total pressure was observed at all points of the buffer and at the bentonite/rock contact. After 15 years, the total pressure reached a maximum value of 6.4 MPa on the rock wall at Section F2 (blue line in Fig. 2-3 and Tab. 2-1), which corresponds to the expected swelling pressures. The final values before the decommissioning of Heater #2 are listed in Tab. 2-1.

The expected swelling pressure under confined conditions was estimated to be between 4 and 6 MPa for a dry density of 1.6 g/cm^3 (ENRESA 1998b, 2006a). However, the swelling pressure varies exponentially with dry density, and the regression was estimated to have an uncertainty of up to ± 25%. The measured total pressures are therefore consistent with the expected swelling pressure at high saturation.

Tab. 2-1: Total pressures (MPa) in the buffer on 24 April 2015, day 6'630

Sensor locations are the same as in Fig. 2-3, line colour in brackets.

	Section E1 [not shown]	**Section P** [green]	**Section G** [yellow]	**Section I** [red]	**Section F2** [blue]	**Section E2** [purple]	**Section B2** [black]
Radial direction	Rock surface 0.78	–	–	–	Rock surface > 6.4	Rock surface > 5	–
Tangential direction	–	–	–	Middle ring 2.20	Middle ring 2.14	–	–
Axial direction	–	Middle ring 5.41 – 5.74	Centre of section 5.67	–	–	–	Middle ring 5.97

2.5 Pore pressure

There was no clear evidence of a consistent ongoing rise in pore pressure with time in any buffer section. The most consistent trend was recorded in Section H (light purple line in Fig. 2-4). Pore pressures typically stayed low relative to the geosphere pressure (~ 1 MPa away from the open drift); pressures reached up to 390 kPa where saturation was high as, for instance, at the right-hand side of Section E2 (dark purple line in Fig. 2-4). This behaviour could be related to the fact that the barrier was not yet fully saturated after the operational phase.

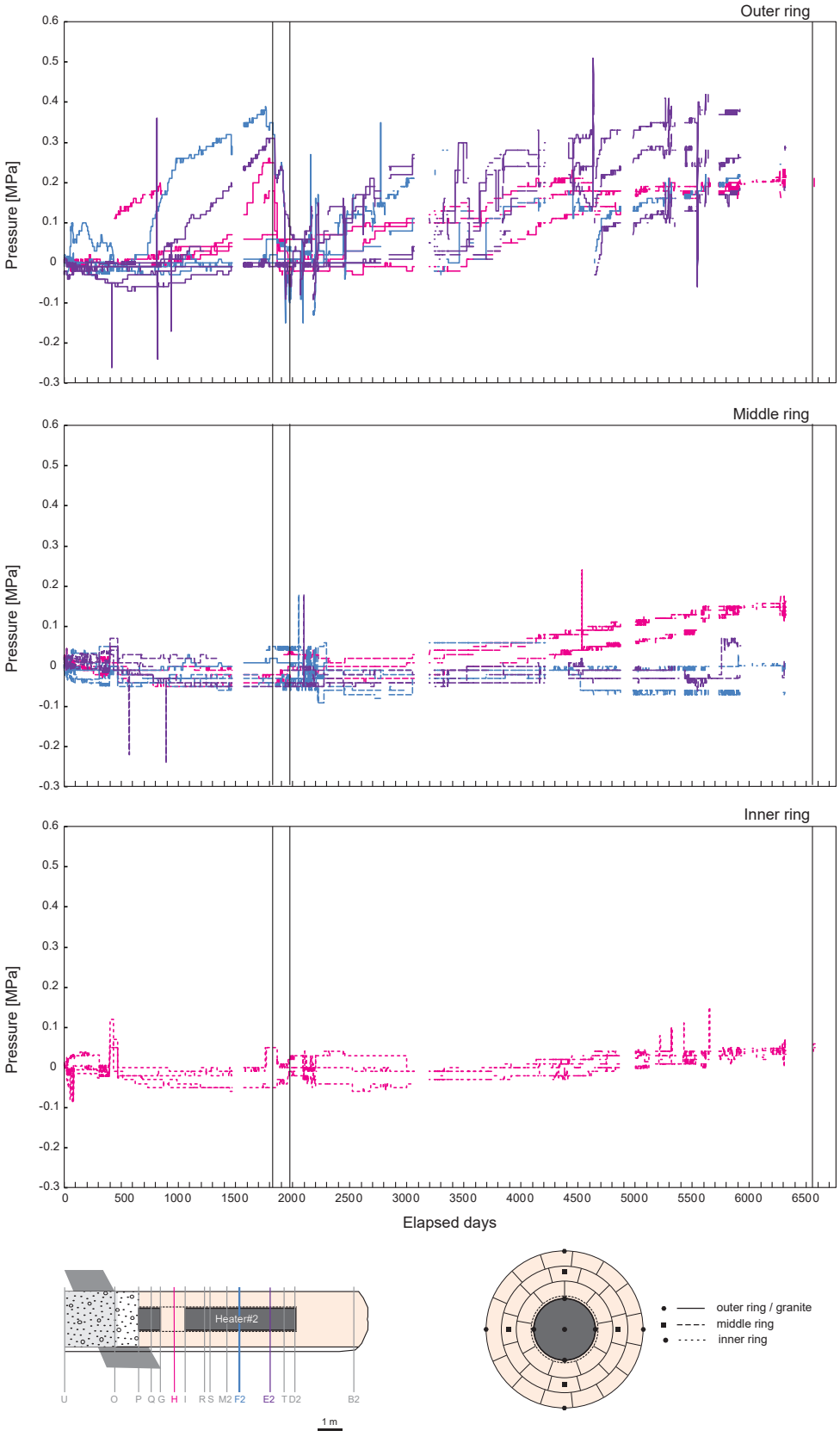


Fig. 2-4: Pore pressure rise (relative) at different locations in the buffer during the full operational phase

Vertical lines mark major events related to the dismantling of the experiment.

When Heater #1 was switched off, the positive pore pressure values around it plunged to zero. Around Heater #2, the positive values in the most humid parts showed a small decrease during the cooling period, and a gradual decrease during the dismantling of the bentonite before reaching Heater #1, but pressure values plunged to zero between two and three days close to day 1931 (12 June 2002), as can be seen in Section E2 (dark purple in Fig. 2-4). This could be due to the thermal dilatation/contraction of the porewater in the bentonite. Afterwards, pore pressure values recovered slowly to reach the values given in Tab. 2-2.

Tab. 2-2: Pore pressure (relative) values on 1 May 2014, day 6272 (MPa)

	Section H [0.5 m from the heater]	**Section F2** [middle of heater]	**Section E2** [1 m from middle of heater]
Outer ring	0.16 – 0.23	0.24	0.18 – 0.39
Middle ring	0.08 – 0.16	-0.06 – 0.00	-0.03 – 0.05
Inner ring	0.03 – 0.05	–	–

2.6 Water content/suction

The outer ring of the buffer quickly reached high relative humidity levels. During the first year, drying was recorded in the inner ring close to the heaters (hot parts), followed by a steady slow increase (Fig. 2-5). The middle ring showed a range of initial fluctuations (rise/fall) but subsequently (after the first year) values typically rose slowly. The effect was largely controlled by distance to the heaters, and it was visible in the central part of the slice between the two heaters (light purple line in Fig. 2-5, Section H).

Results from the partial dismantling after five years of operation confirmed that the water content distribution was axially symmetric with similar average values in the sections studied. In the hot sections around the heater, a higher water content gradient and no influence from geological structures were observed; water content showed strong radial symmetry regardless of the presence of fractures in the rock (see Section 5.2).

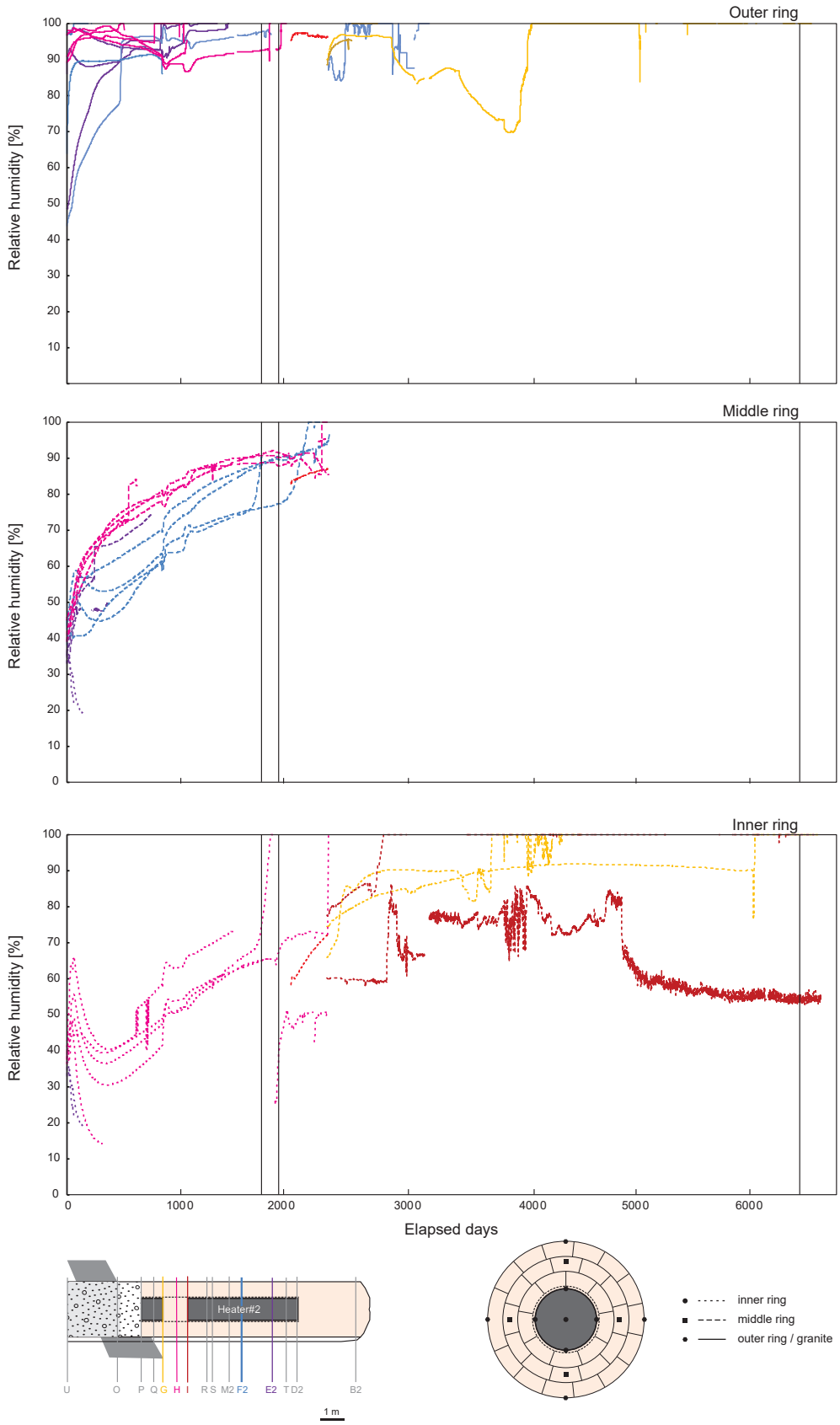


Fig. 2-5: Evolution of relative humidity at different locations in the buffer

Vertical lines mark major events related to the dismantling of the experiment in the buffer.

After a transient period associated with the partial dismantling in 2002, relative humidity in the buffer resumed a slow increase in all but the outer buffer ring, which was already highly saturated. After 7.5 years of operation, relative humidity in the middle ring was also high (almost 100%, and were out of order, Martinez et al. 2019). In the inner ring, RH was around 90% in colder sections, 60 – 90% close to the heater and 40 – 60% around the heater (Fig. 2-5). Note that the majority of the initially installed sensors stopped working during the first five years. Hence, only the newly installed sensors for suction and the TDRs were able to provide information since then. By the end of the operational phase, relative humidity showed high saturation in the outer and middle rings. In the inner ring around the dummy canister, only the sensor in the inner ring close to Heater #2 showed a lower relative humidity (Tab. 2-3).

Tab. 2-3: Capacitive sensors on 24 April 2015 (% relative humidity)

	Section G [1 m from the heater]	**Section I** [heater front]	**Section F2** [middle of heater]
Outer ring	100	100	100
Middle ring	100	100	–
Inner ring	100	54	–

In general, there was good consistency between the different sensor types (suction and gravimetric water content) as provided by TDR measurements in section M2 (Fig. 2-6).

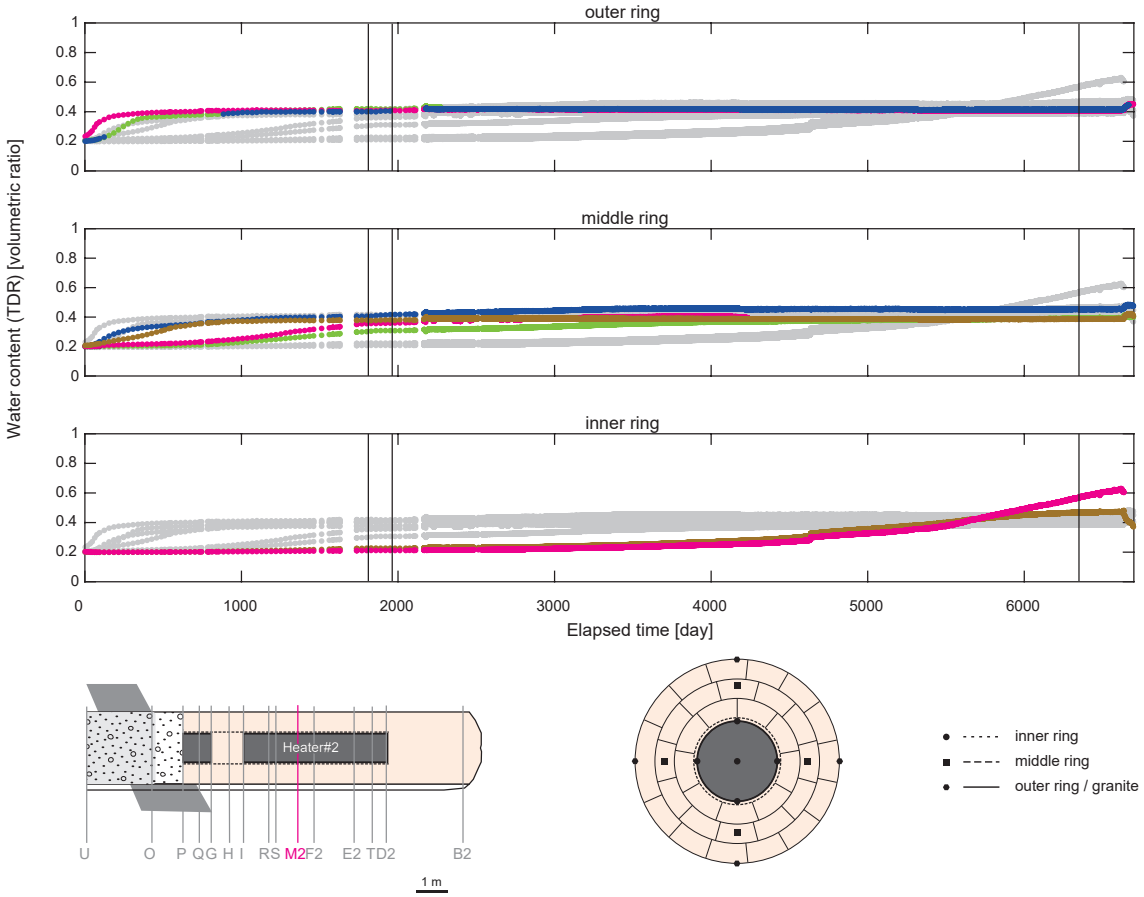


Fig. 2-6: Evolution of volumetric water content in section M2 until final dismantling

Vertical lines mark major events related to the dismantling of the experiment.

2.7 Effects of heater shutdown and dismantling

Temperatures dropped after heater switch-off, most quickly close to the heater. The temperature drop resulted in a gradual decrease in the already low pore pressures. During the subsequent dismantling, the pore pressures sensors dropped to zero when approaching the sensor location, which was consistent with the total pressure cell readings (indicating buffer decompression). The change in the thermal field caused a redistribution of the water content in the clay buffer, with condensation of water vapour close to the heater (see Section 5.2.2). This was reflected in a decrease in relative humidity values in the middle bentonite ring and a fast increase in relative humidity in the inner bentonite ring (see Section 5.2).

2.8 Measurements at the service area

Relative humidity recorded in the service area showed typical winter-summer cycles, with the winter season being generally drier (Fig. 2-7), while the displacement sensors located at the shotcrete plug surface showed little compression with time that could be related to its expected deformation, i.e. a very slight expansion (Fig. 2-8).

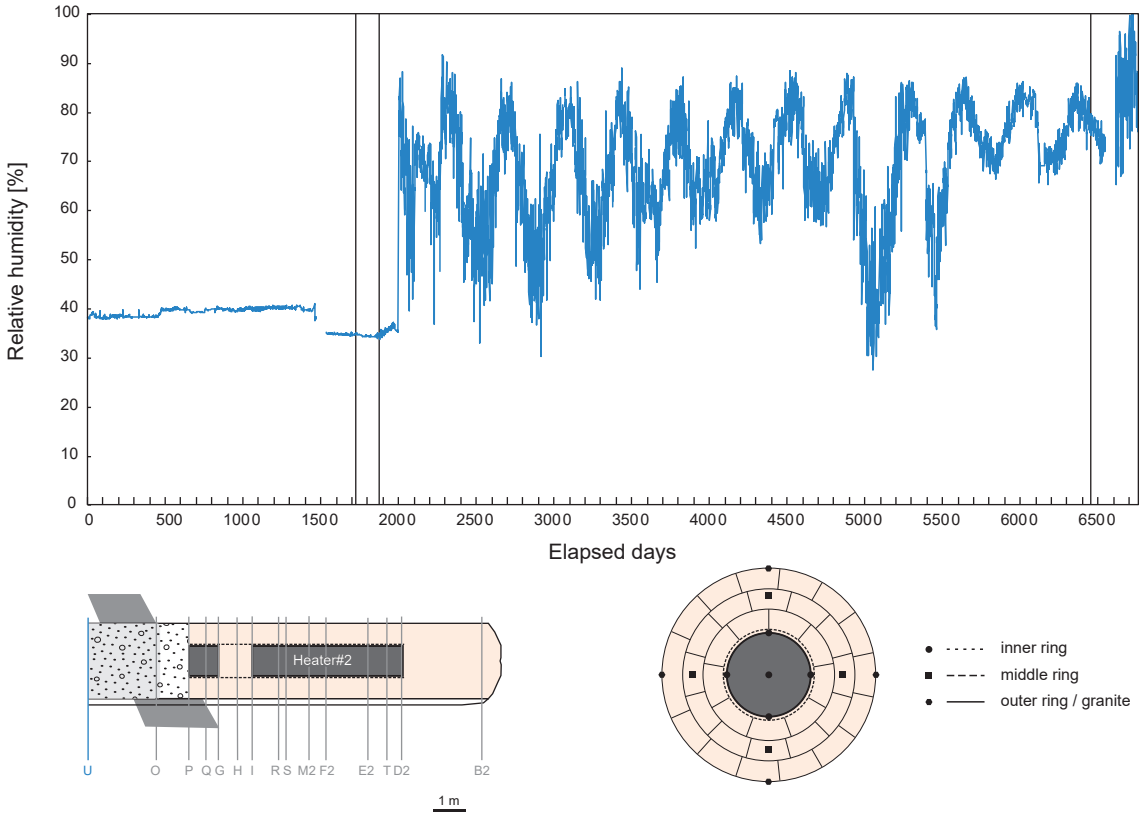


Fig. 2-7: Recorded relative humidity in the air of the service area, beyond section U outside the confined test section

Change in variability after the dismantling is related to a ventilation change of the gallery.

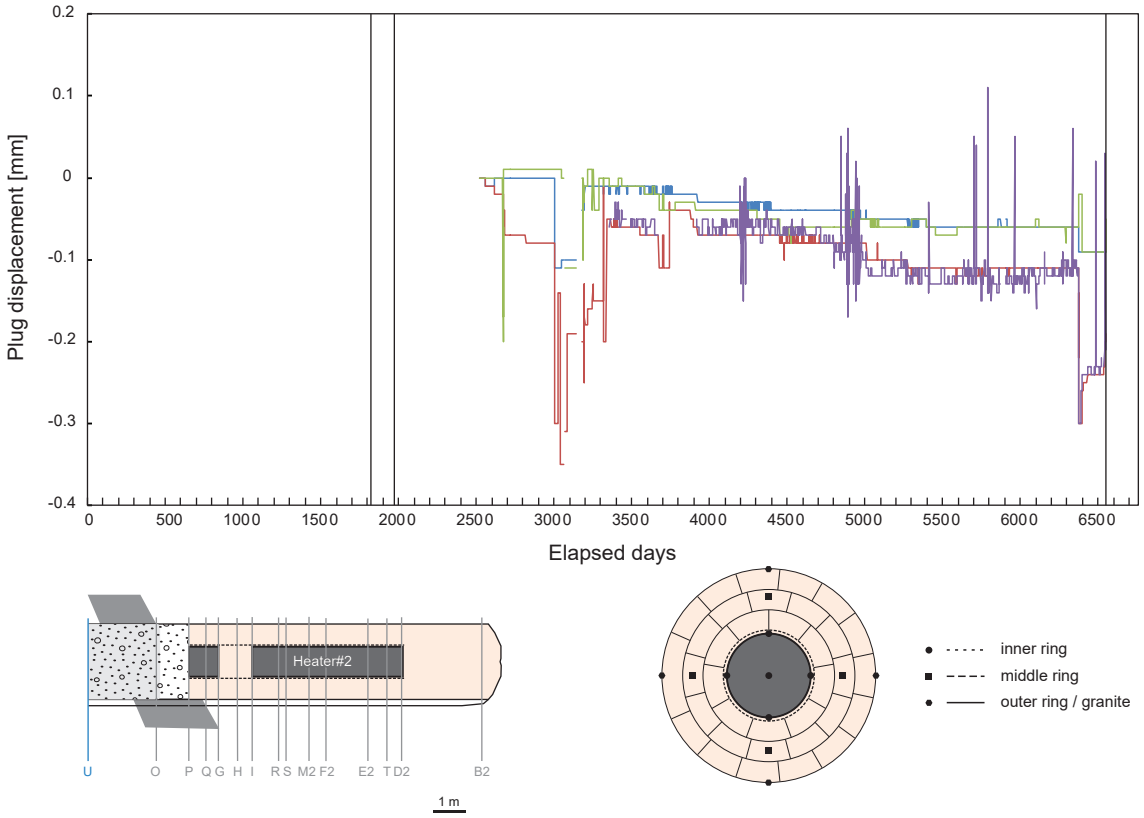


Fig. 2-8: Displacements measurements obtained at the shotcrete plug in section U, colours refer to different sensors

2.9 Near-field/rock evolution

The evolution of the near-field/rock was as expected: temperatures increased during the early operational phase following a radial thermal gradient pathway from the drift. Temperatures dropped after switching off Heater #1 and established a new near-steady-state with a slight upward trend related to the increase in power for Heater #2. Finally, temperatures dropped again after switching off Heater #2 (Fig. 2-9).

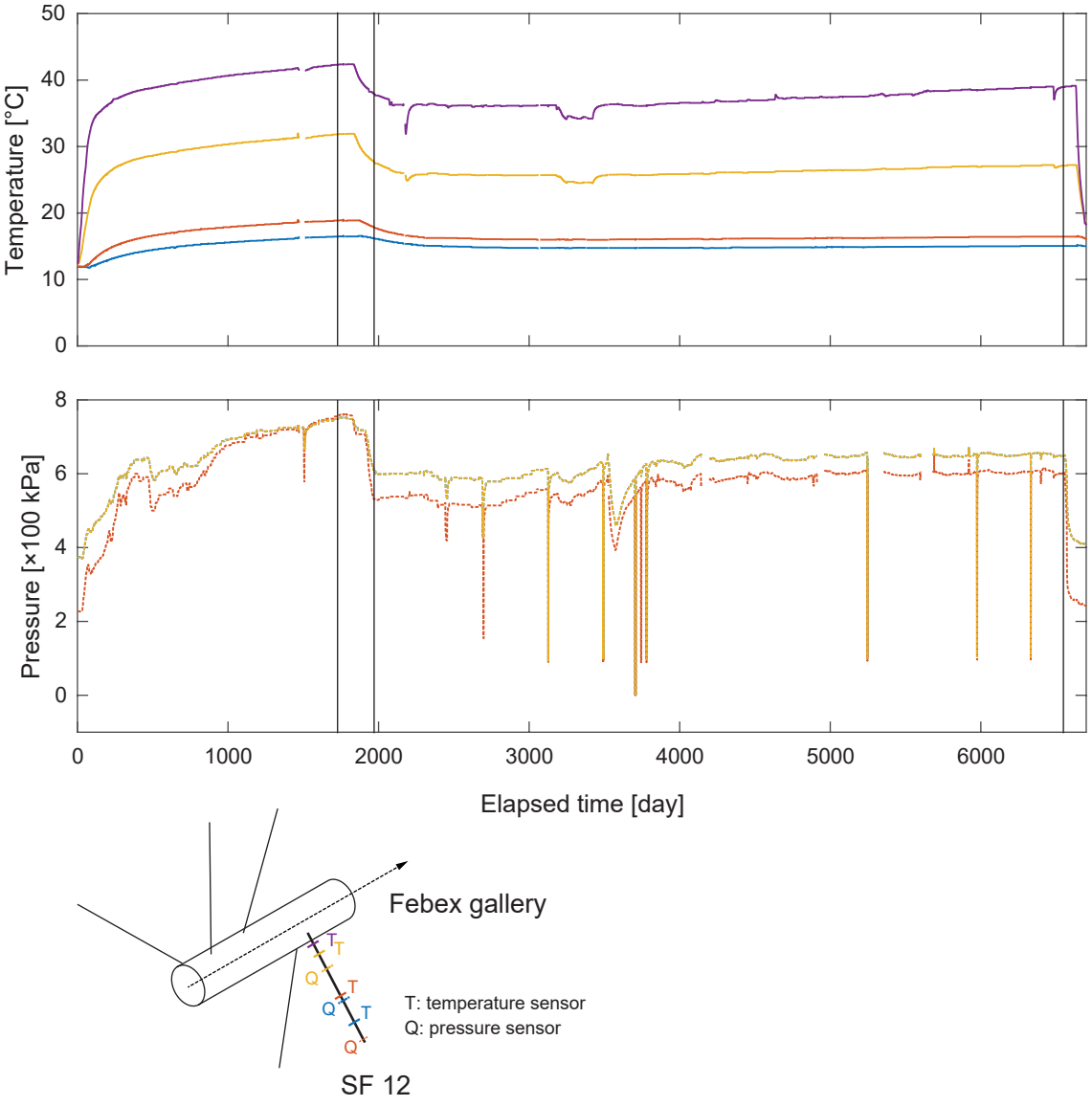


Fig. 2-9: Temperature and pressure evolution in the SF12 borehole

The variable range of hydraulic conductivity in the rock resulted in differences in the speed of pore pressure response to sealing of the open drift and to dismantling operations, but pressures were typically stable after the first years after the partial dismantling (Fig. 2-9). Total pressure (stress) responded to the development of buffer swelling pressure, showing a general radial dependence as would be expected. In general, the buffer was largely unaffected by far-field/rock events (Lanyon & Gaus 2016). Similarly, there appeared to be little influence on the rock, other than the rise in temperature, due to the EBS emplacement and heating.

2.10 Final sensor status after Heater #2 shutdown

The monitoring system, sensors and data acquisition units showed excellent performance during the experiment, providing continuous control of the heating system, and generating a large experimental monitoring database (Martínez et al. 2016). The few incidents that occurred were caused by external factors, and in particular by lengthy power shutdowns that exceeded the capacity of the uninterrupted power supply of the system. Nevertheless, these incidents did not have any real impact on the experiment control or on the continuity of the database.

The power control algorithm developed to keep a constant temperature of 100 °C at the hottest point of the liner surface was very effective, providing smooth operation of the heaters and a good adaptation to the changes occurring in the environment of the heaters, such as the progressive hydration of the buffer or the partial dismantling operation.

Sensors and data acquisition systems typically functioned well beyond the expected lifetime of the experiment (see Chapter 6). A high percentage of sensors was still operational after 18 years. Of the non-operational sensors, around 30% were saturated relative humidity sensors, while other failures occurred either at installation (4%), dismantling of Heater #1 and resealing, or progressively during the experiment. Results from post-excavation characterisation and recalibration further support the quality of the initial design and implementation of the in-situ test. Sensor recalibration has, in some cases, provided an improvement in data quality and was retrospectively applied to data (see Chapter 6).

3 Pre-dismantling investigations

Prior to the dismantling activities, the redox state of the buffer was characterised in order to plan sampling strategies appropriately (Section 3.1). Over the course of the 18 years of the FEBEX experiment, numerous campaigns were performed to obtain gas-water samples from pipes installed in the buffer (Section 3.2). The aim of these studies was to characterise the undisturbed gaseous phase within the buffer prior to dismantling and exposure to the atmosphere.

Furthermore, given that various laboratories were receiving samples and performing similar analyses, an interlaboratory comparison was performed based on existing data (Section 3.3) to facilitate comparison of data from samples obtained from the final dismantling.

Finally, an auxiliary study on colloid formation was conducted from 2005 in two boreholes parallel to the gallery. The results obtained as part of the FUNMIG project (see Section 1.3) are summarised in Section 3.4.

3.1 Redox state prior to dismantling

Prior to the final FEBEX dismantling, the redox conditions in the buffer were evaluated to support subsequent discussions on the potential alteration or contamination that may have affected the samples as compared to their "undisturbed" in-situ conditions (Giroud 2014). The status was based on information and knowledge of the environment before the completion of the experiment (design, chemistry and mineralogy of the bentonite buffer, the plug(s) and equipment, characterisation of the near-field hydrological and geological settings, partial dismantling, monitoring and sampling).

One difficulty in assessing the redox conditions was the very high sensitivity of the redox potential to contamination by the atmosphere. Therefore, all sampling procedures that did not consider this sensitive redox conditions severely limited the interpretability of the data, particularly if the samples had been in contact with the atmosphere. In addition, even when the sampling procedure aimed at hindering contact with the atmosphere, air contamination was difficult to exclude and to account for when interpreting the analytical results.

In a totally sealed experiment, the expected behaviour would be a change in redox potential towards strongly reducing conditions. The duration of such changes were previously suggested to vary significantly with time, with predictions varying between a decade and several centuries (see summary and references in Giroud et al. 2018). In contrast, in the FE experiment (Müller et al. 2017, Giroud et al. 2018), the onset of anaerobic conditions occurred within a few weeks to months after the closure of the experiment (e.g. Müller et al. 2017, Nagra 2019). However, it has been observed in FEBEX (ENRESA 2006a) and other experiments (e.g. Svemar et al. 2016, Giroud et al. 2018) that this trend is disturbed or mostly controlled by the potential inflow of O_2 into the buffer through the plug, along cables ducts and pipes, or through the EDZ. The fact that the FEBEX plug design was neither specified for water- or gas-tightness means that the conditions must be assessed with particular care.

During the analyses of the frst operational phase of FEBEX (1996 – 2002), oxygen levels decreased rapidly after the closure of the experiment (see Section 3.2). The low measured concentrations can indicate the presence of O_2 in the experiment but can also be the consequence of minor air contamination of the samples upon sample collection or handling (ENRESA 2006a). The investigation of the corrosion of metallic components and of microbial activity in the bentonite showed a strong influence, respectively presence, of sulphate-reducing bacteria (SRB), i.e.

anaerobic microorganisms, in the parts of the experiment where substantial corrosion had been observed. However, in the same samples, aerobic microorganisms were also detected in similar or even greater counts.

The variability of the oxygen data obtained during the subsequent 13 years of Heater #2 running is greater than that in the first five years, probably due to air contamination before, during, or after sampling, which did not allow the exact redox conditions in the FEBEX experiment to be ascertained before the dismantling of Heater #2. Despite this mixed information and the findings from the first operational phase of FEBEX, it was forecasted that the FEBEX redox state tended towards an anoxic, reducing environment prior to the final dismantling.

3.2 Gas-water sampling in GRS and CIEMAT pipes

In the FEBEX in-situ experiment, gas and porewater composition within the bentonite was analysed using pipes that were introduced inside the bentonite buffer to analyse gas evolution (Fernandez 2019). Gases may have various sources, such as the corrosion of metals, the abiotic and/or biotic (microbial) degradation of organic materials or steam generation. This knowledge, however, developed further over the 19 years of the experiment (gas measurements were taken prior to turning on the heaters), resulting in a shifted focus and objectives for sampling over time (see Chapter 1). It was acknowledged that the FEBEX in-situ test was not designed for geochemical investigations and, consequently, most water samples were discarded.

Initially, in 1996, ceramic filter pipes were installed in the buffer. During the partial dismantling, additional sintered stainless-steel (316L) filter pipes were inserted to sample gas and porewater from the bentonite in-situ from 2003 onwards (Fernández 2019). This was done because the dissolved gas may be transported in solution, thus porewater sampling was deemed necessary.

The stainless-steel sintered filters allowed to assess the gas and porewater evolution in the FEBEX bentonite barrier. They also showed no signs of corrosion apart from one filter that was in contact with the highly corroded dummy canister. A potentially higher water inflow, as well as the complex history of that part of the experiment (see Chapter 1), could be the cause of these phenomena.

The main gases detected during the 18 years of the FEBEX in-situ test were O_2, N_2, CO_2, CO, H_2, CH_4 and other saturated and unsaturated aliphatic hydrocarbons (alkanes up to C5 and alkenes). The highest fluid pressures measured (between 2 and 4.5 bar around Heater #1) over the first five years of the experiment were related to water pressures because of the water inflow during the saturation process of the bentonite. In the second operational phase (after installing the pipes around Heater #2), the measured fluid pressures indicated either low gas production rates and/or low total gas pressures inside the bentonite buffer. Measured fluid pressures were similar to atmospheric pressure, with values ranging between 0.805 and 0.929 bar absolute pressure (variations in the range of atmospheric pressure fluctuations). The highest values were observed in pipe FP2 located at the bottom of the bentonite barrier, which may be related to the influence of hydrostatic pressure in the experiment.

The gases mainly consisted (> 93 vol.-%, range: 93 – 99 vol.-%) of nitrogen and oxygen, the sum of remaining gases being only between 0.5 and 6.7 vol.-% on average. When oxygen decreases (or is consumed), the amount of nitrogen (plus helium in the last two campaigns) increases in vol.-% (> 92 vol.-%), indicating a low generation rate (or deficit due to migration) of other types of gases in the test. The total content of these other gases (H_2, CO_2, CH_4 etc.) was higher when Heater #2 was running, higher as a function of distance to the heater, and higher depending on the nature of the surrounding materials.

Although the concentration of oxygen decreased over time, it was never completely depleted, showing minimum values between 3 and 0.2 vol.-% (around 83% lower than atmospheric in 1 – 2 years, Fig. 3-1). However, the presence of hydrogen, methane and other hydrocarbons indicates special microenvironments where anoxic/anaerobic conditions were established, which was confirmed by the reducing redox potentials calculated from hydrogen contents and measured in some porewaters collected from the different pipes. The presence of the remaining O_2 could be due to:

- incoming atmospheric air transported from the gallery access towards the barrier through the concrete plug and responding to atmospheric pressure variations (see discussion in Chapter 5).
- gas/water sampling artefacts and other monitoring activities (gas permeability measurements, water and colloid sampling from radial and parallel boreholes drilled in the granitic formation, which ended in the test interval of the FEBEX in-situ test), and
- flow through the excavation damaged zone (EDZ)

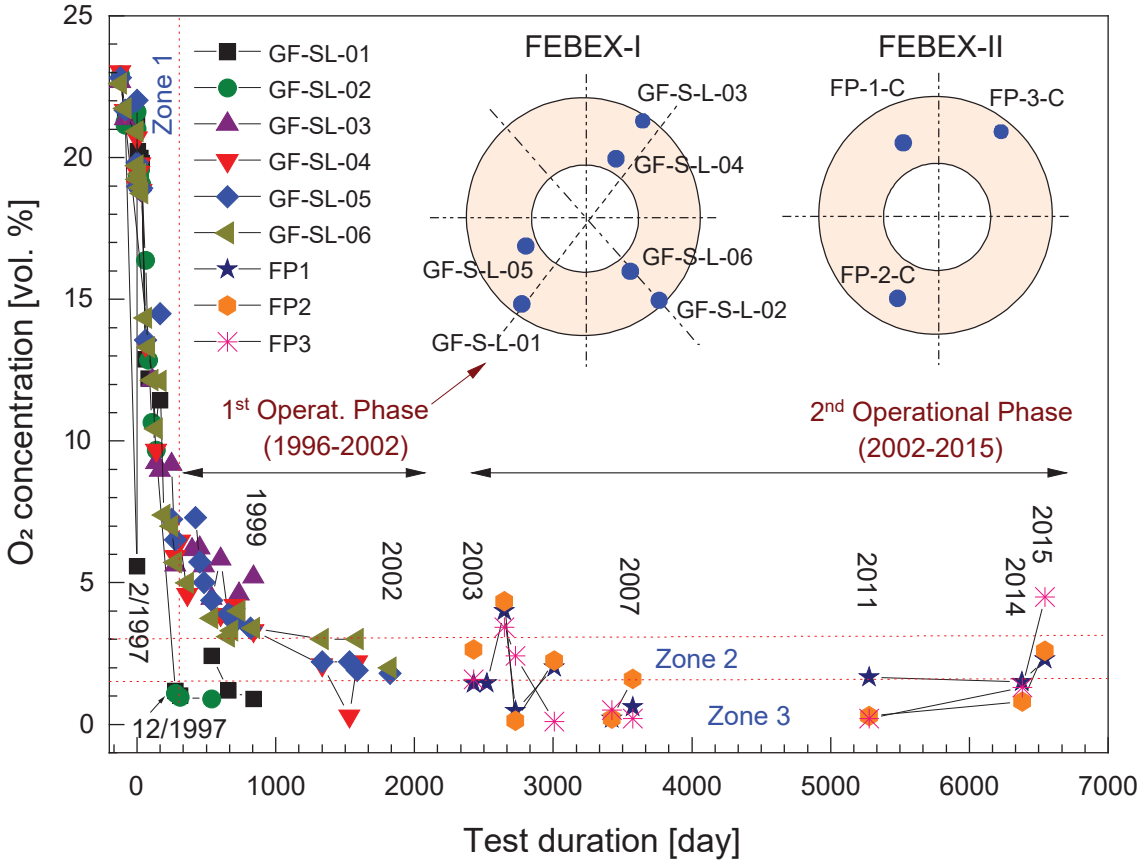


Fig. 3-1: Concentration of oxygen gas (in vol.-%) in the different GRS pipes (GF) obtained during the First Operational Phase (1996 – 2002) and in the CIEMAT pipes (FP) obtained during the Second Operational Phase (2002 – 2015)

Zone 1, Zone 2 ("quasi-anoxic conditions") and Zone 3 indicate different oxygen levels over time. Day 0: 27 February 1997 when heaters were switched on.

Hydrogen was already present before the heaters were switched on and oxygen was consumed; its content showed large fluctuations over time depending on oxygen content, the location of the pipe (close to granite contact or heater contact) and the presence of corroded sensors. Hydrogen is mainly generated through the anoxic corrosion of metals and possibly fermentation of organic matter in its acidogenesis phase. Starting from a high H_2 content (up to 2'000 vpm or ppmv), there was a large decrease in hydrogen, correlated with a decrease in oxygen and an increase in methane and CO_2. Hydrogen increased rapidly after oxygen depletion, and its concentration then remained more or less stable over time or decreased slightly, depending on the location of the pipe and the nature of the surrounding metals and other materials.

Carbon dioxide increased rapidly over time from an atmospheric value to 10 vol.-%. The variations in CO_2 concentration were due to different water/bentonite interactions and/or organic matter degradation since CO_2 is practically absent in the granite groundwater. The higher values were observed during the First Operational Phase during the saturation process of the bentonite and decreased during the Second Operational Phase. The CO_2 content was only measured during the First Operational Phase, and it was always higher than the atmospheric content, increasing over time up to ~ 40 vpm.

The chemical composition of the sampled porewaters is mainly Na-Cl type with ionic strengths ranging between 0.01 and 0.4 M. The composition of the collected waters was in the range of those found from squeezed bentonite block samples (outer, middle and inner blocks) obtained during the dismantling operations in 2002 and 2015 (see Chapter 5). Chloride contents increased towards the inner parts of the bentonite barrier due to the infiltration of granite groundwater and advective transport of solutes as well as due to cations being controlled by dissolution/precipitation processes and exchange reactions, as observed in squeezing and aqueous leaching experiments (Fernández et al. 2018a). Differences in the chemical composition were found among all extracted porewaters with respect to location in the experiment.

The corrosion of metallic compounds consumes O_2, H_2O and CO_2 (by carbonate precipitation) and produces H_2 under anaerobic conditions, whereas the degradation of organic compounds, whether microbially mediated or by abiotic oxidation reactions, may produce H_2, CO_2, CO, CH_4 and other hydrocarbons, and consumes O_2. However, the impact of these possible reactions was not homogeneous over the entire bentonite barrier, as observed in the gas content variations in the different pipes over time (e.g. hydrogen content was higher in pipes close to corroded metals). The variations in gas content depended on the location of the pipes (close to granite interface or to heater contact) and on the surrounding materials (metals, plastics, cellulose, etc.).

Electrochemical redox potential measurements indicated Eh values below -50 mV, suggesting strongly reducing conditions in the bentonite barrier. In addition, Eh values obtained by geochemical modelling from dissolved H_2 concentrations pointed to theoretical redox zones in the range between -221 mV (sulphate-reducing) and -244 mV (methanogenic) during the First (1996 – 2002) and Second Operational Phases (2002 – 2015) (Fernández 2019).

Lessons learned from gas/water sampling in the FEBEX in-situ test

Although ceramic filter pipes are preferred for collecting gas and water samples because they are less reactive to chemical and mineral species from both the rock and porewater and better for redox measurements, they are not recommended in a non-saturated compacted bentonite barrier. The ceramic pipes used during the FEBEX in-situ test during the First Operational Phase were broken, at least partially, due to the generation of high swelling pressures.

After gas collection, a carrier gas was used for flushing the gas/water sampling lines from the pipes to extract additional porewater samples. Nitrogen gas was used in most of the sampling campaigns, and helium gas was used in the last two campaigns (2014 and 2015). The drawback of nitrogen is that it is the main gas dissolved in granitic waters and is generated and/or consumed in different bio-geochemical reactions. Therefore, the use of unreactive gases such as argon or helium is recommended.

Most of the gas contents measured during the FEBEX in-situ test were analysed from the gas phase (at equilibrium with water samples, but as a separate phase). This was because the initial aim of GRS was to only analyse the gas phase, and most of the water samples were discarded. Therefore, the gas concentration dissolved in the water phase was not characterised in the FEBEX in-situ test.

For a complete understanding of the processes and redox conditions involved in an engineered barrier system (EBS), a complete characterisation of gas and porewater composition (including Fe^{2+}, NH_4^+ S^{2-} and TOC) would be needed. This should include not only the main components of both phases, but also the isotopic gas and water composition, as well the characterisation of organic species (pyruvate, lactate, acetate, other organic acids, etc.). Similarly, a microbiological analysis of water samples should be performed. However, because of the low bentonite permeability and the small time gap between the last FEBEX sampling campaigns (five months), not enough water could be obtained for a complete analysis.

3.3 Round robin of key buffer variables for materials characterisation

Prior to the final dismantling of the FEBEX in-situ test, a materials characterisation comparison (geotechnical, geochemical/mineralogical) was performed that was supplied by various organisations associated with FEBEX and aimed at identifying the degree of uncertainty in the reference values for important parameter values in the interpretation of the dismantling data (see Kober & Van Meir 2017). Data from FEBEX bentonite and Wyoming (MX80) were used for this comparison.

Within the bounds of conditions present in the FEBEX bentonite, the geotechnical parameters are predominantly influenced by density and water content, although geochemical properties and conditions also have an effect. Therefore, it was proposed that it would be extremely important to ensure that the methods used to recover FEBEX samples (and measure these parameters) were performed in a consistent manner and subject to minimal procedure-induced variability. Furthermore, the need to obtain samples that are exposed to as little disturbance as possible for conducting tests such as swelling pressure, hydraulic conductivity and gas permeability was stressed.

Within the geochemical and mineralogical parameters, a certain degree of scatter/uncertainty was observed for several of the considered parameters and the various analytical methods, which highlighted the need for careful sampling and data interpretation to ensure that any interpreted changes in parameters are clearly outside the range of normal variation in the baseline data. Within the FEBEX-DP analysis, the data scatter observed inthe round robin was not further explored.

As part of the dismantling planning, partners were not required to follow a single protocol, but the laboratories involved in the mineralogical analyses were required to fully document their analytical methods.

3.4 Colloids in radial and FUNMIG boreholes

The objective of this stuy was to analyse the possible generation and migration rates of bentonite colloids under in-situ conditions around the FEBEX experiment (Missana et al. 2018).

Analyses of waters from different intervals of different boreholes at different distances (see Section 1.3) from the bentonite surfaces were performed to verify the existence of colloidal particles and to identify their nature. In relation to the reference water signal, various colloids were present in the water samples: natural colloids, (possibly) bentonite colloids but also "contaminants" in particulate form (metals, organic and rock fragments). The experimental work conducted from 2006 to 2014 showed that colloidal particles exist at the site in concentrations higher than those expected for Grimsel water (0.2 ppm). However, it was shown that different artefacts existed, possibly caused by the drilling of new boreholes, which biased the identification of bentonite colloids. High amounts of metals (Zn, Ni, W, Cu, Pb) and organic carbon (TOC) were identified.

In comparison with laboratory tests, it was observed that the Al content in Grimsel water is very low, with an Al contribution that could be derived from different aluminosilicates present in the granitic rock and fracture fillings; Mg can originate from the dissolution of some minerals; Fe and Ti can result from oxides, naturally present or also from oxidation of tubings/taps, as detected in the instrumentation of the tunnel. Nevertheless, the presence of Al is the indispensable condition for assessing the existence of bentonite colloids.

The aluminium content was quite low in all the studied intervals of the FUN-1 and FUN-2 boreholes (see Map 2) and was only rarely observed to be higher than the level expected for Grimsel water. The maximum concentration of bentonite colloids (considering that the entire aluminium signal comes from the bentonite) was around 0.8 ppm, but these data alone do not ensure the presence of bentonite colloids. Not even in the intervals where water was clearly affected by the presence of the bentonite (e.g. higher chlorine or sodium contents, or elevated electrial conductivity, for example in FUN-4) could bentonite colloids be identified with certainty. In the regions chemically affected by the bentonite, the ionic strength of the water increased, and this may have important effects on colloid stability, causing their aggregation and sedimentation.

The expected diffusion of colloids under the FEBEX tunnel conditions at a distance of 20 cm from the bentonite surface (minimum approximate distance from FUN-1 to the bentonite) was quantified after 13 years (Missana et al. 2011) and after 18 years (Missana et al. 2018). The fractures and intact granite around the bentonite barrier in the FEBEX gallery have a very low transmissivity ($10^{-10} – 10^{-11}$ m^2/s), thus the colloids potentially generated from the bentonite surface will move by diffusion. The diffusion coefficient, D, for colloids 300 nm in diameter in water is 1.6×10^{-12} m^2/s, so that the concentration at time t [C(t)] at 20 cm from the source after 18 years would be approximately 6.7×10^{-4} mg/L. This calculated value would agree with experimental observations from in-situ testing (< 0.8 mg/L). These simple calculations do not account for the retention of colloids on the granite surface largely seen in laboratory experiments, especially under low water flow conditions, which could additionally decrease the concentration of transported colloids. However, advection processes and gradient changes as well as fracture and preferred mineral orientations cannot be fully excluded for colloid transport but were not further considered.

Many possible agents limiting the stability and migration of bentonite colloids (calcite on fracture surfaces, presence of iron oxides, increase in electrical conductivity, low water flowrates) have been clearly observed and support the general conclusion that bentonite colloids, possibly formed at the bentonite/granite interface, have not been mobilised in significant quantity during the timeframe of this experiment.

4 Dismantling of Heater #2 and buffer sampling in 2015

4.1 Technical pre-dismantling preparations and optimisations

Promising techniques and methods that could be helpful in the dismantling and sampling of the in-situ experiment were studied first in the laboratory, using well preserved bentonite blocks from the partial dismantling and the previously dismantled EB experiment (Mayor et al. 2007) before designing the dismantling. Selected methods were then applied during the operation (García-Siñeriz et al. 2016a). The goal was to identify techniques capable of measuring the state of the buffer at the immediate surface, before the buffer sampling and dismantling operation of each bentonite layer and to minimise the potential perturbation in the sampled material (desiccation, stress release, etc.) that could negatively affect the results obtained from planned on-site analysis of water content and dry density. Details can be found in García-Siñeriz et al. (2016a).

4.2 Dismantling and sampling plan

The objective of the second and final dismantling operation was to dismantle all the remaining parts of the in-situ test, including Heater #2. This operation included carrying out a complete sampling of the shotcrete plug, bentonite buffer and sensors to allow the analysis of the condition of the barriers after 18 years of heating and natural hydration. In addition, samples from the rock, relevant interfaces, metallic components and tracers were also taken. Sampling was aligned to fulfil the requirements of the FEBEX-DP project plan (see Chapter 1.5 and Kober & Van Meir 2017).

All details about the planned dismantling operation were included in specific test plans (Bárcena & García-Siñeriz 2015a) and the sampling programme was described in depth by Bárcena & García-Siñeriz (2015b) and in its update (Rey et al. 2015). Its purpose was to support and clarify the sampling procedure during the dismantling process and provide a complete guide on how to perform the intended sampling operations, which could be followed by any operator without specific information or previous experience with that type of work.

The general layout of the sampling sections is given in Fig. 4-1. Tab. 4-1 contains a breakdown of all the collected samples by materials and zones.

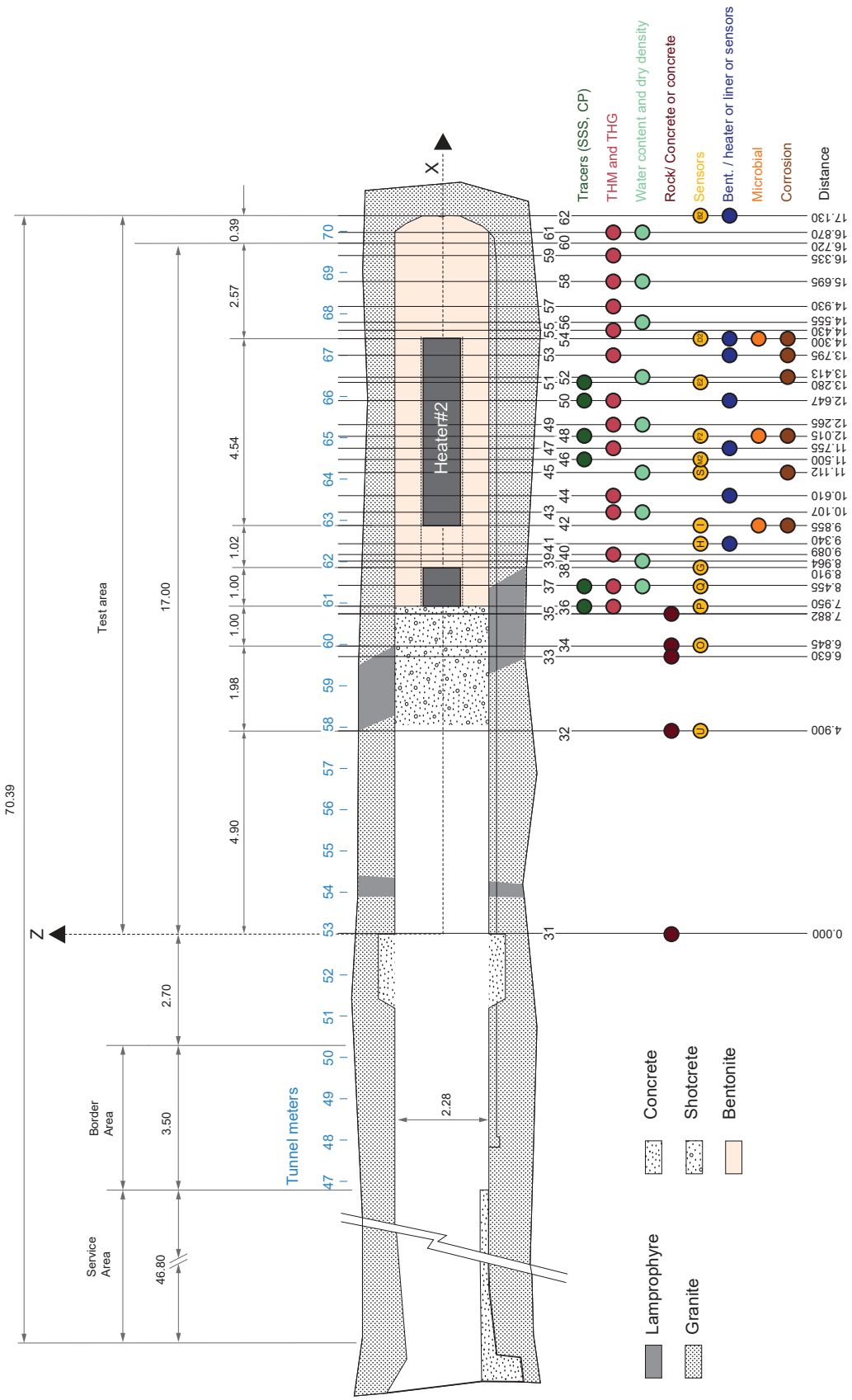


Fig. 4-1: General layout of the sampling sections

Note that individual sampling sections comprise several bentonite slices (see Fig. 1-4).

Tab. 4-1: Breakdown of all the collected samples

Shotcr = shotcrete, Bent = bentonite, Sens = sensor, Met = metal

Zone	Secction	Shotcr/ Rock	Shotcr	Bent/ Shotcr	Bent	Bent/ Granite	Bent/ Met	Sens	Met	Subtotal
Service area	31	2								2
Concrete plug	32 – 35	4	28	8	0	0	0	6	2	48
Clay barrier and heater	36 – 62	0	0	3	968	46	72	168	11	1'268
Total		6	28	11	968	46	72	174	13	1'318

4.2.1 Sample labelling

The code used for sample labelling was T-Y-NN-ZZZ according to the description given below:

T: Sample Material

- B: Bentonite
- C: Concrete
- G: Granite
- L: Lamprophyre
- M: Metal
- S: Sensor

- BC: Interface Bentonite-Concrete
- BG: Interface Bentonite-Granite
- BL: Interface Bentonite-Lamprophyre
- BM: Interface Bentonite-Metal

- CG: Interface Concrete-Granite
- CL: Interface Concrete-Lamprophyre
- CM: Interface Concrete-Metal

- GM: Interface Granite-Metal
- LM: Interface Metabasic dyke/Lamprophyre – Metal

Y: Sample Type

- B: Block
- C: Core
- D: Dice (cube shape)
- S: Any shape
- T: Liner (for metal samples)
- H: Heater (for metal samples)

NN: Sampling section number (31; from 1 to 62)

ZZZ: Sample number for same type of samples in each section or alternatively number of radii – position in radii (increasing clockwise – from those closest to the rock)

Sampling was documented in dedicated sample sheets, while the daily activities were documented in daily reports.

4.3 Dismantling operations

The main operations during dismantling and the results obtained are reported in García-Siñeriz et al. (2016b), and their sequence is described in the following section.

4.3.1 Preparations

The status of the existing dismantling equipment from the previous partial dismantling was checked to determine whether any necessary actions had to be performed in advance of the planned final dismantling operation. The preparations are summarised below:

Preparation of existing equipment: The heater extraction car with the rolling bed, side-dump wagon and winch engines and its cable-pulley system were cleaned/painted, and all bearings and mechanisms were checked, verified and greased. In addition, the mobile electrical crane was prepared and checked, including the main power distribution box. Finally, the entire system was tested by moving the side-dump wagon and then the extraction car in and out the gallery.

Removal of instrumentation at the plug face: The extensometers and their attachment system were removed from the plug face, as well as several other metal remnants (bolts, etc.). The reference vertical and horizontal axes and centre of the plug were marked (see e.g., Fig. 4-2). A portable structure was installed for the positioning of the lasers to be used for providing references at the dismantling front. Finally, the locations of the first drilling and overcoring campaigns were painted at the plug face.

Protection of cabinets inside the drift: The remaining data acquisition cabinets and instrumentation racks within the FEBEX drift were protected by plastic covers to avoid dust entering them during the dismantling work.

Completion of steel tracks up to the plug: Rail parts were emplaced in the gap formerly occupied by the original plug, welded to those already in place and secured. A metal pathway was placed on top of the new rail section for easier personnel movement in the drift. The return pulley was cleaned and greased and fixed next to the end of the tracks to ease the installation of drilling and excavation machinery. As much water as possible was pumped out of the area of the former plug, and a pump was installed permanently to drain the water from overcore drilling and plug demolition.

4.3.2 Plug sampling and overcoring

Plug drilling for specialised sampling of the shotcrete plug and of shotcrete/bentonite interfaces was performed before the plug was dismantled and the heater was turned off (Fig. 4-2). As planned, six good quality cores were obtained, three of them containing an intact sample of the shotcrete/bentonite interface (C-C-32-4/5/6; Tab. 4-2).

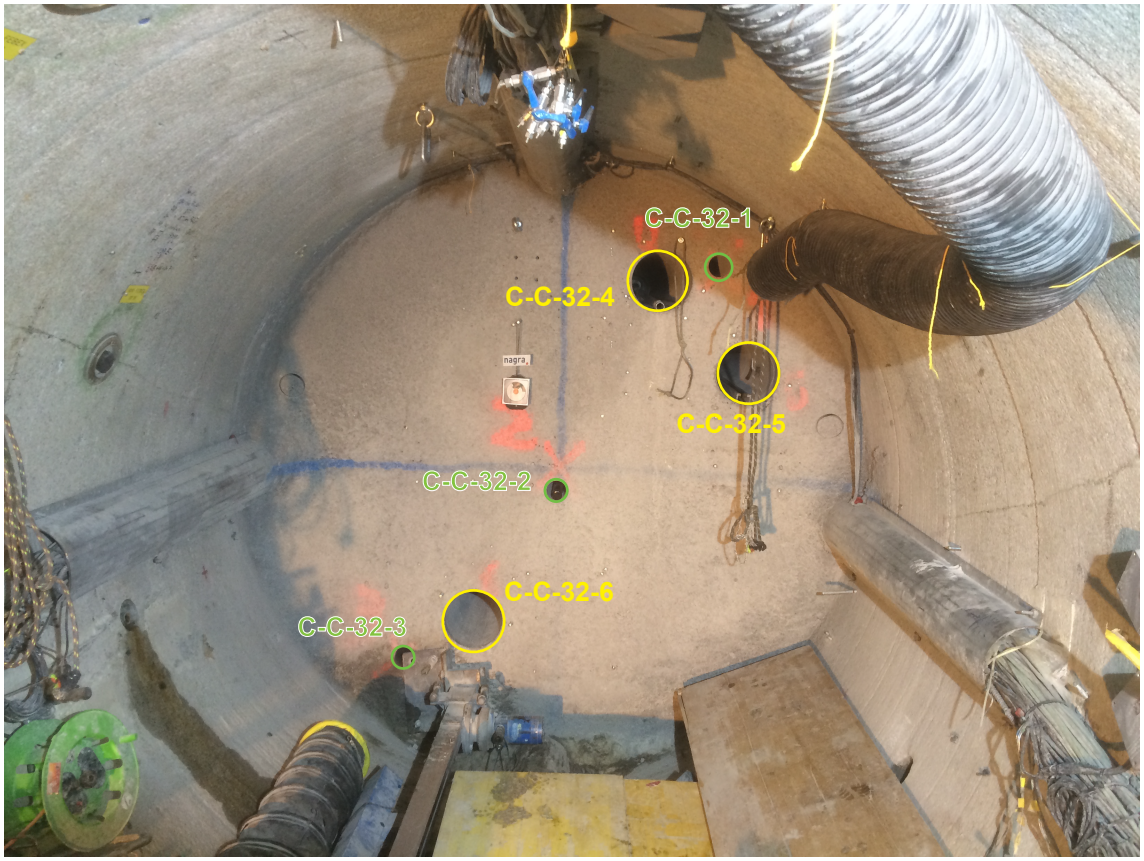


Fig. 4-2: Location of long core boreholes at the plug surface
Sampling Section 32, see Fig. 4-1.

Tab. 4-2: Summary of long cores obtained

Borehole	Purpose	Characteristics
C-C-32-1	Shotcrete	L < 3 m & 78 mm OD, last 10 to 20 cm drilled dry
C-C-32-2	Shotcrete	
C-C-32-3	Shotcrete	
C-C-32-4	Shotcrete/bentonite interface	Approach boreholes of 220 mm OD (L = 2.6 – 2.7 m) and stabilised interface coring of 132/124 mm OD/ID (L = 70 cm)
C-C-32-5	Shotcrete/bentonite interface	
C-C-32-6	Shotcrete/bentonite interface	

Overcored samples (Fig. 4-3) were measured, inspected and properly packaged to be transported to the University of Bern where they were cut into 12 quarter cores to be distributed to partners and their associated analytical teams (Mäder et al. 2016).

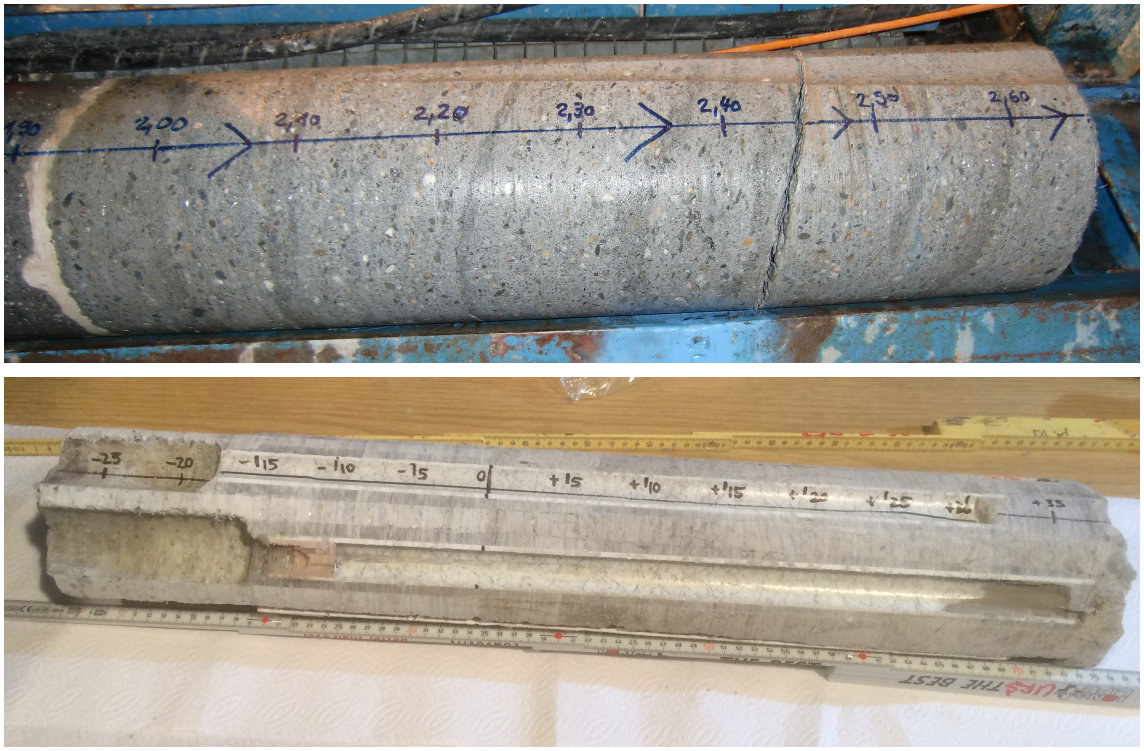


Fig. 4-3: Shotcrete core C-C-32-4 and following overcore, after retrieval

Top: Note that the white band at length '190 (cm)' is the waterproof membrane between the first and the second stage of the shotcrete (see Figs. 1-4 and 1-9).
Bottom: bentonite is to the right (from mark '0' = interface shotcrete/bentonite in the middle of the core onwards) (Mäder et al. 2016).

4.3.3 Plug demolition, concrete sampling and switch-off of Heater #2

Plug demolition was conducted in two main steps as described below.

First part of shotcrete plug demolition (Step I)

The demolition was performed using a Brokk 90 robot, an autonomous arm-shaped small robot that was selected to perform the operation faster, more safely and with greater precision than the hydraulic splitting used in the partial dismantling (Fig. 4-4).



Fig. 4-4: Robot installation in the drift (left) and in operation (right)

The red line marks the former start of the shotcrete plug, while the whitish part in the upper third of the image is the waterproof mebrane that was placed between the first and the second section of the shotcrete plug (see also Fig. 5-1).

The first section of the plug comprised approximately two metres of concrete, from Sampling Section 32 to 34 (Figs. 4-1 and 4-2) and was isolated from the next by a waterproof membrane made of MASTERSEAL X345 polymer compounds (Fig. 1-4). Attention was paid to the position of the cable ducts and total pressure cells in the rock in order to avoid hitting and damaging them. About 12 tonnes of shotcrete were disposed of in this first section of the plug in six working days. A small number of sampling operations were performed in between:

Interface concrete/rock coring (Sampling Section 33): Samples of concrete/granite and concrete/metabasic dyke (lamprophyre) interfaces were taken following a simplified overcoring approach (drilling three stabilisation boreholes with an outer diameter (OD) of 30 mm and in a 120° arrangement filled with fast-hardening resin and overcored with OD 85 mm) at positions where concrete was preserved. Both attempts resulted in cores breaking in the interface. Another approach consisting of drilling only one central stabilisation borehole and then overcoring also failed to produce an intact core.

Plug sampling & concrete coring (Sampling Section 34): Sampling was performed as planned but three samples (C-C-34-1 to 3 planned in the lower-right part) were discarded (due to conflict with cables extending farther back) and total pressure cells PSO-01 & 02 were retrieved (Fig. 4-5).

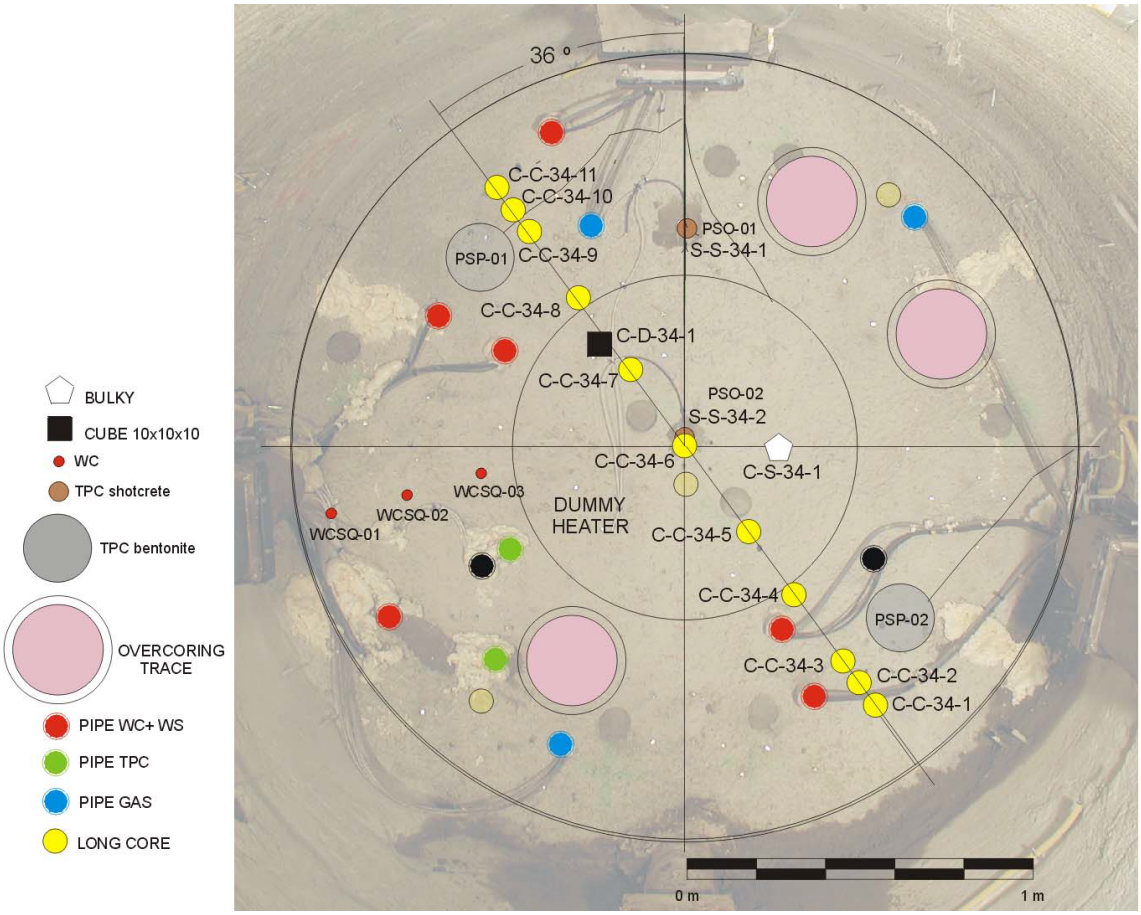


Fig. 4-5: Dismantling plan layout of Section 34 (short cores C-C-34-1 to 11 in yellow)

Switching off Heater #2: The heater was switched off on 24 April 2015, before reaching the buffer, to achieve a temperature level appropriate for the upcoming dismantling work (<30 °C). Working conditions were achieved in about 20 days compared to the 30 days needed during the first dismantling.

Second part of shotcrete plug demolition (Step II)

This comprised the part from the waterproof membrane to the plug-bentonite interface (sampling Section 36). Small hand-made gypsum markers/trackers were placed in the plug/rock contact to check potential movements of the remaining plug (about one metre) during the excavation work. These markers showed no movement whatsoever. The same equipment and procedure were used as for Step I and it took eight working days to complete the works.

Sampling of shotcrete/bentonite interface (sampling Section 35): Several pieces of 5 cm in diameter were extracted using a handheld drilling tool. Concrete and bulky bentonite/concrete pieces were sampled by hand from the excavated parts at the planned locations. The shotcrete/rock interface samples were left in place to be collected later.

4.3.4 Buffer/bentonite dismantling and sampling before dummy retrieval

The initial plan was to remove the dummy canister before starting the dismantling of the bentonite around the liner of the former Heater #1. However, this was not possible because the dummy was stuck in the liner (see Fig. 4-6) due to the pressure developed by the bentonite and the intrusion of bentonite into the inner gap via the holes in the liner. Therefore, it was decided to dismantle the bentonite layers from layers 74 to 66 (dismantling sections 36 – 38, Fig. 4-1) around the first liner segment. This was performed from 12.05.2015 to 22.05.2015.



Fig. 4-6: View of the dummy canister (left) and its adhesion to the liner segment (right)

Electric percussion hammers were used for the removal of the bentonite layers (Fig. 4-7, upper left). As a rule, two blocks of the inner ring were broken first and removed in order to facilitate the extraction of the surrounding blocks. Dismantling operations were coordinated with sampling needs without slowing down the excavation progress too much or jeopardising sample quality. Daily work concluded with leaving at least one bentonite layer in place in front of the next sampling section to avoid exposure to drift conditions. Ventilation in the working area was minimised to prevent samples from becoming drier.

Samples were wrapped and packaged as soon as possible to avoid further loss of water. Each bentonite layer was also fully documented. The x local coordinates for each bentonite layer were measured from the x = 0 coordinate at three places: along the left and right rock walls (mid-height) using a laser device and at the upper part of the bentonite front using the metric tape placed during FEBEX installation.

The instruments contained in the dismantled bentonite buffer were sampled for inspection and calibration, but those installed in the rock walls or boreholes were left in place, for instance the total pressure cells installed in the granite wall.

Sampling was performed in dismantling Sections 36 – 38 by obtaining bentonite core and block samples. Additionally, bentonite samples were taken between the liner and the dummy canister and sensor anchors showing corrosion products as well as iodine filter paper samples were taken.

Before finishing the removal of bentonite layers around the liner, the unit 'liner/dummy canister' was secured with a steel support located at the bottom (Fig. 4-8).



Fig. 4-7: Percussion hammers (left) were used to obtain bentonite core samples of 4.5 cm in diameter (right); microbiological sampling (bottom)



Fig. 4-8: Dummy canister secured with a steel support

4.3.5 Dummy retrieval

On 26.05.2015, the dummy canister plus the surrounding liner section were extracted. The operation was carried out with the help of a light wagon that was placed directly on the gallery floor below the liner. The wagon was then carried over the fixed tracks and could be moved to the gallery entrance where the liner was sampled and the 'liner + dummy canister' was packed and stored (Fig. 4-9).



Fig. 4-9: Dummy canister extraction (in liner section)

4.3.6 Removal and sampling of bentonite and liner up to the front of Heater #2

Following the dummy retrieval, eight layers of bentonite blocks were dismantled, from layers 67 to 60 (dismantling Sections 39 – 42) up to the front side of Heater #2, following the same rules and procedures as described in the previous section. About 14 tonnes of bentonite blocks not required for analysis were disposed of during this dismantling operation performed from the concrete plug to the front of Heater #2 (García-Siñeriz et al. 2016b).

4.3.7 Extraction of Heater #2

The extraction of Heater #2 took place on 04.06.2015. The machine used for the extraction of the heater from the liner and for its transport along the drift was based on that used for the emplacement (ENRESA 1998) and already modified for the extraction of Heater #1 (Bárcena et al. 2003). The gap between the liner and the heater (Fig. 1-6) was found to be filled with bentonite (see Fig. 4-10, right photo) but the heater was extracted gently with a peak pulling force of about 4.6 tonnes at the moment of mobilisation and decreasing later to 3 – 4 tonnes during the rest of the extraction. As a reference, these values were 2 tonnes and 1 tonne, respectively, for the extraction of Heater #1.

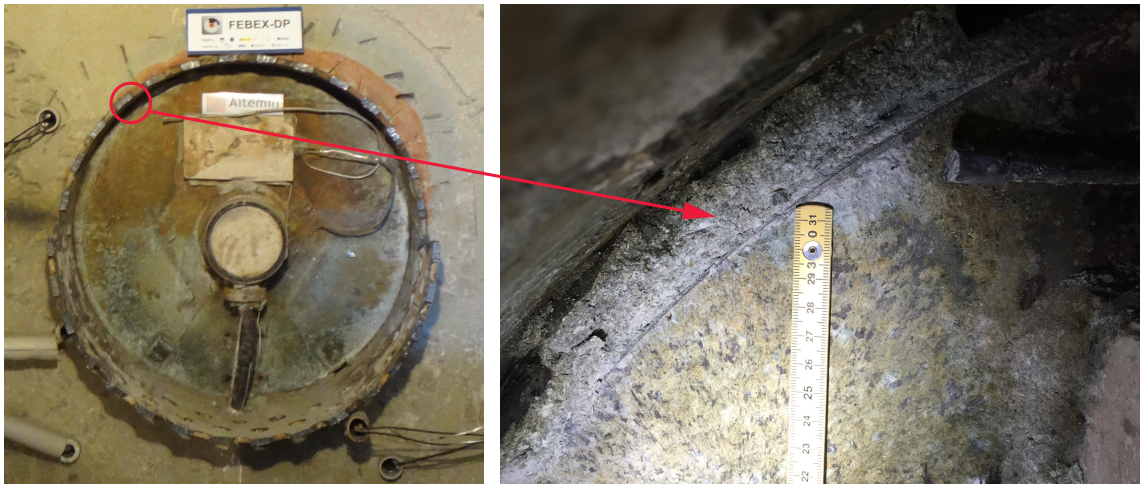


Fig. 4-10: Uncovered heater front (left) and close-up of the gap filled with bentonite (right)

The extraction wagon with the heater was then moved to the gallery entrance where the heater was packed and stored (Fig. 4-11).



Fig. 4-11: Extraction of Heater #2 (left) and general view of the heater at the drift entrance (right)

After removal of the heater, protrusions through the liner could be seen to have resulted in a full bentonite enclosure at the front and end of the heater. Individual protrusions were only visible in the middle of the heater and only where the gap was largest (10 to 2 o'clock regions) (Fig. 4-12). This phenomenon was not observed during the partial dismantling of Heater #1 after only 5 years of saturation.



Fig. 4-12: Inner view of the liner once the heater was extracted (left) and detail of the bentonite protrusions inside the liner (right)

4.3.8 Removal and sampling of the remaining bentonite and liner

After sampling around the extracted Heater #2 section (still in place due to the liner, which was sequentially removed in one m-sections), the buffer dismantling continued up to the end of the FEBEX gallery. Approximately 7.5 metres of buffer length were dismantled in this phase, comprising 59 bentonite layers, from slices 59 to slice 1. The layers were dismantled one by one, and the planned sampling programme was carried out at the same time. The same tools and procedures used for previous dismantling and sampling were applied, but in this case the blocks in the ring were broken first.

A total of 21 sections were sampled in this step, from dismantling section S42 to S62 (e.g., Fig. 4-13). The daily routine was the same as for the previous buffer sections. About 53 tonnes of bentonite were disposed of during the dismantling operation between the front of Heater #2 and the gallery end.

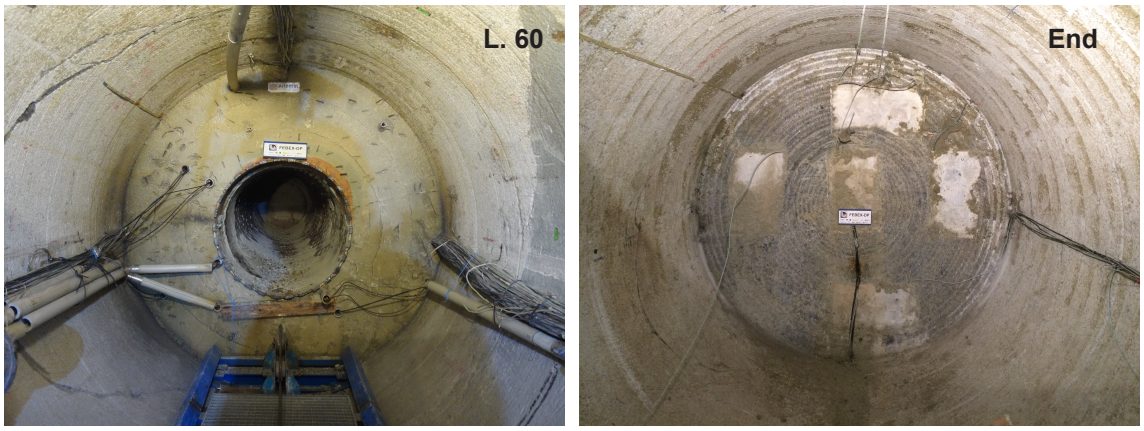


Fig. 4-13: Start (bentonite layer 60, left) and end (granitic back end showing the cemented total pressure sensor slots, right) of the dismantling of the remaining test section

4.3.9 Sampling and sensor dismantling

More than 1'300 samples were taken from 31 sections (Fig. 4-1 and Tab. 4-1), carefully preserved and distributed for laboratory analysis (concrete, rock, bentonite, metals and sensors). Besides, up to 440 samples of bentonite were taken to be analysed in-situ to determine dry density and water content. Results of these analyses are given in Chapter 5.

During dismantling, the sensors appeared in better condition than those gathered during the first partial operation: visibly lower corrosion or mechanical damages except for the crack meter, which was not correctly sealed against the wall during installation. Field observations immediately suggested that no bacterial corrosion was found this time, which was confirmed in the corrosion analysis report (see Section 5.4, Wersin et al. 2017). This is related to the lower frequency of voids left around the sensors in this part of the buffer (see Section 5.2). Further details concerning sensor status and performance are given in Chapter 6.

4.3.10 Sampling for corrosion and microbiology

Microbiological samples were obtained by extracting bentonite cores using a hole saw technique based on first drilling a circular core followed by inserting a sterile metal tube (length 12 cm, diameter 8 cm) that was pushed into the dismantling section wall above the drilled core, thus leaving a sample inside the tube upon retraction. The sections were selected to achieve a large resolution of bentonite exposed to both high and low water content and higher and lower temperatures. In addition, for each section, bentonite samples were taken in straight lines from close to the rock wall, over the middle of the cross-section to the heater to investigate differences in bacterial viability as a function of distance to the heater or to the centre of the buffer. Immediately after sampling, the metal tubes containing bentonite cores were wrapped in a sterile plastic bag to keep out humidity and packed in double aluminium foil bags which were sequentially flushed with argon gas, evacuated at least three times, and then sealed in an evacuated state to keep the samples in an inert, anoxic atmosphere. During the time awaiting shipment, the samples were stored in a refrigerator at the GTS at 4 °C.

4.4 Overall dismantling conclusions

Overall, the dismantling operation can be summarised as follows.

Plug dismantling: The use of a demolition robot was more effective (faster and cheaper) than the hydraulic splitter used for the partial dismantling, and it provided the required accuracy and care to avoid damaging the cables, sensors and gas pipes. Some minor disadvantages of the robotic dismantling of the shotcrete plug included having to wet the concrete to avoid dust emission, and the vibration of the robot affected and loosened the concrete/rock interface/contact, which could thus not be preserved intact.

Heater removal: Although legitimate doubts were raised because of the difficulties encountered when extracting the dummy because it was stuck to the liner, the extraction of the heater proceeded as planned and without major difficulties using the pulling machine designed for this purpose. However, the evident intrusion of bentonite into the inner gap through the holes of the liner should be evaluated when considering the reversibility of waste emplacement concepts (using liners) as well as buffer homogeneity issues close to the heater/liner (see Section 5.2).

Buffer dismantling: Dismantling and excavation tools were demonstrated to be appropriate for the purpose although the operation was slower than expected due to several factors: the difficulties in extracting the dummy canister (excavation around the canister), logistical problems resulting in delays in receiving materials and equipment required to continue, and debris evacuation

and the adjustments required to perform the sampling procedures, including the request for additional samples. Initially, it was planned to take 1'056 samples during the dismantling and recover 172 sensors (Bárcena & Siñeriz 2015). However, during the dismantling activities, on-site decisions and additional partner wishes resulted in an increase in the sample number to 1'318 (additional samples mostly within the buffer). These extra samples required additional time and occasionally delayed the sampling plan, but increased confidence in buffer characterisation (see Chapter 5.2)

The hydrogeology of the region around the drift provided a stable environment able to supply enough water to the buffer for ongoing saturation controlled by the bentonite's ability to take up water (see Chapter 5). There was no evidence of any piping or erosion of the bentonite during the decommissioning operation, nor was water inflow from the rock observed.

Sampling: A small number of sampling procedures related to the bentonite/metal or bentonite/rock interfaces were found to be impractical/unrealistic, and alternatives should be developed. Log documentation was too complex. The procedures should be simplified, and manual filling out of documentation forms should be avoided in order to speed up the dismantling/sampling process and minimise errors. The assistance of partners during sampling was useful and improved the dismantling speed when problems arose, but occasional requests for additional samples increased the duration.

In-situ analysis: In-situ analyses for determining dry density and water content were carried out as expected, although they required more effort than initially foreseen. This was mainly due to the fact that the number of analysed samples was doubled by the addition of new sampling sections and that additional safety measures were required for mercury handling during analysis.

Packaging and shipping of samples: This was more complex than anticipated. In particular, shipping of refrigerated microbiological samples was very complex and expensive because these had to be delivered within 48 hours. Coordination of samples to be shipped to 18 different organisations and partner laboratories always had to be arranged from the country of origin. For FEBEX-DP, this operation was managed by AITEMIN (Spain).

Dismantling team and partner cooperation: It was beneficial to have the same contractor onboard for the dismantling who carried out the installation 20 years earlier and the partial dismantling 13 years earlier, thus providing a wealth of knowledge; this helped to save time and improved the quality of the entire operation. Cooperation with Nagra was successful; in particular, personnel at the GTS contributed significantly to reaching the objectives. Cooperation with the partners requiring samples was also very good, and the assistance of CIEMAT was very valuable.

Comparison of partial and final dismantling on-site activities: The final dismantling showed fewer relevant difficulties, for example the problems with the mercury-filled pressure cells faced in the partial dismantling (ENRESA 2006a). Overall, the dismantling activities were accomplished without major complications. It is evident that this was the result of the lessons learned from previous experience.

5 Analysis and laboratory tests

This chapter is dedicated to reporting the analysis of the major barrier components and interfaces. It follows the steps of the dismantling procedure by beginning with an analysis of the shotcrete plug, its interfaces with the bentonite and the rock, and then continuing with an in-depth THM/THMC analysis of the buffer and its interfaces with metal components and the granitic rock. The chapter ends with summaries of the corrosion and microbiological investigations.

5.1 Concrete and interfaces with bentonite and granite (NAB 16-18)

5.1.1 Introduction and scope

The concrete[5] plug of the FEBEX in-situ test was installed in 2002 – 2003 after the dismantling of the first heater and consists of two different sections (see also Figs. 1-9 and 5-1). Due to initial technical difficulties during the shotcrete installation of the concrete plug, the concrete recipe for the plug was optimised for Section 2 to improve workability. This resulted in a more heterogeneous Section 1, which also exhibits a lower strength compared to Section 2 and contains steel fibres rather than the polymer fibres used for Section 2. The interface between the two sections is a 1 – 2 cm thick polymer sealing layer. The dead volume of the former first heater was filled with a closed steel dummy cylinder (dummy canister). The surrounding bentonite section has therefore experienced a complex heating history, hot during the first phase of FEBEX, but relatively cool during the second phase. A fractured metabasic dyke (lamprophyre, dark grey in Fig. 5-1) intersects the gallery at the location of the shotcrete plug and is a zone of preferential water inflow to the tunnel.

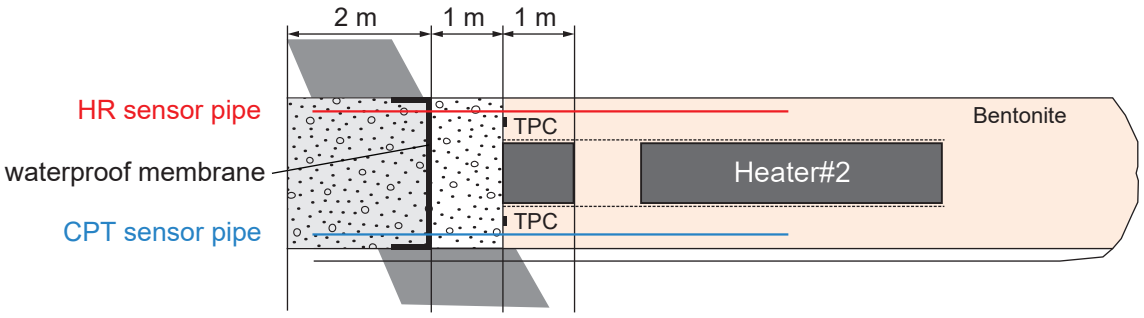


Fig. 5-1: Design of the concrete plug installed after the dismantling of the first heater in the FEBEX in-situ experiment

Section 1 comprises the first shotcreted metre next to the bentonite buffer, Section 2 consists of the remaining two metres of shotcrete closing the experiment to the gallery. It is separated from Section 1 by a waterproof membrane. HR: relative humidity, CPT: cone penetration test

[5] Throughout the report, shotcrete and concrete are used interchangeably. The second plug was constructed by shotcreting. Of interest are the cement interactions that are independent of the aggregates they are composed of.

Within FEBEX-DP, the concrete plug and the interfaces towards the bentonite and the granite rock were investigated mineralogical and physico-chemical alterations that may have occurred during the 13-year-long heating period since installation. Because the concrete plug is – relatively speaking – far removed from Heater #2 (2 metres), interactions are not driven by a large temperature gradient, but by differences in mineralogy and the pH of porewater between the concrete and bentonite. Of particular interest for the design of a repository and its long-term safety are the microstructural and mineralogical changes that occur at the concrete-bentonite/granite interfaces because these may impose a first-order control on transport of water, solutes and gas.

5.1.2 Methods

The studies of the concrete, concrete-bentonite interface and concrete-granite interface were carried out by seven different institutions: BGR (Germany), CSIC-IETcc (National Research Council, Spain), CIEMAT (Spain), Obayashi (Japan), Sandia National Laboratories (USA), UAM (University of Madrid, Spain) and the University of Bern (Switzerland). The results from all studies are documented in Turrero & Cloet (2017).

The majority of the core sampling was planned by AITEMIN and carried out by the GTS drilling team (García-Siñeriz et al. 2016), while the stabilised overcoring of the concrete-bentonite interface was designed and carried out by the University of Bern and the GTS team (Mäder et al. 2016) and the concrete-granite sampling was carried out by Obayashi with GTS support. The concrete plug was dismantled in two sections, 32 and 34 (Fig. 5-2). The concrete sampling and overcoring of the concrete-bentonite interface took place before dismantling. Cores were taken at different radial distances for concrete characterisation and evaluation of the impact of the groundwater coming from the rock. Each core was further analysed as a function of depth (distance to the bentonite/heater interface). Some samples of the concrete-bentonite interface were hand-picked from the last remaining chunks of concrete attached to the bentonite. The concrete-granite interface samples were collected after dismantling from some remaining concrete material attached to the side walls of the tunnel.

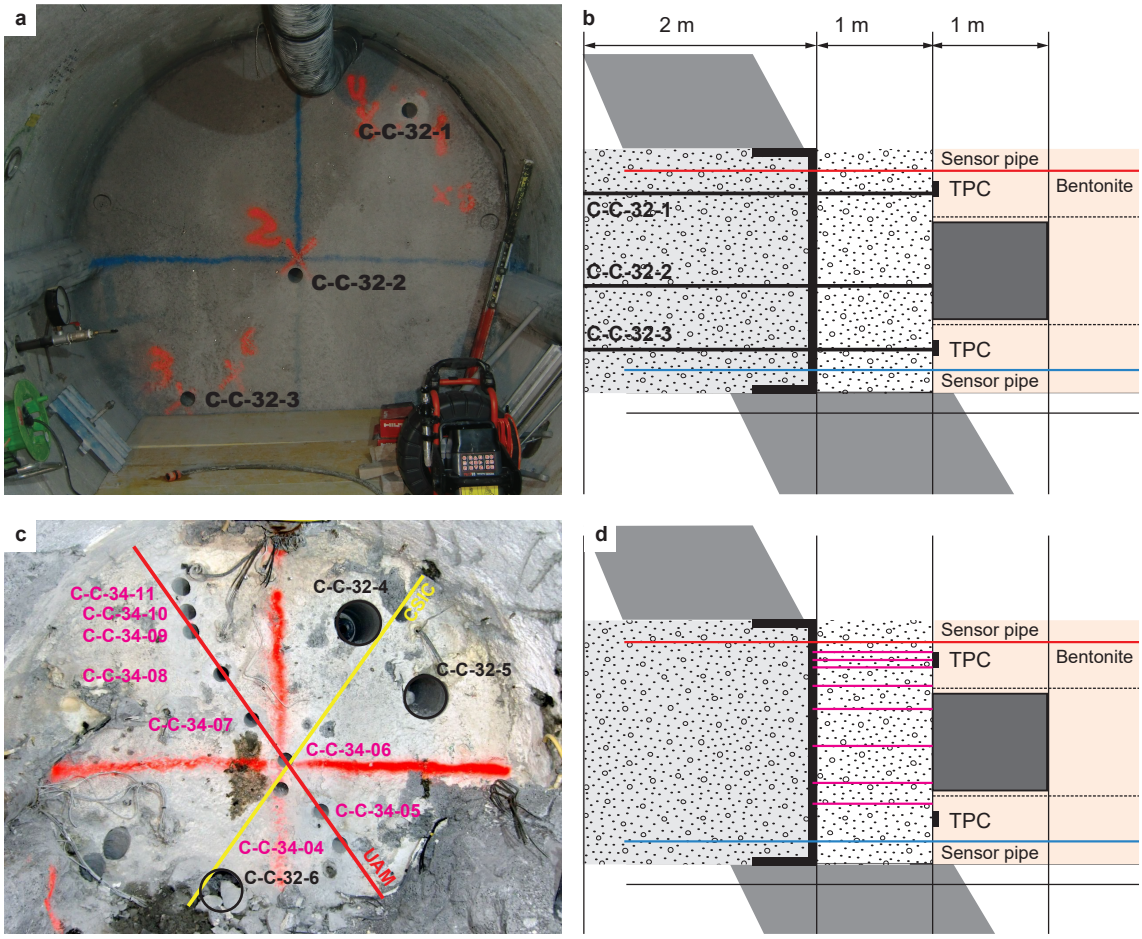


Fig. 5-2: Pictures of sections 32 (a) and 34 (c), both sampling for concrete; (c) shows three large boreholes from interface overcoring; schematic cross-sections of sample locations in section 32 (Fig. 5-2b) and section 34 (Fig. 5-2d)

The analytical methods employed to characterise the samples are summarised in Tab. 5-1.

Tab. 5-1: Concrete, concrete-bentonite and concrete-granite interfaces analysed by the different teams, sections, sample type and methods

Organisation	Section studied	Sample type	Properties studied
CSIC	32	Concrete core	(Water) permeability, mechanical properties, capillary suction, hydraulic conductivity, water absorption, porosity, pore size distribution, microstructure (SEM), carbonation, mineralogy (XRD, EDX, TGA-DTA), pH, soluble ions
UAM	32	Concrete core	Aqueous extracts, C and O stable isotopes, mineralogy, chemical composition, microstructure
	34, 35	Concrete-bentonite core	Carbonation, mineralogy, soluble salt migration, CEC, specific surface area (BET), porosity, pore size distribution
	35	Hand-picked concrete-bentonite	Porosity, specific surface area, soluble salts, CEC, mineralogy
Uni Bern	32	Overcore concrete-bentonite	Macroscopic observations (macro-porosity), texture, temperature, elemental distribution (SEM/EDX), CEC, microstructure and pore network (X-ray computed tomography)
BGR	35	Hand-picked concrete-bentonite	Physical properties, CEC, mineralogy
Ciemat	34, 35	Concrete-bentonite core	Porosity, pore-size distribution, soluble salts, mineralogy, specific surface area
	35	Hand-picked concrete-bentonite	Porosity, specific surface area, soluble salts, CEC, mineralogy
	36	Bentonite block	Porosity, soluble salts
Obayashi	NA	Concrete-granite	Mineralogy, microstructure and pore network (X-ray computed tomography)
	32	Overcore concrete-bentonite	Microstructure, mineralogy, elemental distribution (EPMA), CEC

SEM: scanning electron microscopy, XRD: X-ray diffraction, XRF: X-ray fluorescence, EDX: energy-dispersive X-ray spectroscopy, TGA-DTA: thermogravimetric analysis differential thermal analysis, EPMA: electron probe microanalysis

5.1.3 Concrete evolution

The macroscopic analysis of the concrete cores from Section 32 (see Fig. 4-3) showed the layered structure of the concrete plug, which was caused by the spray application during shotcreting and is particularly prominent in the front section adjacent to the bentonite. The differences in quality between Sections 1 and 2 were already observed immediately after installation of the concrete plug in 2002 – 2003. Samples of the fresh concrete were analysed at that time for compressive strength, which proved to be higher in shotcrete Section 2 than in Section 1. This difference in compressive strength was preserved and observed after the plug dismantling in 2015. Other properties of the concrete cores were investigated (dynamic elastic modulus, water absorption and capillary suction) and confirmed the higher concrete quality of Section 2. The lowest part of Section 1 contained abundant coarse porous layers rich in aggregate resulting from rebound of the spraying action; this zone was water-logged and yielded free outflow into some sampling boreholes, presumably originating from the metabasic dyke.

The differences in accessible and total porosity between the two sections can also be explained by the heterogeneous quality of the sections (Fig. 5-3). In Section 1, the total porosity was higher than in Section 2 and there was a larger number of large pores (0.1 – 5 µm) in Section 1. Finally, the pH of the concrete leachate was observed to be lower in Section 1 compared to Section 2, again indicating the reduced quality of Section 1. The reduced quality of Section 1 could be questioned, as it is unclear whether this observation is due to interaction with the nearby bentonite or to a quality difference. Steel fibres were used in the application of Section 1, but not in Section 2. No oxidation of the steel fibres was observed in preserved samples protected from the atmosphere.

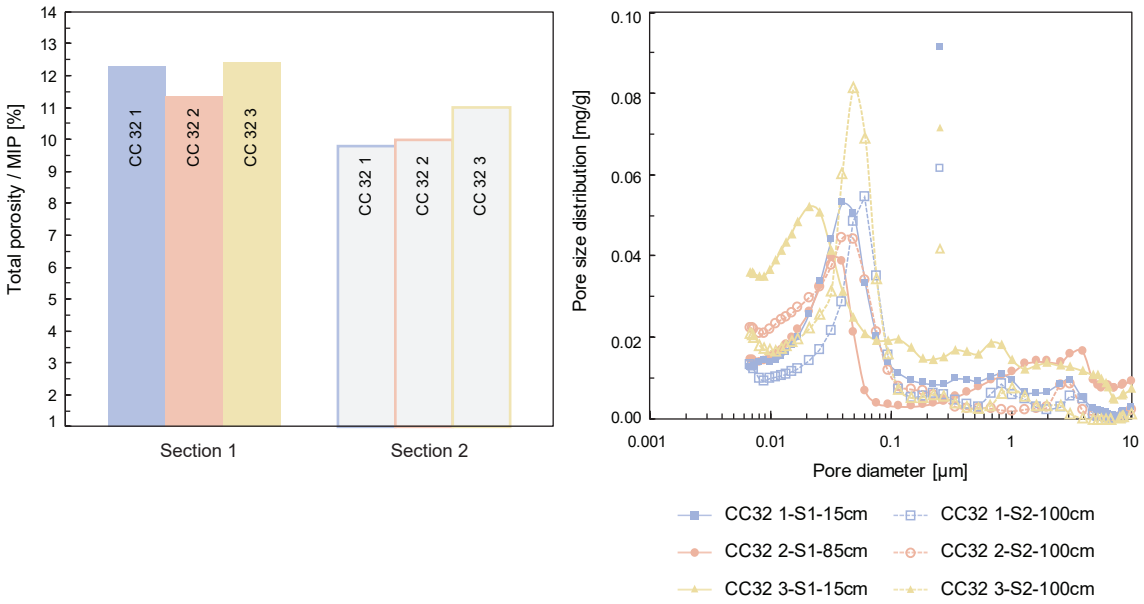


Fig. 5-3: Total porosity (left) and pore size distribution (right) of the samples of core C-C32-2 in both plug sections (Sections 1 and 2)

Samples are shown as a function of location in the plug (C-C-32-1 is at the top, C-C-32-2 is in the middle, C-C-32-3 is at the bottom of the plug, Fig. 5-2). All measurements were obtained by mercury intrusion porosimetry (MIP).

The mineralogy of the bulk concrete changed slightly as a function of distance to the bentonite interface. Portlandite and ettringite could be identified by XRD and showed an inverse relation with distance to the interface. Closer to the bentonite interface and towards the bottom of the concrete plug, the portlandite content decreased, while ettringite increased. A random distribution of calcite was observed, with no observable decrease towards the bentonite interface. Because C-S-H phases are amorphous, they could not be observed by XRD.

The concrete plug not only contacts the bentonite blocks but also the granite host rock. The impact of the granite host rock can be isolated from the concrete-bentonite interaction by analysing cores C-C-32-1 to C-C-32-3 from Section 2 of the concrete plug, which is further away from the bentonite interface. The porewater pH, portlandite content and porosity of the cores showed no significant differences between the cores from the middle compared to the cores close to the tunnel wall (see also Fig. 5-3). Some ettringite formation, calcium and potassium leaching were the only indicators that indicated an impact of the granite on the concrete in the lower part of the plug.

5.1.4 Alterations at the concrete-bentonite interface

The concrete-bentonite cores were of very high quality and succeeded in preserving the concrete-bentonite interface (Fig. 5-4) without causing fractures or delamination. From the macroscopic observations, a clear layering within the concrete and the bentonite can be observed. The zone of macroscopically visible alteration is approximately 10 mm on both sides. It cannot be clearly distinguished whether the discolouration in the bentonite is caused by the presence of the concrete or whether it is an effect of the ambient conditions to which the bentonite was exposed after the first dismantling and before shotcreting started. The natural heterogeneity and granular aspect of this type of bentonite can also be seen in Fig. 5-4.

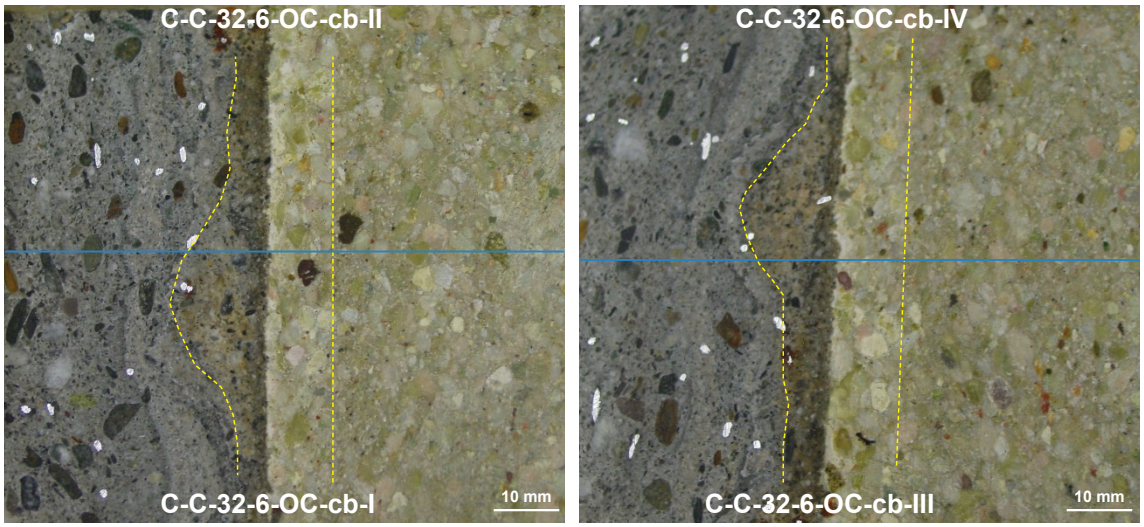


Fig. 5-4: Images of cut surfaces of half cores from C-C-32-6-OC-cb viewed through a liquid epoxy layer

Yellow lines indicate visible alteration areas within the concrete (material on the left side of the interface) and in the bentonite (material on the right side of the interface). Blue lines indicate subsequent cuts to produce quarter cores. Field of view is around 60 × 75 mm. Glossy components in concrete represent steel fibres.

Physico-chemical parameters

The porosity and pore size distribution were analysed at and across the concrete-bentonite interface. Mercury intrusion porosimetry (MIP) was used to measure the interparticle porosity (macropores and mesopores) on dried samples (Fig. 5-5). The number of micropores which could not be intruded by mercury was calculated by subtracting the MIP-measured void ratio from the actual void ratio calculated from the dry density of the sample. Within the bentonite, the porosity was 42.7 ± 0.7%, which is very similar to the bentonite reference porosity (42%, at 1.55 g/cm^3 dry density, Fernández & Rivas 2005; Villar et al. 2018a, see Section 5.3). Only the sample closest to the granite showed a higher total porosity in the bentonite (56.8 ± 2.6%, BC-C-35-2 in Fig. 5-5). While the number of mesopores[6] remained constant as a function of distance to the granite interface, the number of macropores decreased and the number of micropores increased towards the interface.

A similar pattern of porosity distribution was found in the concrete and also here, samples closest to the granite exhibited an increased inter-particle porosity (39% vs. 10%, see Fig. 5-5). The porosity measurements within the concrete might, however, not be very representative of the processes at the concrete-bentonite interface, as the shotcrete was heterogeneous in quality from the start. Furthermore, the number of samples used for this analysis is relatively small.

An insight into the spatial heterogeneities and micro-texture of the concrete-bentonite interface was obtained from X-ray computed tomography (X-ray CT). Only a few fissures along the interface were observed, which were probably induced by sample preparation and drying. Within the bentonite, drying/shrinkage cracks with different apertures from a few hundred microns to a millimetre were observed. The largest cracks were observed at the interface, but many cracks were also found in the bulk region. From the CT scans, it could be seen that the cracks were connected in a network (up to 1'000 micron in length) and that the cracks were not preferentially oriented. Within the concrete, an irregular distribution of aggregates and pores (no cracks) was identified. The pores in the concrete were possibly created by air entrapment during installation.

[6] Macropores > 50 nm, mesopores 6 – 50 nm, micropores < 6 nm

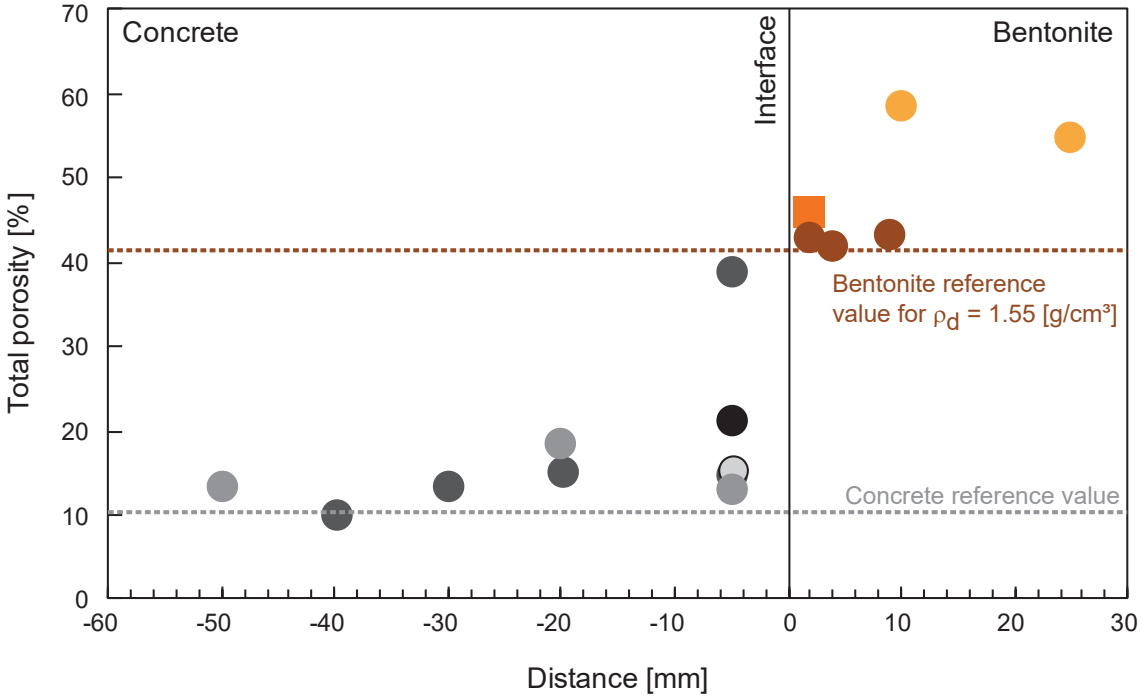


Fig. 5-5: Total porosity (MIP) of the concrete and the bentonite as a function of distance to the interface in dry-drilled samples C-C-34-10 and 12, BC-C-35-1 and 2, BC-S-35-3 and B-B-36-7

Average reference values for concrete and bentonite are plotted for comparison purposes. Varies color codes reflect different samples (see Turrero & Cloet 2017)

Mineralogical changes

The pH gradient between concrete and bentonite/granite is the driving force for starting the interactions that follow. Thanks to the large cation exchange capacity of the clay minerals, bentonite can partially buffer the incoming alkaline solution, but some minerals are nevertheless dissolved. Vice versa, the bentonite porewater (pH = 7 – 8) has a pH-neutralising effect on the concrete (pH = 12 – 13), which destabilises portlandite, C-S-H phases and ettringite, and concurrently releases calcium and provides magnesium. Together with the incoming bentonite/granite porewater, which contains carbonate, calcium precipitates as $CaCO_3$ at the interface. Isotope analysis showed that the precipitated carbonates at the granite interface indeed preferentially contained lighter carbon (^{12}C related to meteoric water), while lighter carbon at the bentonite interface seems to be preferentially dissolved. This suggests that the precipitated carbonate at the granite interface originates from the inflowing granite groundwater, while carbonates at the bentonite interface are formed by carbonate from the bentonite porewater. Precipitation of $CaCO_3$ particles in the nanometre to micrometre scale occurs preferentially at the bentonite interface. Small quantities of calcite precipitation within the bentonite are observed as well. TEM (transmission electron microscopy) analysis further suggested that recurrent recrystallisation at the interface might occur, as both aragonite and calcite were found.

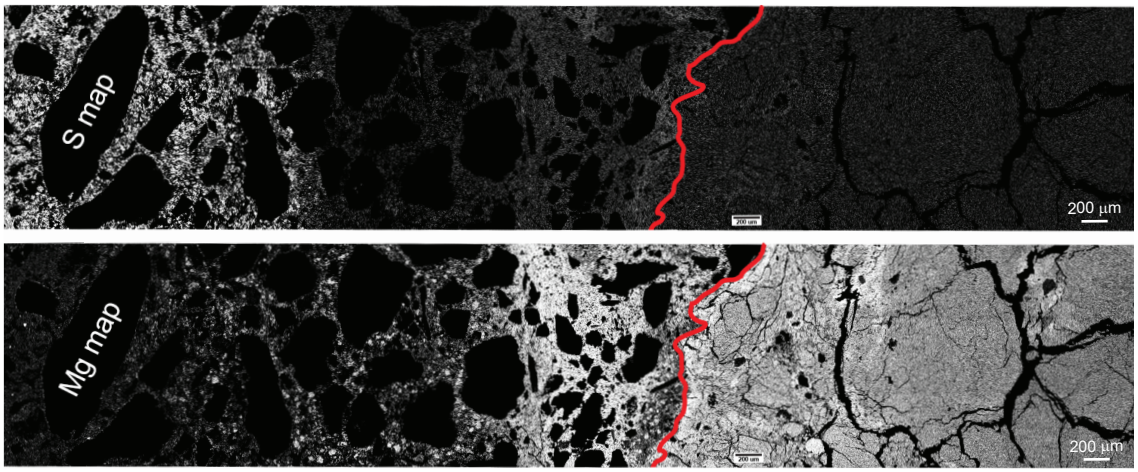


Fig. 5-6: SEM-EDX elemental map for S (top) and Mg (bottom)
Concrete is on the left, bentonite on the right side of the interface (red line).

The $CaCO_3$ precipitation at the interface is at the same time linked to the decalcification within the concrete. A region of approximately 3 mm from the interface contains less Ca and Si, leading to a reduced Ca activity in that region. In CT imaging, a faint zone with higher attenuation is seen surrounding bentonite granules, and this correlates with the Ca distribution observed in element mapping. Calcium is transported further into the bentonite, where it competes with the cations on the cation exchange sites of the clay minerals. Following this influx of Ca, magnesium, which occupies initially approximately 30% of the cation exchange capacity (CEC), is released from the exchange sites. The elevated pH in the bentonite allows the stabilisation of Mg-rich minerals on both sides of the interface (see Fig. 5-6). Various analytical tools (SEM-EDX, EPMA, FTIR (Fourier transform infrared spectroscopy), TGA, DTG (derivative thermogravimetry)) suggested a precipitation of an (Al-poor) Mg-silicate, which could be magnesium-silicate-hydrate (M-S-H) or some layer-structured silicate. The analysis of the hand-picked sample by simultaneous thermal analysis (STA), XRD and Rietveld refinement suggested the formation of brucite or another Mglayered phase. Mg-enrichment can be seen up to 1 – 3 mm on both sides of the interface. Further support for Mg-enrichment and precipitation is provided by the low Mg contribution to the measured CEC in this area. An inverted distribution of Ca and Mg was also observed in the bentonite surrounding the heater (see Section 5.2), where Ca accumulated towards the granite interface and Mg content in bentonite increased towards the heater. As there is no pH increase at the heater, no Mg-silicates precipitated, but Mg is accommodated on the clay exchanger.

In the first 3 – 4 mm of the bentonite, the smectite content was reduced, as observed by XRD, Rietveld refinement, reduction of CEC and SEM-EDX. The CEC was reduced from 98 meq/kg to 85 meq/kg on average and locally at the interface even to 55 meq/kg. The released Si and Al then react with the incoming Ca from the concrete to form calcium aluminate silicate hydrates (C-A-S-H) phases on both sides of the interface. The C-A-S-H phases could also explain the large specific surface area that was measured (BET analysis, following the Brunauer-Emmett-Teller method of adsorption of an inert gas). Besides these phases, also secondary ettringite ($3CaO{\cdot}Al_2O_3{\cdot}CaSO_4$) is formed in the voids of the concrete. As the Ca activity in the concrete is reduced at the interface due to the decalcification, the initially present ettringite is destabilised, and a thin layer depleted of sulphur is found in the concrete (2 mm). However, further away from the interface, the Ca activity is sufficiently high again, and secondary ettringite may recrystallise

in some of the concrete voids. Ettringite was also observed on the bentonite side of the interface, where the Ca activity is also higher. Several different crystal shapes of ettringite have been observed by SEM-EDX (nodules, elongated needles, fibrous needles, see Fig. 5-7).

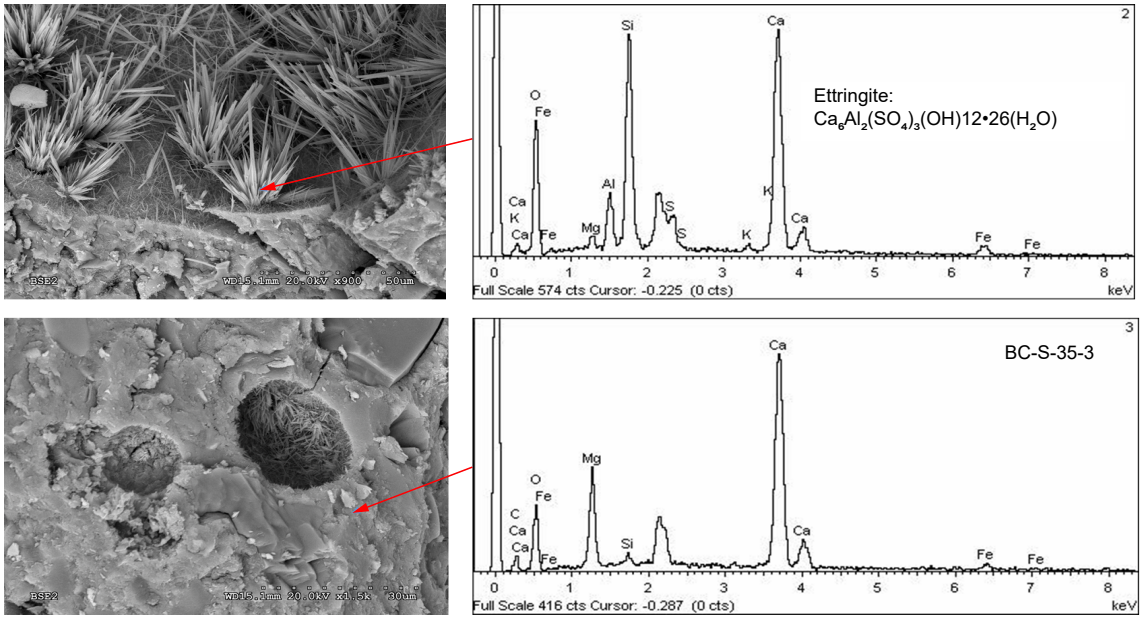


Fig. 5-7: SEM images of concrete scraped from the bentonite surface in the BC-S-35-3 sample (UAM)

Ettringite precipitation in the concrete pores can be observed. EDX analysis of the concrete paste around the pores (red arrow) shows significant concentrations of Mg in addition to Ca.

Further changes in the chemical composition of the concrete-bentonite interface include the redistribution of aqueous ions such as potassium, sodium and chloride. The cation exchange sites were increasingly occupied by K^+, whereas Na^+ remained the same or decreased slightly. A strong migration of Cl^- towards the concrete was observed, where it precipitated as Friedel's salt and could be found up to 5 cm from the interface. Increased quantities of Friedel's salt were found towards the lower half of the plug. In the bentonite buffer surrounding the first heater (which was dismantled and replaced by a dummy), a reduced chloride content was linked to the precipitation of NaCl at the heater (see Section 5.3 and Villar (2017)). From the available information, it is difficult to determine whether the reduced Cl content at the concrete-bentonite interface is influenced by the heater or only influenced by the nearby concrete.

When considering the variations of the elements across the concrete-bentonite interface, it is important not to misinterpret porosity changes, natural inhomogeneities of the bentonite or the layering of the shotcrete for interaction-driven element transfers. A comparison with the porosity map or a normalisation of the elemental distribution could be a help to distinguish the two processes.

5.1.5 Interactions at the concrete-granite interface

The mineralogical changes at the interface between the concrete and the granite were investigated by XRD-CT on two different samples. The first sample originated from the concrete plug surrounding the previously dismantled Heater #1 (2002). The remaining concrete in this sample had been exposed to air for 13 years and was thus rather desiccated. Besides the shrinkage due to drying of the concrete, calcite and illite were formed as a result of the alkaline interaction with the granite. The second sample of the concrete-granite interface was taken from the concrete plug after the dismantling of Heater #2 (2015 in FEBEX-DP) and showed no signs of desiccation. The concrete exhibited a high porosity, which could be related to the lower quality of Section 1 of the concrete plug. Calcite was also found at the interface, but illite was not observed.

5.1.6 Impact on long-term safety – a concrete perspective

The extent of the interaction zone after these 13 years of interaction after plug installation is limited to 40 mm (Friedel's salt, portlandite, ettringite) within the concrete and 4 mm (Mg-minerals, smectite, CEC) within the bentonite. The mineralogical changes in the bentonite did not lead to any observable changes in safety-relevant properties such as dry density and swelling pressure. These are key parameters related to the safety function of the bentonite barrier for long-term safety. Sufficiently high dry densities are also needed to restrict microbial activity near the canister. It could thus be concluded that, after 13 years of interaction, no safety-relevant properties of the bentonite were affected and that the concrete-bentonite interaction therefore has no safety-relevant impact. However, some mineralogical changes in the bentonite did occur, such as limited smectite dissolution and the change of cations at the exchange sites. The impact of a changing cation population on the exchanger, which potentially extended much further than the analysed sample size, on the long-term behaviour of clay minerals should be further explored.

The concrete, on the other hand, experienced more significant changes, such as increased porosity, mineral changes and a lower compressive strength, some of them due to macroscopic heterogeneity related to shotcreting. Depending on the functionality of the concrete in the repository layout (as a plug, a barrier or a support structure), these mineralogical changes might be safety-relevant. These aspects should be considered accordingly in the design assessment of the long-term safety of the repository.

5.1.7 Lessons learned, remaining questions and recommendations

Each of the seven research partners applied one or more analytical tools to identify the dissolved or precipitated minerals at the concrete-bentonite interfaces and the related properties. Reassuringly, the results obtained by the different analytical tools agree well and correlate with concrete-bentonite studies from other laboratory and in-situ experiments. The latter might be surprising, as each experiment uses different clays or cement types. Even though some differences do exist, the general trends are identical, which indicates that the major processes governing the interaction are similar and transferable between the various experiments.

The impact of the heater on the concrete-bentonite interaction could not be elucidated by the FEBEX-DP experiment. The heater was – relatively speaking – too far away from the concrete-bentonite interface and did not lead to a significantly higher temperature (28 – 29 °C were measured after overcoring directly at the interface while Heater #2 was still switched on). The chloride migration in the bentonite towards the concrete was suggested to be enhanced by the heating, but this region experienced a complex thermal history during the first phase of the FEBEX experiment. This remains an open question, as it would mean that some phenomena and processes did indeed extend beyond the analysed sample size and that, within 13 years of interac-

tion, a distance as far as 2 metres was influenced by an acting gradient. It is expected that in the FEBEX-DP experiment some cation exchange effects (Ca-Mg competition) might have occurred beyond the analysed sample size.

In a next step, the insights and data collected in this experiment should be used to improve reactive transport models. For example, given the importance of the coupling between porosity/permeability and solute transport/reactivity, the acquired data on microstructure and pore network could be used to support reactive transport models. Understanding the porosity evolution in both concrete and bentonite will be needed to predict how far the interaction front moves forward at any given time.

5.2 Buffer on-site analysis and laboratory tests (NAB 16-12)

5.2.1 Physical state of the barrier determined on site

Buffer removal and sampling took place between May and August 2015. Numerous bentonite samples were taken in selected sections evenly distributed along the gallery (Fig. 5-8) for the on-site determination of their dry density and water content. Samples were obtained according to a predetermined sampling scheme by positioning a template and by using a crown drill bit (Fig. 5-9). In the sections around the liner, six samples were taken along each radius and, in those without liner, ten or eleven samples were taken along each radius. The samples had a length of 6 cm and a diameter of 4.8 cm. They were immediately wrapped in plastic foil and taken to the on-site laboratory (see Section 1.3), which was located at the start of the laboratory gallery at the northern end of the GTS. Care was taken to cause as little disturbance as possible to the recovered samples.

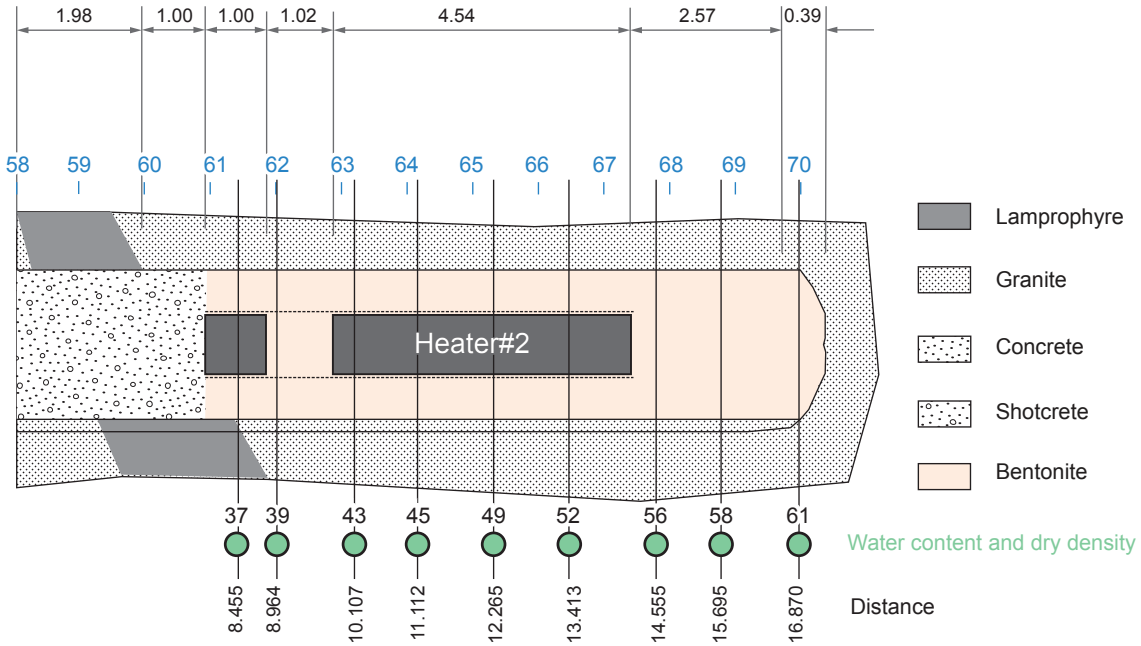


Fig. 5-8: Location along the gallery of the sampling sections used for determination of bentonite water content and dry density on-site

Once in the on-site laboratory, the samples were cut and trimmed into two sub-samples, each of which was between 5 and 37 cm^3 in volume (average volume 18 cm^3) with masses of between 10 and 75 g (average mass 35 g). The external part of the sub-samples that had been in contact with the crown drill bit was removed and the surfaces smoothed. Water content and dry density were determined in each of these sub-samples. The gravimetric water content (w) is defined as the ratio between the mass of water and the mass of dry solid expressed as a percentage. The mass of water was determined as the difference between the mass of the sample and its mass after oven-drying at 110 °C for 48 hours (mass of dry solid). The precision of this measurement is about 0.2%. Dry density (ρ_d) is defined as the ratio between the mass of the dry sample and the volume occupied by it prior to drying. The volume of the specimens was determined by immersing them in a vessel containing mercury and by weighing the mercury displaced, considering a mercury density of 13.6 g/cm^3 for the calculation of volume. The precision of this measurement is between 0.01 and 0.02 g/cm^3. For the determination of water content, the same samples were used whose volume had been determined (García-Siñeriz et al. 2016, Villar et al. 2016).

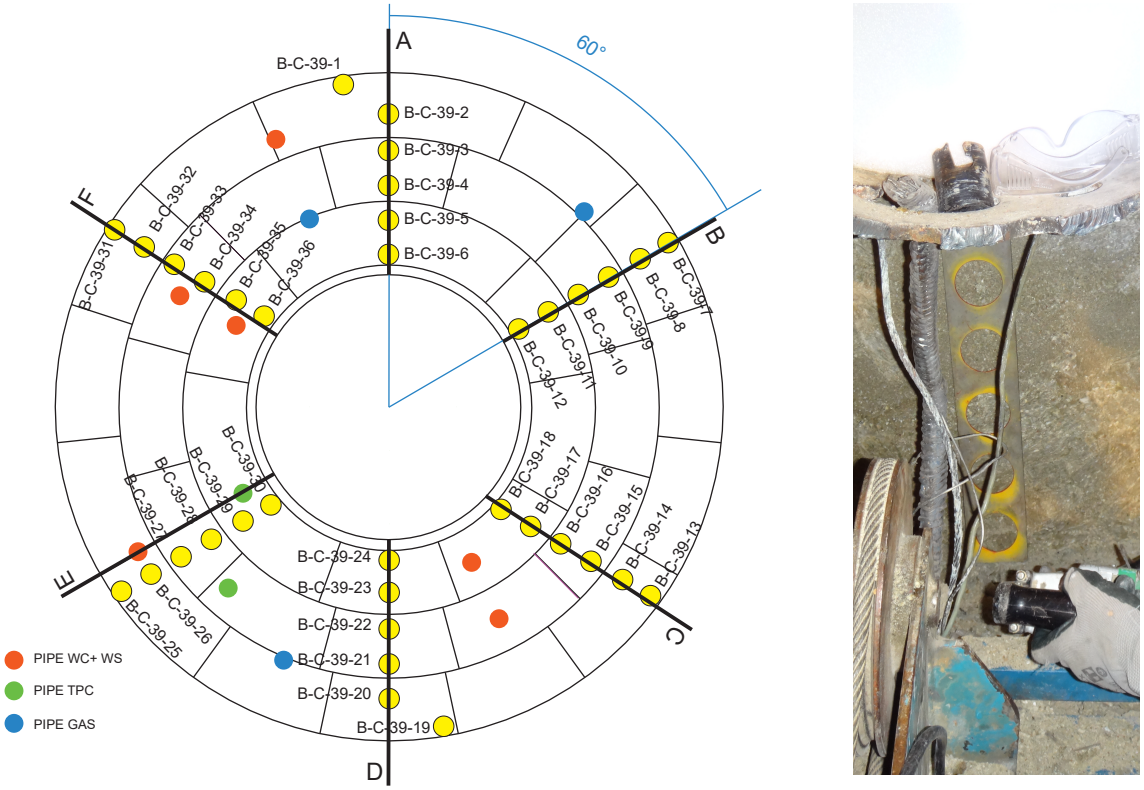


Fig. 5-9: Position of sampling radii in a section and photo of the template used to locate the drillings and the crown drill bit

Example for dismantling Section 39 (Bárcena & Siñeriz 2015a)

Additionally, the dimensions of some blocks were measured, as well as the x-coordinate changes for the block sections.

The results obtained were analysed in detail in Villar et al. (2016) and are summarised in the following sections. Basically, the on-site measurements showed that the physical state of the barrier after 18 years of operation was very much affected by the processes to which it had been subjected, namely hydration from the granite and redistribution of water by the thermal gradient.

5.2.2 Changes in the barrier during dismantling

The bentonite dismantling operations took three months and started after the heater had been switched off for 24 days. The temperatures in the barrier during operation of the experiment were between 100 °C and 36 °C in the sections around the heater (see Section 2.3). Upon switching off the heater, the temperatures dropped to values below 30 °C at all points in the barrier and were mostly around 20 °C when actually dismantled. This temperature change had an impact on the water distribution around the heater, where water in the vapour phase might have condensed because of cooling. Since the inner part of the barrier closest to the heater was not fully saturated, water movement from the outer, saturated part of the barrier toward the drier middle part cannot be ruled out, which would have been driven by the suction potential. Hence the bentonite state in terms of water content observed upon dismantling did not exactly reflect the state of the barrier during operation. Coupled THM modelling to assess the influences of these redistribution processes is discussed in Section 7.3.

In addition to temperature changes, other processes may have occurred between the heater shutdown and the onsite measurements that would need to be identified, evaluated, and considered in a conclusive assessment of the condition of the barrier at the time of removal:

- The water content of the bentonite in contact with the liner was probably lower during operation than the values measured during dismantling because of the water transfer caused by cooling. Conversely, but with similar reasoning, the water content of the middle barrier ring in these areas could have been higher than measured.
- Core drilling and sub-sample trimming could introduce a decrease in dry density that would affect all the samples, but particularly those with higher water content. Hence, the overall as-built dry density of the barrier was slightly higher than that measured. Consequently, the degree of saturation would also be higher than indicated by the measurements.
- The dry density and degree of saturation of the front sections may have been higher during FEBEX operation than those measured because of the decompression and expansion of the bentonite experienced upon plug demolition.

5.2.3 Radial symmetry

The water content and dry density in every section followed a radial distribution around the axis of the gallery, with the water content decreasing from the granite towards the axis of the gallery and the dry density following the inverse pattern. These effects were identifiable as lighter block colours in the inner ring of the barrier, which were an indication of its lower water content. However, the state of those sections around the heater (Fig. 5-10) was different to the state of the cold sections placed towards the back of the gallery (Fig. 5-10) and of those that were subjected to a thermal gradient during the First Operational Phase but were cool during the Second Operational Phase. This aspect is further analysed in Section 5.2.5. The water content and density gradients were more noticeable in sections affected by the heater, although the water content at all points in the barrier, even those close to the heater, was higher than the initial one, i.e. greater than 14%.

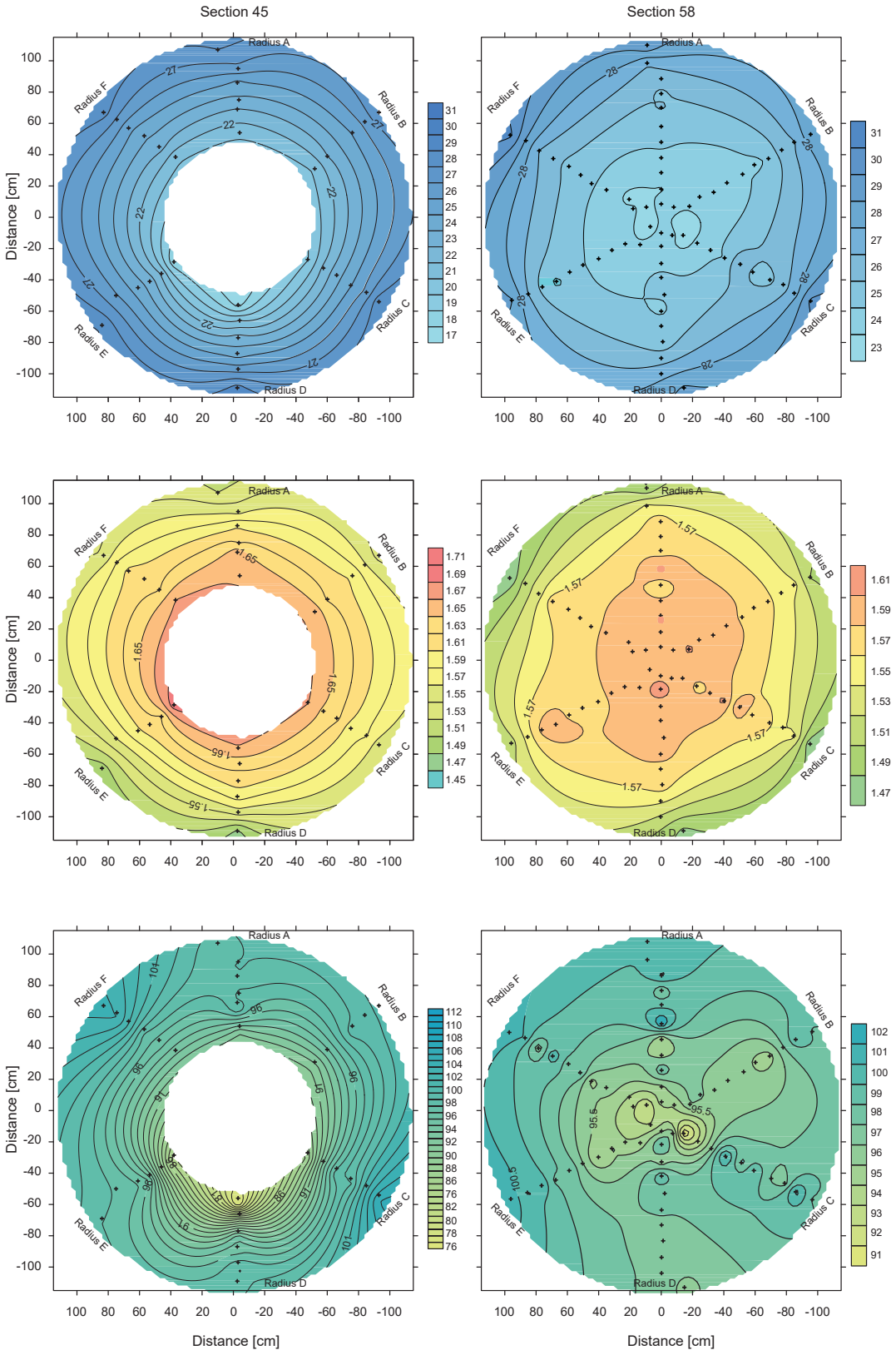


Fig. 5-10: Contour maps for water content, dry density and degree of saturation in a section around the heater (S45) and in a "cold" section (S58): water content (%, upper panel), dry density (g/cm^3, middle panel) and degree of saturation (%, bottom panel)

In most sampling sections, the differences between the six sampled radii were negligible, especially with respect to water content, which is the cause of the clear radial symmetry. Natural features (lamprophyre, fractures) or artifacts (filter paper, plastic sheeting, the latter to prevent early damage to the blocks due to water leakage from the rock during placement) that could potentially alter the water input to the bentonite therefore had no systematic effect on the water content distribution in the buffer and would likely only be found in a few locations

Consistent with the observed water content and dry density distributions, the radial dimensions measured on the surface of the blocks during dismantling usually indicated the expansion of the outer and middle bentonite rings and the compression of the inner one. The radial dimension of the blocks decreased from the outer ring to the inner ring all along the gallery, but particularly around the heater where the radial dimension of the outer ring increased notably with respect to the initial one, whereas the inner ring exhibited the strongest shrinkage (Fig. 5-11). The reduction of the radial dimension of the inner ring could have been enabled by the intrusion of bentonite through the liner holes (Fig. 4-12).

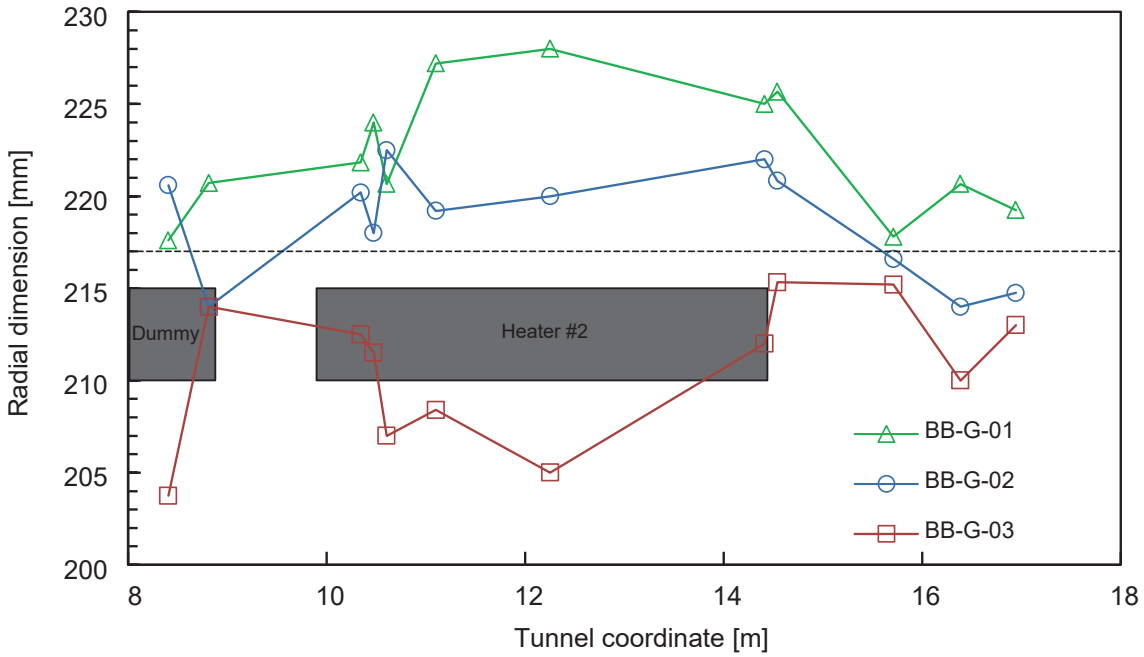


Fig. 5-11: Radial dimension of different types of blocks measured along the gallery on dismantling

The dotted line shows the initial dimension ('c-axis' in Tab. 1-3, see Section 1.4.1). BB-G-01 – outer blocks, BB-G-02 – intermediate blocks, BB-G-03 – inner blocks,

5.2.4 Role of gaps during the course of the experiment

On removal of the shotcrete plug and exposure of the bentonite slices, it was observed that all the construction gaps between blocks had sealed, both those between blocks of the same slice and the gaps between bentonite slices. This was evidenced by the difficulty found in separating sampling sections. There was no effect of the vertical gaps between bentonite slices on the water content and dry density distribution. Also, the granite/bentonite contact was tight at all locations, and the gaps carved in the blocks for passing through cables had been completely filled by the swelling of the bentonite (Fig. 5-12). This had already been observed during the partial dismantling in 2002

(see Section 1.1.4). The water availability at the test site (both in the liquid and vapour phases) was sufficient to allow quick swelling of the external part of the barrier. In turn, the quick swelling prevented preferential paths remaining open.

These results highlight the expansion potential of the bentonite and its adequate performance for a long period of time, even under a thermal gradient.



Fig. 5-12: Appearance of the bentonite barrier around Heater #2 during installation in 1997 and during dismantling in 2015

Dismantling section 24/bentonite slice 59, see Fig. 1-4.

5.2.5 Longitudinal changes

The uniform distribution of sampling sections along the axis of the gallery allowed longitudinal contour plots of the water content and dry density (Fig. 5-13). These show that the back of the gallery had the highest water contents and the lowest dry densities. The highest dry densities were found around the rear half of the heater and at its lower part, where the temperatures were higher and the water content lowest. Around the dummy canister, dry densities below the average of the barrier were observed. The distribution of water content/dry density corresponds with the observed total pressures (and thus predominantly swelling pressures) being highest at the outer, wetter parts of the experiment (see Section 2.4). Plots of the average water content and dry density for each of the sampling sections show similar patterns (Fig. 5-13).

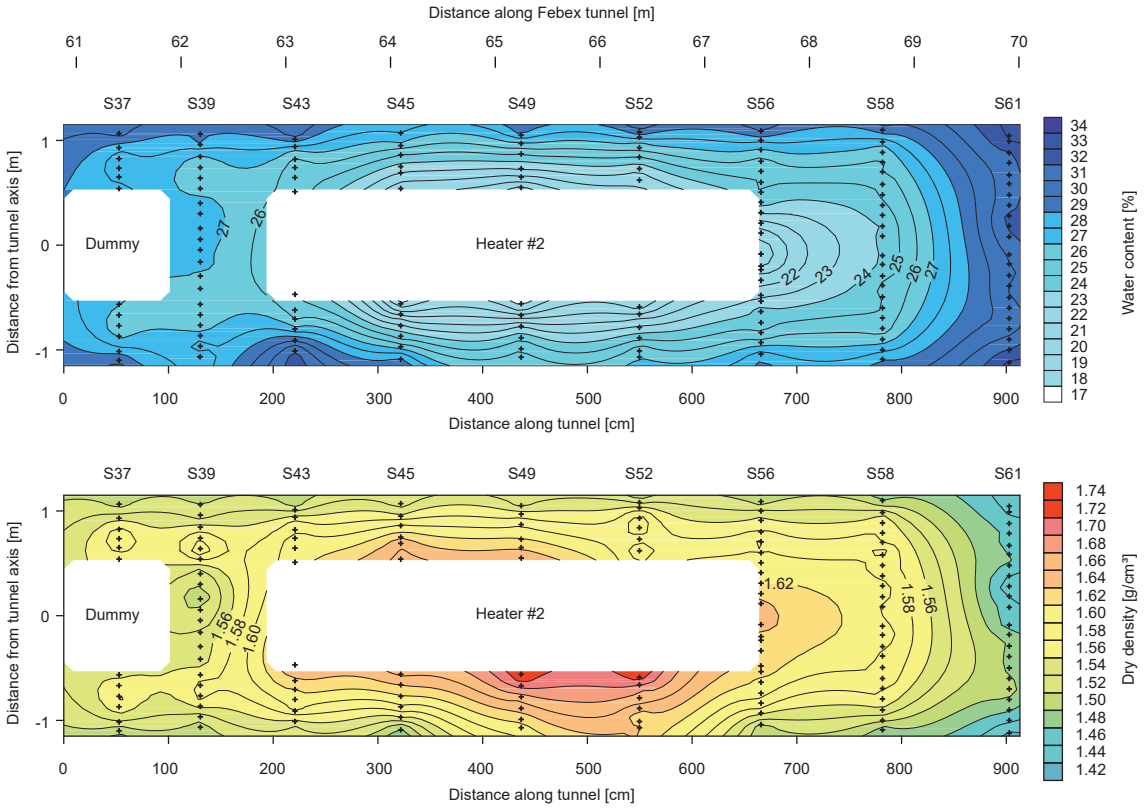


Fig. 5-13: Dry density (top) and water content (bottom); distribution in a vertical longitudinal section

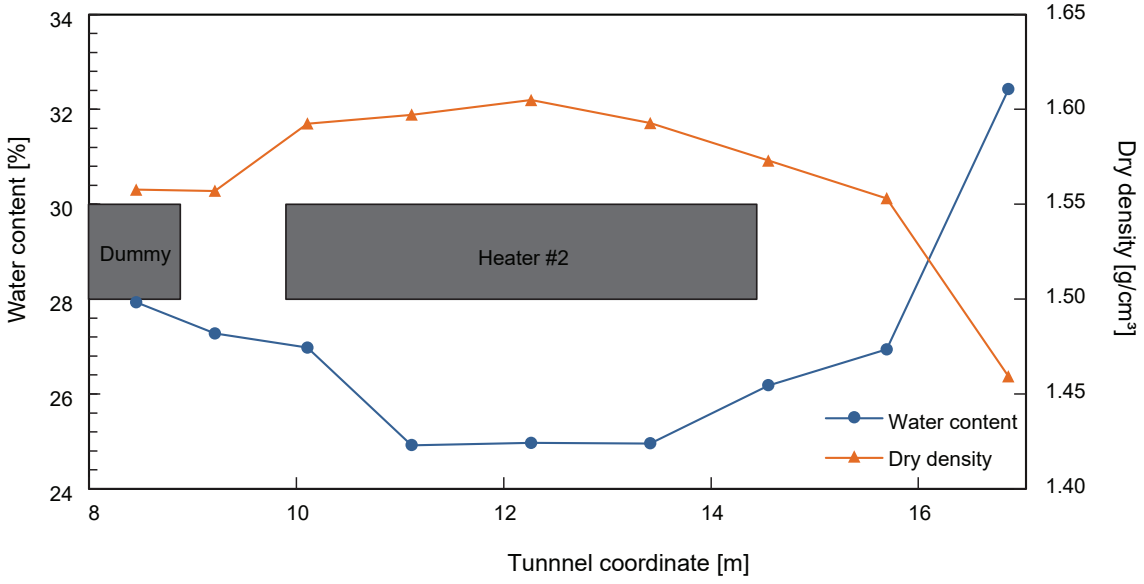


Fig. 5-14: Average water content and dry density for the sections sampled along the barrier

A summary and interpretation of the figures above, which show significant changes in dry density and water content along the axis of the tunnel, is given below:

- The highest water contents and lowest dry densities were found in the rearmost portion of the gallery. This was most probably caused by a larger volume of construction gaps, which resulted in a lower installation density, a condition that, to some extent, remained unchanged until the end of operation. The hydration surface of the first bentonite slice (at the back of the gallery) was larger than for the subsequently installed slices, and this probably contributed to the higher water content observed at the gallery end.
- The highest dry densities were found around the rear half of the heater, where the temperatures were higher and water content lowest.
- Around the dummy canister, dry densities below the average of the barrier were found. This density decrease was related to the displacement of the slices towards the gallery entrance upon plug demolition and pressure release (see below). The bentonite around the dummy canister had also been subjected to a high thermal gradient during the First Operational Phase but it was cool during the Second Operational Phase, which may also have affected its condition. Also, the water from the concrete plug likely contributed to the higher water content of the bentonite slices closest to it.

The best estimates for the final average water content, dry density and degree of saturation of the whole bentonite barrier are 25.5%, 1.59 g/cm^3 and 97%, respectively. The average dry density value is lower than the initial average value given during installation (1.61 g/cm^3). This change can be attributed to a combination of factors: the slight decompression suffered by the barrier on dismantling and sampling, the intrusion of bentonite into the liner (Fig. 4-12) and the sampling and measuring procedures (see Section 5.2.2).

The measurements of the *x*-coordinate of the bentonite slices during dismantling showed that the slices closest to the concrete plug moved towards the entrance of the gallery, which is assumed to have happened as the concrete plug was demolished and the total pressure (about 6 MPa at the concrete/bentonite interface) released. The net forward displacement of the slices decreased towards the back of the gallery. The rear sections of blocks, located beyond the heater, moved in the opposite direction, probably during the operational phases and in response to the less densely installed buffer and construction gaps at the back of the gallery. As a consequence of this longitudinal displacement, the external part of the blocks of the outer ring frequently showed grooves in the direction of the gallery axis, which were caused by friction with the granite, whereas the granite surface was covered with a film of bentonite showing striation parallel to the gallery axis (Fig. 5-15). This gave it an appearance similar to slickensides observed in geological formations.

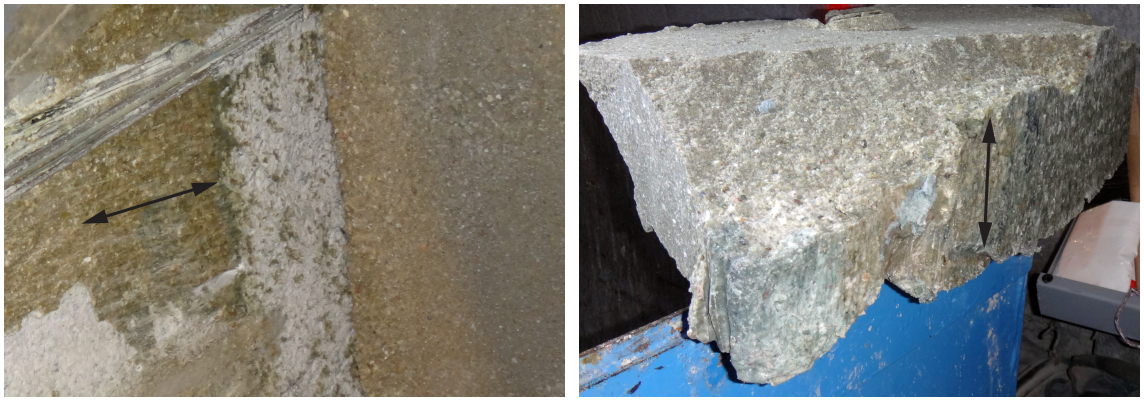


Fig. 5-15: Bentonite adhered to granite showing striation parallel to the axis of the gallery (indicated by an arrow)

5.2.6 Degree of saturation

The degree of saturation tended to be homogeneous and very high in all the sections, with no clear spatial trend, except in those sections around or close to the heater where the degree of saturation decreased towards the heater but was higher than 80% at all points (Fig. 5-10).

In many samples, the degree of saturation was above 100%, which is attributed to using a water density value of 1 g/cm^3 (corresponding to free water) for its computation, whereas most of the water in compacted bentonite is adsorbed water with different properties and assumed higher density. This is further discussed in Villar et al. (2016).

5.3 Buffer/bentonite studies including interfaces (bentonite characterisation and assessment) (NAB 16-17)

During dismantling, numerous bentonite samples were taken in the form of blocks, cores or irregular fragments, carefully vacuum-packed and sent to the laboratories (Fig. 5-16). These samples are called FEBEX-DP or retrieved samples in the discussion below. A detailed summary of the results obtained by different laboratories on the characterisation of the bentonite retrieved during the dismantling was presented in Villar (2017). The aim of the study was to evaluate the effect of temperature and hydration on the properties and characteristics of the barrier and assess the potential changes that occurred during operation with respect to the reference bentonite (ENRESA 1998a). The concrete/bentonite interaction is addressed in detail in Section 5.1 (Turrero & Cloet 2017), and the interaction of the bentonite with the metallic elements of the experiment (sensors, liner, etc.) is specifically analysed in Section 5.4 (Wersin & Kober 2017).

Prior to dismantling, during the 18 years of operation time of the in-situ test:

- The bentonite barrier was hydrated with groundwater coming from the granitic host rock.
- The part of the barrier surrounding Heater #2 – whose surface temperature was 100 °C – had been subjected to a steep thermal gradient for the entire test (see Section 2.3 for information about the temperatures measured in the bentonite during the last part of the test), and experienced an associated redistribution of moisture and consequent swelling-induced heterogeneity (compression of inner ring).

- The bentonite slices at the front of the gallery surrounding the dummy canister were subjected to a thermal gradient during the first five years of operation and then continued hydrating under isothermal, cooler conditions. In addition, the front bentonite slice (sampling section S36) had been in contact with the shotcrete plug constructed after the partial dismantling for the last thirteen years of operation.

To assess the potential changes in the properties investigated that occurred during the FEBEX operation, the values obtained in the FEBEX-DP samples were compared to those of the reference, untreated FEBEX bentonite (ENRESA 2006a). The methods followed by each laboratory were often different, and this had an impact on the results obtained, but in most cases, it was possible to assess how the experimental procedures affected the results.

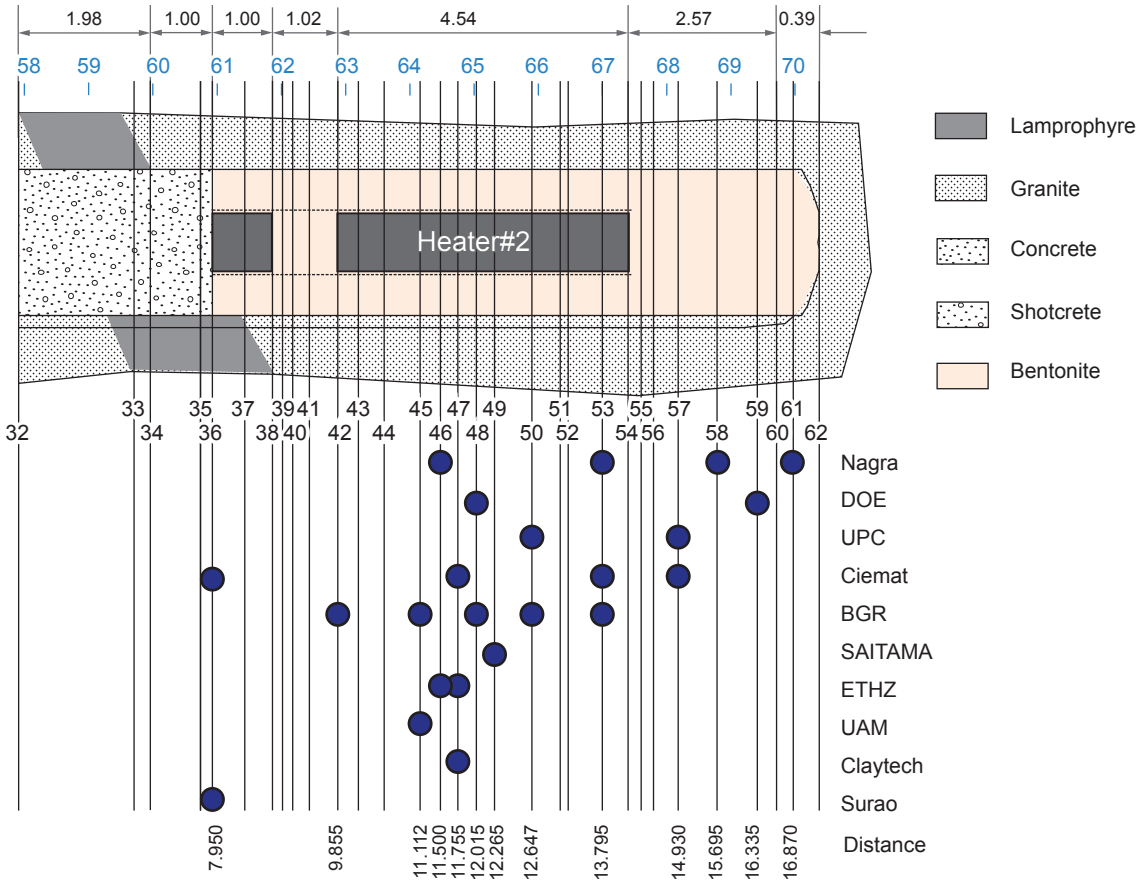


Fig. 5-16: Location of the sampling sections used by each organisation for bentonite characterisation

See location of x = 0 coordinate in Fig. 4-1.

5.3.1 Physical state and microstructure

Most of the laboratories determined the water content and dry density of the samples received before conducting further tests. Despite the large range of time lapses from retrieval at the GTS and sampling in the laboratories, and the different methods used (particularly for the determination of dry density), the values obtained were comparable. The laboratory determinations showed a clear radial distribution pattern: the water content decreased from the granite towards the axis of

the gallery whereas the dry density increased. Hence, the void ratio of the samples (inversely related to dry density) was lower with their proximity to the gallery axis. There was also consistency between the results obtained in the laboratories and on-site tests (see Section 5.2), with the laboratory determinations also reflecting the variations observed in-situ along the gallery. This suggests that the packaging and transport conditions were appropriate for preserving the in-situ state of the bentonite samples even several months after their retrieval.

The water content of all the samples was above the initial condition (14%) and most of them were saturated. To analyse the hydration state from a microstructural point of view, CIEMAT measured the basal reflection (*d*001 value) using X-ray diffraction, which gives a measure of the interlayer distance between smectite particles. All the values were above the initial one (~ 1.48 nm). Most of them were in the range from 1.50 to 1.65 nm, which, despite the changes in the exchangeable cation complex observed (discussed below), corresponded mostly to a completely developed 2-layer hydrate in transition to a 3-layer hydrate. The samples taken at less than 20 cm from the heater with a water content below 25% had lower basal spacings. Above this water content, the basal reflection tended to increase with water content, i.e., as the distance from the axis of the gallery increased. A few samples had basal reflections close to those corresponding to the 3-layer hydrate. The values obtained for the FEBEX-DP samples for water contents below 27% were similar to those measured in FEBEX bentonite samples with the same water content saturated with deionised water.

The water adsorption capacity of the bentonite, analysed by CIEMAT and Clay Technology by determining the water adsorption isotherms of ground samples, remained unchanged for most of the materials recovered. Only those samples closest to the heater showed higher water adsorption capacity for the higher relative humidity. CIEMAT also determined the water retention curves (WRC) in samples trimmed from the blocks, following wetting paths under isochoric conditions (these samples were kept in cells) and using the vapour transfer technique (Campos & Villar 2018). Samples taken from the drier blocks in the barrier were used, i.e., those closest to the heater and those from the core of the barrier in cool areas, since the aim of the tests was to check the effect of prolonged and intense drying on the water retention capacity of the bentonite. The samples closest to the heater reached higher water contents for the lowest suctions than the rest of the samples, which is coherent with the results of the water adsorption isotherms in powder samples and show that the water adsorption capacity was not lost as a result of prolonged drying.

Additionally, the suction of the bentonite blocks was measured by CIEMAT and UPC using psychrometers or capacitive sensors. Consistent with the changes in water content and dry density observed, the bentonite sections around the heater showed a clear increase in suction from the external part of the barrier towards the heater. The materials recovered from the cooler sections showed the same inward increase, but changes were less substantial. WRCs were obtained by relating the suction values measured with the degree of saturation or water content of the samples in which they were measured. For degrees of saturation lower than approximately 95% – corresponding to suctions above 10 MPa − suction decreased logarithmically as the degree of saturation increased. Suction did not drop to zero when the clay approached full saturation. This remaining total suction was mainly a consequence of the block retrieval operation, which had the effect of an undrained unloading on the material. The relationship between suction and water content for suctions below 7 MPa was basically dependent on dry density: the higher the dry density, the lower the water content for a given suction.

The WRCs obtained from suction measurements agreed very well with those obtained with the vapour transfer technique in cells. In addition, the comparison of the WRCs obtained in the retrieved samples with those for the FEBEX reference bentonite compacted at similar densities using different methods shows that there were no changes in the water retention capacity during

operation and that the water adsorption capacity of the bentonite under constant volume conditions is mostly conditioned by dry density (Fig. 5-17). This corroborates the preservation of the water adsorption capacity of the bentonite that the other determinations discussed above had also confirmed.

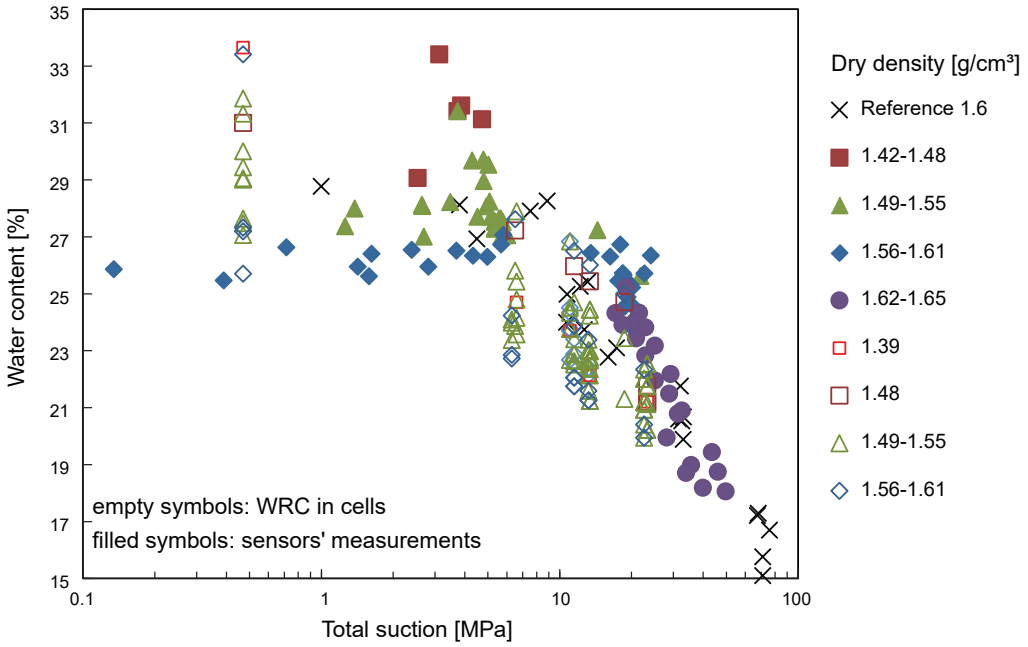


Fig. 5-17: Water retention curves of the reference bentonite compacted at 1.6 g/cm³ (crosses), obtained by measuring the suction of blocks (NAB 16-17, filled symbols) and obtained in cells with the vapour transfer technique

Campos & Villar (2018)

The pore size distribution was analysed by CIEMAT, ETH and UPC using the mercury intrusion porosimetry (MIP) technique. The results obtained by the three groups consistently showed two major pore families in all the samples: a macropore family, with sizes between 10 and 60 µm, and a mesopore family with sizes between 8 and 20 nm. The diameter modes of these families were higher than those for the reference material (which were 17 ± 3 µm and 9 ± 2 nm, respectively), which was probably related to the overall increase in the water content of the bentonite during operation and associated swelling. Although there was not a good agreement in the exact sizes of the pore families determined by the three groups, the results were very consistent in terms of proportion and evolution of each family.

All the MIP results indicated a clear increase in the proportion of void ratio corresponding to pores smaller than 50 nm (mesopores and micropores) at the end of FEBEX (Fig. 5-18). More than 65% of the void ratio corresponded to this pore size at the end of the in-situ test, a notable increase from the original 54%. The reason for these changes is assumed to be the hydration that occurred during FEBEX, which brought about an increase in the percentage of micropores, i.e., those that cannot be intruded by mercury. This agrees with the average increase in interlayer thickness and would point towards the ongoing homogenisation of the pore sizes towards a smaller size range. In the hot sections, the void ratio corresponding to pores smaller than 50 nm decreased towards the heater. In contrast, the void ratio corresponding to macropores decreased

during operation, both in cool sections and in those around the heater. The overall decrease in void ratio towards the axis of the gallery was mostly "absorbed" by the macropores, since the void ratio corresponding to pores larger than 50 nm decreased towards the internal part of the barrier.

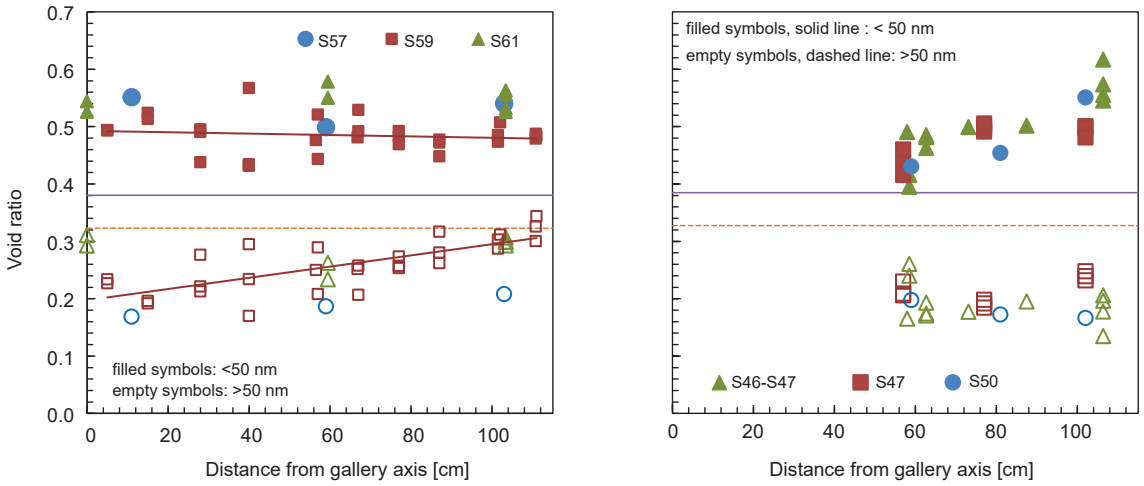


Fig. 5-18: Distribution of void ratio for pore sizes greater and less than 50 nm in samples from cool sections (left) and sections around the heater (right)

The thick horizontal lines indicate the values for the reference FEBEX bentonite compacted at 1.6 g/cm^3 with a 14% water content.

Computerised tomography was used to analyse the texture of the samples at a larger scale than that investigated using the techniques mentioned above. In particular, to study the fracture network of the retrieved bentonite, LBNL used the non-destructive Synchrotron X-Ray Micro Computerised Tomography (SXR-µCT) technique to look at the interior of the sample, in samples as much as possible undisturbed. The samples were found to be permeated by a network of thin fractures that probably had several origins, with sizes in the order of a few tens of microns. Cracks larger than 45 µm were uncommon, but the samples closer to the granite tended to have a larger amount of large fractures compared to the samples close to the heater or to the centre of the section. This observation agrees with the higher proportion of macropores (> 50 nm) found in the MIP analyses towards the gallery wall and suggests that the increase in water content under low stress brought about the creation of larger voids. In contrast, the sample closest to the heater had the largest relative amount of smallest microfractures of all the samples.

The interfaces between blocks were studied at Saitama University using a Microfocus X-Ray Computerised Tomography (MFX-CT) system. The study of the interfaces inside the barrier was motivated by the impacts that unhealed block boundaries might have on density homogenisation, fluid transport, and consequently on the performance assessment of the barrier system. The images clearly showed the interfaces between blocks close to the heater, where conditions were drier. However, the interfaces between blocks recovered from the external, wettest part of the barrier were generally not visible. This indicates that the original block joints had closed up tightly during the long period of water adsorption in the barrier. No significant heterogeneity was observed near the joints.

The external specific surface area, which represents the surface of the intra-aggregate and inter-aggregate voids but not that of the interlayer space, was determined by CIEMAT, ETH and UAM using the BET method. In the FEBEX-DP samples analysed, this parameter was related to the

water content of the samples after dismantling. The BET specific surface areas of samples with a water content above 22% increased slightly with water content but remained in the order of the reference value. Thus, in the cool sections and in the external part of the barrier in sections around the heater, the values found were close to, or slightly higher than, that of the reference value (55 – 56 m^2/g). However, for water contents below 22%, the external specific surface area decreased sharply as water content decreased. The measured external specific surface area dropped to values as low as 22 m^2/g towards the heater (Fig. 5-19). This effect could be attributed to the aggregation of smectitic particles under shrinkage induced by the initial thermal loading of the buffer.

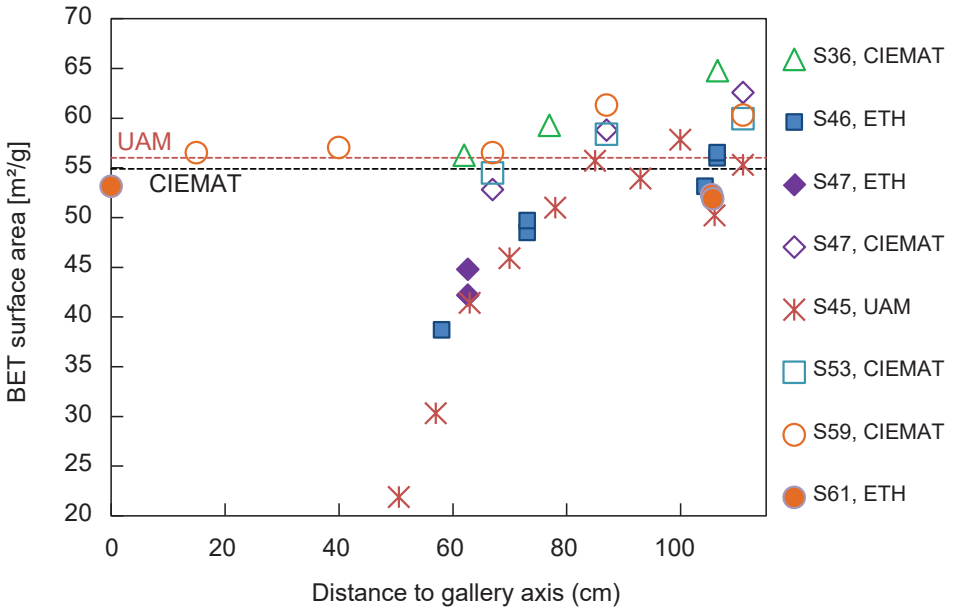


Fig. 5-19: BET specific surface area measured by CIEMAT, ETH and UAM in bentonite samples taken from different sections

The dashed lines indicate the values for the reference sample as determined by CIEMAT and UAM.

The specific weight of the bentonite was determined by CIEMAT in 22 FEBEX-DP samples, and an average value of 2.70 ± 0.04 g/cm^3 was measured, which is the same range of variation as for the reference bentonite. The values determined or used by Clay Technology and Saitama University were within this range.

5.3.2 Mineralogy and geochemistry

5.3.2.1 Mineralogy

The mineralogical composition of the bentonite was determined by CIEMAT, ETH and UAM using X-ray diffraction. Overall, the composition did not change during operation. Depending on the sample and laboratory, the proportion of smectite found was between 82 and 96%, and K-feldspars, quartz, cristobalite, calcite and plagioclase appeared in proportions lower than 5%. ETH also found contents of illite of around 3% in all the samples, whereas UAM found traces of illite in the reference sample and in those samples taken at less than 30 cm from the granite. The acces-

sory minerals detected by CIEMAT in the samples retrieved by SEM were the same as those found in the reference bentonite: carbonates, sulphates, zircon, monazite, biotite, muscovite, ilmenite and apatite.

According to CIEMAT's analyses, the smectite phases were made up of an R0 smectite-illite mixed-layer (R0 meaning that the layering was disordered), with 5 – 23% of illite layers, although most samples had between 5 and 13%. The smectite had a basal reflection around 1.46 nm, which is typical of a predominantly divalent montmorillonite. The crystal thickness of the smectite particles ranged between 7.65 and 10.31 nm, and the number of TOT (tetrahedral-octahedral-tetrahedral) layers in the quasicrystals was 5 – 6. The smectite particles prior to and after the FEBEX in-situ test could be classified as low-charge smectites, with the location of the charge mainly in the octahedral sheets. The mean layer charge of the retrieved samples determined by three laboratories (CIEMAT, UAM, ETH) was on average 0.37 MLC/hfu (mean layer charges/half unit cell), the same as for the reference bentonite. The structural formulae of the smectite in the samples retrieved did not show any changes with respect to those of the reference bentonite, with substitution in the tetrahedral sheets between 5 and 15% that confirmed their classification as Wyoming-type montmorillonites (Tab. 5-2). Hence, the results of all these analyses indicate that no structural changes took place in the montmorillonite during FEBEX operation. The crystal-chemical analyses performed by UAM showed a subtle increase in layer charge of the montmorillonite towards the heater, but no evidence of illitisation.

Tab. 5-2: Structural formulae calculated from the chemical analyses of the < 2 μm grain size fraction of the samples (number of samples analysed in parentheses)

Sample	Structural formula
FEBEX ref [a] – CIEMAT	$(Si_{3.94}Al_{0.06})^{IV}\ (Al_{1.35}Fe^{3+}_{0.21}Mg_{0.49}Ti_{0.01})^{VI}\ O_{10}(OH)_2\ X_{0.29}$
Average retrieved [b] (16) – CIEMAT	$(Si_{3.96\pm0.01}Al_{0.04\pm0.01})^{IV}\ (Al_{1.35\pm0.01}Fe^{3+}_{0.20\pm0.01}Mg_{0.48\pm0.01}Ti_{0.01})^{VI}\ O_{10}(OH)_2\ X_{0.20\pm0.01}$
FEBEX ref [c] – UAM	$(Si_{3.94}Al_{0.05})^{IV}\ (Al_{1.41}Fe^{3+}_{0.09}Mg_{0.50})^{VI}\ O_{10}(OH)_2Ca_{0.24}K_{0.04}$
Average retrieved [c] (11) – UAM	$(Si_{3.96\pm0.02}Al_{0.04\pm0.02})^{IV}\ (Al_{1.41\pm0.02}Fe^{3+}_{0.09\pm0.01}Mg_{0.50\pm0.02})^{VI}$ $O_{10}(OH)_2Ca_{0.25\pm0.02}K_{0.04\pm0.01}$

[a] not homoionised, [b] Ba-homoionised, [c] Ca-homoionised

5.3.2.2 Solid chemistry

The chemical composition of the different bentonite samples analysed by CIEMAT and BGR did not show significant changes with respect to the reference bentonite (ENRESA 1998a). There was a small apparent increase in iron and calcium and a decrease in sodium.

The general spatial distribution of the elements was relatively homogeneous across the barrier and did not seem to follow any particular trend for most elements. Nevertheless, the magnesium content increased from the granite towards the axis of the gallery, both in the sections around the heater and in the cool sections, whereas the calcium and especially sodium contents increased from the internal part of the barrier towards the gallery wall (Fig. 5-20). These relative changes were probably linked to the changes in the exchangeable cation complex described below.

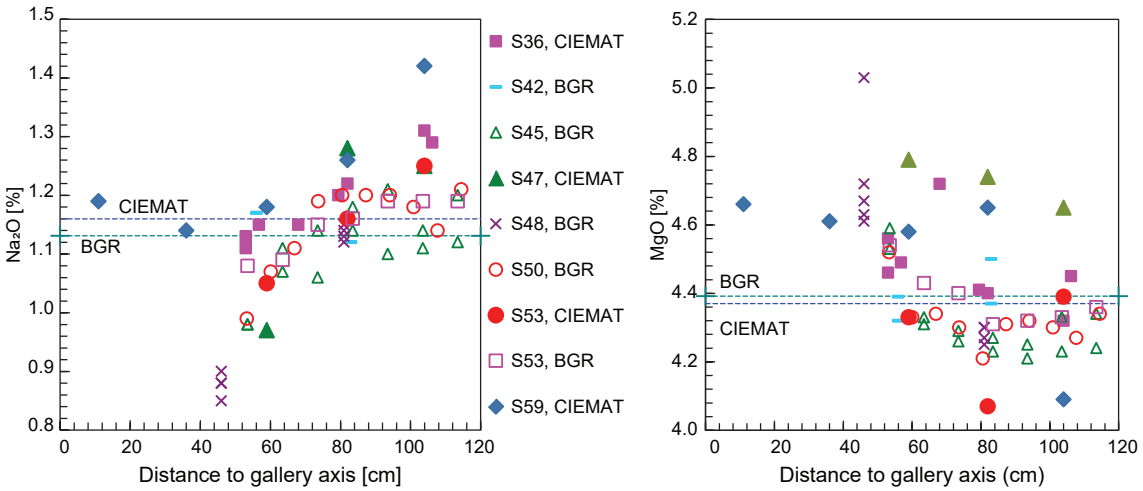


Fig. 5-20: Sodium and magnesium content in bulk samples from different sections analysed by BGR and CIEMAT

Horizontal dashed lines indicate the reference values.

Among the trace elements, the increase in chlorine from the granite towards the gallery axis was clear, and agreed well with the soluble salts analyses, which also showed an increase in chloride towards the internal part of the barrier (see next section, Fig. 5-22). The fluorine content, probably coming from the granite groundwater (see Chapter 9, Garralón et al. 2017), exceeded the reference value overall.

Most of the carbon measured was inorganic and seemed to be related to the calcite content. The total carbon content increased from the axis of the gallery towards the granite, particularly in the sections around the heater. However, microorganisms and organic matter were observed by SEM in samples from the outer and middle rings of some bentonite sections, i.e., in the wettest part of the barrier, although it was not possible to assess if these were living or viable microorganisms. In this context, the microbiology studies showed that cells could be cultivated in large numbers in the samples from moist, low temperature positions of the barrier (see Section 5.5, Bengtsson et al. 2017a).

The results of CIEMAT for the cation exchange capacity showed an overall decrease with respect to the reference value: the retrieved samples had CECs from 89 to 100 meq/100 g (average 95 ± 2 meq/100 g), whereas the reference value is ~98 meq/100 g. Despite the uncertainty of the analytical methods and the differences among laboratories (CIEMAT, BGR), no spatial trends

were found for this property. The assumption that a slight decrease in CEC took place is supported by the overall decrease in exchangeable cation positions (as determined by the sum of exchangeable cations). The sodium concentration in the exchange complex decreased towards the internal part of the barrier, particularly in the heated sections (Fig. 5-20, left). The distribution of exchangeable magnesium and calcium was affected by temperature, since it was quite homogeneous in the cool section S59, whereas the exchangeable magnesium concentration increased towards the heater (Fig. 5-20, right), as did that of calcium in the hottest section S47. Hence, both exchangeable calcium and magnesium responded to temperature, which is probably related to the temperature dependence of the ion exchange selectivity coefficients. The fact that the exchangeable sodium content decreased towards the heater, while exchangeable magnesium and calcium contents increased, made the exchangeable complex more heterogeneous towards the heater. The concentration of exchangeable potassium was higher overall than the reference value, and this consistent with the observed decrease in CEC.

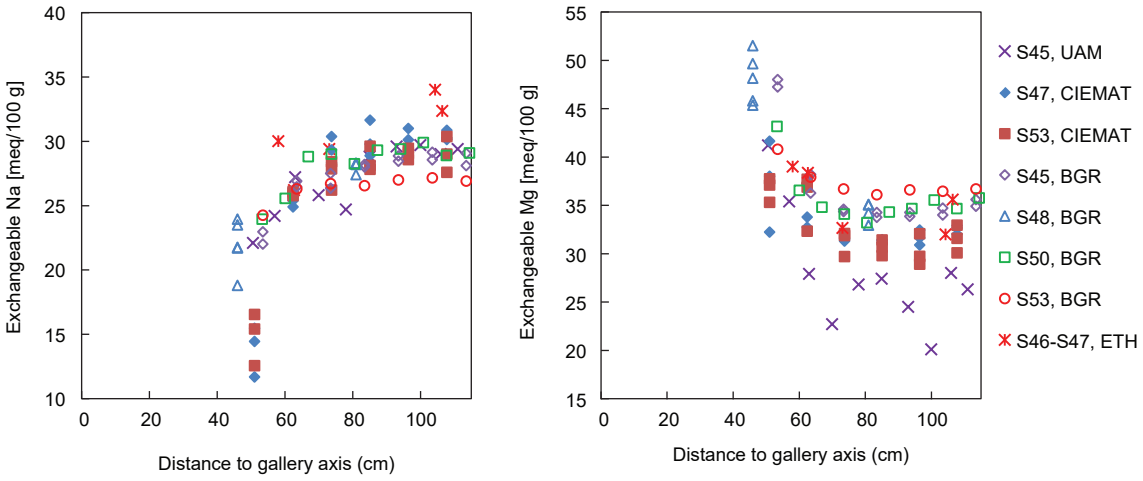


Fig. 5-21: Exchangeable sodium and magnesium determined by different laboratories in samples from sampling sections around the heater

See Fig. 5-16.

5.3.2.3 Porewater chemistry

The porewater composition was studied by CIEMAT using two techniques: preparing aqueous extracts and extracting porewater by squeezing (Fernández et al. 2019). The chemical analyses of the water obtained do not provide the actual porewater composition for either method, particularly in the case of the aqueous extracts, because of the dilution involved in their preparation. On the other hand, the squeezed porewater can be affected by ultrafiltration processes. Therefore, although the water obtained by squeezing is more representative, in both cases it is necessary to perform modelling and make some assumptions to obtain the porewater composition of the bentonite in the barrier. Nevertheless, the results obtained with both methodologies were very consistent and showed clear patterns. An overall increase in the content of most soluble ions occurred because of the general increase in water content and the consequent dissolution of mineral species, which in some cases could have been enhanced by the high temperature.

The overall increase in ionic content was particularly significant for soluble potassium. The main soluble ions in the bentonite were sodium and chloride. In the external part of the barrier, close to the granite, the concentration of these ions decreased below the original values, especially in the heated sections. Sodium in particular, and mainly chloride, were leached out of the 40 cm closest

to the granite and concentrated in proximity to the heater, where they precipitated (Fig. 5-22). The process of ionic redistribution was similar but less intense in the cool section S59. Calcium, magnesium and potassium behaved similarly, with increases in their concentration towards the axis of the gallery that were remarkably sharp in proximity to the heater. This pattern indicates that these soluble species were dissolved in the wettest part of the barrier (because of the water content increase), transported by advection and concentrated in inner parts of the barrier. The movement was enhanced under the thermal gradient, indicating that processes other than advection were also active in concentrating these ions. The soluble species precipitated close to the heater because of their high concentration and the lower water content in this area.

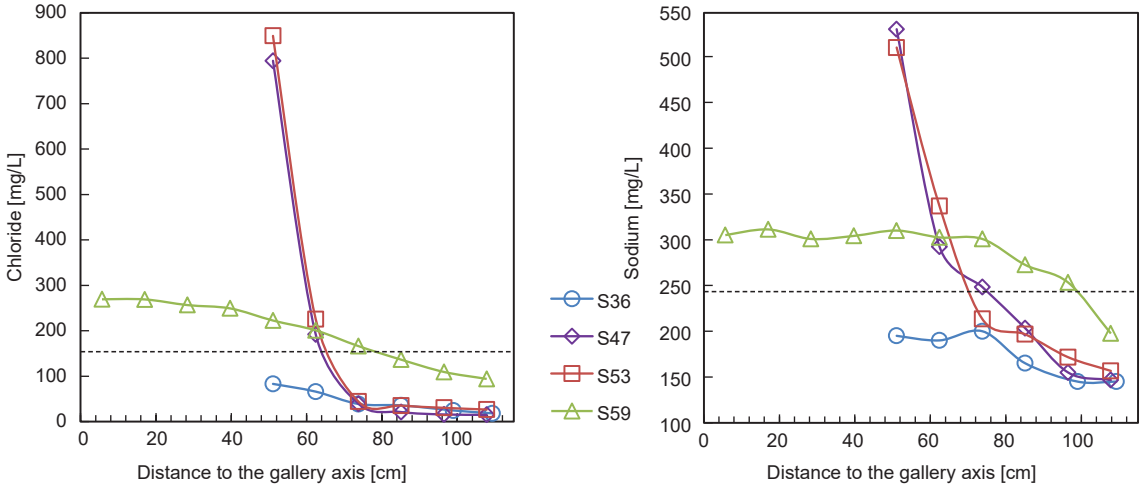


Fig. 5-22: Concentration of soluble chloride and sodium in 1:4 aqueous extracts of samples from several sampling sections

Average for all the samples taken at the same distance from the heater. The dashed horizontal lines indicate the concentration for the reference bentonite.

Sulphate was also depleted close to the granite and its concentration increased towards the interior of the barrier, reaching a maximum at a temperature-controlled distance from the gallery axis (Fig. 5-23). The high temperature also seems to have hindered movement of sulphate towards the gallery axis, likely as a result of dissolution/precipitation processes.

The bicarbonate content showed the opposite trend and was higher than the reference value in all the more hydrated samples. The bicarbonate could come from the granitic groundwater or from carbonate dissolution from the clay. Towards the core of the barrier, the bicarbonate concentration in the aqueous extracts maintained values similar to those of the reference bentonite in cool sections. In the hot sections, the bicarbonate concentration decreased with respect to the original value. These differences are related to the precipitation of carbonates triggered by the decrease in their solubility with increase in temperature. The pH ranged from 8 to 9.2 (7 in the contact with the liner, as determined by UAM) in the aqueous extracts and from 6.8 to 7.9 in the porewater extracted by squeezing. The pH changes followed similar patterns to those of bicarbonate, with a sharp decrease towards the heater.

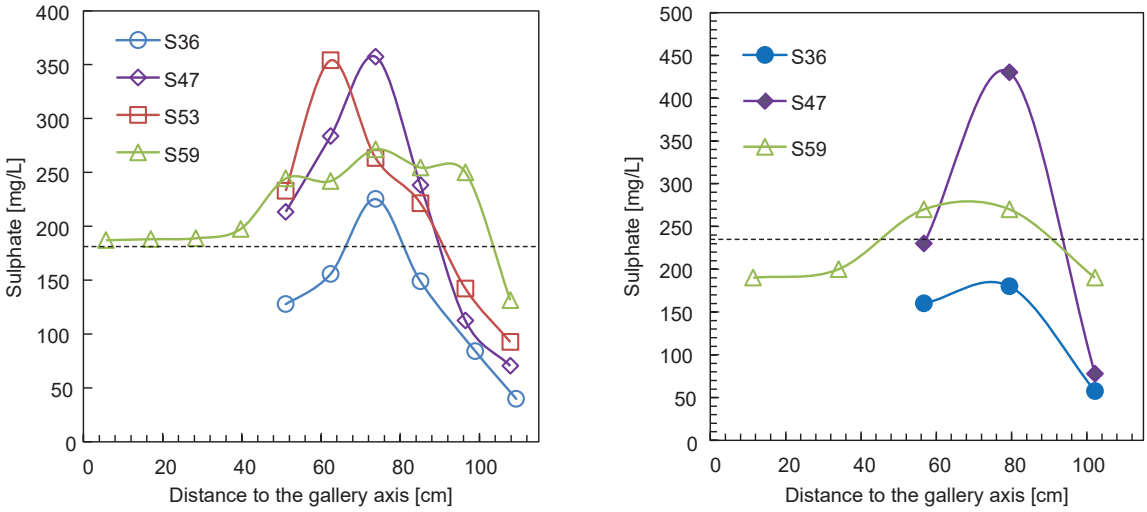


Fig. 5-23: Concentration of soluble sulphate in 1:4 aqueous extracts (after equilibration) of samples from several sampling sections (left; each point represents the average for all the samples taken at the same distance from the heater) and in porewater obtained by squeezing (right)

The dashed horizontal lines indicate the concentration for the reference bentonite.

5.3.3 Thermo-hydro-mechanical properties

Most thermo-hydro-mechanical (THM) properties of bentonites depend on their dry density and water content. In addition, when analysing the hydro-mechanical properties of the bentonite retrieved from the FEBEX in-situ test, the changes experienced by the bentonite during sampling on site and during preparation of specimens in the laboratory have to be kept in mind. Although the samples were preserved carefully and their water content did not seem to have changed since operation, the stresses in the barrier (which at some points were as high as 6 MPa during operation, see Section 2.1) were released on dismantling. This probably resulted in a decrease in the bentonite dry density and a suction increase. Additionally, the preparation of specimens to fit the testing rings required drilling and trimming, causing a decrease in the final dry density of the samples tested compared to that of the bentonite blocks from which they were taken. This decrease was not of the same magnitude in all cases since it depended on the sample conditions and on the operator.

Consequently, the values obtained for some of the THM properties are not identical to those of the bentonite during operation. Nevertheless, the main aim of the THM studies was to check if these properties changed during operation. To accomplish this, two approaches were used:

- The samples to be tested were obtained by trimming the blocks to the appropriate size for the testing cells, attempting to preserve their dry density and water content, i.e. the same condition in which they were received. The results were compared either with those obtained in samples trimmed from a reference block or with those obtained with empirical correlations resulting from previous investigations (e.g., ENRESA 2006a), relating these properties to the water content and dry density of the reference bentonite compacted to various dry densities and water contents.
- The retrieved samples were remoulded to different dry densities and water contents and tested. The results obtained were then compared with those corresponding to samples of the reference bentonite prepared in the same way.

5.3.3.1 Thermal properties

The thermal conductivity of the bentonite blocks was measured in-situ (Nagra) during dismantling and in the laboratory (CIEMAT). The values obtained in-situ ranged between 1.2 and 1.4 W/m·K, with no clear spatial variation (Fig. 5-24), probably because the degree of saturation was very high almost everywhere in the bentonite barrier (see Section 5.2.6).

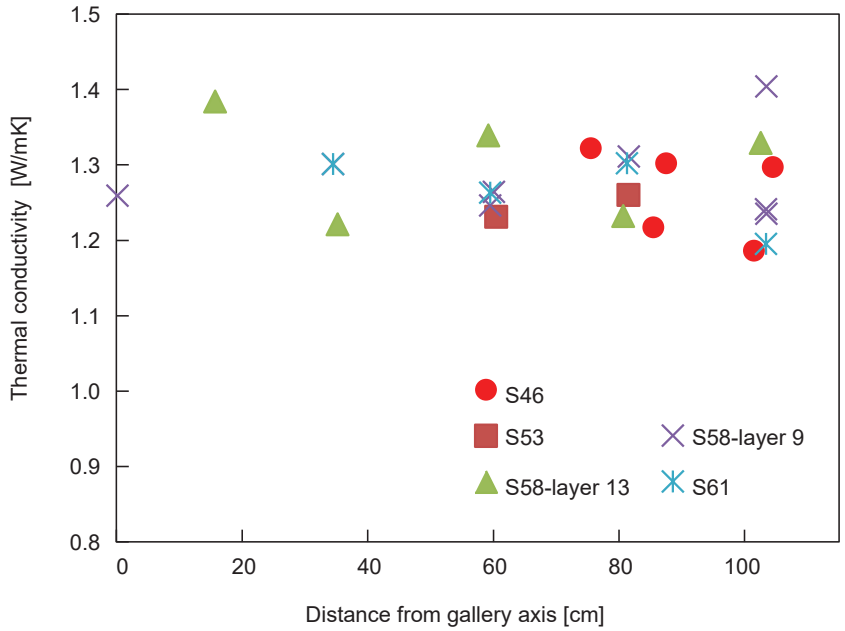


Fig. 5-24: Thermal conductivity measured in-situ by Nagra in different sampling sections

The thermal conductivity values determined in-situ and in the laboratory are plotted in Fig. 5-25. They increased with water content and dry density in the same way as was observed for the reference bentonite. Hence, the thermal conductivity of the bentonite was preserved after operation. However, the values obtained in-situ tended to be higher than those measured in the laboratory for samples of the same dry density and water content. The cause would be the unavoidable decrease in dry density that occurred in the process of obtaining and preparing samples (see Section 5.2.2).

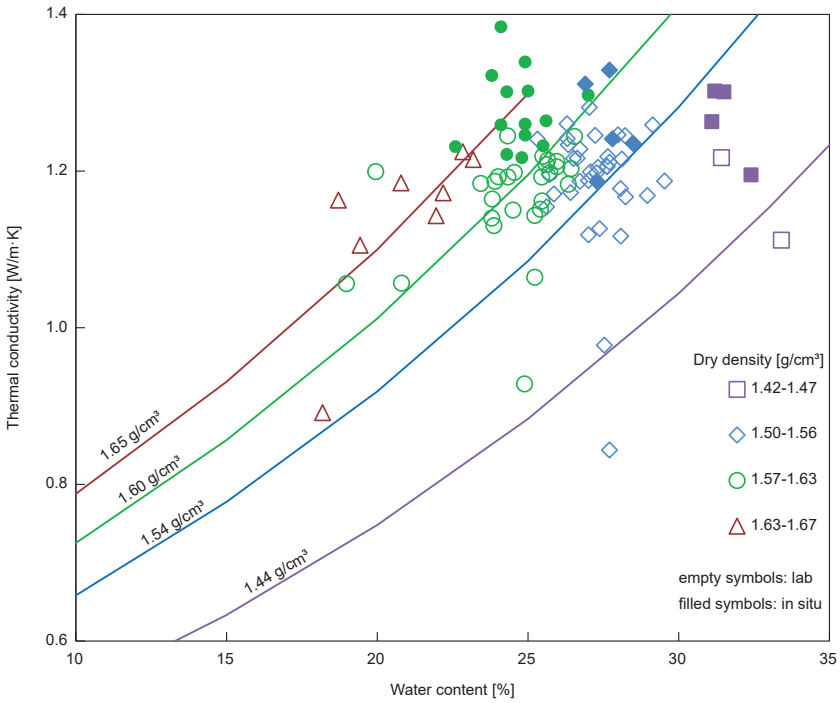


Fig. 5-25: Dependence of thermal conductivity of bentonite measured in-situ (filled symbols) and in the laboratory (empty symbols) on water content and dry density, and empirical relationships for the FEBEX reference bentonite (lines)

5.3.3.2 Swelling properties

The swelling pressure was determined by Clay Technology in the saturated samples (both trimmed and remoulded) kept at constant volume. In both cases, as well as in the samples obtained from a reference block, swelling pressure increased exponentially with dry density. Overall, no significant deviations were found with respect to the reference values. The exception to this was a slight reduction in swelling pressure observed in some of the remoulded specimens from the inner ring of the barrier (Villar 2017).

The swelling capacity of the samples was tested by CIEMAT by letting samples trimmed from the blocks saturate with deionised water in oedometers under a vertical load of 0.5 MPa. The final strain of the samples was linked to their initial dry density and water content. The comparison of the results with those obtained for the reference bentonite tested under the same conditions showed that, on average, the vertical strains measured in the FEBEX-DP samples were slightly lower than the theoretical ones for the reference bentonite. However, although most samples from the external, more saturated bentonite ring swelled less than expected, the samples from the inner, drier ring tended to swell as expected or more, which would mean that prolonged drying did not impair the swelling capacity (Fig. 5-26, Villar et al. 2018a).

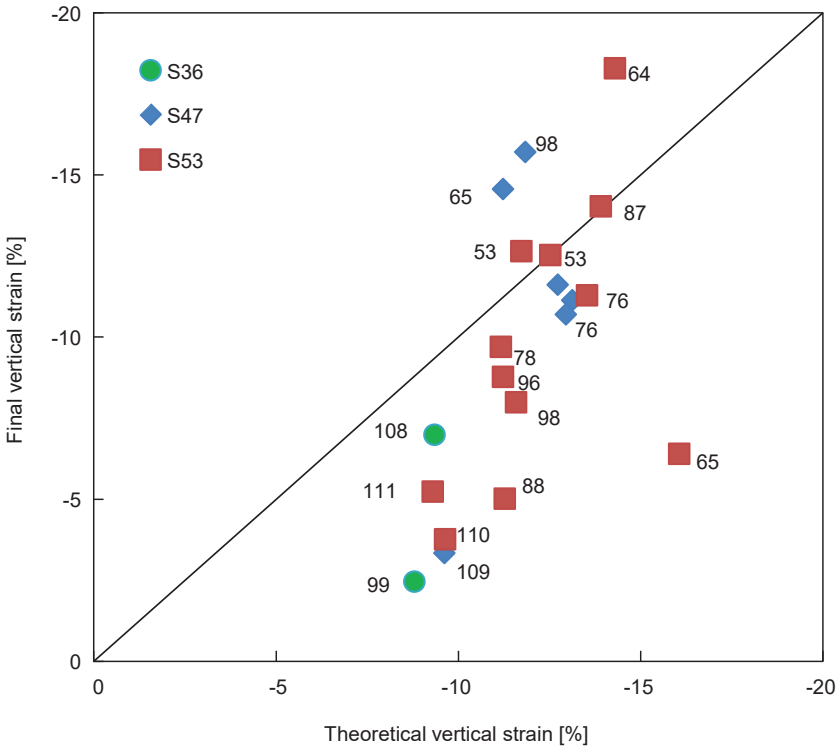


Fig. 5-26: Comparison between the vertical strain measured at the end of the swelling under load tests for samples from different sampling sections and the strain for equivalent samples of the reference bentonite tested under the same conditions

The distance to the gallery axis of each sample is indicated in cm.

5.3.3.3 Compression testing

The high-stress oedometric and isotropic consolidation tests carried out by UPC and CIEMAT allowed the post-mortem pre- and post-yield compressibility and the pre-consolidation stress of the bentonite to be determined.

During the laboratory tests, the coefficient of consolidation decreased as the vertical stress increased to approximately 30 MPa. For further loading/unloading steps, the coefficient of consolidation remained approximately constant. Moreover, on loading at high stresses, the compressibility curves tended to move towards matching that of the reference block. The apparent pre-consolidation stresses determined in the samples retrieved were between 11 and 24 MPa. The blocks installed in the FEBEX in-situ test at Grimsel were manufactured by applying uniaxial vertical pressures of between 40 and 45 MPa, which should correspond approximately to the pre-consolidation stress of the clay. This decrease in the apparent pre-consolidation pressure of the retrieved samples with respect to the reference samples can be explained by the volume increase experienced by the bentonite during hydration and the decrease in suction. The apparent pre-consolidation pressure values tended to be lower as the initial void ratio was higher, and suction was lower (Fig. 5-27). As expected, the compressibility of the samples retrieved was higher both in the plastic and the elastic zones because of their higher initial void ratio. The post-yield compressibility in particular increased for the samples that reached the lowest suction during barrier operation, i.e., those from cool sections or taken closest to the granite. Also, both the pre- and post-yield

compressibility of samples from a section around the heater were lower than those of samples from a lower temperature section, which can be related to the higher degree of saturation and void ratio in these cooler regions.

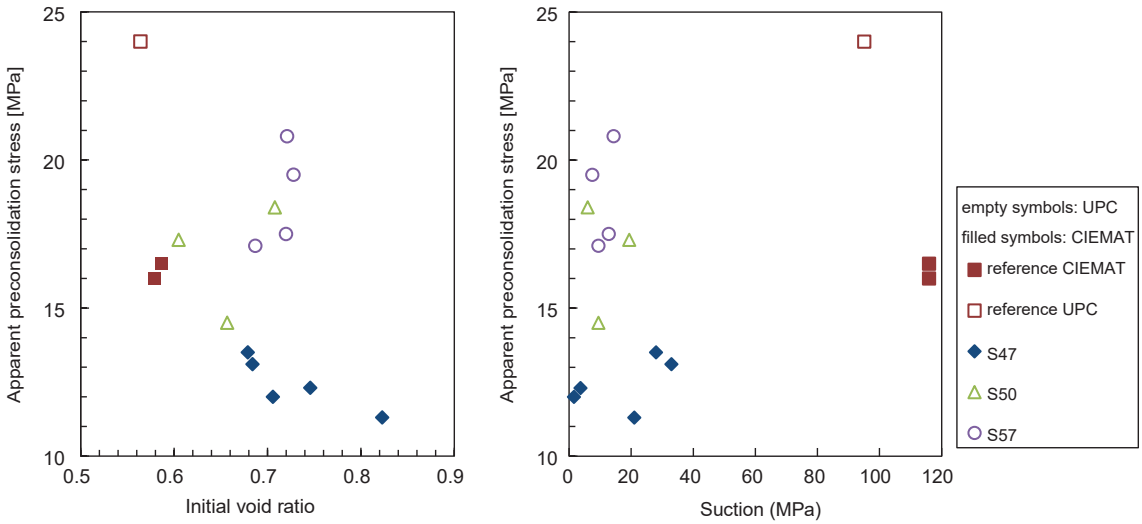


Fig. 5-27: Apparent pre-consolidation stresses estimated from the oedometer tests for samples trimmed from blocks retrieved from different sampling sections, for a reference block (UPC) and for compacted samples of the reference bentonite (CIEMAT)

The consolidation tests performed under isotropic conditions showed that some samples displayed an anisotropic deformational response with lower radial straining. This behaviour could be inherited from the uniaxial compaction used to manufacture the blocks. Upon saturation and volume increase, the initial anisotropy tended to disappear in some cases. The mean pre-consolidation stresses determined from these tests were between 13 and 15 MPa.

The unconfined compressive strength of specimens from a section around the heater was determined by Clay Technology by means of unconfined compression tests on pre-saturated samples obtained by trimming. The compressive strengths were between 1.0 and 1.8 MPa and increased exponentially with the dry density of the samples (Fig. 5-28, left). The values obtained were in the same order as those for remoulded samples prepared from a reference block. The vertical strain at failure clearly decreased from the gallery wall towards the liner (Fig. 5-28, right), indicating a more brittle behaviour in the samples that had been subjected to higher temperature. Some of the specimens from the field experiment showed a lower strain at failure than the samples from the reference block, which is consistent with results of other large-scale field tests (e.g. Dueck et al. 2011).

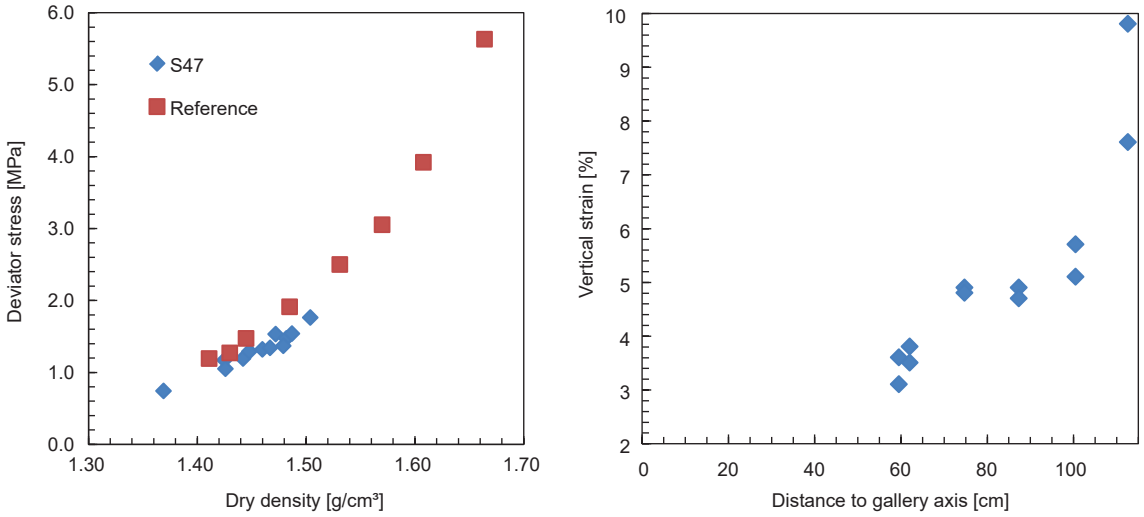


Fig. 5-28: Maximum deviator stress for samples trimmed along a radius of section S47 and samples recompacted from a reference block (left) and corresponding strain (right)

5.3.3.4 Hydraulic properties

The hydraulic conductivity was measured by CIEMAT and Clay Technology in samples saturated with deionised water obtained both by trimming from the blocks and by remoulding. The values obtained were clearly related to the dry density of the samples, with hydraulic conductivity decreasing with increasing dry density. Once the trimmed samples of dry densities below 1.5 g/cm^3 were allowed to hydrate and swell into a homogeneous specimen (most of those measured by Clay Technology), their permeability was higher than the values that would be expected for reference bentonite at the same dry density. Changes in the pore size distribution during swelling of the bentonite in the permeability cell – with an increase of the macropore volume – could be responsible for the increase in permeability observed for these samples. For higher dry densities, where less swelling of the recovered samples occurred, the permeability measured by CIEMAT in retrieved samples tended to be below the expected range of variation of this property. Although there is no final conclusion possible regarding the change in hydraulic conductivity, it can be stated from these tests that the saturated permeability of the bentonite remained very low (< 10^{-13} m/s at the end-of-test densities).

The gas permeability of the FEBEX-DP samples was determined by CIEMAT in core samples drilled on site at different positions across the barrier, some of which were drilled between two blocks, i.e., they crossed an interface (Fig. 5-29). Two-phase flow seemed to be the main gas transport mechanism under the testing conditions. The gas permeability of the samples was related to their position in the barrier (Fig. 5-30), tending to be lower towards the granite, where the degree of saturation was higher and hence the accessible void ratio lower. The latter expresses the ratio between gas-accessible volume and particle volume and is computed as e(1-Sr) (accessible-void ratio). The gas permeability of the samples also depended on their stress state, decreasing noticeably as the confining pressure applied during the tests increased up to 4 MPa. As the confining stress increased, the tortuosity of the gas pathways also increased, which causes the decrease in gas permeability, and eventually the closing of pathways. In fact, beyond a confining stress of 4 MPa, no gas flow took place through any of the wetter samples. For higher confining pressures, the decrease of gas permeability with stress was less significant, except in samples with a block interface. As ecpected, samples with an interface had higher gas permeability than samples of similar accessible void ratio with no interface, and it was necessary to apply higher confining

pressures to reduce or suppress gas flow through them. The decrease in permeability that occurred during loading was not reversible, and the gas permeability of the samples after unloading was lower than the initial one. The dry density of the samples at the end of the tests in which confining pressures above 2 MPa were applied was higher than initial values.

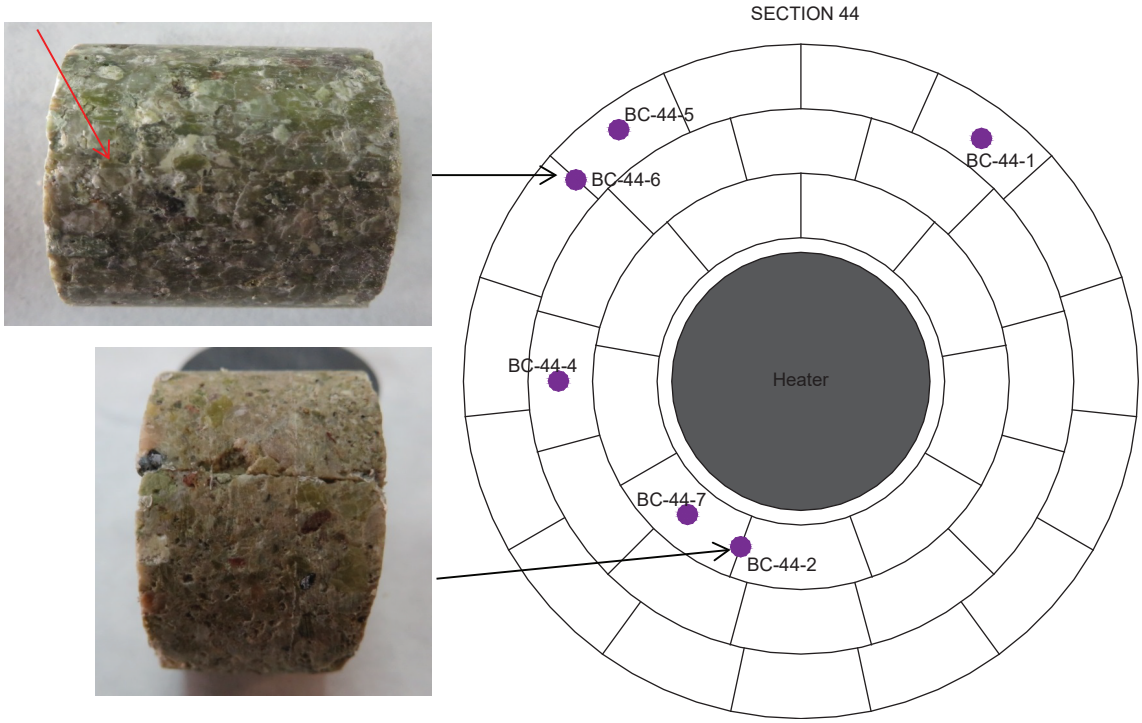


Fig. 5-29: Samples taken for gas permeability in sampling section S44 and appearance of the interface between blocks in a sample from the outer ring (barely visible, indicated by an arrow, BC-44-6) and another from the inner ring (BC-44-2)

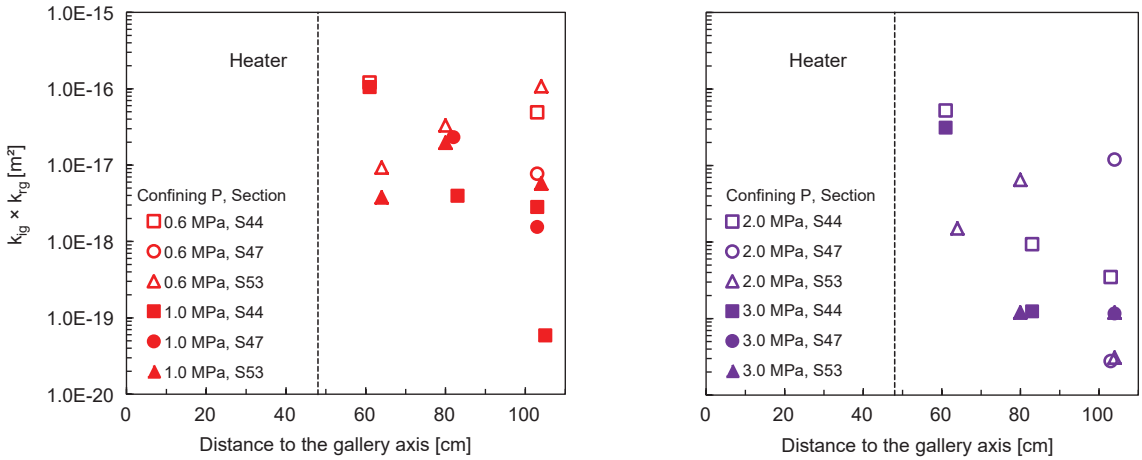


Fig. 5-30: Effective gas permeability values of samples from different sampling sections for different confining pressures as a function of the position in the barrier (no samples with interface are shown)

k_{ig} - intrinsic permeability, k_{rg} - relative permeability

Overall, the gas permeability depended on the accessible void ratio of the samples in the same way as was to be expected for the FEBEX reference bentonite, decreasing with it according to a power law (Fig. 5-31). The void ratio accessible for gas flow was below 0.15 in all the samples tested, given their high degree of saturation. However, samples with an interface drilled in the inner ring of the barrier had higher permeability than samples with a similar accessible void ratio in the reference bentonite. In contrast, wetter samples drilled along interfaces of the middle and outer rings of the barrier (which had a very low accessible void ratio due to saturation) had permeabilities closer to that corresponding to the same accessible void ratio in the reference bentonite. In the latter samples, the interfaces were barely visible and already looked sealed prior to gas testing (Fig. 5-29). This indicated the closing and healing of the interface, resulting in gas transport properties that are dominated by the matrix structure and not by the interface. The closing of interfaces in the more hydrated samples of the external part of the barrier was also confirmed by the MFX-CT studies (see Section 5.3.1). Consequently, it seems that no changes in the gas transport properties occurred as a result of the THM conditions to which the bentonite was exposed (Carbonell et al. 2019).

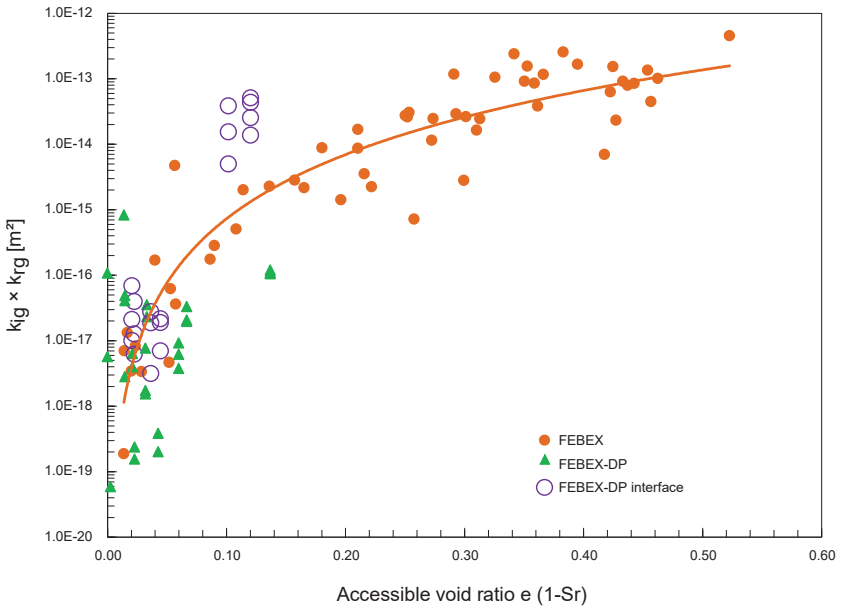


Fig. 5-31: Gas permeability as a function of the accessible porosity for the FEBEX reference and for FEBEX-DP samples with and without interface

Villar et al. (2018b)

5.4 Metal corrosion and iron-bentonite interaction studies (NAB 16-16)

5.4.1 Introduction and scope

Most repository concepts contain metal components in the EBS, such as iron or copper canisters, rebar in cement or rock bolts. These metals are susceptible to corrosion processes in the near-field environment. The degradation of metals by corrosion may lead to degradation of the clay and thus affect the integrity of the bentonite barrier. Microbial activity may enhance both corrosion and degradation processes in the clay.

The FEBEX experiment offered a unique possibility to study in detail corrosion phenomena and their effect on the bentonite in a repository setting. It contained a variety of different metal components, including heaters, the dummy, the perforated liner, small metal coupons and various metal sensors (see Section 1.4). The largest metal fraction consisted of carbon-based steel materials. These materials exhibited prominent corrosion features which had already been observed after the first dismantling period (ENRESA 2004b, 2006a). The scope of the corrosion-related studies in FEBEX-DP was to build on the preliminary FEBEX I study and to investigate both corrosion and iron-bentonite interaction in more detail. These studies focused on the corrosion of metal coupons (copper, titanium, stainless steel, carbon steel), the steel heater, the perforated steel liner and various metal sensors. The impact of steel corrosion on the bentonite was investigated predominantly in the contact area with the liner.

5.4.2 Methods

The corrosion-related studies in the FEBEX-DP project were carried out by seven teams: Tecnalia (Spain), CIEMAT (Spain), Obayashi (Japan), University of Bern (Switzerland), BGR (Germany), SKB (Sweden) and University of Bristol (UK) (Fig. 5-32, left). All the studies are documented in NAB 16-16 (Wersin & Kober (eds.)).

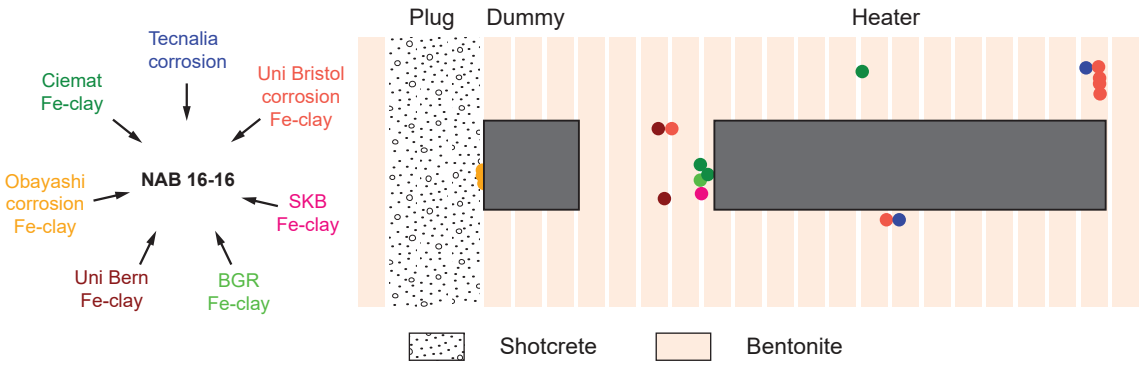


Fig. 5-32: Left: teams involved in Corrosion and Fe-clay interaction studies, Right: locations of corrosion and Fe/clay interface samples

Sampling was carried out by AITEMIN together with Nagra. Selected samples were conditioned by the University of Bern which then sent them out to the different laboratories. The locations of the samples analysed by the different teams are shown in Fig. 5-32 (right). As illustrated in this figure, the majority of the samples came from the central part of the gallery where most areas were not completely saturated (see Section 5.2). Furthermore, the sampling of interfaces was based on visual observations and not on a statistical approach.

The analytical methods that were employed to characterise the samples are summarised in Tab. 5-3.

Tab. 5-3: Samples analysed for corrosion and Fe-bentonite interaction listed by the teams, sections, sample type and methods

Organisation	Section studied	Sample type	Methods
Tecnalia	54	Sensors	Visual, SEM/EDX, XRD, optical microscope
	48	Coupons	Same as sensors, Raman spectrometry
	45, 52	Liner	Same as sensors
	54	Heater	Same as sensors
CIEMAT	42, 54	Clay (interface heater)	Bulk properties, SEM, TEM, XRD, FTIR, MIP, BET, wet chemistry on Fe speciation
	45, 52	Clay (interface liner)	Same
	37	Clay (between liner) and dummy)	Same
	47	Clay (interface sensor)	Same
Obayashi	35	Liner-clay interface	SEM/EDX, µ-Raman, lab corrosion test, CT-XRD, Tof-SIMS
	35	Dummy	SEM/EDX, µ-Raman
BGR	36	Liner-clay interface	XRF, XRD, FTIR, STA, CEC
	42	Liner-clay interface	XRF, XRD, CEC
	54	Clay-heater	XRF, XRD, FTIR, STA, CEC, SEM
	E2-E8	Liner (corr. products)	XRF, XRD, FTIR, STA, CEC
SKB	42	Clay (interface metals)	XRD, XRF, CEC
Uni Bristol	41	Liner-clay interface	XRD, SEM/EDX
	54	Clay (close to sensor)	XRD, SEM/EDX
	48	C-steel coupon	SEM/EDX, µ-Raman
Uni Bern	41	Clay (interface liner)	SEM/EDX, Mössbauer, XRF, XRD, µ-Raman

Tof-SIMS: time-of-flight secondary ion mass spectrometry, STA: simultaneous thermal analysis

5.4.3 Metal coupons (Cu, Ti, stainless steel): macro/micro observations and corrosion studies

Metal coupons were assembled on Teflon racks, placed in pre-fabricated holes in the bentonite blocks in the vicinity of the liner and then filled with loose bentonite powder. Some disturbance occurred during the first dismantling due to drilling of pipes and during the second dismantling period due to partial exposure to air (details in Wersin & Kober 2017). The appearance of the carbon steel/stainless steel racks and the Cu/Ti racks is shown in Fig. 5-33, left and right, respectively. The surrounding bentonite showed a powdery aspect, indicating rather dry conditions because of the proximity to the heater.



Fig. 5-33: Metal coupons from section 48 after extraction

Left: stainless steel rack 1A (left) and carbon steel rack 2A (right). Right: copper coupon rack 4A (left) and titanium rack 3A (right)

5.4.3.1 Copper coupons

These coupons consisted of Cu-Ni alloys and almost pure copper (Cu-ETP, 99% Cu). For the two analysed Cu-Ni alloy specimens, general corrosion seemed to be the dominant mode and no signs of localised corrosion were found. In one sample, cuprite (Cu_2O) could be identified as a corrosion product.

For the "pure" Cu coupon (Cu-ETP) specimen, corrosion seemed to be generally uniform, yielding a corrosion layer with a brownish colour mixed with greenish areas (Fig. 5-34, left). Cuprite was identified as a corrosion product. From weight-loss measurements on one specimen, a corrosion depth of 8.5 µm, giving an average corrosion rate of 0.47 µm/a, was derived. Small areas of localised corrosion were also found. The pits were filled with clay, but with no or only very little corrosion product material. A fairly systematic analysis of the pits indicated depths of about 20 – 60 µm (Fig. 5-34) with a maximum depth of 100 µm observed at one location.

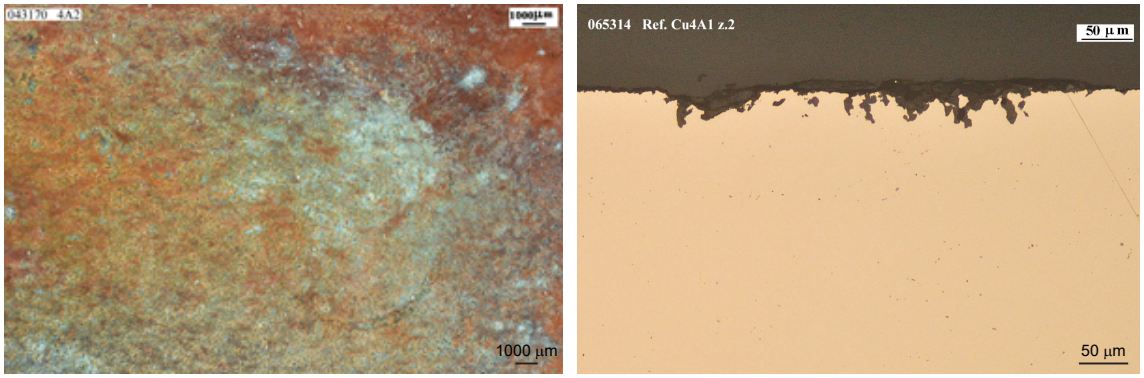


Fig. 5-34: Photograph of Cu-ETP coupon and optical micrograph of pit analyses at 0 mm depth from the surface

Left: photograph of Cu-ETP coupon (sample 4A2). Right: optical micrograph of pit analyses at 0 mm depth from the surface (sample 4A1)

5.4.3.2 Titanium coupons

In general, very little or no corrosion was observed from visual inspection, both in the unwelded and welded samples. It is to note that the Ti rack had been partially damaged during the first dismantling process.

5.4.3.3 Stainless steel

No signs of general corrosion were detected. Pitting, however, was observed in all of the studied coupons and, in one of them, also some cracking. The pits were filled with brownish-blackish corrosion products whose nature was difficult to identify. In one pit, a mixture of magnetite and hematite could be identified. The maximum pit depth was 300 µm. Crack analysis showed evidence of stress corrosion cracking.

5.4.3.4 Redox conditions

The corrosion analysis indicated that the metal coupons had been exposed to variable redox conditions (see Chapter 3). These were initially aerobic and subsequently became anaerobic. It cannot be ruled out, however, that aerobic corrosion after dismantling contributed to the observed corrosion products.

It is worth noting that the corrosion features on the Cu coupons are entirely explained by aerobic corrosion and that no signs of anaerobic or microbially induced corrosion were found.

5.4.4 Carbon steel-related studies

5.4.4.1 Macroscopic observations

All carbon and low-alloy steel materials were covered with a corrosion layer, but the extent and visual appearance of corrosion features varied. This behaviour could largely be explained by differences in moisture content.

The retrieved heater, for example, revealed a fairly homogeneous compact brownish corrosion layer (Fig. 5-35, upper left). A similar, albeit somewhat darker corrosion and less homogeneous layer formed on the perforated liner. Some sensors exhibited more pronounced reddish corrosion products (Fig. 5-35, lower left). A striking observation was the colouration of the clay in contact with some of the steel parts (dismantling sections 41 and 42, see Fig. 4-2). Thus, in some areas, a reddish halo followed by a bluish-greenish one was visible (Fig. 5-35, upper right). Reddish to brownish halos in the clay were found around a number of steel objects. Occasionally, they formed concentric shapes, as for example around a corroded fissurometer (Fig. 5-35, lower right).

In general, the macroscopic observations highlight the heterogeneous nature of the corrosion and Fe-clay interaction process. Water saturation of the buffer blocks and air movement occurred unevenly, leaving strong imprints on steel corrosion. The inner zones close to the heater remained unsaturated until the final state, whereas the outer and "colder" inner zones reached saturation (see Section 5.2). Thus, the latter zones generally displayed more extensive corrosion with corrosion layers and surrounding halos in the clay. There seems to be less correlation with regard to temperature which, however, had an indirect impact by affecting moisture evolution.



Fig. 5-35: Heater after extraction and transport to AITEMIN workshops, end of extensometer SHSD2-01, steel liner in contact with clay and corrosion halos in bentonite induced by corroding fissurometer

Upper left: heater after extraction and transport to AITEMIN workshops. Lower left: end of extensometer SHSD2-01 (stainless steel) showing corroded carbon steel screw. Upper right: steel liner in contact with clay (section 41). Lower right: corrosion halos in bentonite induced by corroding fissurometer (section 48)

5.4.4.2 Corrosion studies

On a macroscopic descriptive level, two layers adjacent to the iron metal can be distinguished: the corrosion layer attached to the iron surface and the interaction zone. The extent of these layers was found to be variable, in particular the interaction zone which varied from 0 to 250 mm (Fig. 5-36).

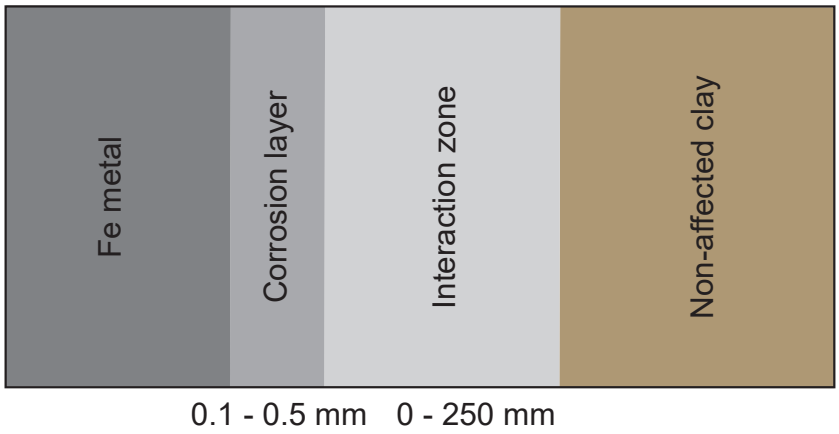


Fig. 5-36: Schematic view of the different compartments between carbon-steel-based materials and the bentonite clay (not to scale)

(See text for discussion.)

On a microscopic level, consistent data were obtained for the different steel components studied. The corrosion layers were generally dominated by Fe(III) oxides, but magnetite and siderite were also encountered. As illustrated in Tab. 5-4, the nature of Fe(III) oxides was variable depending on the iron component and the location. In the case of the heater and liner, which constitute the largest Fe mass, goethite was found to be the dominant corrosion product. However, microcrystalline iron oxyhydroxides likely occurred as well, but could not be identified by most of the applied techniques (e.g., XRD).

Tab. 5-4: Fe phases identified on carbon steel surfaces and in the Fe/clay interface zone

Object	Fe phases identified	Section	Team
Liner	mag, aka, hem, sid	45	Tecnalia
	hem, sid, goe, aka	35	Obayashi
	goe, (hem)	41	Uni Bern
	goe, mag	36,42	BGR
	mah, goe, lep	45,52	CIEMAT
Heater	aka	Variable	Tecnalia
	goe	54	BGR
	mah, goe, lep	42,54	CIEMAT
Sensors	mag, sid	54	Tecnalia
	mah, goe, fer	47	CIEMAT
Coupon (TstE355)	mag, sid, hem	48	Uni Bristol

mag: magnetite, aka: akageneite, hem: hematite, sid: siderite, goe: goethite, mah: maghemite, lep: lepidocrocite, fer: ferrihydrite

Coupons and sensors

All studied carbon-steel coupons had a thick blackish-reddish crust. They showed strong corrosion effects which resulted in cracking in some cases. General corrosion was the main corrosion mode. Identified corrosion products were siderite, hematite and magnetite.

Only few corrosion data for steel sensors were acquired. Reddish-brown corrosion products were observed for a sensor located close to the rock wall which could be attributed to magnetite and siderite and likely to non-identified Fe(III) oxyhydroxides.

Heater and liner

As indicated above, the heater displayed a fairly uniform reddish-brown corrosion layer with a thickness of about 200 µm. General corrosion was the main corrosion mode. At the end parts of the heater, some localised corrosion had occurred with corrosion layer thickness up to 400 µm (due to slightly higher water contents).

The liner exhibited corrosion layers (CL) on both sides. The CL at the outer surface contacting the clay was slightly thicker (max. thickness 200 – 250 µm) than that on the inner surface (max. thickness 180 µm). No localised corrosion or pitting was observed, thus indicating that general corrosion was the main corrosion mode.

The corrosion depths can be roughly estimated from the CL thicknesses accounting for densities of the corrosion products and carbon steel. This leads to corrosion depths in the range of 100 – 200 µm.

A somewhat intriguing result was the predominance of Fe(III) oxides in view of the anaerobic conditions which should prevail after the depletion of the oxygen initially present in the tunnel (air in the gaps and bentonite pores). To test whether the amounts of Fe(III) oxides could be explained by the initial amount of O_2 in the tunnel reacting with the steel surfaces, a mass-balance estimate for a section comprising the heater and liner was carried out (NAB 16-16). This calculation showed that the amount of Fe(III) modelled was much smaller than was actually measured. In fact, 10 – 20 times more Fe(III) oxides occurred in the corrosion layers than were estimated to form with the O_2 initially present, strongly suggesting the presence of a further O_2 source during the experiment (discussed in Section 5.4.5) and a prolonged aerobic phase. Gas sampling prior to dismantling indicated a general trend from oxidising to reducing (Chapter 3.2). However, considerable spatial variation in O_2 and H_2 was observed, suggesting variable redox conditions within the tunnel. It should be noted that O_2 was not entirely depleted at the end of the measurements, thus qualitatively supporting results from corrosion studies.

5.4.4.3 Interface studies

Most of studies focused on the clay side of the Fe/clay interface, and a number of analytical methods were applied to characterise the clay close to the interface and compare these data with the clay located further away from the contact. As stated above, the studied samples were taken from locations where macroscopic corrosion features were visible. Therefore, they are not statistically representative as, at many interfaces, no visible interaction zone in the clay was observed.

Extent of Fe front

The extent of the Fe front from the interface into the clay correlates with the colour changes observed in the clay. Thus, the larger the interaction zone in the clay, the large the Fe increase relative to the unaffected clay. The Fe content close to the iron source was found to be 1.5 to 3 times higher than farther away. Conversely, in areas where no interaction was observed, no increase in the clay occurred (Fig. 5-37). The thickness of the zone of increased Fe thus varied from 0 to about 30 mm.

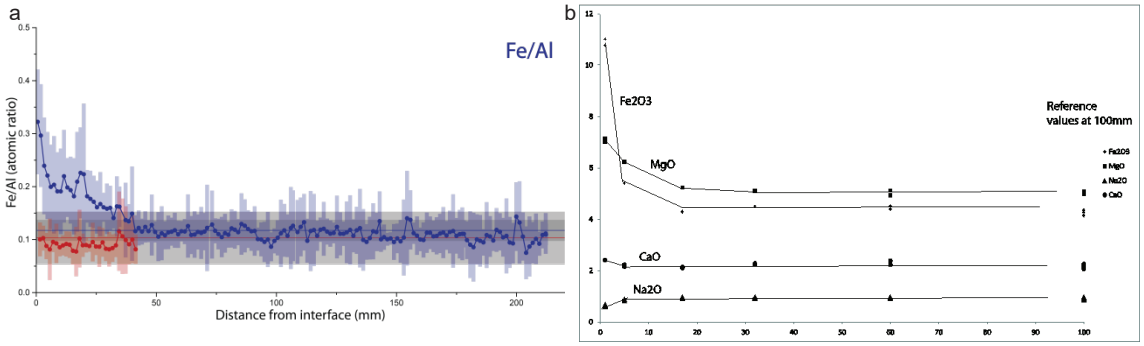


Fig. 5-37: a) Fe/Al ratio (EDX data) as a function of distance from the interface for two samples in Section 41 (blue and red curves); b) contents of elements (wt.-% oxides) (XRF data) as a function of distance from the interface for one sample in Section 42

Curves in a) represent average and the range (bars) of five measurements with identical distance to interface.

Nature of Fe species

The identification of the Fe species in the clay turned out to be more challenging than in the corrosion layer. In general, Fe(III) oxides prevailed adjacent to both sides of the interface. The occurrence of newly formed Fe(II) minerals in the clay could be expected from the redox evolution in the experiment, but such phases could not be unequivocally identified in the clay. Nevertheless, the combination of SEM/EDX, XRF and Mössbauer spectroscopy on one interface sample in Section 41 showed that Fe(II) species (which could not be further identified) increased together with a second small front in the clay (Fig. 5-38). Fe(II) also increased towards the metal side (not shown in Fig. 5-38) and could be attributed to magnetite and siderite.

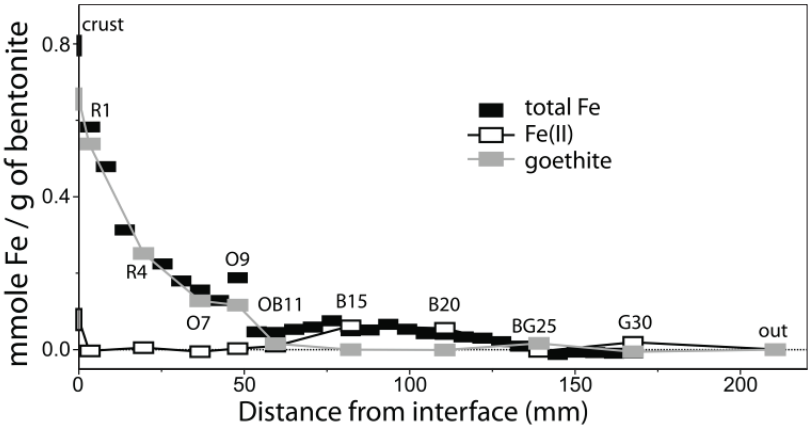


Fig. 5-38: Speciation of Fe (shown as excess iron relative to natural clay) as a function of distance from the steel contact determined from Mössbauer spectrometry and XRF in Section 41

5.4.4.4 Other findings at the Fe/clay interface

Some accumulation of salts was observed close to the heater. This is explained by evaporation induced by the heating of the bentonite in conjunction with the limited amount of water available in the clay. As a result, chloride accumulated as did – to a lesser extent – sulphate and carbonate salts. This is consistent with the results on aqueous extracts (Section 5.3.2.3). Chloride is known to be a strong corrodant under oxidising conditions, and the evaporation process likely enhanced corrosion rates at the heater and liner surfaces. Calcite and aragonite precipitates were also observed close to the heater.

The cation exchange capacity (CEC) showed no or only small changes as a function of distance from the heater. Only a limited amount of newly formed silicate minerals was identified. The formation of minor trioctahedral smectite (saponite) "domains" in some samples in direct contact to the heater was indicated by XRD. All these findings suggest that the alteration of smectite was very limited or even negligible in the FEBEX experiment. Support for this is provided by the noted constant Al/Si as a function of distance from the heater.

An Mg increase towards the iron contact was observed in some of the samples. This increase is not correlated with the increase in Fe and therefore does not appear to be related to the corrosion process but rather to the effect of temperature.

5.4.4.5 Tentative model for corrosion and Fe-clay interaction process

From the combined dataset of microscopic and spectroscopic analyses, the following phenomenological corrosion and Fe-clay interaction model was proposed:

Phase 0: Carbon steel is covered with a thin oxide layer (mainly magnetite). Bentonite has a low moisture content and the main species is structural Fe(III).

Phase 1: Aerobic corrosion of steel leads to the formation of Fe(III) oxides. Depending on moisture content, anhydrous Fe(III) oxides (hematite, maghemite) or Fe(III) oxyhydroxides (mainly goethite, lepidocrocite) are formed. O_2 and H_2O transfer to steel decreases as corrosion proceeds and the corrosion layer thickens.

Phase 2: Anaerobic corrosion of steel inside of the corrosion layer leads to the generation of Fe(II) and the formation of magnetite and siderite in the corrosion layer. Furthermore, (rapid) electron transfer across the corrosion layer occurs, generating Fe(II) at the corrosion layer/bentonite interface which reacts with the remaining O_2 to further produce Fe(III) oxides.

Phase 3: Anaerobic conditions everywhere: continuation of anaerobic steel corrosion, generation of Fe(II) (and magnetite/siderite) and (rapid) electron transfer across the corrosion layer. Diffusion of Fe(II) into bentonite and accumulation of Fe(II) in clay. Further transport of small fluxes of Fe(II) into clay. The mechanism of this transfer process still has to be established but probably involves redox reaction with structural Fe(III) and with previously formed (and pre-existing) Fe(III) oxides.

It should be pointed out that the main drivers of the corrosion process in the FEBEX experiment were the availability of water and O_2.

5.4.5 Implications for repository conditions from a corrosion perspective

In general, the FEBEX experiment was not initially designed for detailed studies of corrosion processes and was not set up in an ideal way to study corrosion without inducing disturbances during dismantling and sampling. Nevertheless, useful information regarding conditions of the early stage in the near-field after repository closure could be deduced. These conditions can be characterised by variable moisture contents and a predominantly oxidising environment. The slow water ingress from the "cold" host rock and the heat emanating from the central part induced a humidity gradient and salt accumulation on the hot side, which lasted until the end of the experiment. Movement of air and moisture likely occurred in an uneven and partly "channelled" manner in the central part of the buffer. Thus, corrosion effects were more pronounced in areas with a higher moisture content, but accumulation of chloride probably adversely influenced corrosion in some of the drier areas.

A somewhat unexpected result was the large amount of Fe(III) oxides produced by the corrosion process. The initial O_2 present in the package at the time of emplacement can only explain a small proportion of the total Fe(III) produced by corrosion, suggesting the presence of an external source of air which may have entered the system through the cement plug or the EDZ. This is supported by the gas monitoring data (Section 3.2). A further part of the Fe(III) may have been produced during and after the dismantling procedure. In summary, the FEBEX experiment reflects accentuated conditions with regard to aerobic corrosion effects.

In spite of the likely oxic disturbances, the data point to anaerobic corrosion following the aerobic stage. This led to a reduction of previously formed Fe(III) species and diffusion of Fe(II) further into the clay.

From the analyses of the corrosion layer thicknesses and the amounts of Fe transferred, the corrosion depths could be roughly estimated to be in the range of 110 – 440 µm. Considering 18 years of exposure time, this corresponds to average corrosion rates of 6 – 24 µm/a. The upper range is in line with aerobic corrosion rates proposed by Foct & Gras (2003) for the temperature of interest (~ 95 °C). This again supports the importance of prolonged aerobic conditions in some of the sections. The lower corrosion rate range reflects prolonged unsaturated (oxidising) conditions and/or the stronger influence of anaerobic conditions.

The corrosion process induced very little alteration of the clay. There are some indications of the formation of trioctahedral Mg smectite close to the heater contact, but this effect appears to be mainly related to temperature. The results obtained for the clay contacting the hot Fe source are in line with data from other in-situ tests, for example the ABM (Alternative Buffer Materials) and TBT (Temperature Buffer Test; both at ÄSPÖ hard rock laboratory, Sweden) experiments (Wersin et al. 2015, Svensson & Hansen 2013, Svensson 2015).

5.5 Microbiological studies (NAB 16-15)

5.5.1 Scope and objectives

Compacted bentonite is a hostile environment for bacterial life in view of its nanoporous structure, its low water activity and high swelling pressures in the saturated state (King et al. 2012). A number of studies have been carried out to assess conditions which constrain microbial activity in bentonite buffer materials (e.g. Masurat et al. 2010, Bengtsson et al. 2017b, Stroes-Gascoyne et al. 2010). In particular, microbially induced sulphide production by sulphate-reducing bacteria (SRB) has been studied in view of the importance of sulphide as corrodant for Cu and Fe canisters.

The FEBEX in-situ test offered a good opportunity to shed more light on the role of microbes in a repository-type setting. Specifically, the test enabled the study of microbial activity (MA) in a variably saturated environment and a thermal gradient, where not much data was available. Microbiological studies carried out after the partial dismantling in 2002 had indicated that SRB could be cultivated from FEBEX bentonite samples in numbers ranging from 30 to 10'000 cells per gram depending on temperature and water content (ENRESA 2004).

The microbiological studies of FEBEX-DP had the following objectives:

- to contribute to the characterisation of the impact of bacterial activity on the long-term properties of the bentonite barrier
- to gain systematic information on the effectiveness of the bentonite buffer to inhibit bacterial activity by studying parameters such as density, temperature, water content and the related water activity
- to gain information about how the bacterial activity and diversity vary in a cross-section of the bentonite from the wetter parts closest to the rock wall inwards toward the heated canister

5.5.2 Methods

The microbiological studies in FEBEX-DP reported here were carried out by two teams: Micans (Sweden) and BGR (Germany). These are documented in NAB 16-15 (Bengtsson et al. 2017a). Further studies by SCK CEN (Belgium) and the University of Manchester (UK) were conducted within the scope of the EU MIND project (www.mind15.eu).

Numerous samples were extracted from various sections along the buffer (Figs. 4-1, 5-39, left) at different distances from the tunnel centre (see example Fig. 5-39, right). Appropriate measures were taken to minimise contact with O_2 during sampling and sample preparation.

A suite of methods was employed to identify and quantify the microorganisms, to assess their activity in the clay and to relate this to the physical conditions (temperature, density and water content). A major focus was on the cultivability, with the determination of the maximum probable number (MPN) under aerobic and anaerobic conditions and different media favouring sulphate-reducing (SR), iron-reducing (IR) or nitrate-reducing (NR) cultures. Furthermore, adenosine triphosphate (ATP) analysis was carried out to obtain further information on the microbial activity in the in-situ experiment. The study was complemented with DNA extraction and quantification and Illumina sequencing (Meyer & Kirchner 2010).

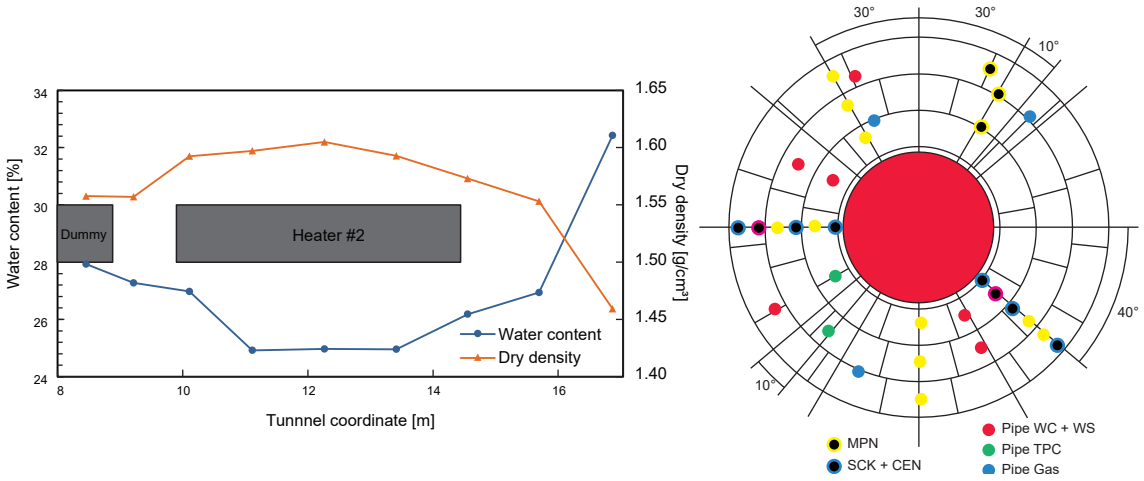


Fig. 5-39: Water content and dry density along the tunnel axis and with respect to the heater and location of samples for mineralogical studies

Left: The water content and dry density along the tunnel axis and with respect to the heater. Right: location of samples (Section 42 taken as an example)

5.5.3 Results

Visualisation of bacteria was attempted, which is known to be difficult because of strong attachment of organic surfaces to the clay. Indigenous bacteria were evidenced in one sample in section 60 as illustrated in Fig. 5-40.

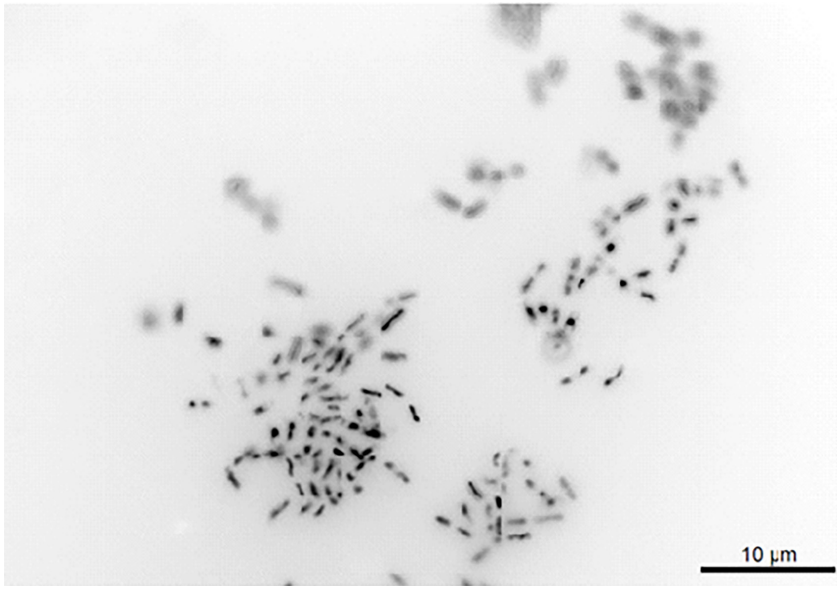


Fig. 5-40: Extracted cells from sample B-C-60-18 stained with DAPI (4',6-diamidino-2-phenylindole) in 1'000× magnification

Some of the cells have a blurred appearance as they are out of the focal plane of the microscope.

MPN and ATP analysis

In general, the maximum probable numbers for most samples were found to be low and often below the detection limit as shown in Tab. 5-5, which lists the results from Micans. There is a clear tendency of MPN increase towards the far end of the tunnel. A trend with higher water content/lower dry density towards the end of the tunnel can be also observed as illustrated in Fig. 5-41. On the other hand, no obvious trend with temperature conditions in the in-situ experiment can be observed. The MPN notably drop at a cultivation temperature of 70 °C compared to 30 °C.

The low amount of cultivable MPN in the central parts is explained by the high dry densities of about 1.6 g/cm^3 (Fig. 5-39) and to some extent by the unsaturated conditions that prevailed there. The MPN obtained are in a similar range to those derived in the first dismantling phase. This suggests that conditions regarding bacterial survival have remained stationary for a long time.

ATP could be extracted in one sample from Section 60 in amounts that were consistent with MPN data. This supports the presence of living cells and suggests that MA occurred in that section.

Tab. 5-5: Most probable numbers of SRB, NRB and IRB in FEBEX bentonite core samples with lower and upper confidence limits (CL) from Micans study

gww = gram wet weight

Sample code	SRB gww^{-1}	Lower-upper CL	NRB gww^{-1}	Lower-upper CL	IRB gww^{-1}	Lower-upper CL
B-C-42-01	< 4	–	8	2 – 34	< 4	–
B-C-42-02	< 4	–	< 4	–	< 4	–
B-C-42-03	< 4	–	< 4	–	< 4	–
B-C-48-04	< 4	–	< 4	–	< 4	–
B-C-48-05	< 4	–	< 4	–	< 4	–
B-C-48-06	< 4	–	< 4	–	< 4	–
B-C-48-13	< 4	–	< 4	–	< 4	–
B-C-54-01	< 4	–	< 4	–	< 4	–
B-C-54-02	< 4	–	16	6 – 48	< 4	–
B-C-54-03	< 4	–	< 4	–	< 4	–
B-C-54-20	< 4	–	< 4	–	< 4	–
B-C-60-13	4	2 – 20	< 4	–	< 4	–
B-C-60-15	12	4 – 36	2'600	1'000 – 7'800	< 4	–
B-C-60-16	60	20 – 220	120	60 – 360	4	2 – 20
B-C-60-17	46	18 – 172	2'200	800 – 6'000	22	8 – 58

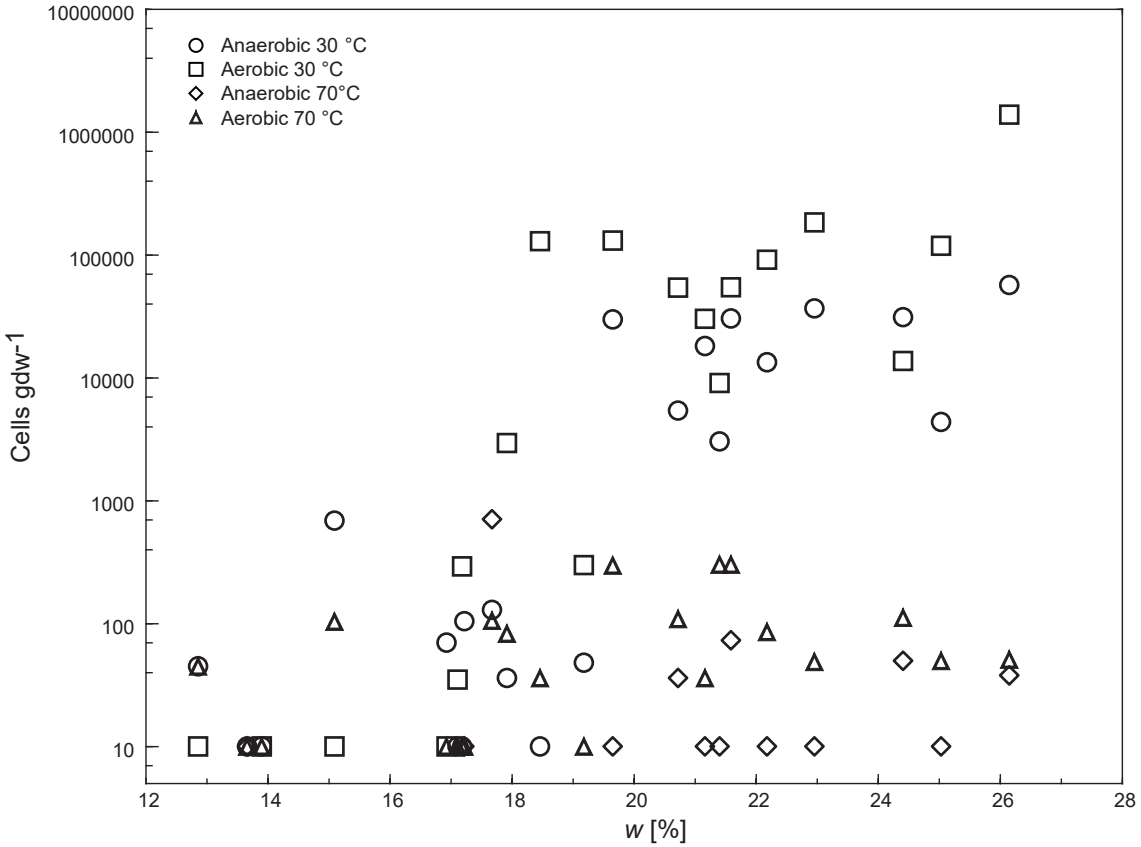


Fig. 5-41: Numbers of aerobic and anaerobic cells cultivated by BGR at 30 °C and 70 °C as function of gravimetric water content (w)

Data below detection < 10 cells gdw^{-1} (gram dry weight) are shown as 10 in the graph.

DNA extraction and Illumina sequencing

DNA extraction from MPN tubes was carried out in samples from Section 60. The concentrations obtained showed good correlation with MPN results. Direct extraction from the clay yielded low DNA amounts, which is explained by the experimental difficulty of extracting cells from the clay.

Illumina sequencing did not show clear taxonomic differences between the different cultivable media, except for some samples cultivated for SRB that had a slightly divergent core population. In general, the large majority of the samples could not be attributed to a specific genus. The genus *Desulfosporosinus* was found in many of the cultures and includes spore-forming, mesophilic sulphide-producing bacteria with the ability to grow with molecular hydrogen as source of energy. The detection of a large diversity of spore-forming genera was expected because spores will survive for a long time in dry clay until water saturation is reached. When water is available, spores can germinate to active bacteria.

5.5.4 Conclusions

The samples around the heater did not yield any cultivable bacteria. This can either be explained by viable but not cultivable cells due to desiccation effects or by cells killed during the experiment by desiccation and possibly also by the high temperature. The MPN results are also consistent with corrosion data in that area that did not indicate any signs of microbially induced corrosion, such as sulphide-related corrosion (Section 5.4).

Despite a fairly high dry density (~ 1.5 g/cm^3) and swelling pressure (> 5 MPa), it was possible to cultivate numerous bacteria in some of the sections after 18 years (see Tab. 5-5 and Fig. 5-41). Consequently, no cut-off density or pressure below these values seems to exist for when microorganisms in highly compacted FEBEX bentonite are completely eradicated. Cultivability and viability of bacteria in compacted bentonite clays likely depend on several variables such as density, pressure, water availability and, most importantly, the type of clay.

6 Sensor evaluation

This chapter focuses on the observations and analyses performed on the sensors recovered during the final dismantling operation. The conclusions about their performance are of great importance because the information provided evidence on the reliability of the obtained data for improving the understanding of THM processes. The complete results can be found in two reports: Rey et al. (2016) and Sakaki et al. (2017). The operational status of the sensors has been documented in Martínez et al. (2016) (see also Chapter 2).

6.1 Sensor sampling and observations

The sampling procedure was designed in consecutive steps in which the sensors had to be properly recovered while the dismantling operation was in progress and included the following steps:

- recording the position (coordinates) to quantify changes from installation (if any)
- recording the status (Figs. 6-1 and 6-2), describing visible corrosion signals, fractures, or mechanical damage, flooded filters, etc.
- photo documentation
- careful removal, re-labelling for lab analysis, if required, and packaging

All sensors and cables were found to be in good contact with the bentonite, while those close to the rock walls or the liner were strongly pressed against them. In general, the sensors retrieved in 2015 appeared in better shape than the ones gathered during the first dismantling in 2002, i.e., they showed less corrosion and mechanical damage, with no clear reason for this.

No noticeable changes in the sensor positions with respect to the surrounding buffer material were found due to the bentonite swelling, and no movements of the heater were encountered during the inspections made when dismantling the test set-up. Nevertheless, the mechanical effects of the bentonite swelling on some sensors were clearly visible (squashed cables, bent or broken filters, crushed or bent body), in particular for those close to rigid surfaces or when the sensors extended across bentonite block joints.



Fig. 6-1: Status of a psychrometer (left), a capacitive moisture and pore pressure sensor before being retrieved (centre) and detail of a pore pressure sensor (right)



Fig. 6-2: TDR probes with various types of damage at the time of on-site inspection

Some were badly damaged when the power chisel partially scraped off the coating film, electrode and teflon rod. Damage included cracking of the surface coating film, shearing at the bentonite block joints and cracking of cable protection.

6.2 Post-mortem sensor evaluation

Retrieved sensors were analysed, verified and calibrated in the laboratory, except for the TDRs that were analysed on site to determine the main causes of failure of some of them and thus evaluate their performance and options for improving them for future re-use. A full breakdown of the sensors installed and retrieved during the whole operational phase is given in Tab. 6-1. Examples of the results obtained during the verification and calibration carried out in the laboratory are shown in Fig. 6-3 for selected different sensor types.

The qualitative and quantitative performance of each sensor type analysed in FEBEX-DP is described hereafter.

a) **Temperature sensors** (T type, thermocouples): The performance was excellent and, except for those damaged by corrosion, up to 72% survived. The accuracy of the still-operating sensors had not varied since installation (below ± 1 °C), showing maximum errors below 5.3% of the reference temperature.

b) **Moisture/humidity sensors** (capacitive, psychrometers and TDR type): The readings provided by the different moisture sensor types matched relatively well with each other. The capacitive-type sensors (WC type) remained functional for a duration far beyond the initially expected operating lifetime (six months). Twelve out of 31 lasted for more than five years and one operated until 2005 (almost nine years). Their readings were accurate and, given their wide range, the data obtained from them are very useful for tracking the slow bentonite buffer hydration process that started from low initial water content. Psychrometers (WP type) proved to be very fragile for the bentonite buffer environment with the arrangement used and only 5 out of 24 remained operational, but were damaged during dismantling. They also seemed to be highly sensitive to contamination by salt (laboratory results from surviving ones) but data recorded from those installed in the outer buffer ring seemed to be sufficiently accurate and they matched the ones from the capacitive type sensors. The TDRs (WT type) in the bentonite buffer performed well in the harsh environment (combination of temperature, stress, high moisture, and salt precipitation) and, although a few suffered damages (Fig. 6-2), 7 out of 10 remained operational and provided consistent data after re-scaling.

Tab. 6-1: Breakdown of FEBEX sensors

Parameter (and instruments)	Code	Sensor type	Location area*				Total FEBEX I	Removed during partial dismantling	Febex II (added)	Total Febex II	Removed during final dismantling
			G	B	H	S					
Temperature (bentonite)	T	Thermocouples [mV]	62	91	36		189	55	8	142	80
Total pressure in rock matrix (3D)	PB	Vibrating wire (frequency)	4				4			4	
Total pressure in rock or heaters	P	Vibrating wire (frequency)	30	6			36	3	3	36	6
Total pressure in buffer	P	Piezoresistive [mV]							10	10	10
Hydraulic pressure in rock	QB**	Piezoresistive [0 – 20 mA]	62				62			62	
Pressure in borehole packers	PP**	Piezoresistive [0 – 20 mA]	62				62			62	
Pore pressure in bentonite	Q	Vibrating wire (frequency)		52			52	24		28	28
Humidity and temperature	WC	Capacitive + Pt–100 [20 × 0 – 20 mA]		58		1	59	27	21	53	52
Humidity and temperature	WP	2 Thermocouples [mV]	28	48			76	24		52	24
Humidity	WT	TDR (reflectogram)	4	20			24	10		14	10
Rock extensometer	3S	Vibrating wire (frequency)	6				6	2		6	
Heaters displacements	SH	Vibrating wire (frequency)		9			9	4		7	7
Bentonite block expansion	SB	Vibrating wire (frequency)		8			8	6		4	4
Displacements in bentonite	SS	Potentiometer (resistance change)		6			6			0	0
Plug displacements	S**	LVDT				4	4	12		4	4
Inclinometers	IT	LVDT		12			12			0	0
Crack meter	3S	LVDT		3			3	4		3	3
Gas pressure in clay buffer	GP**	Piezoresistive		4			4	6		0	0
Gas flow	GF**	Manual reading		6			6			0	0
Atmospheric pressure	P**	Piezoresistive [0 – 20 mA]				1	1			1	0
Ventilation air flow	A**	Hot wire [0 – 20 mA]				1	1			1	0
Heating element current	V**	Electrical converter [0 – 20 mA]				6	6			6	0
Heating element voltage	C**	Electrical converter [0 – 20 mA]				6	6			6	0
Total			258	323	36	19	636	177	42	501	228

* G: granite, B: bentonite buffer, H: heater, S: service area

** Sensors located outside the test sealed section

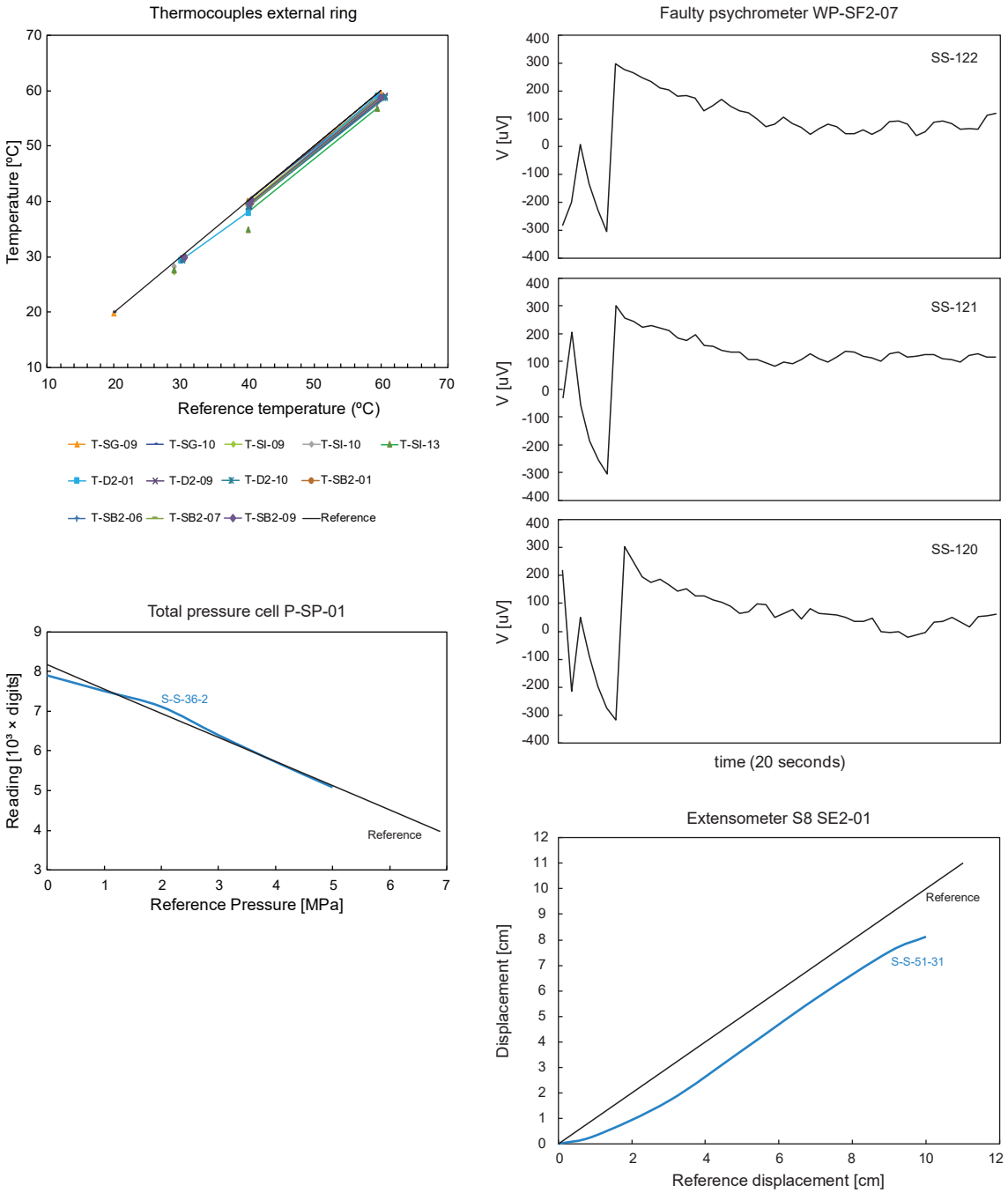


Fig. 6-3: Results of the verification of different types of sensors

c) **Total pressure cells** (P type): In general, all sensors based on the vibrating wire technique (Geokon ones) showed good behaviour. The only difficulty resulted from the weakness of the embedded thermistor that failed in some cases; half of these during operation. Malfunctioning was also caused by the cables, which were most likely damaged during operation.

d) **Pore pressure sensors** (Q type): Overall, these sensors provided very low pressure readings, showing positive values only in the most humid parts located at the outer part of the buffer. This type had the highest survival rate, although 11 out of 28 showed problems during operation, usually due to damage to the cables. Once repaired, up to 22 units functioned well in the laboratory.

e) **Heater displacement sensors** (SH type): only 1 out of 7 remained operational and all the recovered sensors showed damage due to corrosion in the anchoring pieces only (Wersin et al. 2017); the tube of the sensors was bent in several cases, hindering precise measurement of the displacement. Therefore, the confidence in the readings obtained from these sensors was poor.

f) **Bentonite block displacement sensors** (SB type): only 1 out of 4 sensors remained operational throughout the entire operation. These displacement transducer sensors, installed by "floating" in specific bentonite blocks in the middle ring of the buffer, yielded very small length variations (in the range of 1 – 2 mm). Again, the problem was mechanical deformation as shown in Fig. 6-4 (frequent blockage).



Fig. 6-4: (Slightly) deformed (bended) extensometer

g) The **crack meter** (3S type, prototype sensor) failed quite early due to complete flooding and damage to the associated electronics.

Sensor performance evaluation according to the type of measurement technique showed the following results:

Vibrating wire type pressure cells: these proved to be robust and most of them remained operational. They were well designed and built for the harsh conditions, i.e., appropriate materials (stainless steel and tough plastics) and correct isolation at the cable entry. However, the cable entry was the weakest point, most probably due to the loss of flexibility of plastics with time combined with the differential movements of the cable in relation to the metal body.

Prototypes of new sensors: fisurometers – these need further improvement/development (mechanical protection and water isolation).

Sensors that measure in a chamber isolated by a filter: these became damaged over time due to flooding, salt deposition and bentonite intrusion, which led to corrosion and mechanical breakage.

Long-body sensors: these showed clear deformations due to bentonite swelling, making them unoperational with time.

In general: the plastic materials used for the cables were not good enough. Many of them were significantly degraded, losing their initial properties and becoming damaged. The effects of metal corrosion were generally negligible and not a relevant cause of malfunctioning.

The causes of sensor failure are summarised in Tab. 6-2 based on the results from data recorded during the operational lifetime, from the dismantling operation and from the post-dismantling evaluation/assessment analysis.

Tab. 6-2: Summary of sensor failure causes

García Siñeriz et al. (2019)

Type	Retrieved	Out of order	Causes			
			Saturated**	Flooded	Mechanical	Broken cable
T (bentonite)	54	15			15	
T (heater)	118	2*			2	
T (instrumented pipe)	8	0				
P (pz, plug)	2	2		2		
P (pz, inst. pipe)	8	5*			5	
P (VW)	6	3			3	
Q	28	11				11
WC (bentonite)	34	34	20	11		3
WC (inst. pipe)	18	12*	12			
WP	24	19	8			11
WT	10	3			1	2
SH	7	6			6	
SB	4	3			3	
3S	3	3				
S	4	0				
Total	228	99	40	16	35	27
Percentage	100.0%	43.4%	40.4%	16.2%	35.4%	27.8%

* Not analysed in the laboratory, ** reached 100%

6.3 TDR re-scaling

The TDR signals reflect the amount of water (i.e., volumetric fraction) within a certain sampling volume rather than gravimetric water content and the results were therefore compared with the laboratory sample analyses performed at the ETH (Villar et al. 2017). The differences found are related to unquantifiable changes in the temperature correction and/or the effect of damage to some of the probes over the long monitoring period. In consequence, the data were subjected to re-scaling so that their values satisfy the volumetric water contents obtained from the barrier in the years 1997, 2002 and 2015 (see details in Sakaki et al. 2017).

6.4 Conclusions and lessons learned

The performance of the installed sensors was satisfactory and significantly better than initially expected, as illustrated by Fig. 6-5. Most sensors kept providing reliable and valuable information on THM parameters for more than 18 years. Furthermore, a significant amount of information was obtained regarding the real status of the sensors after more than 18 years of in-situ operation, in conditions similar to those of a HLW repository, except for the radiation. The inspection of the sensor status yielded some recommendations for improvements for future experiments and monitoring programmes.

The use of high TRL (technology readiness level) sensors using passive measuring methods (such as the vibrating wire technique) proved to be the best choice. The failure rate for the low TRL sensors could be minimised for future applications by improving the mechanical protection using corrosion-resistant metals and avoiding weak plastic parts.

If they cannot be replaced by e.g. wireless devices, the cables should be armoured, made of long-lasting materials and routed to provide flexibility so that pulling forces due to bentonite swelling/movements are avoided.

The sensor bodies should not be too long and the joints between the bentonite blocks/layers should be avoided whenever possible to minimise mechanical deformations (see Fig. 6-4) largely resulting from shearing, which could lead to critical damage to the sensor functionality.

The TDR-estimated volumetric water content was considered to be representative of the qualitative trend of its temporal evolution, although the quantitative accuracy required refinement by "re-scaling". The checking/evaluation and re-scaling of the sensors that survived indicated that the accuracy of the data generated by these sensors remained relatively unchanged and that most of them showed negligible or very low drift (not for all parameters), and that the obtained data were trustworthy. Therefore, the confidence in the recorded data has increased significantly.

The conclusions reached from the evaluation of the sensors status after dismantling are of great importance because the information provided by the sensors helps to improve the understanding of the THM processes (Papafotiou et al. 2017). The database created is being used to validate several existing modelling codes. Furthermore, the obtained results will be used as a basis for designing other generic large-scale in-situ tests or future monitoring system of a repository, a task that has been also a part of the EU Modern2020 project (http://www.modern2020.eu/).

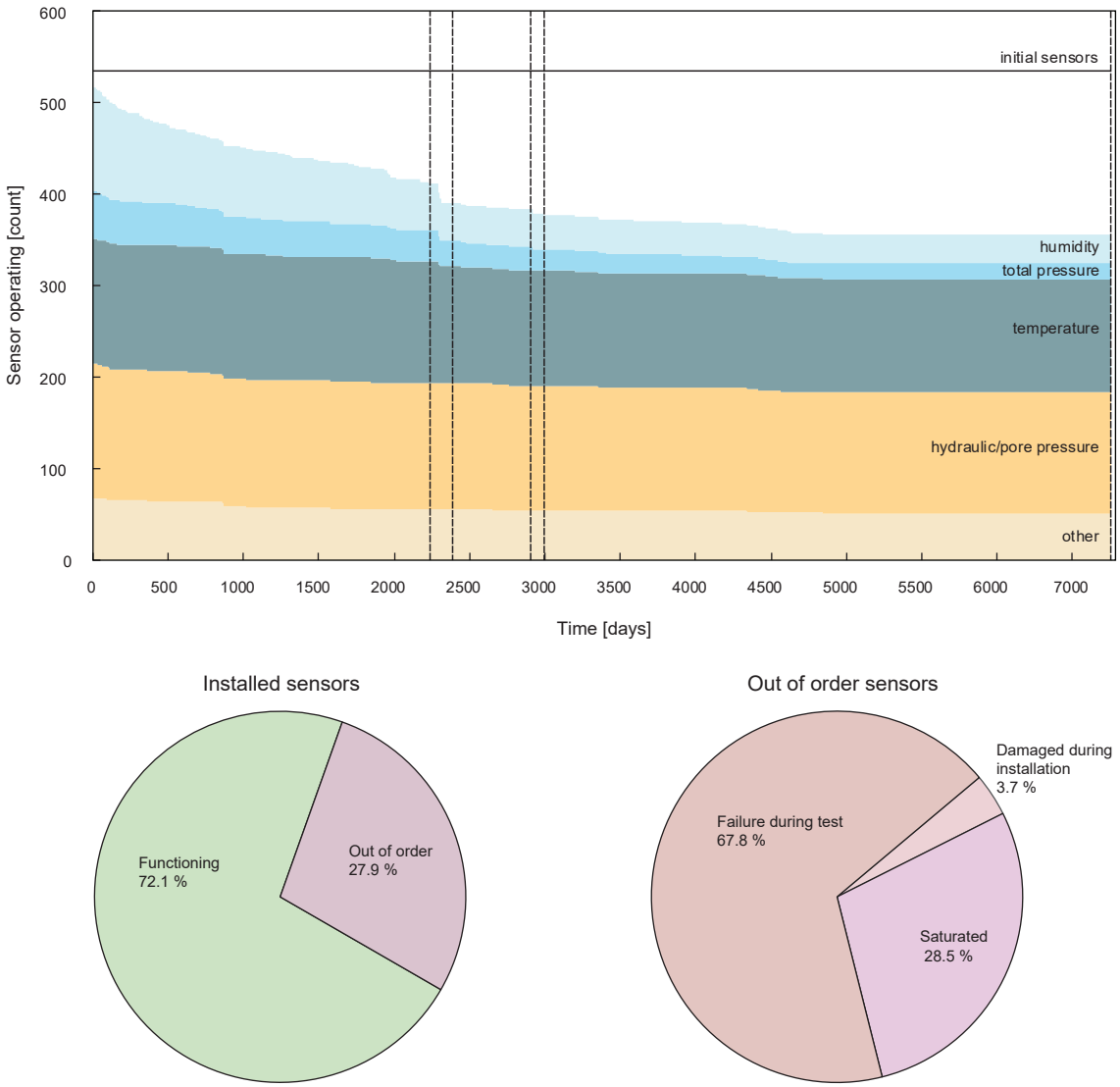


Fig. 6-5: Evolution of sensors operating throughout the lifetime of the experiment (top) and breakdown of defective sensors (bottom)

From Martínez et al. (2016)

7 Pre-dismantling modelling activities and synthesis of modelling activities

Apart from the objective of demonstrating the feasibility of constructing a specific design of an engineered barrier system, the FEBEX project also aimed to study the thermo-hydro-mechanical (THM) and thermo-hydro-(geo)chemical (THC) processes in the near-field. The examination of the THM and THC behaviour of the experiment is greatly assisted by the performance of numerical analyses. For this reason, THM and THC modelling of the in-situ test has been an ongoing activity throughout the project (Lanyon & Gaus 2016). In this chapter, the FEBEX modelling activities carried out previously (prior to dismantling) is presented in Sections 7.1 and 7.2., followed by a review and summary of the THM and THC modelling performed within the FEBEX-DP project (Sections 7.3 and 7.4). The current ongoing modelling activities are reported in Section 7.5. The chapter closes with a general synthesis of the modelling performed and an outlook for future activities.

7.1 Overview of THM modelling and codes until dismantling

The majority of the THM analyses of the FEBEX in-situ experiment before final dismantling were carried out by CIMNE (Centre Internacional de Mètodes Numèrics en Enginyeria, Barcelona, Spain) using the CODE_BRIGHT computer code. THM modelling was also performed by EPFL (Ecole Polytechnique Fédérale de Lausanne, Switzerland) using the LAGAMINE code. In addition, the early part of the FEBEX experiment was used as a benchmark within the DECOVALEX III international collaborative project. Significant modelling of the FEBEX in-situ test was also carried out within the NF-PRO and FEBEX-e projects. These modelling exercises are briefly reviewed below.

7.1.1 Modelling by CIMNE

The THM analyses by CIMNE using CODE_BRIGHT (Olivella et al. 1996) were based on a coupled THM formulation that involves the simultaneous solution of the balance equations of solid (mineral) mass, water mass, air mass, internal energy and momentum (equilibrium). The solid mass equation can be eliminated through the consideration of a material derivative leading to an auxiliary equation that provides the changes of porosity with time. In the analyses of the in-situ test, the gas pressure has generally been assumed to be constant, and the air mass balance equation is thus dropped. Therefore, the basic unknowns to be determined are displacements, liquid pressure (or suction) and temperature.

The formulation includes appropriate constitutive laws and equilibrium conditions designed to take into account the following phenomena:

- heat transport by conduction and advection
- water evaporation and condensation (including consideration of latent heat)
- liquid flow
- vapour diffusion
- deformation of the materials due to changes in stresses, suction, liquid pressure and temperature. The mechanical constitutive law is based on the Barcelona basic model (BBM, Alonso et al. 1990) formulated in terms of net stresses and suction.
- deformation of solid, liquid and gas constituent phases

The basic formulation has remained largely unchanged throughout. It is described in detail in ENRESA (2006b). Extensions of the formulation were developed to take into account a potential threshold gradient in Darcy's law, thermo-osmotic flow and evolution of the microfabric of compacted bentonite via the double-structure BExM model (Sánchez et al. 2005, 2007, 2010, 2012a). These extensions have had only a very limited use in the analysis of the in-situ test as they either have no significant effects or lead to worse predictions (Rodríguez-Dono et al. 2018). For this reason, those extensions of the formulation are not discussed further here.

THM modelling of the in-situ test has been performed at all stages of the experiment. Specifically, the following modelling stages (prior to pre-dismantling modelling) can be distinguished:

- pre-operational modelling
- operational modelling
- modelling of first dismantling
- modelling within the framework of the NF-PRO European project
- modelling during the FEBEX-e phase

The goal of the pre-operational modelling (ENRESA 1998c, 2000) was to gain a better understanding of the THM processes involved in the experiment and to assist in the design. At the time, available laboratory tests were limited and there was some uncertainty regarding the final test protocol. Consequently, significant knowledge was acquired, especially from a set of 1D parametric analyses that revealed the complexity of some interactions and allowed the identification of a number of key parameters, notable examples being permeability and retention curve. Fig. 7-1 shows an example of the results of the 1D sensitivity analyses. A limited set of 2D analyses (axisymmetric and plane strain) were also performed. The axisymmetric calculations yielded very similar results to the 1D analyses (in the heater central section) whereas the plane strain analyses showed that the problem was basically axisymmetric. Results of this stage of analyses have also been reported in Gens et al. (1998, 2002).

An analysis was developed at the start of the heating stage of the test (once the heating protocol was known) in order to establish comparisons with observations as the test progressed. This operational modelling analysis was named Operational Base Case (OBC). It remained unchanged during the experiment and has provided the numerical results for comparison with observations. The main features of the OBC analysis are described in ENRESA (2000, 2006a, 2006b). The OBC results provided a very adequate qualitative description of the various THM observations demonstrating their capability to properly consider the complex interactions between different types of processes (Gens et al. 2009). Quantitatively, temperatures were well predicted (although there were some unexplained discrepancies concerning heater power), the evolution of bentonite hydration was adequately captured, and more differences were observed concerning swelling stresses potentially affected by the lower reliability of stress measurements. The behaviour of the rock was far simpler and is well represented in the analysis. As an example of the results of the calculations, Fig. 7-2 shows the comparison of computed and observed relative humidity for a Section across Heater #1 (Section E1) at different radial distances r (m) from the tunnel axis.

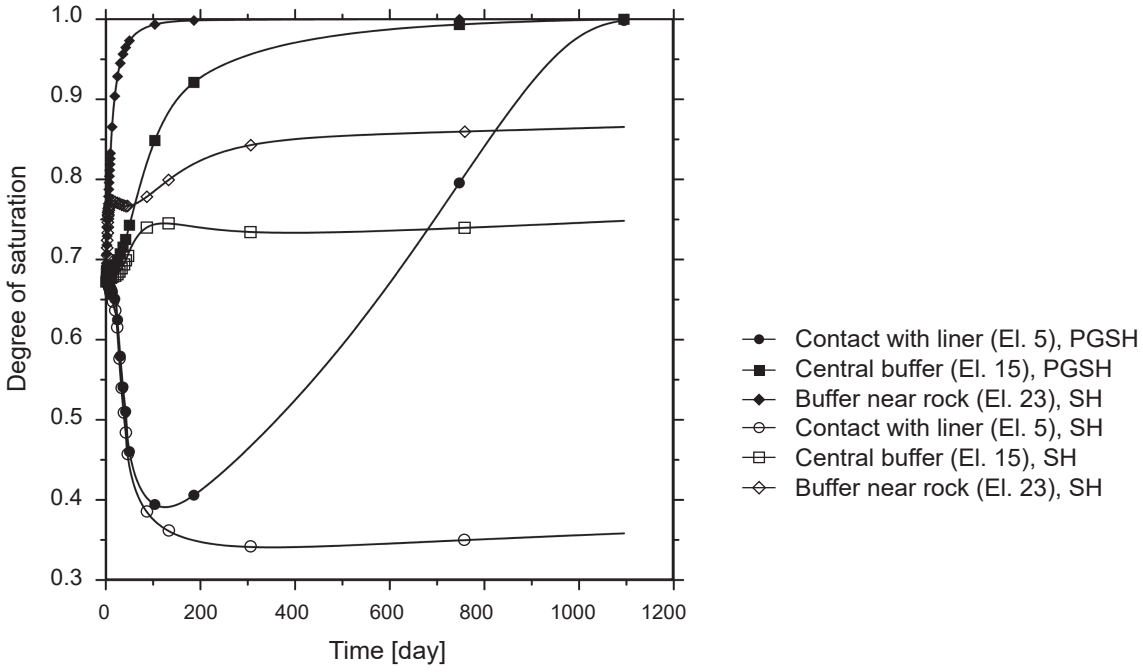


Fig. 7-1: Evolution of degree of saturation with alternative retention curves for the bentonite resulting in granite desaturation (SH) and no granite desaturation (PGSH)

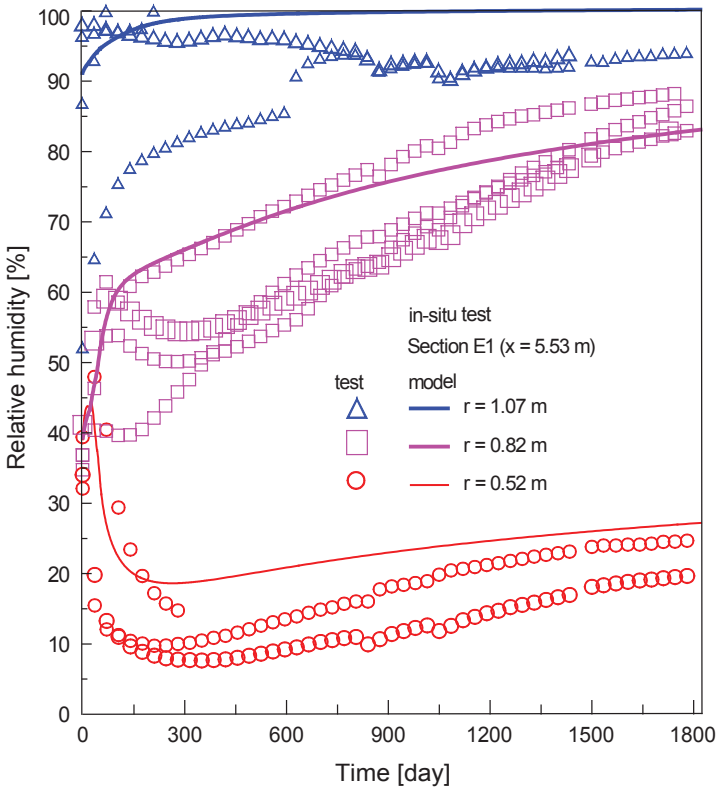


Fig. 7-2: Computed (OBC analysis) and observed evolution of degree of saturation in Section E1 (across Heater #1, Fig. 1-4) at different radial distances r from the tunnel axis

The OBC was modified to incorporate the removal of Heater #1 after five years of heating (ENRESA 2006a, 2006b, Sánchez et al. 2012b). The dismantling modelling considered the shut-off of Heater #1 and the various stages of bentonite removal and heater extraction (Fig. 7-3). The analyses provided data that could be compared with the state of the barrier determined during the dismantling (ENRESA 2006b, Gens et al. 2009). As illustrated in Fig. 7-4, the modelling results agreed remarkably well with the observations considering that they were based on a prediction without additional calibration. This enhances confidence in the soundness and relevance of the THM modelling performed. A closer look at the comparisons reveals that the computed degree of hydration lags a little behind observations. The analysis was continued (ENRESA 2006b) beyond dismantling and again yielded adequate agreement with observations, although the number of monitoring points was now drastically reduced through sensor removal and a number of sensor failures.

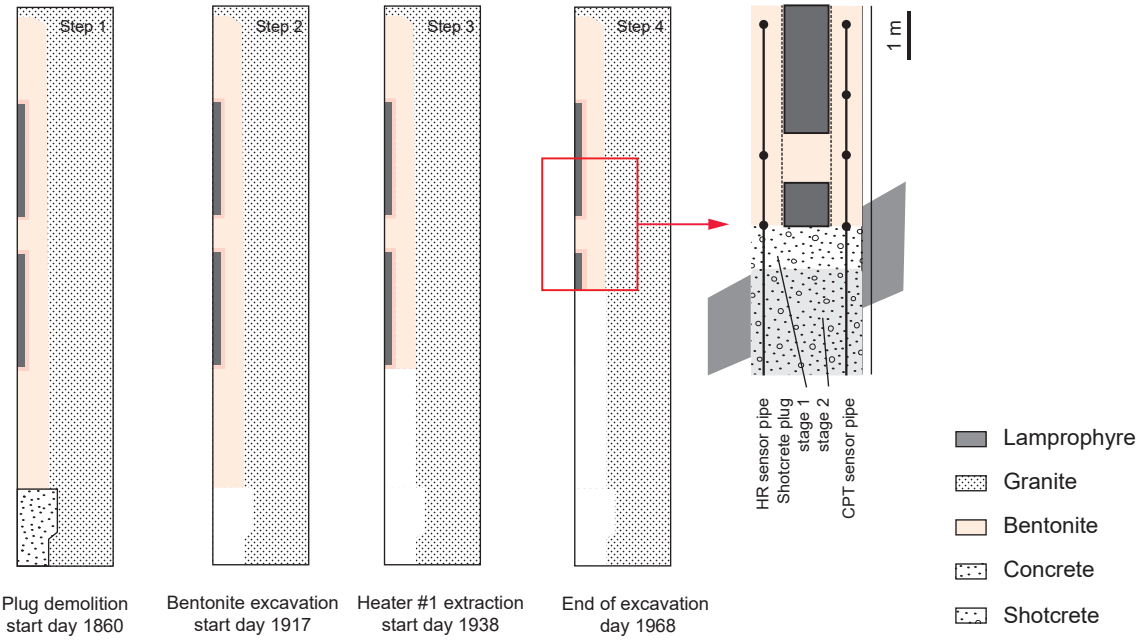


Fig. 7-3: Stages considered in the dismantling modelling

Modelling of the in-situ test continued as part of the work package WP3.3 of the European NF-PRO project that ran from January 2005 to December 2007. No significant new modelling activities were undertaken, as the goal was to check and review the comparisons of the OBC (modified to include the first dismantling) and observations up to 11 years of testing. No significant deviations were observed, and modelling continued to provide appropriate predictions of the limited set of sensor measurements available. The results of this modelling were reported in Sánchez & Gens (2007, 2008). Analyses were also performed during the FEBEXe phase of the experiment that ran from 2008 to 2014 (Rodríguez-Dono et al. 2018). Although slight modifications were introduced (use of standard van Genuchten law for retention curve and the adoption of an unstructured mesh for the granite), the model produced similar results to previous analyses. However, increasing the bentonite permeability led to results somewhat closer to measurements. Incorporation of thermo-osmosis led to larger differences with observations, whereas the consideration of double structures in the bentonite did not noticeably modify the outcome of the analyses.

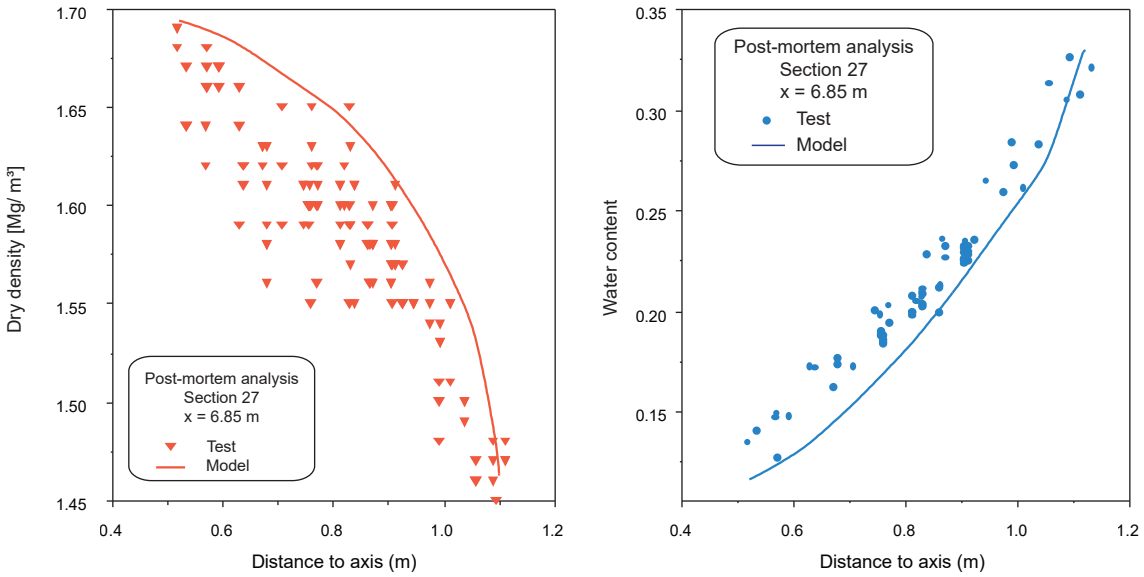


Fig. 7-4: Predicted and observed distributions of dry density and water content in a section across Heater #1

7.1.2 Modelling by EPFL

Modelling of the in-situ test was carried out by the EPFL group using the LAGAMINE code (Charlier et al. 2001). The work is reported in Dupray et al. (2013). The basic coupled formulation is similar to that employed in CODE_BRIGHT but there are a number of differences. The behaviour of the bentonite was modelled based on the ACMEG-TS thermoplastic constitutive model (Laloui & Francois 2009) for saturated and unsaturated soils that incorporates irreversible effects due to temperature. The parameters of the model were derived from back-analysis of oedometer tests under controlled suction and temperature. The ACMEG-TS model is formulated in terms of effective (Bishop) stress differing from the net stress formulation of the BBM constitutive model used in CODE_BRIGHT. In addition, the water retention behaviour of the bentonite includes the effects of hysteresis, temperature and mechanical strains.

Temperatures were predicted quite accurately by the analyses performed, and the simulation of the pattern of hydration and stress development was also adequate, although some quantitative differences from observations can be seen such as the evolution of relative humidity for a section across Heater #2 shown in Fig. 7-5. Overall, the type of results obtained using LAGAMINE are not significantly different from those derived from CODE_BRIGHT analyses. Dismantling was not modelled and the state of the barrier after five years of heating was not computed at this stage.

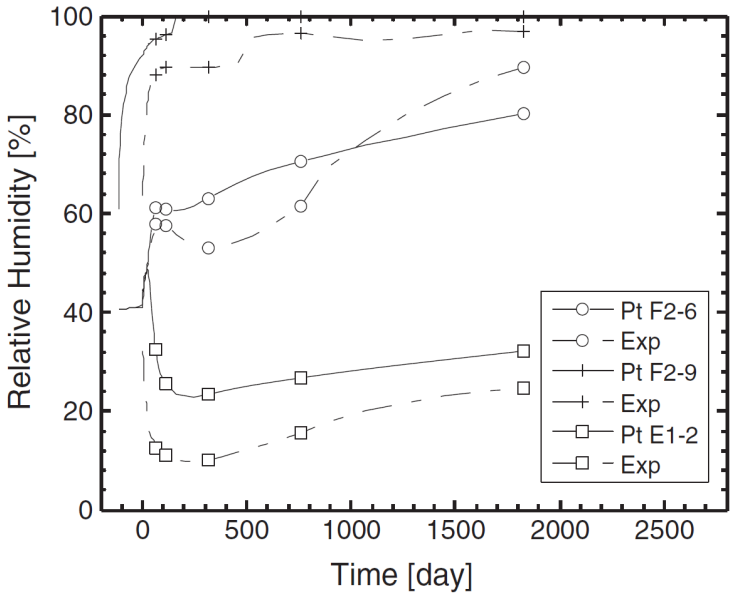


Fig. 7-5: Computed and experimental evolutions of relative humidity in a section across Heater #2

Analysis performed using LAGAMINE code (Dupray et al. 2013)

7.1.3 Modelling performed within the framework of the DECOVALEX III project

The early part of the in-situ test (up to 1'000 days of heating) was adopted as a benchmark by the DECOVALEX III project (Tsang et al. 2005) and was structured in three parts (Alonso & Alcoverro 2005):

Part A: Hydro-mechanical modelling of the rock, which dealt with the excavation of the FEBEX tunnel; water inflow and water pressure changes were required.

Part B: Thermo-hydro-mechanical analysis of bentonite behaviour. Input power, temperature, relative humidity, stresses and displacements were computed.

Part C: Thermo-hydro-mechanical behaviour of the rock during the test. Temperature, stresses, water pressures and displacements were required.

Tab. 7-1 lists the ten different modelling teams that participated in the benchmark together with their funding organisations and the computer codes employed. The benchmark was coordinated by UPC and supported by ENRESA. An important proportion of the benchmark was devoted to the behaviour of the rock, however, the most relevant results were obtained in Part B focused on the THM behaviour of the bentonite. A full account of all the benchmark activities is presented in Alonso et al. (2005).

Tab. 7-2 shows the teams that reported numerical analyses for Part B, i.e., on the thermo-hydro-mechanical behaviour of the bentonite. It can be noted that a variety of approaches was adopted with different degrees of coupling. Four teams (CNSC, US-DOE, SKB and SKI) incorporated the full range of THM processes and only one team (BGR) explicitly considered gas flow.

Tab. 7-1: Funding organisations, modelling teams and computer codes involved in the FEBEX in-situ test DECOVALEX III benchmark

Funding organisation	Country	Modelling team	Computer code
Andra	France	Laboratory "Sols, Solides, Structures" Grenoble. Ecole Polytechnique (G3S)	ANTHYC 3D
Andra	France	Laboratoire Environnement, Géoméch. et Ouvrages. Ecole des Mines de Nancy (LAEGO–ENM)	3DEC-3FLO
BGR	Germany	Federal Institute for Geosciences and Natural Resources (BGR)	RF – RM
CNSC	Canada	Canadian Nuclear Safety Commission (CNSC) & Mc Gill University	COSMOS/M FRACON
US–DOE	USA	Sandia National Laboratories (SNL)	TOUGH2 – JAS3D
IRSN	France	Institute for Radiological Protection and Nuclear Safety (IRSN) & Ecole des Mines de Paris	CHEF – HYDREF – VIPLEF
JNC	Japan	Hazama Corporation, Kyoto University & Japan Nuclear Cycle Development Institute (JNC)	THAMES3D
SKB	Sweden	Clay Technology AB & FEM–Tech AB	ABAQUS
SKI	Sweden	Lawrence Berkeley National Laboratory (LBNL)	ROCMAS
STUK	Finland	Helsinki University of Technology	ELMER

Tab. 7-2: Couplings and phenomena considered by the various teams involved in the modelling of Part B

Team	Couplings	Deformation	Water flow	Vapour diffusion	Phase change	Gas flow	Heat conduction
BGR	TH → HM		•			•	•
CNSC	THM	•	•	•	•		•
US–DOE	TH → TM	•	•	•	•		•
IRSN	THM	•	•				•
JNC	TH		•	•	•		•
SKB	THM	•	•	•	•		•
SKI	THM	•	•	•	•		•
STUK	TH		•	•	•		•

The degree of agreement with observations of the numerical results of the various teams was uneven. For example, Fig. 7-6 shows the results for the evolution of relative humidity corresponding to the first 1'000 days of the experiment for a section located between the two heaters. In general, better results were obtained by the teams that used fully coupled formulations that incorporated the full range of THM processes. Since the benchmark was focused on the early part of the test, the inclusion of vapour diffusion and phase change was particularly important to satisfactorily reproduce that stage of the experiment.

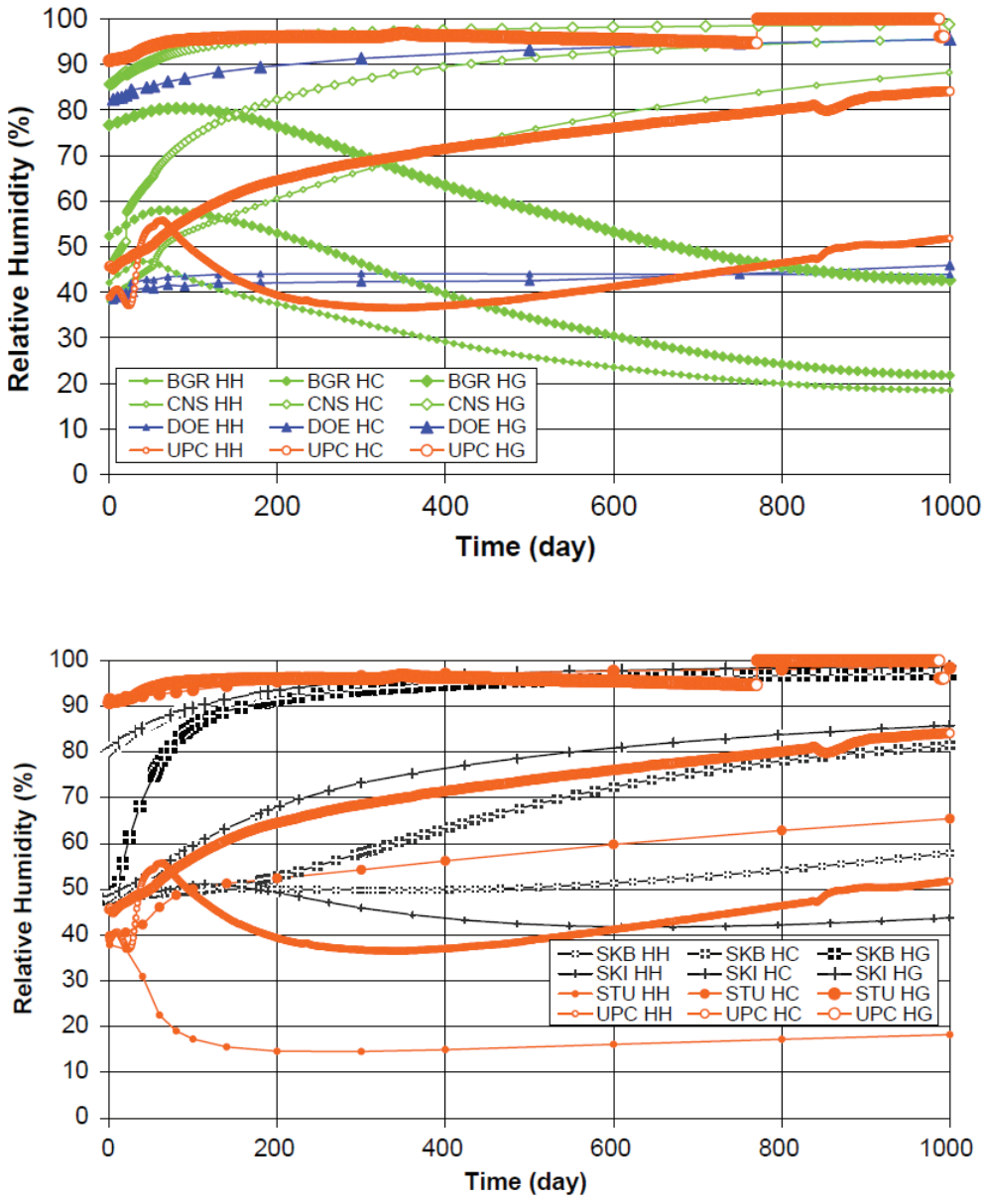


Fig. 7-6: Comparison of computed evolutions of relative humidity by the different modelling teams and observations. Experimental results are in orange and labelled UPC

7.1.4 Summary of THM modelling and codes until dismantling

Most of the initial THM formulations and constitutive laws employed in the modelling reported above were able to adequately reproduce the main trends of THM observations, suggesting that all relevant phenomena had been properly included. Appropriate modelling of vapour production and migration were found to be essential to simulate the early part of the experiment. In contrast, the modelling details concerning the rock mass turned out to be unimportant because, in this case, the permeability of the bentonite and not that of the rock controls the hydration process.

Considering quantitative comparisons between calculations and observations, the temperature field was generally well reproduced, reflecting the fact that heat transport is dominated by conduction and a good estimate of thermal conductivity (and its evolution) is sufficient for a satisfactory simulation. More quantitative discrepancies were observed regarding the progress of hydration. The reason for this is believed to lie in the sensitivity of hydration to small changes in hydraulic parameters and coupling laws rather than in a lack of understanding of the processes involved. Quantitative differences were also noted in the development of swelling stresses that can be due to shortcomings of the mechanical constitutive models used and/or uncertainties of the measurements.

Generally, the first dismantling data were well predicted by CIMNE in both hot and cool sections, although the water content predictions by the Operational Base Case (OBC) appear to lag slightly behind the actual progress of hydration. The dismantling observations and measurements exhibited a basically axisymmetric nature, indicating a very limited role of the rock discontinuities and of the gaps between the blocks.

Some analyses incorporating more sophisticated features (e.g. thermo-osmosis, water retention hysteresis, fabric evolution) provided interesting insights into the nature of the problem but they did not improve the results significantly, indicating a high degree of robustness of the initial THM formulations.

7.2 Overview of THC modelling and codes until dismantling

The bulk of the THC modelling was performed by the modelling group at UDC (Universidad de A Coruña). The CIMNE group also carried out THMC analyses of the in-situ test (Guimarães 2002, Guimarães et al. 2006), but the focus was on the development of the formulation and coupled THMC code rather than on a close reproduction of the experimental results. Therefore, only the THC modelling performed by UDC is reviewed here. The work has been reported in ENRESA (2006a, 2006c) and Samper et al. (2008). Thermo-hydro-geochemical activities are denoted as THG in the ENRESA reports but the more common THC acronym is used here.

In general, THC modelling was less extensive than THM modelling, probably because of the complexity of the subject and the lack of experimental data. Whereas THM observations were abundantly available during the performance of the in-situ experiment, no geochemical data from the in-situ test were obtained until the first dismantling. In spite of these limitations, very valuable THC modelling was undertaken and applied to the interpretation of laboratory tests, the mock-up test and the in-situ test.

Three different conceptual geochemical models were used, based on different bentonite porewater datasets:

- CGM-0. Based on squeezing data (Samper et al. 2001)
- CGM-1. Based on aqueous extraction data (Samper et al. 2005)
- CGM-2. Modified version of CGM-1 including squeezing data (Samper et al. 2005)

Both methods of porewater extraction (squeezing and aqueous extraction) are affected by artefacts and have to be corrected via the application of a suitable geochemical model. This inevitably introduces a degree of uncertainty.

The chemical species considered in the three conceptual geochemical models are listed in Tab. 7-3. Models CGM-0, CGM-1 and CGM-2 incorporated aqueous complexation, acid-base reactions, mineral dissolution/precipitation, gas dissolution/exsolution and cation exchange. These processes were assumed to be at local equilibrium except for calcite and dolomite that can dissolve or precipitate under kinetic conditions in models CGM-1 and CGM-2.

A proper geochemical modelling approach requires knowledge of the thermal, hydraulic and mechanical variables at every point in the analysis domain. Thus, the geochemical module has to be coupled to a TH or a THM formulation of the type described in Section 7.1. This results in a THC formulation (if mechanical effects are ignored) and a THMC formulation (if mechanical effects are considered).

Tab. 7-3: Chemical species considered in models CGM-0, CGM-1 and CGM-2

Samper et al. (2008)

Geochemical models	**CGM-0**	**CGM-1**	**CGM-2**
Primary species	H_2O, H^+, Ca^{2+}, Mg^{2+}, Na^+, K^+, Cl^-, SO_4^{2-}, HCO_3^-, $SiO_{2(aq)}$		
Aqueous complexes	OH^-, $CaSO_{4(aq)}$, $CaCl^+$, $MgCl^+$, $NaCl_{(aq)}$, $MgHCO_3^+$, $NaHCO_{3(aq)}$, $CaHCO_3^+$, $MgCO_{3(aq)}$, $CaCO_{3(aq)}$, $CO_{2(aq)}$, CO_3^{2-}, KSO_4^-, $MgSO_{4(aq)}$, $NaSO_{4(aq)}$, $H_2SiO_4^{2-}$, $HSiO_3^-$		
Minerals	Calcite (equilibrium)	Calcite (kinetic)	Calcite (kinetic)
	Chalcedony (equilibrium)	Chalcedony (equilibrium)	Chalcedony (equilibrium)
	Gypsum/anhydrite (equilibrium, only precipitation)	Gypsum/anhydrite (equilibrium)	Gypsum/anhydrite (equilibrium, only precipitation)
		Dis-dolomite (kinetic)	Dis-dolomite (kinetic)
Exchangeable cations	Ca^{2+}, Mg^{2+}, Na^+, K^+	Ca^{2+}, Mg^{2+}, Na^+, K^+, H^+	Ca^{2+}, Mg^{2+}, Na^+, K^+, H^+
Gases	No condition on $CO_{2(g)}$	Fixed $CO_{2(g)}$ pressure	Fixed $CO_{2(g)}$ pressure

There was continuous development of computer codes to implement the THC and THMC formulations: CORE2D V4 (Samper et al. 2003, 2012), FADES-CORE (Juncosa 2001), INVERSE-CORE2D (Dai & Samper 2004) and INVERSE-FADES-CORE (Zheng & Samper 2004 and 2005). The reported THC analysis of the in-situ test (Samper et al. 2008) was performed using INVERSE-FADES-CORE, a code that solves both forward and inverse multiphase flow and multicomponent reactive transport problems in 1 and 2 dimensions (including axisymmetric dimensions) for porous and fractured media. The analysis used a 1D finite element mesh taking advantage of radial symmetry conditions.

An example of the type of results obtained is shown in Fig. 7-7 that plots the computed radial distribution of Cl^- together with the recalculated experimental data. The general pattern of variation of what is effectively a conservative tracer is reasonably captured by the modelling. In this case, the effect of using different geochemical models is small. Larger differences are obtained with other ions such as Ca^{2+} or Mg^{2+}.

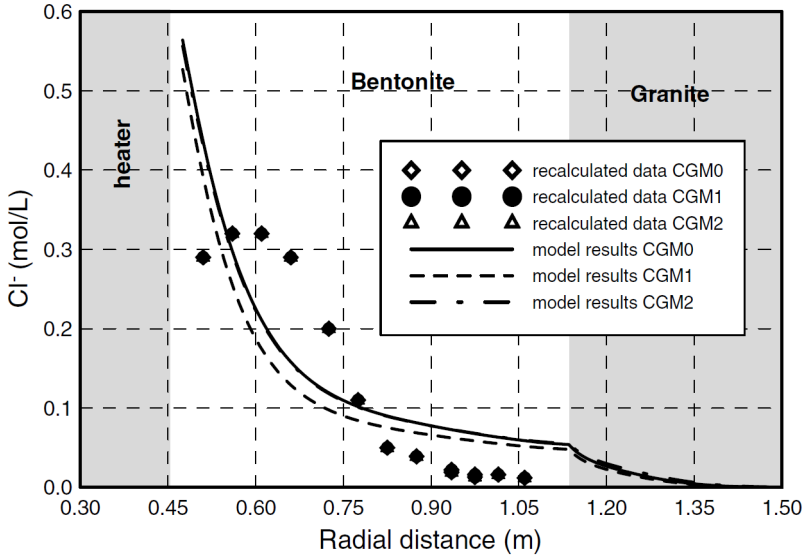


Fig. 7-7: Comparison of computed distributions of Cl^- concentrations with recalculated experimental data after 1930 days of heating (first dismantling)

The distribution of chemical species is the result of the interaction of a number of phenomena that are considered in the THMC model: porewater evaporation near the heater, water condensation in the outer part of the barrier, dilution due to inflow of granitic groundwater, advective advance of the hydration front, and solute diffusion. Dilution and evaporation phenomena appear to be generally dominant, at least during the early part of the experiment. Apart from sulphate (SO_4^{2-}) and bicarbonate (HCO_3^-), the THC calculations reproduced the general trends of most chemical species, albeit with significant quantitative discrepancies.

Subsequently, a more advanced THMC model was applied to the analysis of the in-situ test (Zheng et al. 2011), which includes thermal and chemical osmosis as well as an explicit consideration of the deformation of the bentonite via a state-surface approach (Lloret & Alonso 1985). Fig. 7-8 shows the concentrations of Cl^- obtained in the new analysis. It can be observed that if bentonite swelling is not considered, Cl^- concentrations are severely underestimated.

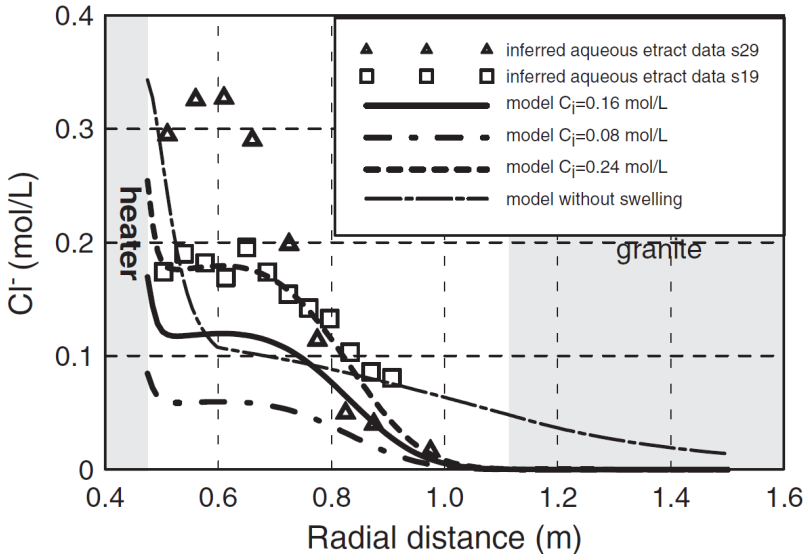


Fig. 7-8: Comparison of computed distributions of Cl^- concentrations with inferred aqueous extract data after 1930 days of heating (first dismantling)

The new analysis yielded a reasonable match for Cl^- and cations (Ca^{2+}, Mg^{2+}, Na^+, K^+) that largely follow the Cl^- trend. Chemical osmosis effects turned out to be negligible. The importance of calcite dissolution, cation exchange reactions and gypsum/anhydrite dissolution/precipitation for the geochemical evolution of the buffer was also highlighted. However, model results deviated strongly from measurements at the interfaces. HCO_3^- and pH data could not be explained by the model either. It is suggested that this may be due to CO_2 degassing and transport within the buffer. In summary, although very important advances were made through modelling, significant uncertainties remain in the understanding of the geochemical evolution of the barrier in the in-situ test.

7.3 Pre-dismantling THM modelling

Prior to the final dismantling, a number of THM modelling activities were undertaken. One of the goals of this modelling phase was to perform a blind prediction exercise comparing selected results of the analyses with observations of dry density and water content from final dismantling. Three modelling teams participated: CIMNE, EPFL and Clay Technology (CT). CIMNE and CT used the CODE_BRIGHT computer code whereas EPFL used LAGAMINE. As indicated above, CIMNE and EPFL had already performed THM analyses in previous stages of the project and the pre-dismantling modelling was therefore a continuation of previous numerical models. In contrast, the analysis of CT was the first one performed by the group regarding the FEBEX in-situ test. The pre-dismantling THM modelling of the three groups is presented in Papafotiou et al. (2017) and includes sections on the joint interpretation of the modelling results and on the comparison of predictions with observations. Only the most salient features and results of the analyses are discussed here.

Two instrumentation sections were selected for the blind prediction exercise: F2 and G (Fig. 7-9). These correspond to dismantling sections S49 and S39, respectively. Computed values of dry density and water content for those two sections were requested from the modelling teams before the dismantling observations were available. Section F2 corresponds to a section through the centre of Heater #2 and is therefore representative of the THM behaviour of the barrier at higher temperature. In contrast, the cooler section G is less representative because of the presence of a perfo-

rated liner dividing the barrier into two parts and the proximity to a dummy cylinder (replacing part of the extracted Heater #1) and to the new concrete plug. Unavoidably, this atypical location introduces uncertainties in the comparison with measurements.

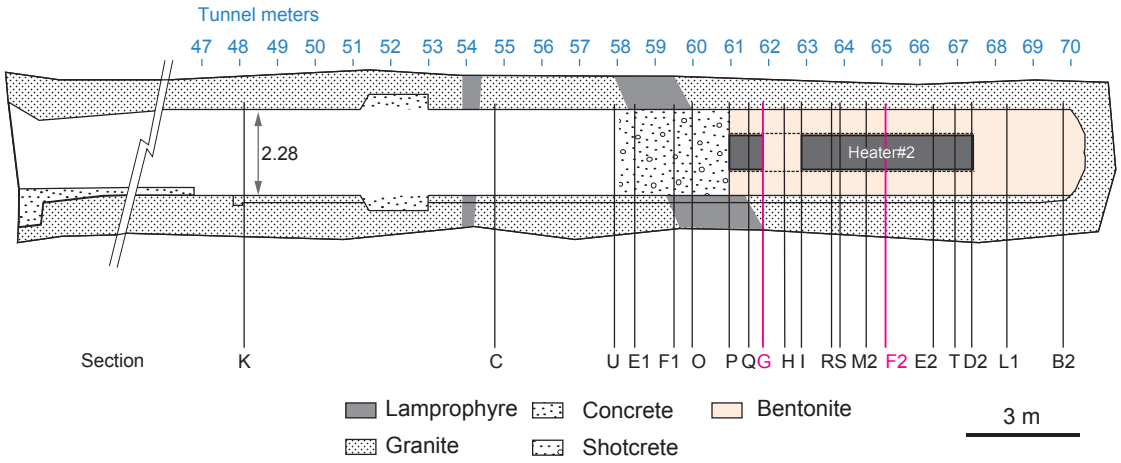


Fig. 7-9: Location of sections F2 and G selected for checking blind predictions

Although the focus is on the dismantling data, the computation of the final state of the barrier requires the simulation of the entire history of the experiment from the initial tunnel excavation, through test installation, heating phase, partial dismantling to final dismantling. In this section, the most significant features of the three modelling exercises are presented first. Afterwards, a joint overview of the three sets of results is presented together with comparisons with dismantling observations.

7.3.1 Pre-dismantling modelling by CIMNE

The pre-dismantling modelling by CIMNE was the continuation of the OBC analysis using the CODE_BRIGHT code already summarised in Section 7.1.1. It was already shown that the analysis was capable of adequately reproducing the observations gathered during the progress of the test as well as the state of the barrier (dry density and water content) observed after the first dismantling in both hot and cooler cross-sections. Although the general pattern of results was satisfactorily replicated, there were, naturally, quantitative differences. For instance, the comparison with water contents obtained during the first dismantling suggested that the computed degree of hydration somewhat underestimated the actual rate of barrier saturation.

The computation of the final state of the barrier required the simulation of the final dismantling and was performed considering the stages shown in Fig. 7-10. These are: switching off Heater #2, plug demolition, heater extraction and two phases of bentonite removal. The predicted distributions of water content and dry density in sections F2 and G are shown in Fig. 7-11. In section G, the OBC model considered the presence of a steel liner at a radius of 0.45 metres. This feature accounts for the discontinuity in the distributions of water content and dry density. Apart from the uncertainty introduced by the possible effects of the presence of the liner, the mesh discretisation in the domain inside the liner was quite coarse, so the computations in that area should be regarded as approximate only.

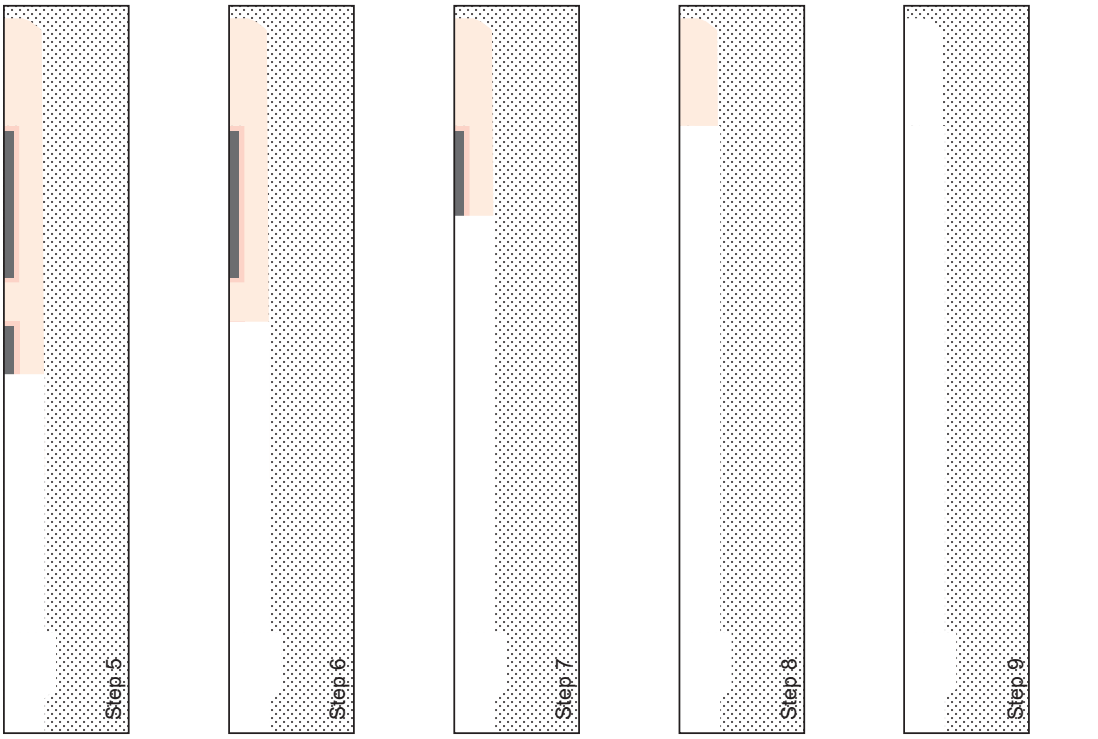


Fig. 7-10: Stages considered in the simulation of the final dismantling (CIMNE model)

Parallel to the OBC analysis, a number of complementary analyses were carried out by CIMNE during the progress of the FEBEX experiment to investigate the potential effects of other parameters and/or phenomena. An interesting set of analyses concerning the effect of the bentonite retention curve are reported in Papafotiou et al. (2017). Specifically, the influence of the parameter P_0 in the Van Genuchten expression (related to the air entry value) has been investigated for P_0 values of 7 MPa (OBC), 12 MPa, 16 MPa and 20 MPa. As Fig. 7-12 shows, all the resulting retention curves are well within the range of experimental results. The full results of this sensitivity analyses are presented in Papafotiou et al. (2017). For greater clarity, Fig. 7-13 shows the results for values of P_0 of 7 MPa and 20 MPa, demonstrating that a rather minor change in retention curve has a significant impact on the rate of hydration, but has only a minor effect on the distribution of dry density.

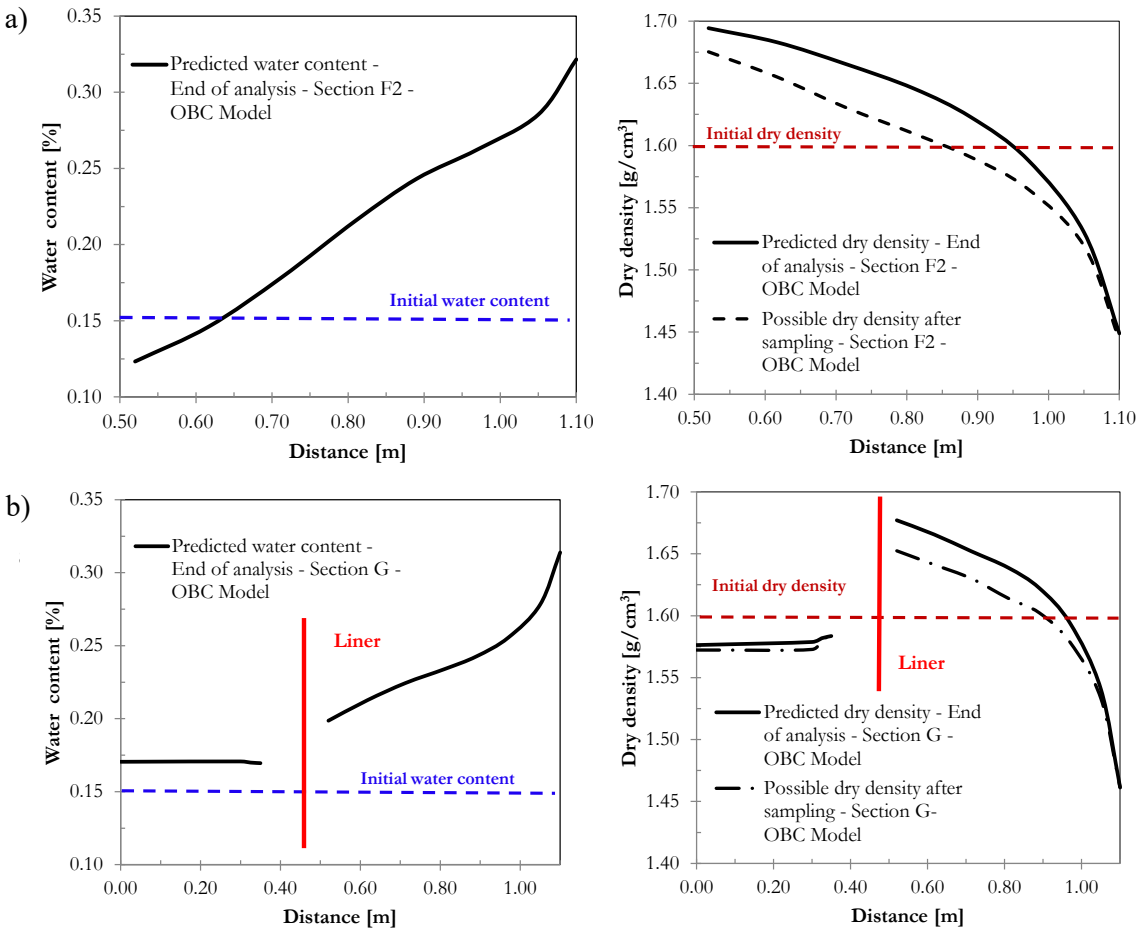


Fig. 7-11: Predictions of water content and dry density for the final dismantling, a) Section F2, b) Section G (CIMNE model)

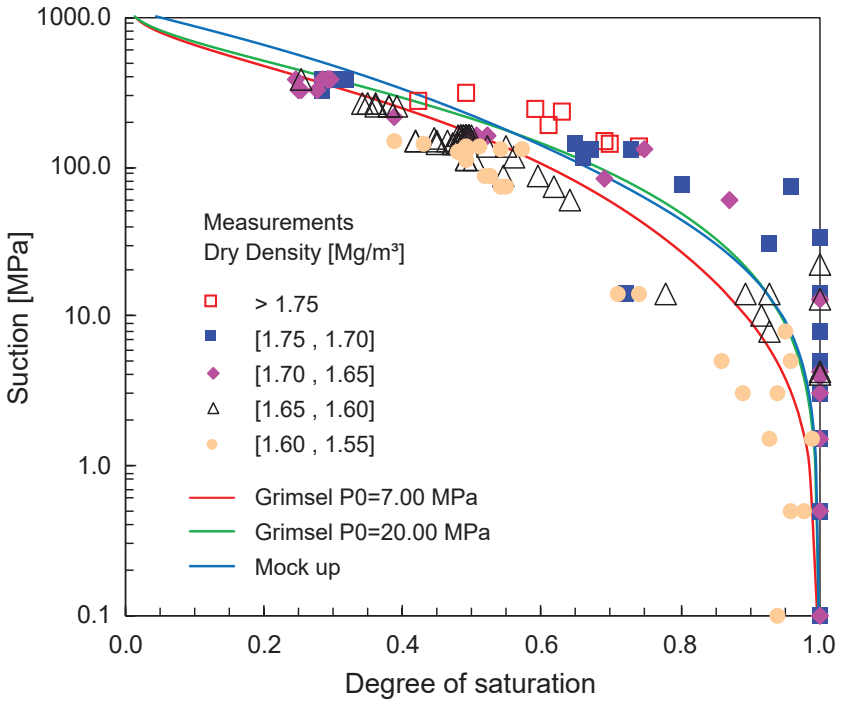


Fig. 7-12: Range of retention curves used in the sensitivity analyses (CIMNE model)

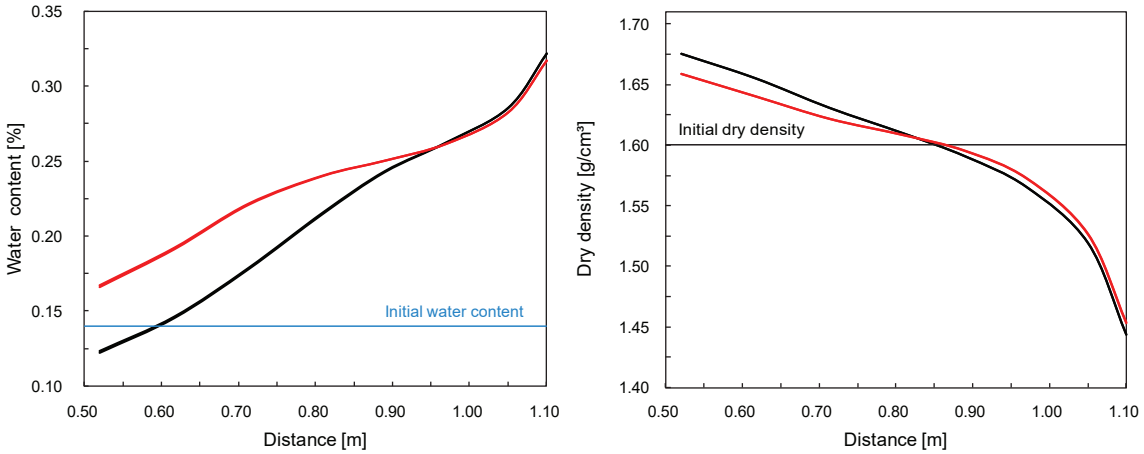


Fig. 7-13: Distributions of water content and dry density with values of P0 of 7 MPa (black line) and 20 MPa (red line), Section F2 (CIMNE model)

7.3.2 Pre-dismantling modelling by EPFL

The pre-dismantling modelling performed by EPFL used the LAGAMINE code, which can be considered the continuation of the simulation program outlined in Section 7.1.2. The formulation shares the same basic features as CODE_BRIGHT but differs significantly in the type of constitutive models used. As indicated above, the mechanical behaviour of the bentonite is defined by the ACMEG-TS thermoplastic constitutive model that incorporates irreversible effects due to temperature. Fig. 7-14 presents a graphical scheme of the bases of the ACMEG-TS model. Furthermore, a general water retention model of the bentonite is used that can incorporate the effects of hysteresis, temperature and mechanical strain.

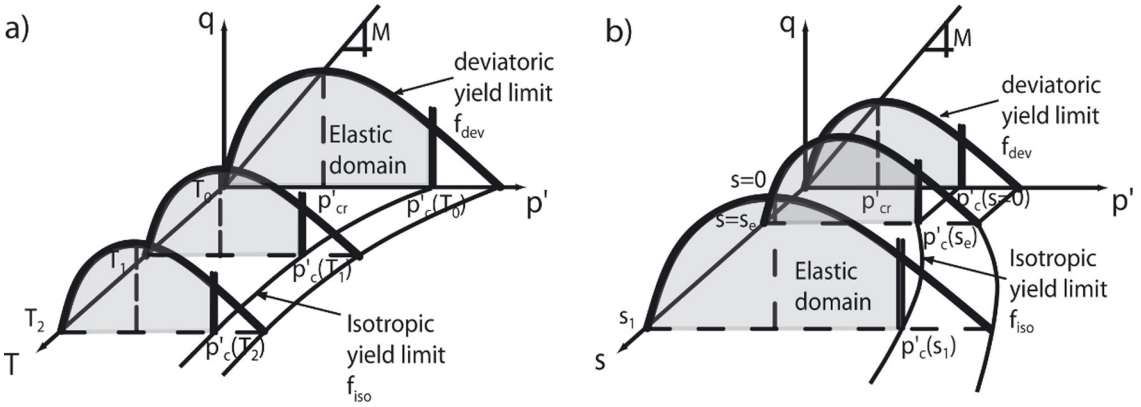


Fig. 7-14: ACMEG-TS model

Effect of (a) temperature and (b) suction on the shape of coupled mechanical yield limits

The pre-dismantling analyses have included the simulation of all the phases of the experiment from tunnel excavation to final dismantling. The same thermal parameters have been used as before but a number of hydraulic and mechanical parameters have been modified for this analysis. The effect of temperature and void ratio changes on the retention curve have now been ignored. The domain size, mesh and boundary conditions are the same as in previous calculations.

The comparisons between computed and observed dry density and water content for the first dismantling are shown in Fig. 7-15 (hot section) and 7-16 (cool section). A quite satisfactory agreement is apparent. Predicted water content and dry density at Sections F2 and G for the final dismantling are shown in Fig. 7-17.

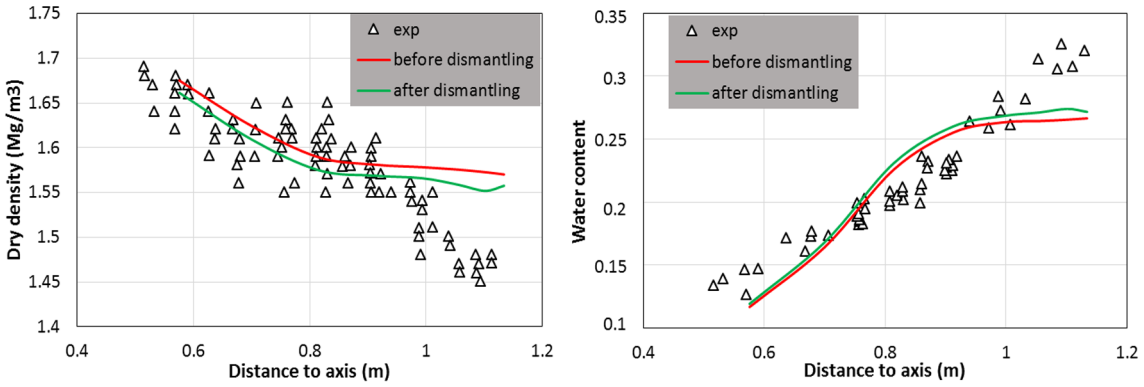


Fig. 7-15: Computed and observed distributions of dry density and water content after first (partial) dismantling of Section 27 (hot section, near instrumented section F1, ~ 6.9 m into buffer from first plug, see Fig. 1-4) (EPFL model)

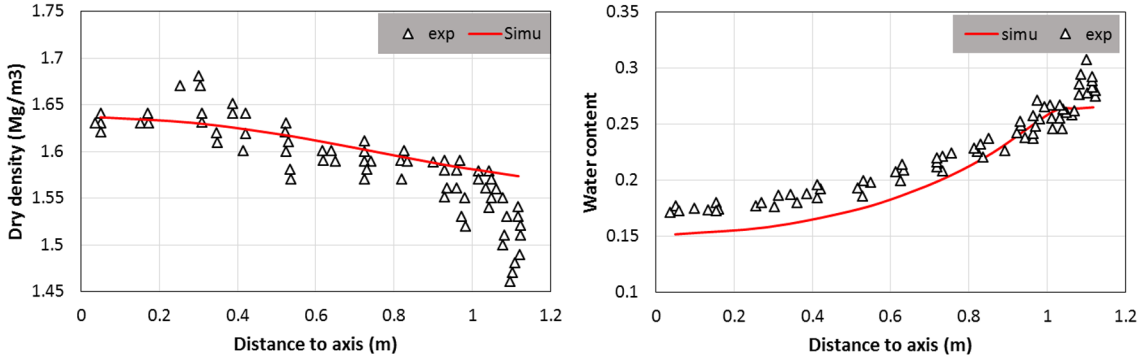


Fig. 7-16: Computed and observed distributions of dry density and water content after first (partial) dismantling of Section 15 (cool section, ~ 3.3 m into buffer from first plug, see Fig. 1-4) (EPFL model)

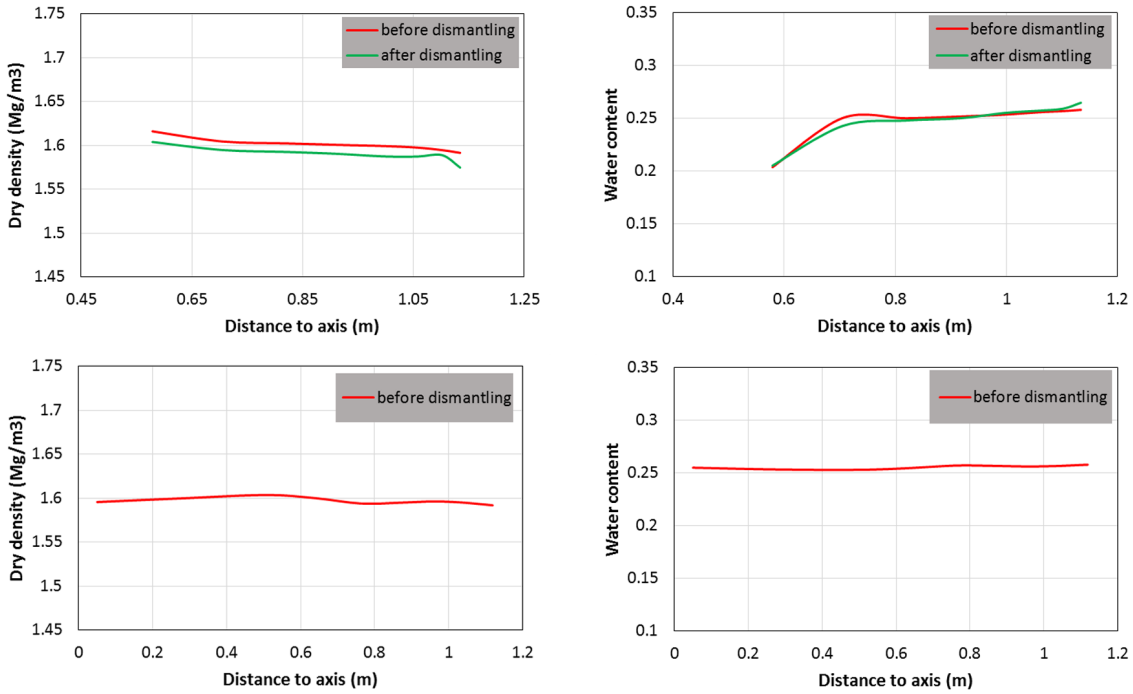


Fig. 7-17: Predictions of water content and dry density for the final dismantling
a) Section F2, b) Section G (EPFL model)

7.3.3 Pre-dismantling modelling by Clay Technology

The pre-dismantling modelling carried out by Clay Technology (CT) was not a continuation of any previous work. The calculations were performed using the CODE_BRIGHT computer code and a version of the BBM model for the mechanical constitutive law. Thus, the basic formulation was similar to those of CIMNE and EPFL, but the modelling strategy was different.

In this case, only one section, across the centre of a heater, was considered. The modelling domain was one-dimensional (with radial symmetry) and encompassed the bentonite barrier only. An analytical thermal calculation (axisymmetric) of the rock was performed, using the measured heater power as input, to provide the temperature boundary condition at the outer edge of the barrier.

An important feature of this analysis is that the initial gap between rock and barrier is explicitly considered. Thus, the initial properties of the bentonite correspond to a dry density of 1.70 g/cm^3 (which is the actual dry density of the blocks) instead of the average value of 1.60 g/cm^3 used by the other two modelling teams. Consequently, the bentonite domain has an outer radius of 1.112 m and the rock radius is 1.14 m, leaving a gap of 28 mm. In addition, all the volumes of the gaps between the blocks have been concentrated in the outer bentonite/rock interface. The gap behaviour is represented by a bi-linear elastic model. Fig. 7-18 shows the geometry of the analysis domain together with the adopted boundary conditions.

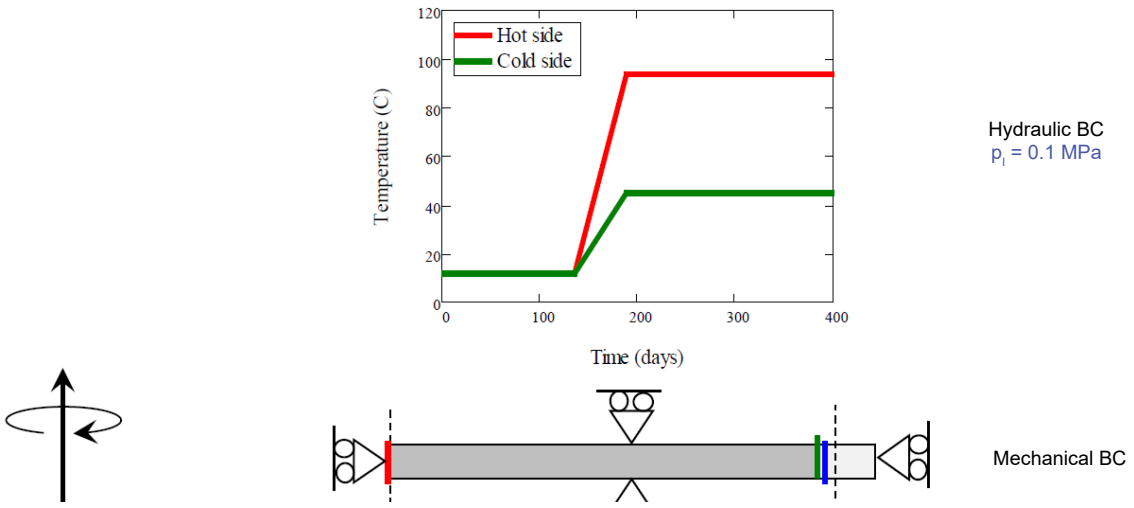


Fig. 7-18: Geometry and boundary conditions of the CT analyses

Because of the one-dimensional nature of the analyses, dismantling operations have not been simulated. The parameters for the mechanical law have been based on tests on MX-80 bentonite rather than on FEBEX bentonite properties, although it appears that the swelling pressures for the two materials at the same void ratio are not very different. The computed distributions of water content and dry density at different times are presented in Fig. 7-19. The results for 1'962 days correspond to the partial dismantling, while the results for 6'710 days are the final pre-dismantling predictions.

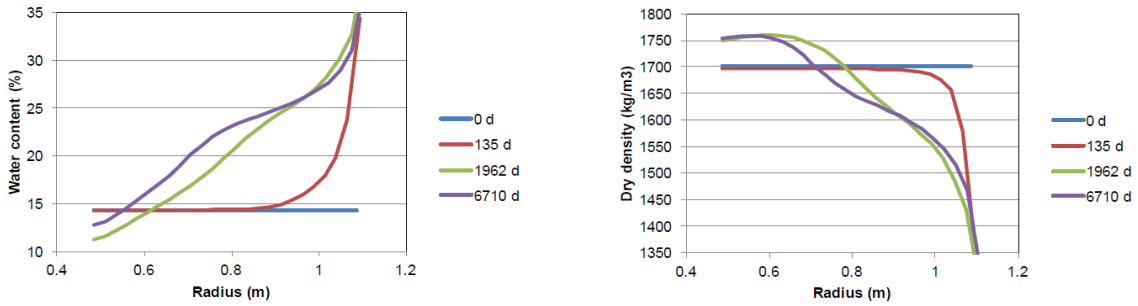


Fig. 7-19: Computed distributions of water content and dry density at different times (CT model)

7.3.4 Summary of the modelling analyses and comparison with test observations

The main features of the three modelling analyses are compared in Tab. 7-4. The basic THM formulation is very similar for all three teams; it is based on the simultaneous satisfaction of the balance equations for water mass, energy and momentum (equilibrium). In all three analyses, gas pressure is considered to be constant and equal to atmospheric pressure, and vapour transport is driven by diffusion. There are differences, however, regarding the mechanical constitutive law and the retention curve between the teams using CODE_BRIGHT and the team using LAGAMINE. The models used by CIMNE and EPFL were a continuation of previous numerical models while the model used by CT was newly developed for this exercise.

Tab. 7-4: Main features of the THM analyses

Modelling Team	**CIMNE**	**EPFL**	**CT**
Formulation	Coupled THM	Coupled THM	Coupled THM
Thermal conduction	Fourier's law	Fourier's law	Fourier's law
Fluid advection	Darcy's law	Darcy's law	Darcy's law
Vapour transport	Diffusion	Diffusion	Diffusion
Air pressure	Constant (atmospheric)	Constant (atmospheric)	Constant (atmospheric)
Mechanical constitutive model	BBM	ACMEG–TS	BBM
Retention curve	No hysteresis	Hysteresis	No hysteresis
Computer code	CODE_BRIGHT	LAGAMINE	CODE_BRIGHT
Analysis domain	2D axisymmetric 100 m × 50 m	2D axisymmetric 130 m × 61 m	1D radial symmetry 1.14 m
Barrier – rock gap	Not included	Not included	Included
Initial dry density of the bentonite	1.60 Mg/m^3	1.60 Mg/m^3	1.70 Mg/m^3
Predictions of w/c and dry density	Sections F2 and G	Sections F2 and G	Section F2

In spite of a number of similarities, there were also significant differences in the details of the constitutive models and in the parameters defining them. This is illustrated in Fig. 7-20 where the variation of the bentonite thermal conductivity with degree of saturation and the variation of the bentonite intrinsic permeability with porosity adopted by the three modelling teams are plotted. It can be noted that they do not coincide although the differences in thermal conductivity are slight. In contrast, the EPFL team uses an intrinsic permeability substantially higher than the other two teams. Another difference is that the parameters for the bentonite have been determined for an initial dry density of 1.60 g/cm^3 in the case of CIMNE and EPFL and of 1.70 g/cm^3 in the case of CT (see details in Papafotiou et al. 2017).

The main difference between the modelling approaches is the geometry of the analysis domain and the boundary conditions. CIMNE and EPFL adopt an axisymmetric domain that includes the rock and the bentonite barrier. The boundary conditions are applied at the inner wall of the barrier and at the outer edge of the rock. In the case of CT, the domain is 1D (with radial symmetry) and

includes only the bentonite barrier, as well as a gap between the barrier and rock. Boundary conditions are applied to the inner and outer walls of the barrier. An analytical thermal analysis of the rock has been performed to obtain the outer thermal boundary condition. CT only provided predictions for section F2.

The thermal observations of the experiment are well reproduced by the three analyses (Fig. 7-20), a consequence of having similar values for thermal conductivity for a heat transport problem dominated by thermal conduction. EPFL considers the influence of porosity on thermal conductivity but the effect is small, as the average density of the bentonite does not vary during the experiment. There are larger differences between the modelling teams concerning the evolution of relative humidity reflectibg that hydration is much more sensitive to slight changes in hydraulic parameters such as intrinsic permeability, relative permeability and retention curve. However, the responses of the models are in good qualitative agreement with sensor measurements, which is a clear sign that the basic phenomena have been correctly incorporated in the formulations. The similarity of the CT results to those of the other two teams indicates that the flow is basically one-dimensional and dominated by the permeability of the bentonite. Swelling stress development is slower in the CT analysis, which is probably due to the presence of the gap. However, at the end of the test, the swelling pressure predicted by CT is higher (around 8 MPa) than that predicted by CIMNE (around 6 MPa). This is probably due to the differences in parameters of the BBM mechanical model that, in the case of CT, was calibrated with MX-80 bentonite data.

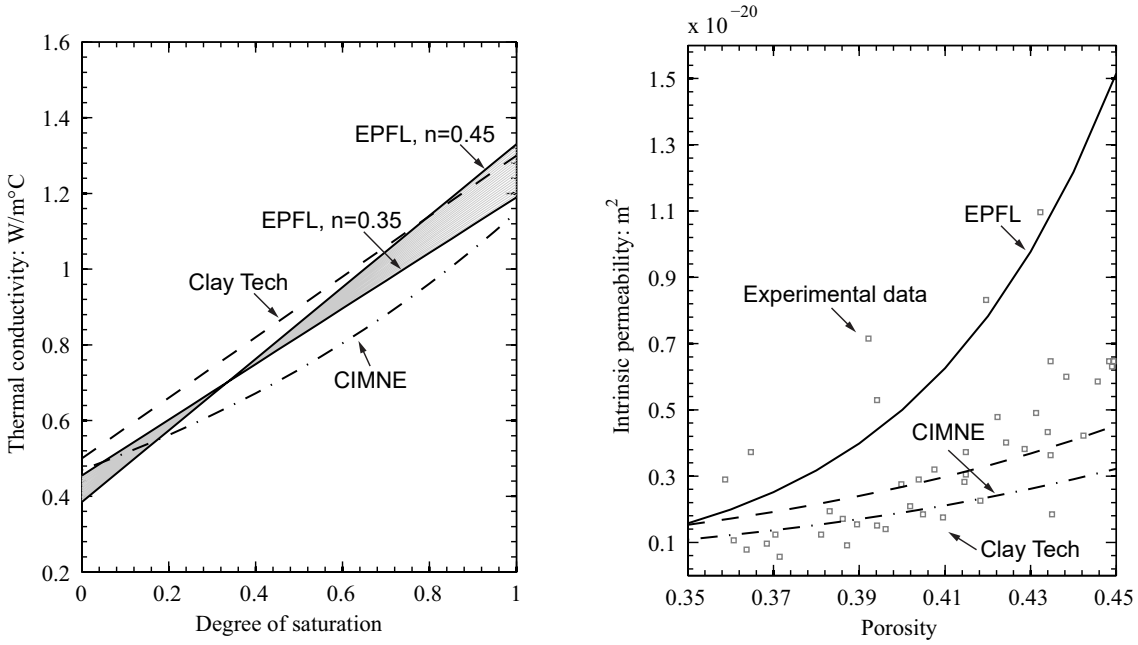


Fig. 7-20: Variation of the thermal conductivity of bentonite with degree of saturation for the three modelling teams (left) and variation of the intrinsic permeability of bentonite with porosity for the three modelling teams (right)

(from Papafotiou et al. 2017)

Prediction of the final state of the barrier in terms of water content and dry density was one of the main goals of the pre-dismantling modelling. The predictions from the three teams for section F2 are shown in Fig. 7-21. Section F2 provides a better representation of the THM response of the experiment and of the three models. Significant differences in the predicted distributions of dry

density can be observed, some of which can be attributed to differences in the mechanical constitutive laws used. Thus, the analysis by EPFL yields a nearly constant distribution of dry density. This is due to the absence in the model of irreversible features such as thermal plasticity and irrecoverable hydraulic swelling. Both CIMNE and CT, using the BBM constitutive model, predict non-uniform distributions of dry density, likely related to the pattern of variation of elastic moduli with applied stress and suction. CT predicts a lower dry density close to the rock, which is probably due to the initial presence of a gap at that location. The same team predicts a higher dry density close to the heater, possibly related to the fact that the assumed initial dry density of the bentonite was higher in their analysis. The predicted water content near the heater is higher in the EPFL simulation, which can be attributed to the use of a larger intrinsic permeability for the bentonite.

The comparisons of the predicted distribution of dry density and water content with the dismantling measurements are presented in Fig. 7-22 for section F2 and in Fig. 7-23 for section G. The comparison with measurements shows a reasonable agreement, especially in section F2 that avoids the uncertainties associated with section G. The predictions draw a consistent picture of the THM evolution associated with the hydration and initial drying of the bentonite in the experiment (Papafotiou et al. 2017).

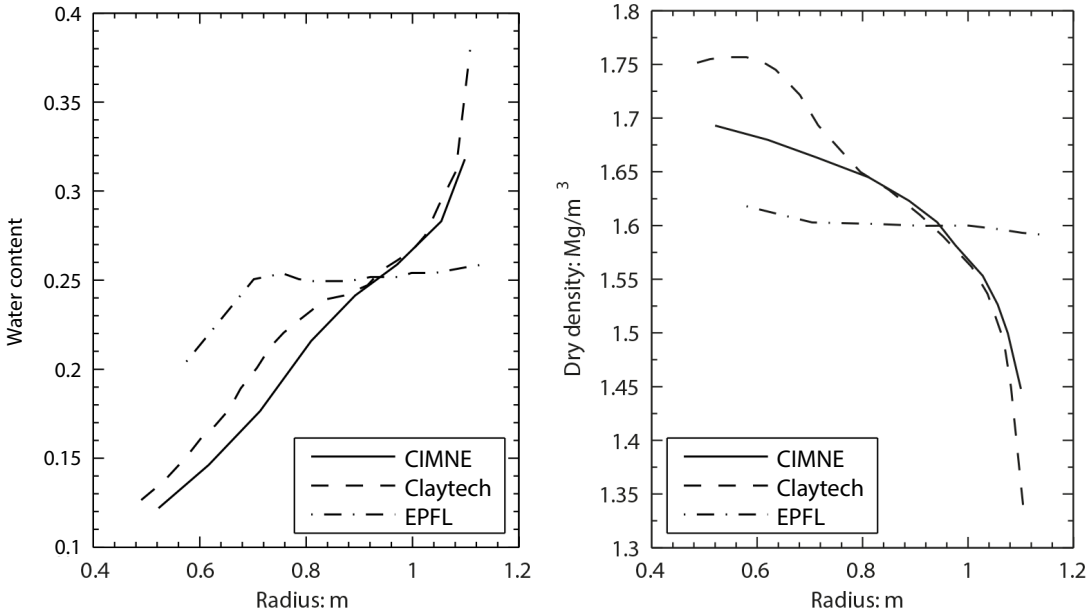


Fig. 7-21: Predictions of distributions of water content (a) and dry density (b) in section F2 from the three modelling teams at final dismantling

From Papafotiou et al. (2017)

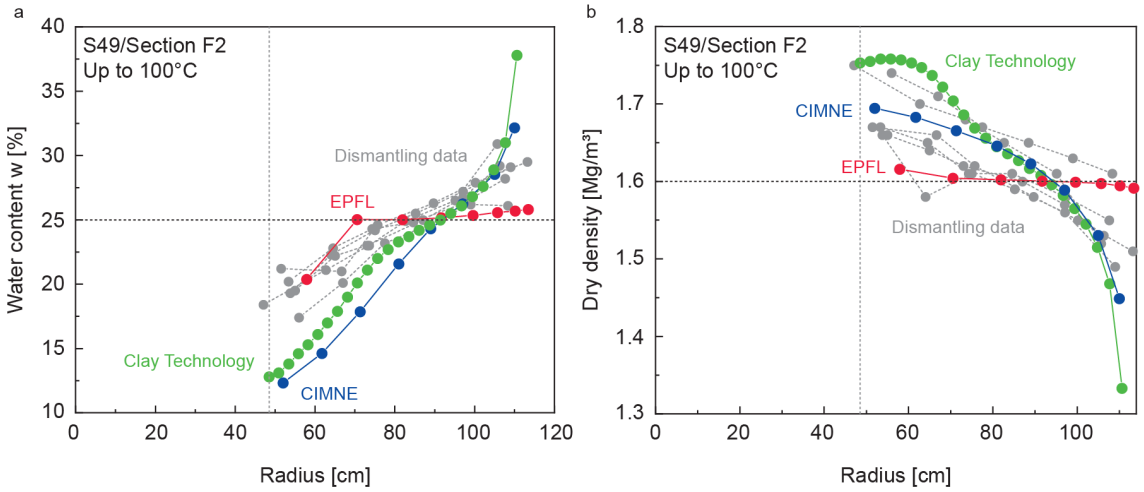


Fig. 7-22: Comparison between predicted distributions of water content (a) and dry density (b) in section F2 with dismantling observations

From Papafotiou et al. (2017)

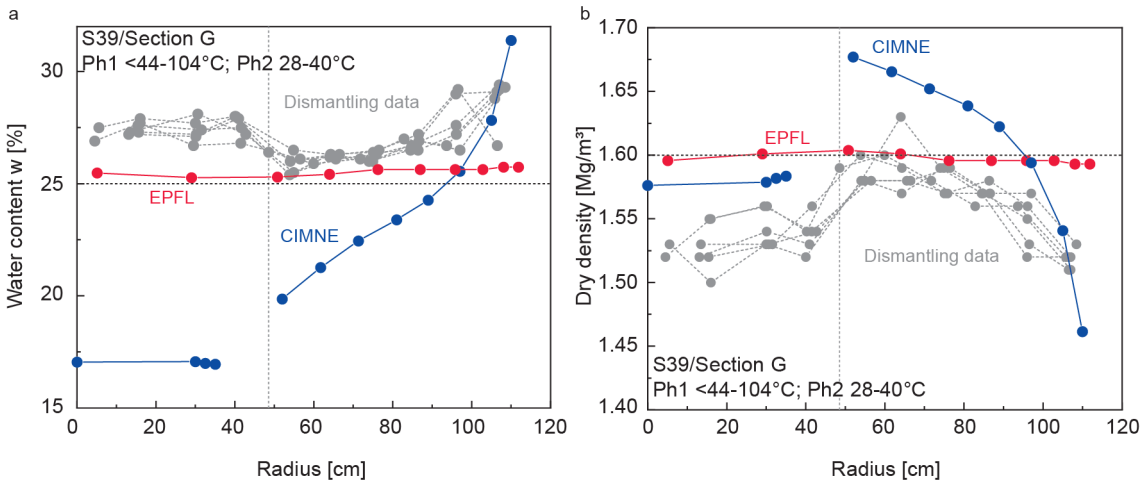


Fig. 7-23: Comparison between predicted distributions of water content (a) and dry density (b) in section G with dismantling observations

From Papafotiou et al. (2017)

In summary, the theoretical formulations adopted by the three modelling teams have a common core incorporating a similar set of physical principles and equations. It suggests that the formulations incorporate all relevant processes and phenomena because the numerical analyses can simulate all the main features of THM behaviour such as the drying of the barrier close to the heater, vapour transport, the subsequent hydration of the barrier and the development of stresses due to bentonite swelling. There are, however, differences in the details of the constitutive laws employed and in the parameters selected, even if they have been derived from the same set of experimental results. Nonetheless, these differences do not seem to affect the capability of the models to successfully simulate the overall THM behaviour of the experiment. An important difference between models, however, lies in the geometry of the analysis domain: 2D axisymmetric, including bentonite and rock, for CIMNE and EPFL and 1D (radial symmetry) including only the bentonite barrier for CT. Crucially, the 1D domain includes a gap between the rock and the bentonite.

Differences can also be observed in the predictions for the state of the barrier after 18 years of heating and hydration. In the hot section, EPFL predicts a uniform final distribution of dry density whereas CIMNE and CT predict a non-uniform state of the barrier with the dry density increasing monotonically from near the rock to the zone around the heater. The lowest dry density is computed by CT near the rock which is possibly due to the inclusion of a gap in that area. Nonetheless, those differences must ultimately depend on the details of the mechanical constitutive model.

7.4 Pre-dismantling THC modelling

Prior to final dismantling, a number of numerical analyses incorporating geochemical effects were carried out. There were three modelling teams: Universidad de A Coruña (UDC), Lawrence Berkeley National Laboratory (LBNL) and Clay Technology (CT). UDC has also reported some results and comparisons with observations of analyses performed after the final dismantling. The computation of chemical results required the performance of associated TH or THM analyses to provide the necessary background and conditions but these are not addressed in this section as it focuses on the geochemical aspects of the analyses. The computer codes used in the numerical analyses are INVERSE-FADES-CORE by UDC, TOUGHREACT-FLAC3D by LBNL and an in-house code by CT. Pre-dismantling THC modelling is described at length in Birgersson et al. (2018); only a synthesis is provided here.

7.4.1 Pre-dismantling modelling by UDC

A large number of numerical THMC simulations have been carried out by UDC as a contribution to the pre-dismantling modelling programme. This is a continuation of the work performed throughout the FEBEX project summarised in Section 7.2. In particular, the conceptual and numerical model used is a continuation and update of the THMC model described in Zheng et al. (2011). The work performed not only addresses the evolution of chemical species in the bentonite but also the prediction of tracer migration and the interaction between concrete and bentonite.

UDC adopted a homogeneous model (Birgersson et al. 2018) where all the water is considered as bulk water and the interlayer pores are treated as cation-exchange sorption sites. In this framework, interlayer pores are considered to have zero volume and exchangeable cations have no diffusion capacity. Aqueous species can be transported by advection, diffusion and mechanical dispersion. Sorption is accounted for by cation exchange and by edge protonation. The geochemical equations are coupled to a THM formulation. The mechanical behaviour of the bentonite (including swelling) is described using a state surface approach (Lloret & Alonso 1995).

Most analyses by UDC have adopted a 1D radial symmetry domain encompassing both bentonite and rock. A hot and a cold section have been considered (Fig. 7-24). A first set of analyses by UDC has been devoted to the performance of a set of sensitivity calculations to identify the potential effects of a series of parameters and conditions: retention curve (specifically the air entry pressure), smectite dissolution and precipitation, gas boundary conditions, bentonite cooling, vapour tortuosity and effective diffusion coefficients in bentonite and rock (Sánchez et al. 2012b). Parameters that affect the hydration regime such as the retention curve are shown to have an effect on solute concentrations (e.g. Fig. 7-25). UDC has adopted the van Genuchten expression to formulate the retention curve:

$$S_l = \frac{(1-9.11\times10^{-7}\,\psi)^{1.1}}{(1+(\alpha\psi)^{1.22})^{0.18}}$$

where S_l is the liquid saturation, ψ is the suction (in kPa) and α is a parameter which is the reciprocal of the air entry pressure. Fig. 7-25 shows the effect on Cl^- concentration of changing α from 10^{-5} kPa^{-1} (base run) to 1.4×10^{-4} kPa^{-1} (retention curve run).

As expected, solute diffusion from the bentonite into the granite is very sensitive to the values of diffusion coefficients. In contrast, computed concentrations are not sensitive to smectite dissolution or to the precipitation of the analcime silicate mineral.

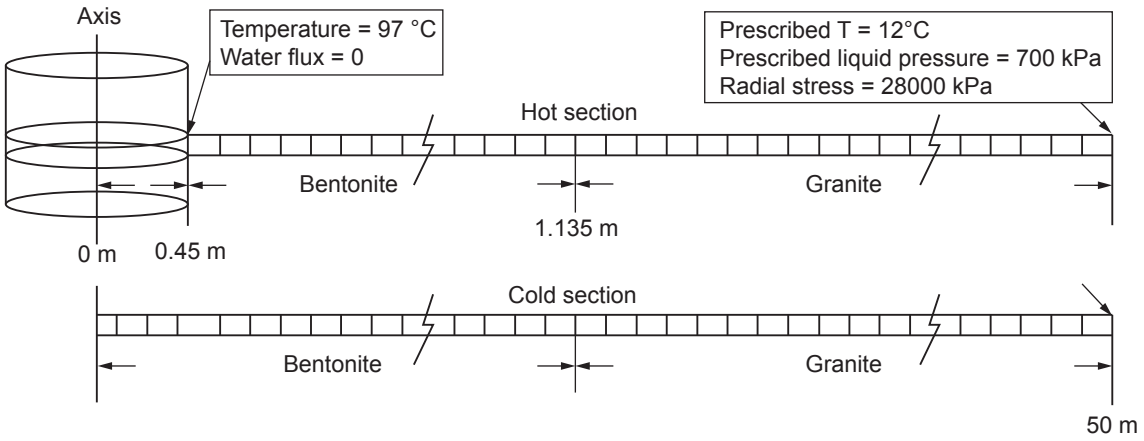


Fig. 7-24: 1D analysis domain used by the UDC team

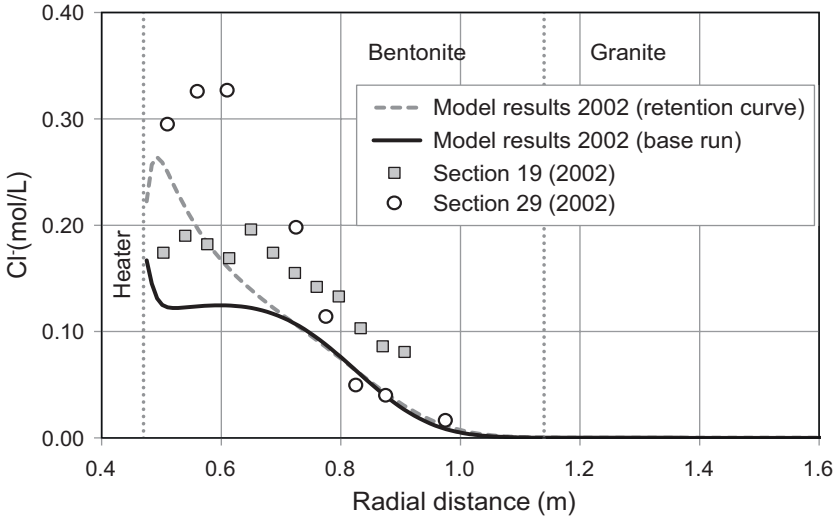


Fig. 7-25: Effect of a change in the retention curve on the distribution of Cl^- concentration at first dismantling

The results observed in two different sections are added for comparison (UDC model).

In addition, the model has been extended from 1D to 2D (axisymmetric) but it has been found that the 1D model outperforms the 2D model, probably because the parameters have been calibrated with reference to the 1D model. In any case, the 2D axisymmetric analysis indicates that the edge effects extend over a distance of only around 0.5 metres to 1 metre.

Based on this information, the previous 1D model was updated by i) improving the boundary condition at the heater-bentonite interface; ii) refining the spatial discretisation of the finite element mesh; and 3) modifying the solute dispersivities of the bentonite and the granite. The updated model leads to a satisfactory agreement with available THM observations. The revised implementation of the boundary condition leads to more water evaporation than the previous formulation. The concentrations of Ca^{2+}, K^{+}, Mg^{2+}, Cl^{-} and Na^{+} near the heater computed with the updated model are significantly larger than the concentrations calculated with the previous reference model. In contrast, the computed pH and the concentrations of SO_4^{2-} and HCO^{3-} using the updated model are similar to those of the reference model. The model has been used to provide pre-dismantling predictions concerning chemical variables such as concentrations of anions (Cl^{-}, SO_4^{2-}, HCO_3^{-}), dissolved cations and pH for both hot and cool sections. As an example, Fig. 7-27 shows the predicted distribution of Cl^{-} concentration at first and final dismantling.

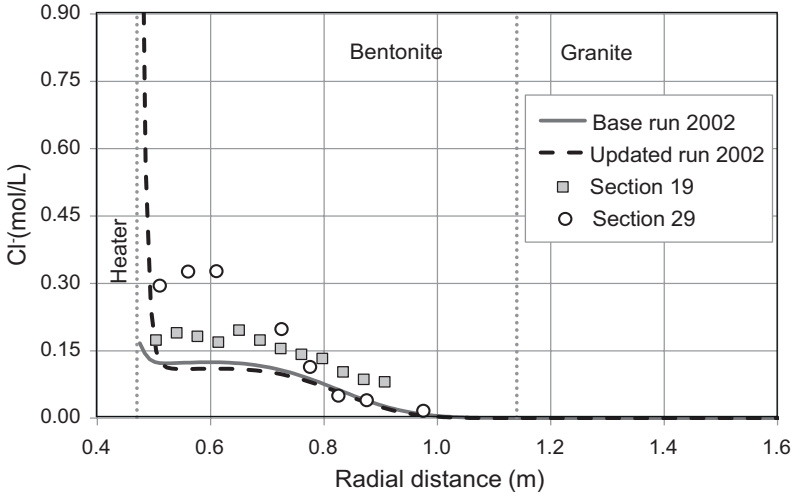


Fig. 7-26: Comparison of the distribution of Cl^{-} concentration at first dismantling computed with the initial and updated model

The results observed in two different sections are added for comparison (UDC model).

In addition, the UDC team supplied predictions for tracer migration that, when compared with measured values, will provide a basis for the partial validation of the THMC models. The interaction of the bentonite with the concrete plug was also modelled by UDC. The calculations indicated that the calcite dissolves in the bentonite and precipitates near the bentonite/shotcrete interface and that the precipitation front propagates into the bentonite. Neither gypsum nor anhydrite precipitate. Other precipitation/dissolution phenomena are small. As a consequence, the porosity decreases slightly in the bentonite near the shotcrete/bentonite interface due to the precipitation of brucite, calcite and sepiolite, while the porosity in the shotcrete increases near the interface due mostly to the dissolution of portlandite. In any case, the UDC modelling suggests that changes in porosity only affect 2 cm in the bentonite and shotcrete on both sides of the interface.

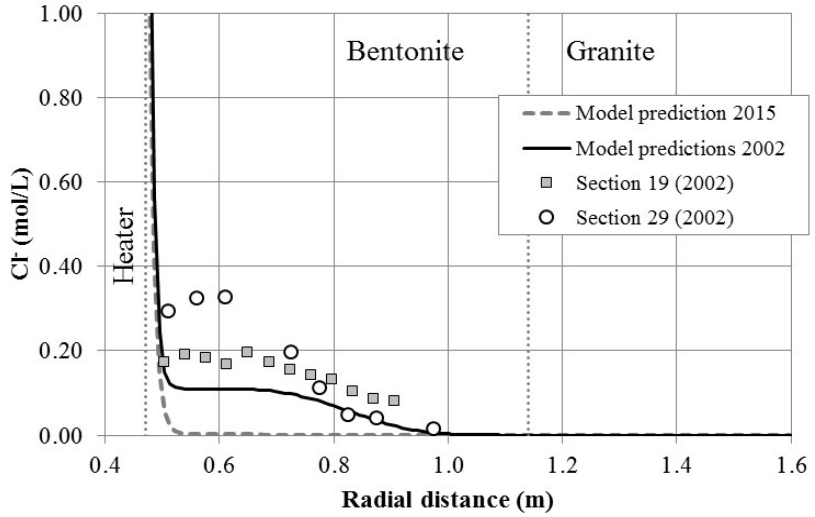


Fig. 7-27: Comparison of the distribution of Cl^- concentration at first dismantling (2002) and final dismantling (2015) computed with the updated model

The results observed at first dismantling in two different sections are added for comparison (UDC model).

7.4.2 Pre-dismantling modelling by LBNL

A conceptual homogeneous model was adopted where all water is considered bulk water; the interlayer space has zero volume and is the location of cation-exchange sorption sites. Aqueous species can be transported by advection, diffusion and mechanical dispersion, whereas exchangeable cations have no diffusion capacity. Sorption is due to cation exchange and edge protonation. The geochemical problem is connected to a THM formulation resulting in THMC analyses. Comparison with the equivalent results of a THC mode (i.e. without mechanical phenomena such as swelling) demonstrated that THMC models clearly outperformed THC analyses because they are able to account for the swelling of bentonite and subsequent porosity and permeability changes. Consequently, the THMC model matches the data at 5.3 years of heating reasonably well.

The numerical simulations are conducted using two sequentially coupled codes, TOUGHREACT and FLAC3D. A 1D domain with radial symmetry was used and only a hot section was analysed. Two options, a linear swelling model and the double-structure BExM elastoplastic model (Sánchez et al. 2005), were assessed to describe the mechanical behaviour of the bentonite (including swelling). Despite being more sophisticated, the BExM model did not outperform the simpler linear swelling model.

The THMC models matched the THM data to a satisfactory degree but they did not match the measured concentration profile of a conservative species (Cl^-) at first dismantling (Fig. 7-28). Changes in diffusion coefficient, relative permeability law and intrinsic permeability led to slightly better predictions, but they still failed to provide an accurate representation of the observations after first dismantling. In conclusion, an additional process or processes are probably required for the model to match both THM and chemical data.

The concentration profiles of cations (calcium, potassium, magnesium, and sodium) were essentially a consequence of transport processes despite the ongoing mineral dissolution/precipitation and cation exchange, which have only a marginal effect. The concentration profiles of pH, SO_4^{2-} and HCO_3^- were largely determined by chemical reactions. Better Cl^- concentration distributions could be achieved by varying hydraulic parameters of the bentonite at the cost of a more inaccurate representation of the THM processes. The full THMC model was used to provide predictions for the final dismantling to be compared with measurements (Fig. 7-28).

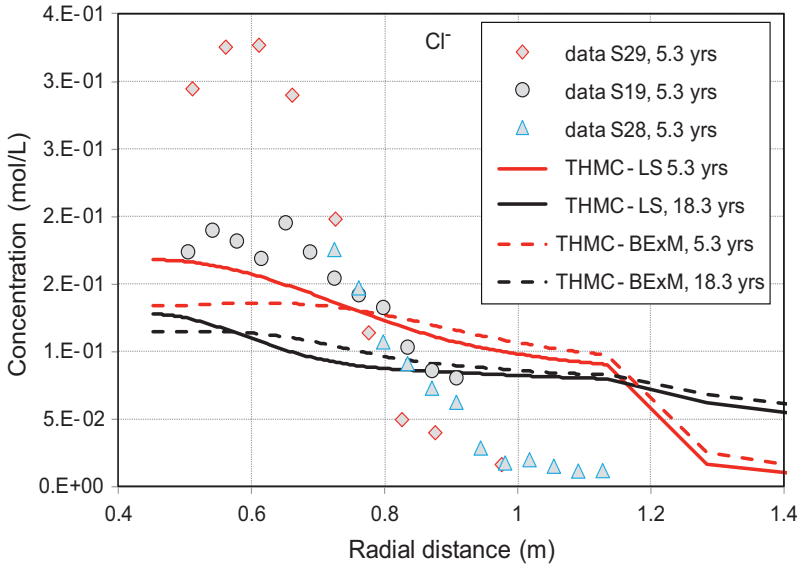


Fig. 7-28: Distributions of Cl^- concentration at first dismantling (5.3 years) and final dismantling (18.3 years) using the linear swelling model (LS) and the BExM model

The observed results at first dismantling in three different sections are added for comparison (LBNL model).

7.4.3 Pre-dismantling modelling by Clay Technology (CT)

CT used a conceptual model very different from those employed by UDC and LBNL. The so-called homogeneous mixture model assumes that all the water is located in the interlayer spaces of the bentonite. In the model, there is no bulk water and the entire porosity corresponds to interlayer space. Donnan equilibrium holds between the bentonite and an external water solution. Diffusion alone governs the interlayer transport, with all species having the same diffusion coefficient. Chemical reactions in the interlayer are treated in the same way as in ordinary aqueous solution, but it is acknowledged that the chemistry in the interlayer can be very different from the chemistry in a bulk water solution.

The calculations by CT were carried out with a computer code that was newly developed in-house based on the formulation described in Birgersson et al. (2018). The analysis considers only the bentonite, and the domain is planar 1D. The barrier is assumed to always be saturated at constant temperature and density. Therefore, no THM phenomena are considered. The mass transfer resistance between rock and bentonite is controlled by the porosity of a fictitious porous element located at the outer edge of the barrier (Fig. 7-29). Predictions have been provided for the

distributions of various species for a time of 5'000 days (Fig. 7-30). This period is shorter than the full duration of the FEBEX experiment and has been selected based on the argument that the unsaturated period of the barrier is not considered in the analysis.

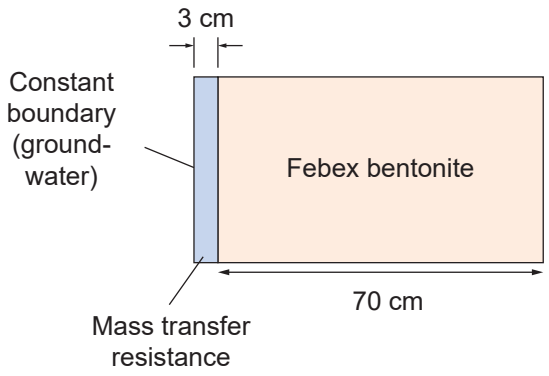


Fig. 7-29: 1D (planar) analysis domain (CT model)

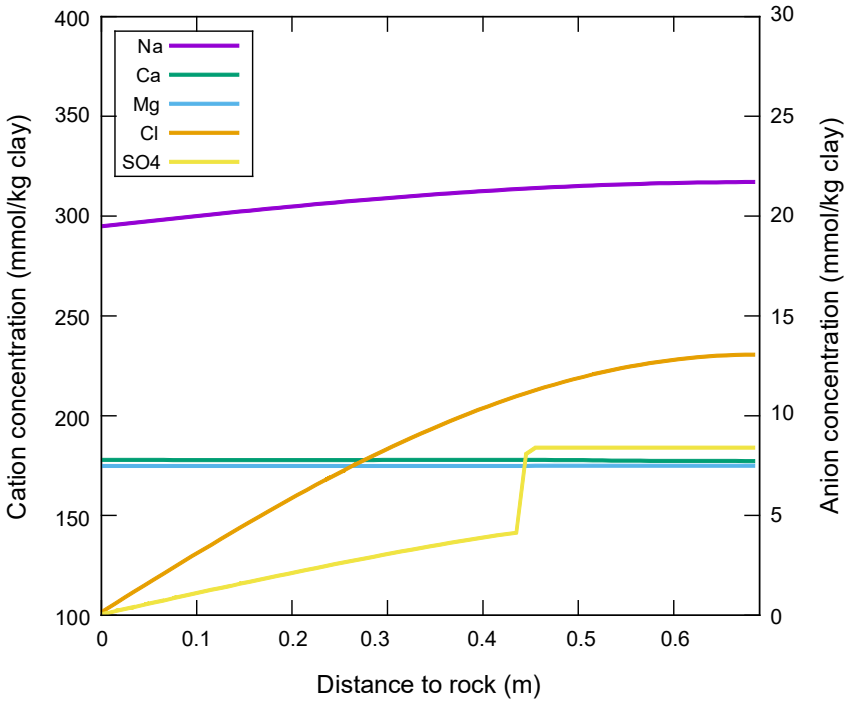


Fig. 7-30: Prediction of distributions of chemical species concentrations after 5'000 days of simulation (CT model)

7.4.4 Combined summary of the three modelling approaches

Due to the complexity of the phenomena, the large number of parameters and variables and the different conceptual approaches, no systematic comparisons between the results of the different modelling teams were envisaged. However, in this section, some considerations concerning the main aspects of the three modelling approaches are presented. A more detailed account is reported in Birgersson et al. (2018). The main features of the three sets of analyses are collected in Tab. 7-5.

Tab. 7-5: Main features of the analyses involving geochemistry

Modelling team	**UDC**	**LBNL**	**CT**
Formulation	Coupled THMC	Coupled THC and THMC	C only
Thermal conduction	Fourier's law	Fourier's law	Not considered
Flow	2-phase	2-phase	Not considered
Fluid advection	Darcy's law	Darcy's law	Not considered
Vapour transport	Diffusion	Diffusion	Not considered
Mechanical constitutive model	State surface approach	Linear swelling model BExM	Not considered
Porewater	Bulk water	Bulk water	Interlayer water
Solute transport	Advection, diffusion, mech. dispersion	Advection, diffusion, mech. dispersion	Diffusion
Sorption	Cation exchange, edge protonation	Cation exchange, edge protonation	No sorption
Computer code	INVERSE-FADES-CORE	TOUGHREACT – FLAC3D	In-house
Analysis domain	1D (radial symmetry), 2D axisymmetric	1D (radial symmetry)	1D planar
Materials considered	Bentonite, rock, concrete	Bentonite, rock	Bentonite

The major differences between the modelling approaches lie in the conceptual model for the chemistry component. CT uses a novel approach in which all the water is considered interlayer water and chemical species move by diffusion in the interlayer pore space. Sorption is automatically accounted for by the establishment of the Donnan equilibrium. Unfortunately, the application to the in-situ test is very elementary using a 1D planar geometry and the assumptions of constant temperature, a saturated barrier throughout and a constant bentonite density across the barrier. The analysis, therefore, fails to reproduce the actual evolution of the barrier that must be an important factor in the distribution of chemical species. A more elaborate model would be necessary to establish comparisons with dismantling observations and thus enable a well-grounded judgement of the merits of the new conceptual formulation.

UDC and LBNL adopt a classical approach where bulk water exists and the aqueous species are transported by advection, diffusion and dispersion. Reactions take place in the aqueous phase and sorption is mainly due to cation exchange phenomena. The primary chemical species considered are similar in the two cases, however, LBNL incorporates more mineral phases (Birgersson et al. 2018). In both approaches, the chemistry formulation is coupled to an advanced THM model

capable of satisfactorily representing the THM observations of the in-situ experiment. The the predicted distributions of chemical species concentrations do not match well the results obtained in the first dismantling, even after varying some key parameters. This suggests that there may be some processes missing from the formulations used. More work is therefore required but the entire database of chemical measurements obtained in the final dismantling should be crucial to improving and validating THMC models. The need for further work is illustrated in Fig. 7-31 where the predictions of chloride (Cl^-) and sulphate (SO_4^{-2}) distributions by the three teams are compared with some early observations from the final dismantling, bringing to light significant discrepancies.

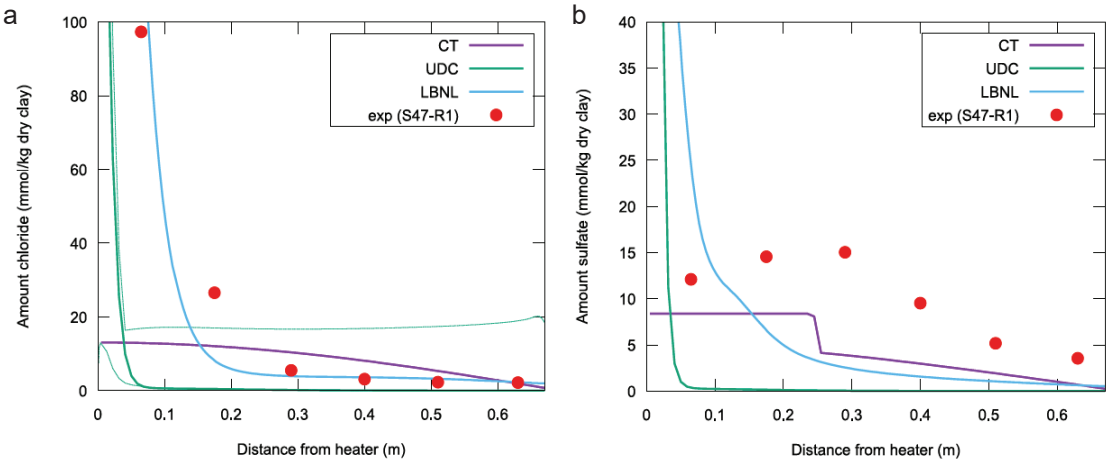


Fig. 7-31: Comparison of predictions of the distributions of (a) chloride (Cl^-) and (b) sulphate (SO_4^{-2}) by the three modelling teams with first observations from final dismantling

Birgersson et al. (2018)

7.5 Post-dismantling modelling

The FEBEX in-situ experiment is exceptional in many respects but chiefly because of its long duration and the fact that two dismantling events were carried out, thus providing direct access to the state of the bentonite barrier at two different times. The database gathered in the experiment therefore offers a unique opportunity to check, improve and validate THM and THC formulation and models.

Two large international cooperative projects, the EBS Task Force (coordinated by SKB) and DECOVALEX 2019 (coordinated by LBNL), have set up benchmarks based on the FEBEX in-situ experiment as part of their work programmes. Only THM modelling is considered so far. In the case of EBS Task Force, it has been used in Task 9, and, in the case of DECOVALEX 2019, it corresponds to Stages 3 and 4 of Task D (hydro-mechanical interactions in bentonite engineered barriers – INBEB). The funding organisations, modelling teams and computer codes involved are presented in Tabs. 7-6 and 7-7. The FEBEX in-situ experiment was also recently selected as one of the three large-scale experiments to be modelled within Work Package 5 (Step 2) of the European BEACON project that will run from 2017 to 2021.

The concurrent analyses by a large variety of teams, approaches and computer codes together with the large database of the FEBEX in-situ experiment should lead to significant advances in the development and validation of THM modelling tools. However, the analyses are still ongoing

and no reports have been released. No definite plans are in place to use the chemistry data from the FEBEX in-situ experiment in a similar manner. However, the EBS Task Force is considering the performance of THMC analyses of the experiment.

Tab. 7-6: Funding organisations, modelling teams and computer codes involved in Task 9 of the EBS Task Force

Funding organisation	**Country**	**Modelling team**	**Computer code**
BMWi	Germany	Gesellschaft für Anlagen– und Reaktorsicherheit (GRS)	COMSOL – VIPER
CODE_BRIGHT Consortium	International	Universitat Politècnica de Catalunya (UPC)	CODE_BRIGHT
CRIEPI	Japan	Central Research Institute of Electric Power Industry (CRIEPI)	LOSTUF
DOE	USA	Sandia National Laboratory (SNL)	COMSOL
ICL (self-funded)	UK	Imperial College of Science, Technology and Medicine (ICL)	ICFEP
SÚRAO	Czech Republic	Technical University of Liberec (TUL)	COMSOL
SKB	Sweden	Clay Technology (CT)	CODE_BRIGHT

Tab. 7-7: Funding or10-1ganisations, modelling teams and computer codes involved in Task D (INBEB) of the DECOVALEX 2019 project

Funding organisation	**Country**	**Modelling team**	**Computer code**
JAEA	Japan	Japan Atomic Energy Agency (JAEA)	THAMES 3D – DACSAR 2D
KAERI	Korea	Korea Atomic Energy Research Institute (KAERI)	TOUGH2–MP FLAC 3D
SÚRAO	Czech Republic	Institute of Geonics of the Czech Academy of Sciences (IGN)	COMSOL
TPC	Taiwan	National Central University (NCU)	HGC 5.3/3D

7.6 Synthesis and outlook

FEBEX is a unique experiment because of its long duration and the fact that two dismantling operations have been performed during its lifetime, allowing the direct observation of the state of the barrier at two different times. THM and THC modelling have been a constant activity throughout the development of the experiment and have proved to be an invaluable tool for achieving a proper understanding and interpretation of test observations and results.

THM modelling has demonstrated the capability to represent the overall behaviour of a large full-scale system encompassing the ensemble of THM phenomena and their interactions. All the formulations used in the simulations share a common core of assumptions and basic equations and incorporate a similar set of processes. The solution of a coupled system of suitable balance equations is necessary to reproduce the interactions between different phenomena. This common core, however, allows for the adoption of different constitutive laws for individual phenomena, different parameters and different geometries and boundary conditions of the analyses. The fact that no unexplained patterns of THM observations have arisen during the experiment indicates that no significant processes have been ignored in the formulations.

In spite of the general success of the THM analyses, quantitative differences with observations arise, which is expected. In general, the temperature field is generally well reproduced. This is probably a consequence of conduction being, by far, the dominant mechanism of heat transport. As the experiment is temperature-controlled, only a good estimate of thermal conductivity (and its evolution) is required for a satisfactory temperature simulation. Larger quantitative departures from measurements are observed regarding the evolution of relative humidity in the barrier. It is likely that these differences result from the high sensitivity of the progress of hydration to small changes in the formulation of hydraulic laws and the respective parameters. The quantitative discrepancies concerning observed stresses in the barrier are probably related to the larger uncertainties of this type of measurements and/or to shortcomings of the mechanical constitutive models. However, in most cases, the computed swelling pressure shows a realistic development throughout the test and reaches reasonable values at the end of the experiment. Interestingly, the inclusion of more sophisticated formulations or the incorporation of new phenomena (e.g., thermo-osmosis, water retention hysteresis, double structure and fabric evolution) does not lead to significantly improved results when compared with the in-situ test observations.

The simulation of the state of the barrier as observed during the dismantling operations is of particular interest. The distribution of dry density and water content displayed a nearly axisymmetric character, implying a very limited role of the rock discontinuities and of the gaps between the blocks in the development of the experiment. All three modelling groups have provided numerical results for comparison, although CT did so only for the final dismantling. The state of the barrier after the first dismantling was quite well reproduced by CIMNE and EPFL, although the predicted water content appeared to somewhat underestimate the actual hydration rate.

The results of the final state of the barrier differed between the different teams. EPFL predicted a uniform distribution of dry density whereas CIMNE and CT computed a non-uniform distribution, with the dry density increasing monotonically from the barrier close to the rock all the way to the zone around the heater. Blind predictions were required from the three modelling groups concerning only two cross-sections, one of which was not especially representative of the overall test. Due to this limited scope, comparisons are inconclusive. The differences between modelling groups are likely the result of different characteristics of the mechanical constitutive laws adopted and may be related to the need to incorporate irreversible/stress path-dependent features of behaviour. The European BEACON project has been specifically set up to address these issues.

The availability of the full database of the FEBEX in-situ experiment (including the final dismantling data for all sections) offers an exceptional opportunity to conduct a systematic study of the THM modelling of a complex large-scale system in order to identify key processes and critical parameters as well as to evaluate uncertainties. Some of these uncertainties can be intrinsic and therefore unavoidable. The activities by a number of international projects (EBS Task Force, DECOVALEX 2019/2023, BEACON) may provide very appropriate platforms in this regard. However, it should not be forgotten that the analysis of a large-scale complex test has limitations when the goal is to identify and characterise specific processes because of all the couplings that occur simultaneously in the experiment. Consequently, it should be envisaged that dedicated small-scale experiments are bound to be necessary as well.

The incorporation of chemical issues in the modelling of the FEBEX in-situ experiment significantly increased the complexity of the problem to be analysed. In addition, while THM data were collected throughout the entire duration of the test, observation of chemical parameters was only possible during the two dismantling operations. However, the THC behaviour of the test was one of the explicitly stated goals of the experiment, and a significant number of numerical analyses involving chemical aspects has been carried out.

Chemical simulations require knowledge of thermal and hydraulic conditions at every point of the domain and, therefore, the performance of associated TH calculations is essential. It has been conclusively shown that the incorporation of mechanical effects (especially bentonite swelling) is also crucial to achieving a good representation of the chemical observations of the test. Consequently, a proper representation of the experiment requires the performance of THMC analyses. Fortunately, all the indications suggest that the coupling from chemical variables towards THM phenomena is minor.

A large proportion of the chemical modelling work performed during the FEBEX experiment has been devoted to the development of conceptual formulations and codes capable of accounting for the observed and expected features of the test. As a result, there have been very considerable advances involving conceptual approaches, numerical methodologies and code development. In particular, many of the efforts have been directed towards the description of geochemical processes affecting the evolution of ion composition, pH and alkalinity. It should be remembered that, at the beginning of the experiment, available THC codes could only handle non-isothermal multiphase flow and transport with no geochemical processes or, alternatively, isothermal saturated flow and reactive transport.

Three modelling groups were involved in the pre-dismantling analyses focussing on chemical aspects. UDC and LBNL used similar classical THMC formulations and provided predictions for the chemical distributions of a set of chemical species at various stages of the test. Although comparisons with the observations at the final dismantling are very limited, significant discrepancies with the observations in the first dismantling suggest that there may be some relevant geochemical processes that are not yet included in the formulation. Some suggestions regarding missing processes have been put forward but not explored in detail. As part of their modelling work, UDC also provided predictions of tracer migration and analyses of bentonite-concrete interaction.

The analyses of CT adopt a very different conceptual model in which all water is considered interlayer water and chemical species move by diffusion in the interlayer pore space. However, it is difficult to judge the relevance of the new model for the FEBEX in-situ experiment because of the very elementary nature of the modelling performed so far.

For the geochemistry of the bentonite barrier, the exploitation of the full database of the FEBEX in-situ experiment (especially including the final dismantling) appears especially crucial. There is a large amount of geochemical data (as well as associated THM variables) that may provide key information concerning the necessary improvements of the models with a particular focus on

potentially missing processes in the formulations. Again, dedicated small-scale experiments are likely to be required to identify and unambiguously characterise specific phenomena. Unfortunately, as yet there seem to be no initiatives for the use of the full chemical database of the FEBEX in-situ experiment similar to those in place for the THM modelling.

8 Geosphere THM response

8.1 Introduction and scope

During FEBEX-DP, a major effort went into the post-heating characterisation of the buffer (as discussed in Chapter 10) and only a very limited characterisation of the geosphere was performed. This is consistent with the objectives of the project and the understanding that the geosphere response is relatively well understood (see DECOVALEX modelling, Alonso and Alcoverro 2005) and that the geosphere has a limited influence on the buffer (essentially providing confinement, inward water flux and outward thermal flux, ENRESA 2004a). Some additional EDZ investigations were made during FEBEX-DP but the geosphere response is otherwise characterised by the monitoring data as discussed in Chapter 2. This chapter presents a short summary of the overall THM response of the geosphere. A more detailed consideration of the hydro-chemical exchanges between the buffer and the rock is given in Chapter 9.

8.2 Investigations and influence of the excavation-damaged zone (EDZ) on buffer evolution

After the partial dismantling, the re-exposed gallery was investigated with regard to microfracturing, porosity and gas permeability; acoustic investigations were also carried out (ENRESA 2006a). The experimental results indicated that the granite matrix was neither damaged during excavation nor by the EBS-THM loading. SEM/EDX investigations of the FEBEX tunnel showed disturbance to the matrix extending 1 – 3 mm with crushed quartz grains and some fractures extending to depths of a few mm from the wall surface. A more extensive region of disturbance (10 – 15 mm) was associated with a metabasic dyke (ENRESA 2004). The absence of a significant EDZ in the Grimsel granite matrix in general (Frieg et al. 2012) showed that the maximum stress developed around the tunnel was much lower than the minimum strength of the rock (ENRESA 2006a). As a result, it was concluded that a continuous pathway for radionuclide migration along the drift was highly improbable.

After the final dismantling, a visual inspection of the granite gallery was performed (Kober & Van Meir 2017) and intact shotcrete/cement-granite interface samples were taken. It was not possible to obtain intact bentonite-granite interfaces (García-Siñeriz et al. 2016, Turrero & Cloet 2017, see also Chapters 4 and 5).

Visually, the granite wall as well the various metabasic dykes (lamprophyres) as shear zones appeared unmodified and undamaged, acknowledging that any modification would have to be investigated on the micrometre scale.

8.3 Geosphere thermal response

Temperatures in the geosphere around the drift rose in response to heating. The initial temperature in the geosphere was ~ 12 °C with some slightly higher temperatures very close to the drift. The temperature then rose relatively quickly in the first few hundred days after the start of heating and peaked when Heater #1 was switched off (day 1827). The temperature then slowly recovered over time until Heater #2 was switched off as shown in Fig. 8-1.

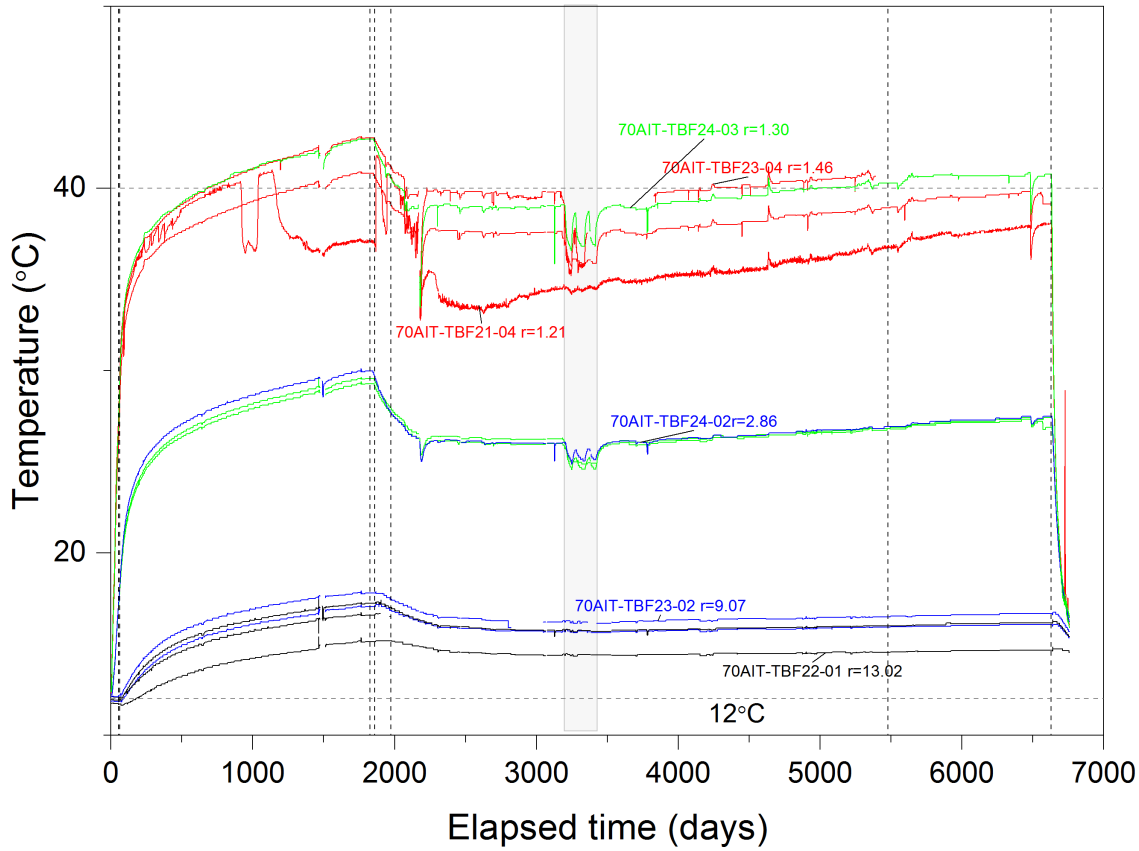


Fig. 8-1: Temperature response in boreholes SF21 – 24

Note: r is the distance of the measurement interval from the centre of the FEBEX drift

The overall temperature pattern in the region around Heater #2 is shown in Fig. 8-2, with an approximately log-linear variation with radial distance from the drift axis. The temperature disturbance extends beyond 13.7 metres (the further measurement interval) although the temperature rise at this point is only small (~ 5 °C).

The overall temperature distribution in the geosphere could be modelled reasonably well (Alonso et al. 2005) as temperature is largely controlled by the thermal conductivity and heat capacity (see discussion in Chapter 7). Convective heat transport is negligible due to the slow groundwater velocity.

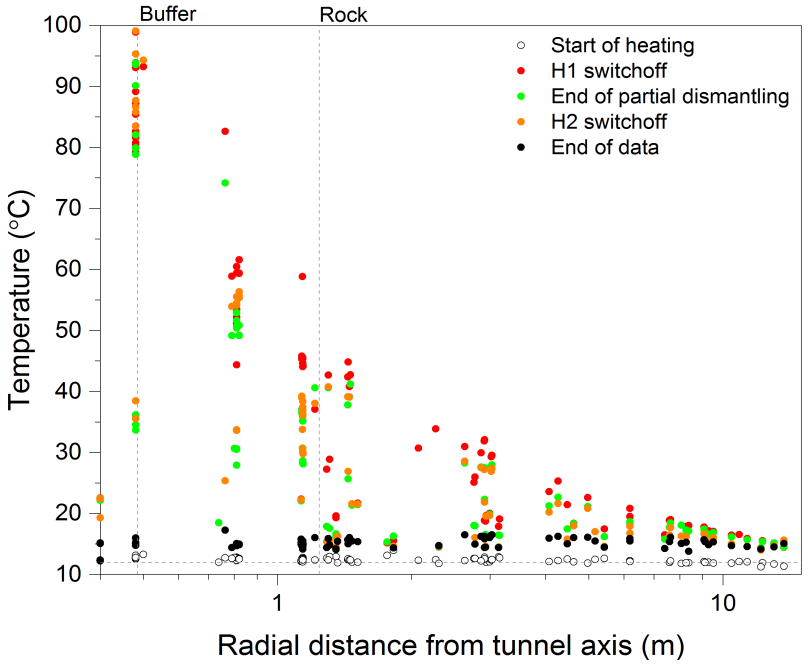


Fig. 8-2: Variation of temperature with radial distance from the FEBEX drift axis at key times during the in-situ experiment for sensors in the Heater #2 section of the drift

End of data – end of data logging

8.4 Geosphere hydraulic response

The hydraulic response in the geosphere was monitored in terms of pore pressure and water content. The TDR water content data show an initial increase up to partial dismantling with a subsequent fall during dismantling, followed by steady conditions.

Fig. 8-3 shows the measured pore pressure in the SF21, 22, 23 and 24 boreholes drilled radially out from the Heater #2 section of the drift (see Fig. 1-3). SF21 was drilled vertically upwards, SF23 vertically downwards, while SF22 and SF24 were sub-horizontal. The boreholes were completed with multi-packer systems, and the interval pressures show a general rise to between 7 and 10 bar from the start of the heating until partial dismantling. The rise is probably due to the ongoing recovery from the open tunnel period.

Removal of the plug and excavation of the buffer during partial dismantling resulted in a reduction in pressure with roughly stable conditions from partial dismantling until the final dismantling. The strong drop in pressure around day 3'520 relates to an event in the BOUS borehole when drilling in 2009 (days 4'633 – 4'660) resulted in a reduction in pressure, particularly on the left side of the drift (closest to the drilling), but also in the vertical boreholes. A drop and subsequent rise in pressure in some boreholes (e.g., SF14 and SF24) from around day 4'980 is believed to relate to changes in acquisition electronics associated with storms.

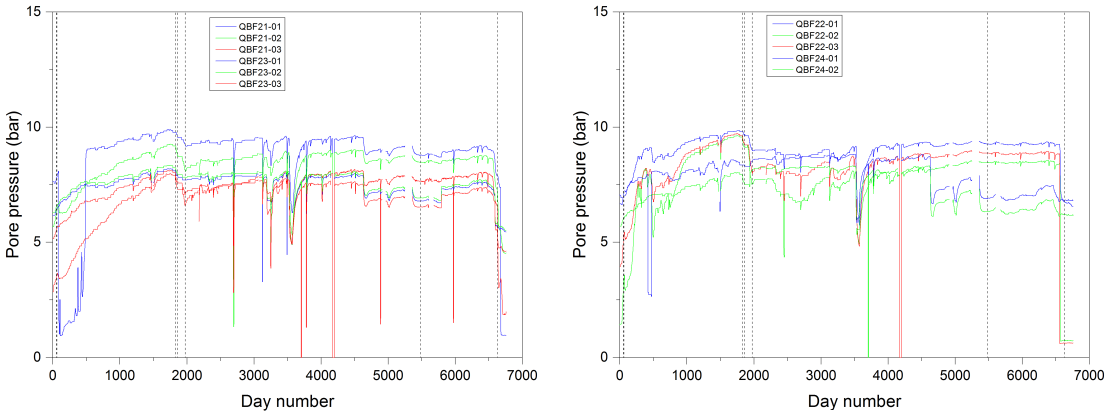


Fig. 8-3: Measured pore pressure in boreholes

a) SF21, SF23 (direction vertical up) and b) SF22, SF24 (direction horizontal)

The overall pattern of pressure with radial distance is shown in Fig. 8-4. While there is some initial pressure gradient into the tunnel (still present at day 0) after this time, pressures are relatively constant with distance from the tunnel axis, indicating only limited flow to the buffer. Pressures are typically higher immediately before partial dismantling and drop down to near the initial values by the end of the final dismantling. There is some variability in pressure between intervals which is probably due to the heterogeneity in the fracture network.

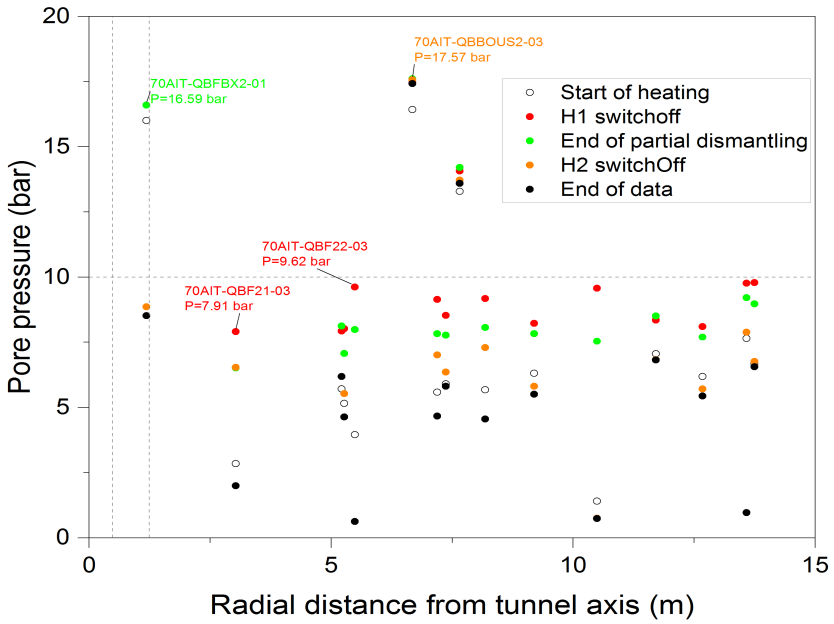


Fig. 8-4: Variation of pore pressure with radial distance from the FEBEX drift axis at key times during the in-situ experiment

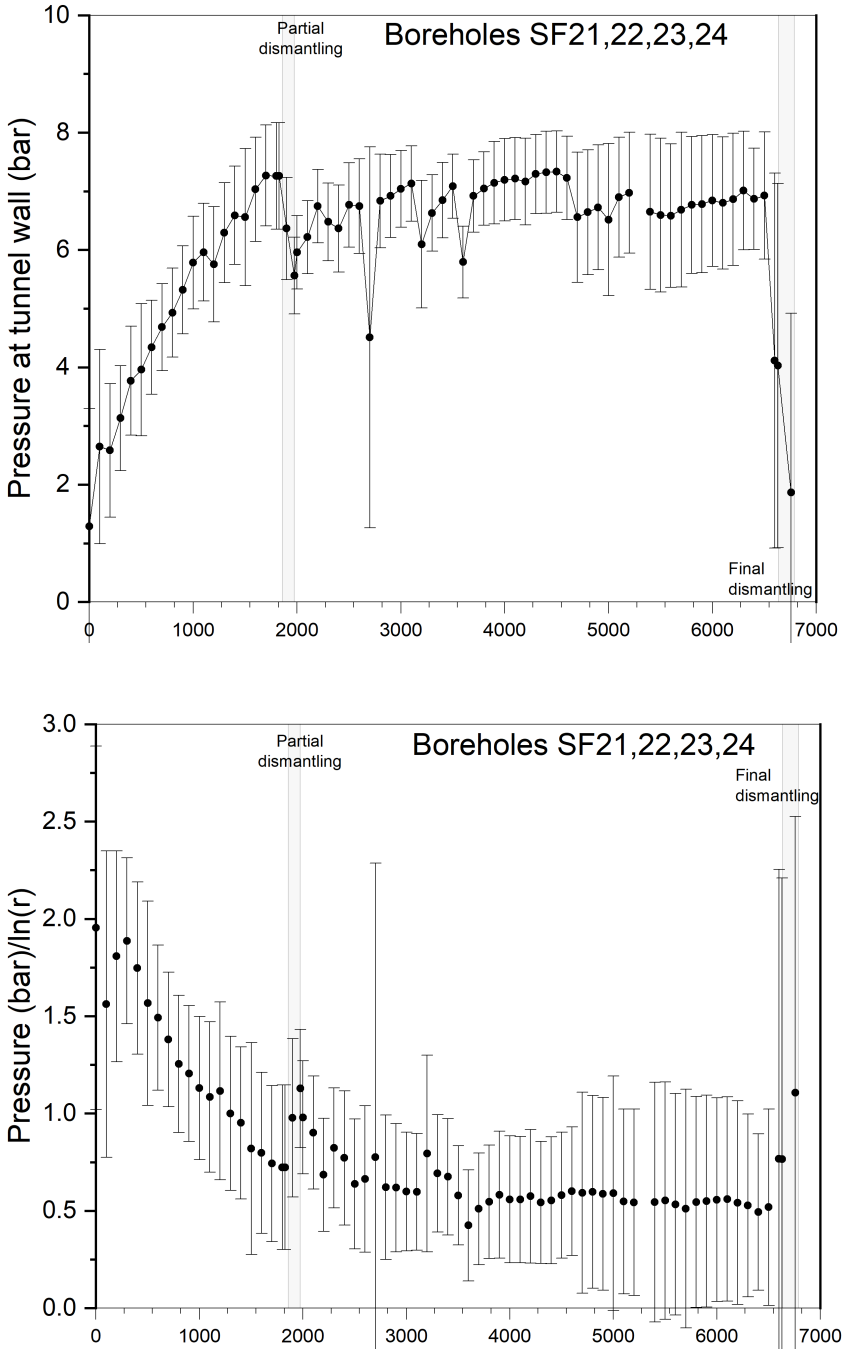


Fig. 8-5: Estimated (upper panel) pressure at the gallery wall and (lower panel) pressure gradient slope with *ln r* based on the measurements from borehole intervals in SF21 – 24

Error bars show the standard errors from the regression.

The pressure data from selected intervals have been analysed assuming radial flow and Fig. 8-5 shows the fitted pressure at the gallery wall and gradient (with ln radial distance) derived from a regression of the pressure data from the SF21 – 24 pressure measurements. The increase in pressure and reduction in slope during the first five years are clearly shown. If radial flow is assumed, the gradient is directly proportional to the flow to the gallery, but there may be some component of axial flow to the open gallery, which may explain the stable flow seen after about 3'000 days in Fig. 8-5.

The average inflow from the rock to the EBS can be estimated from the increase in bentonite water content observed at partial dismantling after 5 years heating, and final dismantling after 18 years (see discussion in Section 10.1). The estimated average inflow, together with the measured inflow to the open cavern is shown in Fig. 8-6. The inflow decreases over time in a manner consistent with the decreasing hydraulic gradient shown in Fig. 8-5b). It can be seen that bentonite saturation is limited by the low permeability of the bentonite (Gens et al. 2009) rather than the ability of the rock to provide water.

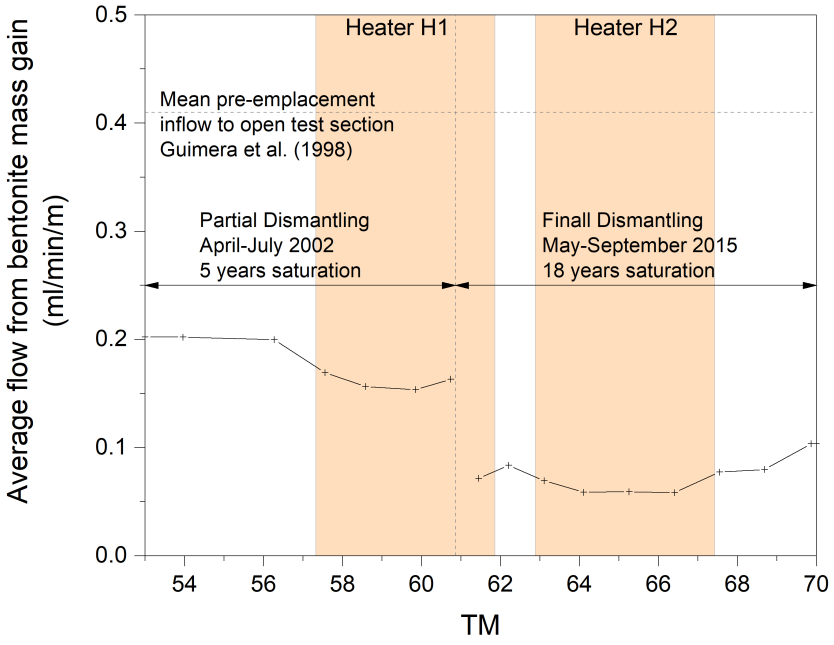


Fig. 8-6: Average inflow (ml/min) estimated from increase in bentonite water content at partial and final dismantling

8.5 Geosphere mechanical response

Stress and displacements were monitored in boreholes around the drift. A total of ten pressure cells were located at varying orientations and depths in both the SG1 (vertical) and SG2 (horizontal) boreholes drilled in the Heater #2 section. The measured total pressures vary with distance along the borehole, cell orientation and borehole orientation. Total pressures rise strongly during the initial response to heating in the sensors close to the drift wall in SG2, peaking at around 100 days. This is followed by a slower increase in total pressure until partial dismantling, when total pressure drops with the removal of the plug and buffer (Fig. 8-7). A similar response to heating is observed in the measured packer pressures. Total pressure then shows a slower but consistent increase from the end of partial dismantling until the start of final dismantling.

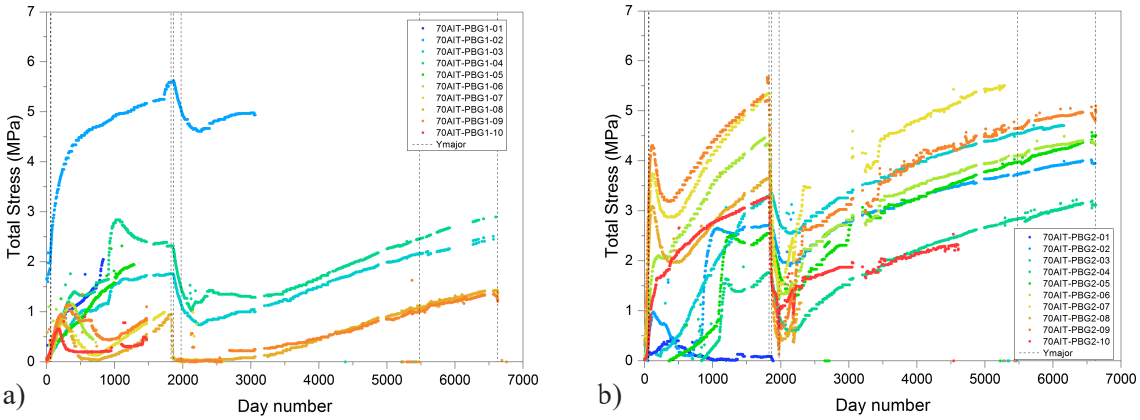


Fig. 8-7: Measured total pressure in borehole: a) SG1 (vertical up) and b) SG2 (horizontal)

Displacements were measured with 4-point extensometers located in boreholes SI1 (vertical up) and SI2 horizontal (Fig. 8-8). The extensometer data show a response to the start of heating and partial dismantling with otherwise roughly constant conditions. The changes in measured deformations are small with ~ 0.1 mm over the heating period (Fig. 8-8).

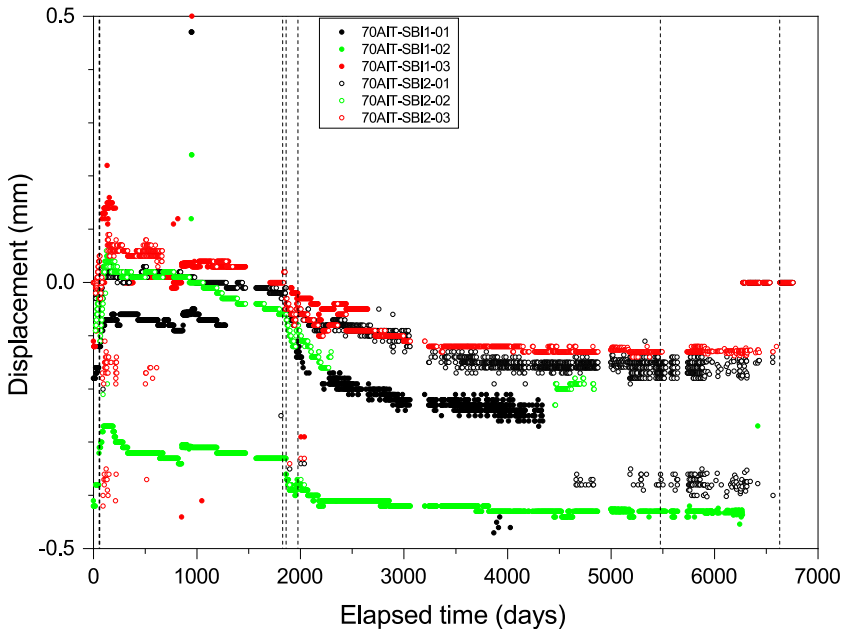


Fig. 8-8: Measured displacements in the SB1 and SB2 boreholes (displaying slight expansions)

8.6 Summary of geosphere THM response

The observations at the drift wall and from monitoring data suggest that:

- EDZ: Changes in stress, pore pressure and temperature appear to have had relatively little effect on the EDZ around the tunnel, although investigations have been limited and the EDZ is relatively small at the GTS, being confined to a few centimetres beyond the tunnel wall.
- Thermal: The overall temperature pattern can be reasonably well explained by conductive transport through the rock from the buffer. There is little evidence of significant heterogeneity in thermal properties or any significant convective flow.
- Hydraulic: Pore pressures show a general increase after plug emplacement and the start of heating up to partial dismantling. The relatively high effective permeability of the rock (compared to the buffer) prevents any significant thermally induced pressure transient (see Alonso et al. 2005). After partial dismantling, pressures are relatively stable with occasional disturbances due to the opening of boreholes, sampling and drilling of new boreholes. The low flow to the bentonite buffer results in a homogeneous pore pressure distribution with no significant "cone of depression" around the remaining buffer. Pore pressures have returned to values comparable to those at the start of the experiment.
- Mechanical: Stresses show a general increase during the heating period together with a strong response to the unloading during partial dismantling. The overall stress response is consistent with thermal expansion of the rock due to an increase in temperature. Stress increases are typically larger in the SG2 borehole (horizontal) than in the SG1 (vertical) borehole. The observed pattern of stress change depends on borehole orientation, distance from the drift wall and cell orientation as would be expected.
- Mechanical: Displacements are typically small but show a rapid initial response to heating and partial dismantling but then ongoing steady conditions until final dismantling.

Overall, the relatively higher permeability of the rock matrix, compared to that of the saturated bentonite, has resulted in a limited influence of the rock on the buffer during the early saturation period. This can be adequately described using homogeneous effective properties, without significant features or processes due to the heterogeneity of the fracture system at the site.

The role of the geosphere in the FEBEX in-situ experiment has been to:

- provide physical containment of the buffer
- provide water for the saturation of the buffer
- conduct heat away from the buffer
- allow a diffusive exchange between bentonite porewater and near-field groundwater

No significant influence of geosphere heterogeneity has been observed on buffer saturation and, similarly, EBS emplacement and heating have had little effect on the geosphere other than to locally raise temperature and pressure. While these results are specific to the FEBEX site and the experiment layout and heating schedule, this suggests that, in low-permeability crystalline rock (and in absence of any significant water conducting features) such as that surrounding the FEBEX drift where saturation is largely controlled by the low permeability of the bentonite, interactions between the EBS and geosphere are limited.

9 Groundwater chemistry characterisation

Groundwater chemistry impacts radionuclide (RN) transport behaviour, as RNs mainly migrate in groundwater as dissolved species. Furthermore, the chemistry of the water (salinity, pH, Eh, complexing agents) is one of the main parameters controlling the aqueous speciation of RNs, their solubility, their retention in the medium and colloid stability. Specifically, in crystalline media, it is important to understand what chemical reactions and sorption processes occur in the host rock and what their effects on RN mobility might be. In addition, the presence of the engineered barriers may possibly influence the chemical composition and reactivity of the groundwater, also through colloidal processes. The FEBEX experiment, with its real repository scale in a granitic rock, offered a unique possibility to study the chemical effects produced and interactions caused by the bentonite (EBS) on the surrounding groundwater, including the formation and release of colloidal particles. Several boreholes, radially from and parallel to the FEBEX drift (see Section 1.3) were used for water sampling for over 20 years.

The main objectives in analysing the groundwater during the experiment were:

- gathering hydrogeochemical information regarding the rock around the FEBEX gallery, prior to, during and after the experiment
- evaluating the main factors (lithological, hydraulic, structural) responsible for the chemical composition of the groundwater around the FEBEX gallery
- obtaining information about the effect of the near-field vs. far-field interface in a granitic environment and gaining information about potential geochemical gradients generated by the bentonite into the granite

Over the duration of the FEBEX experiment, 683 samples were taken from borehole intervals and surface water (Garralon et al. 2017), and it can be concluded that:

- Electrical conductivity increases in groundwater near the bentonite (parallel boreholes) as Cl^- and SO_4^{2-} concentrations increase, while the bicarbonate concentration remains stable. In radial boreholes, water is more dilute than in parallel boreholes, and the concentrations of main dissolved ions remain constant. The pH value of the water samples from the parallel boreholes drilled in the FEBEX gallery is 7.4 ± 0.7 and that from radial boreholes is 8.1 ± 0.7, indicating that waters are generally neutral to slightly alkaline. However, there were difficulties in measuring reliable values from borehole intervals with low flow.
- The order of relative abundance of major cations in the groundwater from the radial boreholes is $Ca^{2+} > Na^+ > NH_4^+ > K^+ > Mg^{2+}$, and the relative abundance of major anions is $HCO_3^- > F^- > SO_4^{2-} > Cl^-$, whereas in the parallel boreholes it is $Na^+ > Ca^{2+} > NH_4^+ > Mg^{2+} > K^+$ and the relative abundance of major anions is $HCO_3^- > SO_4^{2-} > Cl^- > F^-$. Groundwater in the parallel boreholes shows some differences in chemical composition compared to that in the radial boreholes (Fig. 9-1).

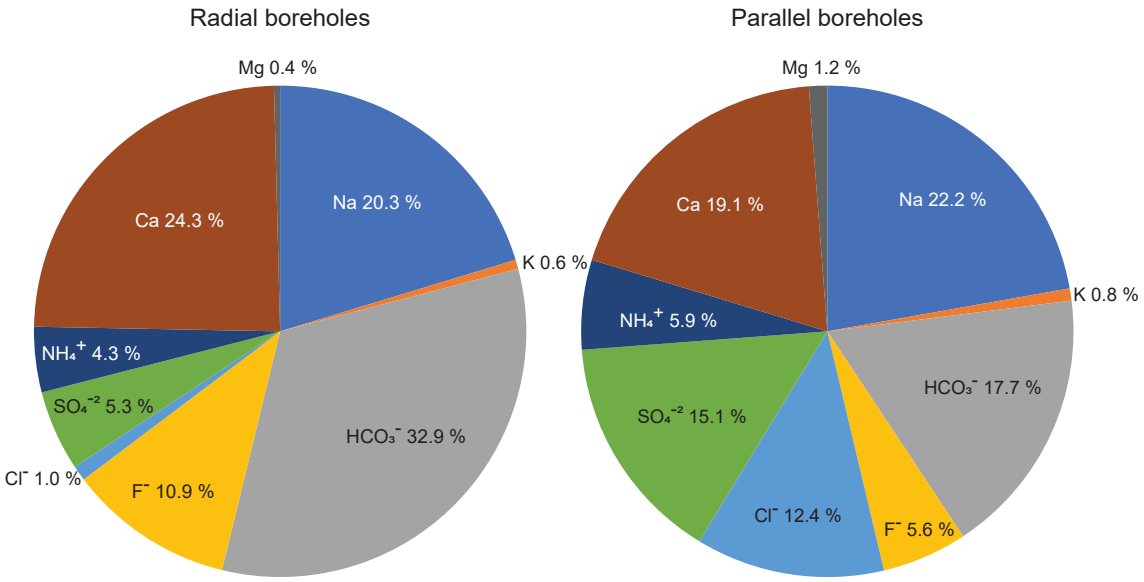


Fig. 9-1: Pie diagram of mean concentration values for major ions in groundwater from radial and parallel boreholes

- The major anion in Grimsel groundwater from radial boreholes is HCO_3^- associated with Ca^{2+} and/or Na^+ due to the interaction with granitic host rock and the minerals of the fracture fillings. Dissolution of carbonates (calcite) and silicate minerals are the main processes responsible for the chemical composition of Ca-Na-HCO_3-type water. As the residence time of groundwater increases in contact with the granite, the influence of plagioclase hydrolysis becomes increasingly important. A compositional transition from Ca-Na-HCO_3- to Na-Ca-HCO_3-type water was observed due to a decrease in the calcium concentration and enrichment of sodium via water-rock interactions such as silicate weathering and cation exchange between Ca^{2+} and Na^+. A small number of water samples from the radial boreholes was classified as NH_4-HCO_3 due to the presence of ammonia in feldspars, micas and clay minerals in which it substitutes for K^+.
- Groundwater samples from parallel boreholes (at 20 and 60 cm from the bentonite) have been classified into five water types: Ca-Na-HCO_3, Ca-Na-SO_4, Na-Ca-SO_4, NH_4-SO_4 and Na-Cl. The distance to the bentonite barrier and the influence of its chemical porewater composition (Na-Cl) was the key to obtaining these different types of water in the parallel boreholes in a granitic system. Diffusion processes took place between the major ions of the porewater bentonite and the granitic groundwater through the small fractures isolated in the intervals packed-off in the boreholes. As a result, the chemical composition evolved from Ca-Na-HCO_3^- to Na-Cl-type water. After the final dismantling of the bentonite (2015), the flowrate decreased in all the borehole intervals and a new change in chemical composition into a NH_4-SO_4-type water was observed.
- The quartz veins and the small lamprophyres represent preferential flow paths that can facilitate the solute mass transfer between the bentonite and the granite groundwater. Intervals with a higher transmissivity (i.e. due to the presence of fractures) are most affected by the influence of the bentonite barrier.
- The hydration of the barriers with Grimsel groundwater provides fluoride to the buffer with respect to the reference material as observed in all samples (Villar, 2017); the fluoride most likely came from the granite groundwater.

- The pH of water in contact with the shotcrete plug was about 10.18, as measured in a water spill. This seems to indicate some interaction with the concrete, which is expected to provide a higher pH (Turrero & Cloet 2017, see also Section 5.1). While the water obtained from radial boreholes is predominantly of bicarbonate and calcium/sodium ion composition and contains very low concentrations of other anions and cations, the high concentration of chloride, sulphate, sodium and potassium in the water spill (observed during short-core concrete drilling, Turrero & Cloet 2017) may also reflect the interaction of the granite groundwater with the concrete plug and the bentonite buffer.
- The Na/Cl ratio in groundwater (0.93) was higher than in bentonite porewater (0.81). The source of Na in the groundwater (classified as Ca-Na-HCO_3^- and Na-Ca-HCO_3-types) is due to cation exchange of Na^+ for Ca^{2+}. The remaining water samples have another source of Na^+ concentration: the dissolution of plagioclase or mass transfer from the bentonite.
- In relation to the silicate weathering processes, most of the samples indicate a position in the stability field of kaolinite. The chemistry of the groundwater system favours kaolinite formation, and chalcedony could control silica concentration in solution. All the waters are in equilibrium with chalcedony. Albite is near equilibrium or slightly supersaturated in some HCO_3-type waters and in Na-Cl type water. In the rest of the samples, water was always sub-saturated. Gibbsite is supersaturated in all samples studied.
- SO_4-type waters show the highest concentrations of trace elements in solution. These waters are characterised by the highest EC values (744 μS/cm) and their chemical composition is influenced by their proximity to the bentonite barrier. Ni, Zn and Sr are the most abundant trace elements in FEBEX groundwater. The Sr content is probably controlled by the chemistry of the Ca-plagioclase. Trace elements such as U, Cu, Th, Pb, Li, Mn and Ba show concentrations that should be considered as intermediate in the range of the trace elements. By normalising these values with the chemical composition of the bentonite porewater, the bentonite barrier could be observed to have an effect on the chemical composition of the waters sampled at the parallel boreholes (in SO_4-type and Cl-type waters).
- The stable isotope characterisation of groundwater from the FEBEX gallery confirms the influence of the bentonite barrier on the waters sampled and analysed at the parallel boreholes. A significant difference between the waters sampled from the radial boreholes and those from the parallel boreholes has been observed and can be explained by the diffusion of water from the bentonite barrier as a function of travel distance.

Some open questions regarding the exchange of FEBEX porewater and groundwater remain:

- The ion diffusion from the bentonite barrier has clearly been observed for Na^+ and Cl^- ions, but how does it affect other ions such as SO_4^{2-}, K^+, Ca^{2+}? Correspondingly, the trace element behaviour is not fully understood and suggests diffusion from the bentonite barrier to the granitic media.
- The presence of NH_4^+ ion in the sampled water in the parallel boreholes is suggested to be related to the feldspar origin, but should be explored in depth.
- Unfortunately, the low flow conditions observed in the boreholes from the FEBEX gallery did not allow a detailed study of the redox conditions.

The hydrogeochemical studies have revealed the importance of the solute mass transfer between the bentonite barrier and the geosphere and have allowed determination, at a real scale, of the effective diffusion coefficients of the natural tracers coming from the bentonite porewater (Garallon et al. 2017). The transport of conservative solutes from the bentonite into the granite can thus be realistically considered in a safety assessment of similar systems.

The transport of conservative solutes from the bentonite porewater to the near-field geosphere has been characterised within the low-permeability crystalline rock around the FEBEX drift, but no significant transport of bentonite colloids has been observed in the near-field, because there were only a relatively small number of sampling locations in the geosphere. However, this, together with the observations of the state of the buffer at dismantling, suggest that, in the absence of highly transmissive structures, there is no evidence of significant bentonite mass loss during the early saturation transient at the FEBEX site.

10 Comparison of the buffer characteristics from the dismantling in 2002 versus 2015

The FEBEX in-situ experiment provided a unique opportunity to obtain long-term monitoring data and particularly large datasets from samples from dismantlings at two different times, thus characterising different stages during the early evolution of the EBS. These data contribute significantly to confirming, testing and verifying concepts and help to test, calibrate and improve THM and THC models. This chapter focuses on the evolution of the buffer, based on the data after five years of heating from the partial dismantling in 2002 which are then compared with data after 18 years of heating at 100 °C (heater surface) from the final dismantling in 2015.

10.1 Comparison results 2002 versus 2015: evolution of the barrier

As mentioned in Chapter 1, the original configuration of the FEBEX experiment included two heaters (Fig. 10-1) and a much longer bentonite barrier. Half of the experiment, including Heater #1, was dismantled in 2002 after five years of operation. A comparison of the results obtained concerning the physical state of the bentonite barrier during this partial dismantling and the bentonite properties determined in the laboratory (Villar et al. 2005, 2008) and those obtained during the final dismantling and in the samples then retrieved (reported in Chapter 1 and Section 5.3, Villar 2017, Villar et al. 2016, 2018a,b, 2020) allows some conclusions to be drawn about the evolution of the barrier over time, with regard to both its physical state and the bentonite properties.

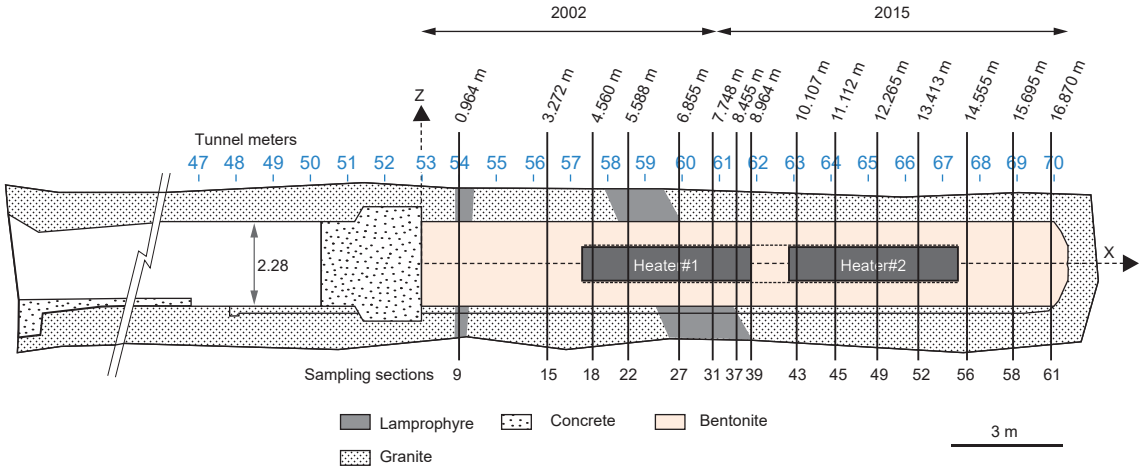


Fig. 10-1: Schematic representation of the FEBEX gallery with indication of the sampling sections used for on-site analyses in 2002 (sections S9 to S31) and 2015 (sections S37 to S61)

10.1.1 Physical state of the barrier

One of the most striking features of the bentonite barrier was that its swelling and sealing capacity had already developed after five years of operation, since all the construction gaps in the barrier were almost entirely filled with bentonite. This meant that the water availability at the test site (both in the liquid and the vapour phases) was sufficient to allow quick swelling of the external part of the barrier. In turn, the quick swelling avoided preferential paths remaining open, which resulted in the water content distribution in vertical sections following a radial pattern that was largely independent of the particular features in the rock (Fig. 10-1). Although the boundaries of the blocks were clearly visible, no gap remained between them, except at the core of the barrier in the cold sections, where the water content had barely increased with respect to the original content, i.e. from 14% to values below 18%. However, after 18 years operation, these internal joints were also sealed (Fig. 10-2).

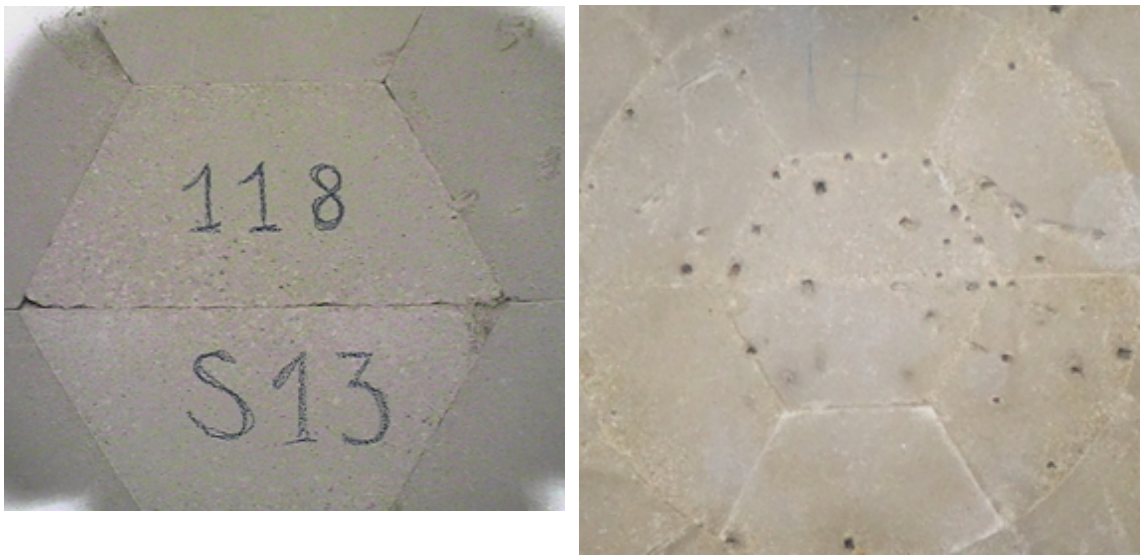


Fig. 10-2: Appearance of the core of the barrier in cold zones after 5 years (left, slice 118) and 18 years (right, slice 17) of operation

The main changes during the Second Operational Phase took place in the internal part, i.e. core, of the barrier. After five years of operation, the cold and hot sections had distinctly different features, and these were also observed in the final dismantling. In particular observations included (for the locations of the sampling sections refer to Fig. 10-1):

- The water content in the 10 cm closest to the granite of the cold sections was the same after 18 years operation as after 5 years, whereas the additional operational time allowed the saturated region to extend further towards the interior of the barrier (Fig. 10-3).
- In the sections around the heater, the water content near the granite, i.e. in the outer ring of the barrier, decreased from that observed at five years after 13 additional years of operation. In contrast, the water content increased in the middle and inner rings of the barrier (Fig. 10-4, left).
- The dry density distribution along the radii around the heaters did not significantly change over time (Fig. 10-4, right).

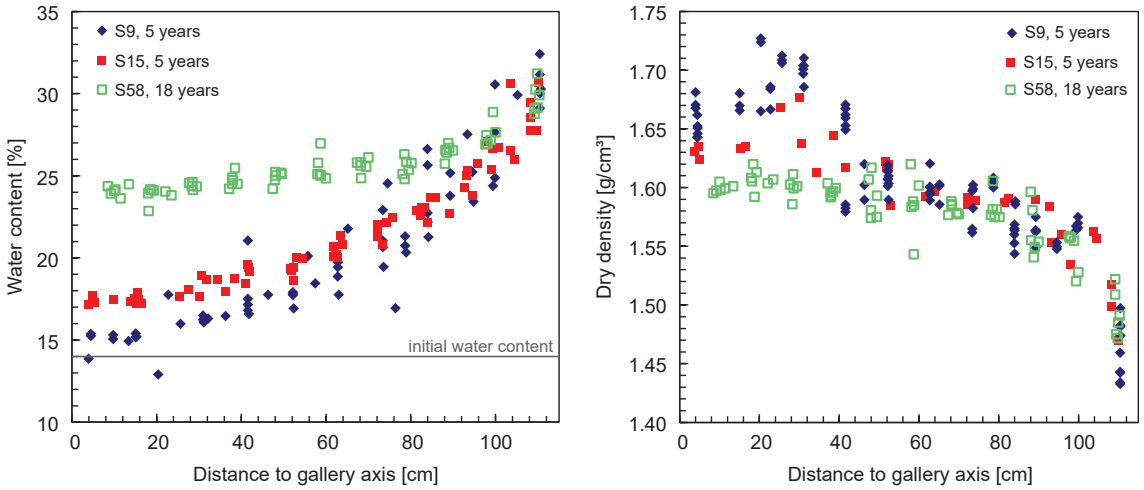


Fig. 10-3: Water content and dry density of the bentonite barrier along the gallery axis in cold sections after 5 and 18 years of operation

After 5 years of operation: Daucausse & Lloret (2003) and after 18 years of operation: Villar et al. 2016

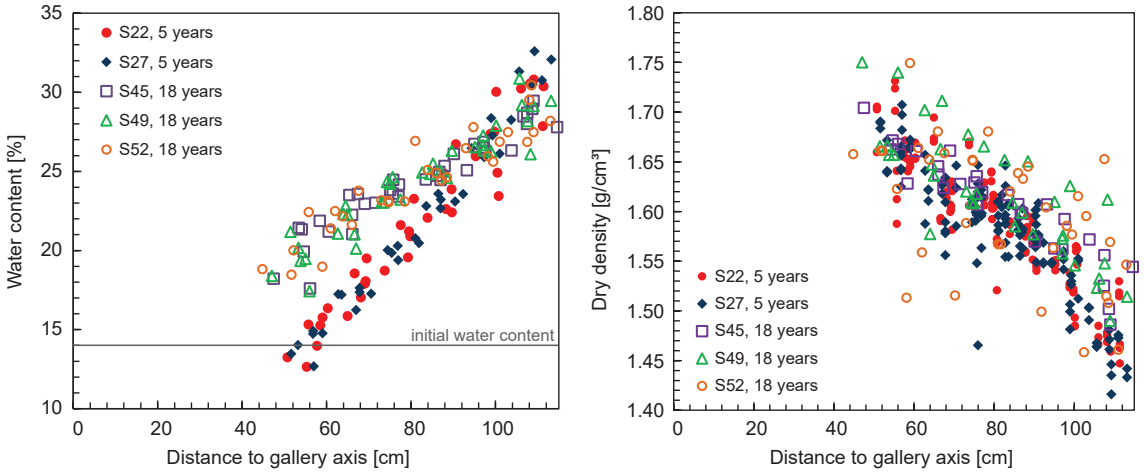


Fig. 10-4: Water content and dry density of the bentonite barrier along the gallery axis in sections around the heaters after 5 and 18 years of operation

After 5 years of operation: Daucousse & Lloret 2003) and after 18 years of operation: Villar et al. 2016 & 2020

Hence, the water content and dry density gradients generated as a consequence of hydration and heating have proved to be persistent, and maybe irreversible since they were already observed after five years of operation and remained stable for a further thirteen years despite the overall high degree of saturation at the end of the experiment.

The average water content (w), dry density (ρ_d) and degree of saturation (S_r) for the bentonite sections sampled in 2002 and 2015 are given in Tab. 10-1. These values are plotted as a function of the distance to the coordinate origin in Fig. 10-5, where the sections around Heater #1 are those dismantled in 2002 after 5 years of operation and the sections around Heater #2 are those disman-

tled in 2015 after 18 years of operation (see Fig. 10-1). The variation of the bentonite installation density along the barrier, taken from ENRESA (1998), is also plotted in this figure. From longitudinal profiles similar to those shown in Fig. 5-14, the overall values for these properties can be computed (Villar et al. 2016) and are shown in Tab. 10-2 for the partial and final dismantling. The initial installation density is also indicated, since the section of the barrier dismantled in 2002 had an average dry density lower than that dismantled in 2015. There is no particular reason for this difference, which is simply a consequence of particularities of the installation operation. The initial water content of the bentonite was considered to be 14.4% for all the blocks (ENRESA 1998a).

Tab. 10-1: Average properties for each section as computed from fitting of polynomial functions

***x*-coordinate** [cm]	**Slice**	**Sampling section**	**Dismantling date**	***w*** [%]	ρ_d [g/cm^3]	S_r [%]
96	129	S9	2002	22.9	1.58	85
327	111	S15	2002	22.8	1.58	86
456	101	S18	2002	23.1	1.58	87
558	93	S22	2002	22.6	1.57	85
685	83	S27	2002	22.6	1.56	84
774	76	S31	2002	22.8	1.58	85
845	70	S37	2015	27.9	1.56	103
921	64	S39	2015	27.3	1.56	100
1'011	57	S43	2015	27.0	1.59	105
1'111	49	S45	2015	24.9	1.60	97
1'226	40	S49	2015	25.0	1.60	98
1'341	31	S52	2015	25.0	1.59	97
1'455	22	S56	2015	26.2	1.57	98
1'569	13	S58	2015	26.9	1.55	98
1'687	4	S61	2015	32.4	1.46	103

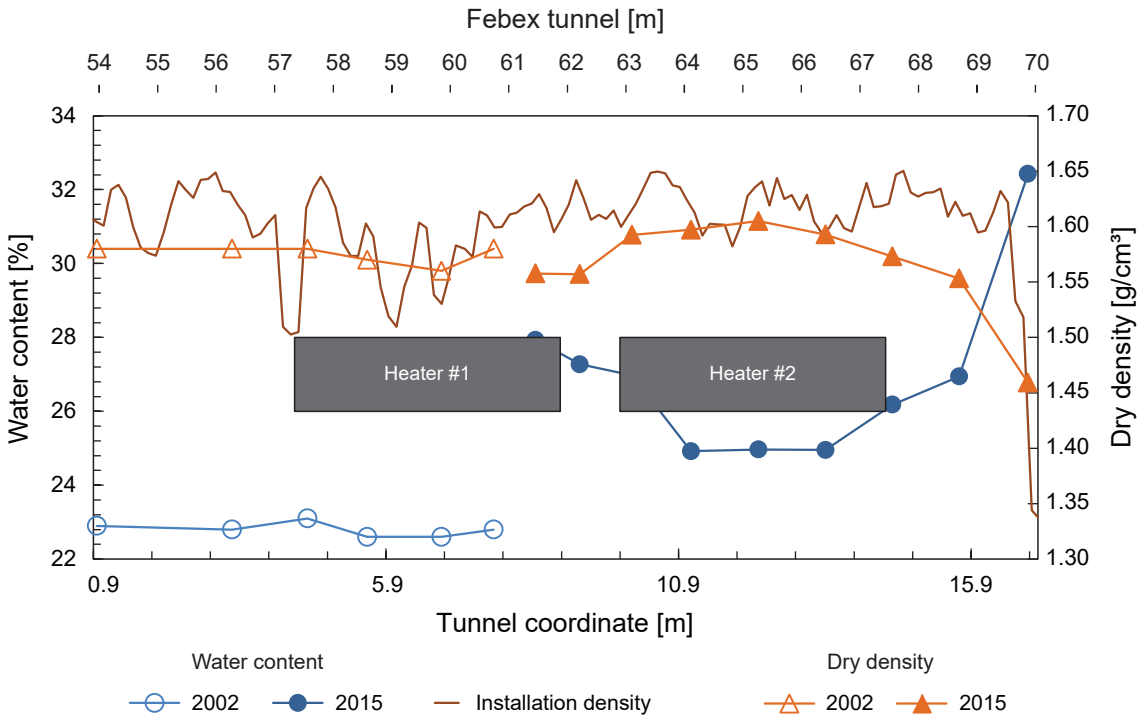


Fig. 10-5: Average water content and dry density for the sections sampled along the barrier in 2002 and 2015

Values from Tab. 1

Tab. 10-2: Average values computed from the longitudinal profiles

Dismantling date	***w*** [%]	**Installation ρ_d** [g/cm³]	ρ_d [g/cm³]	S_r [%]
2002	22.2	1.59	1.58	85
2015	25.5	1.61	1.59	97

After five years of operation, there was a significant overall increase in the barrier water content from the initial value of 14% to an average value of 22%. This increase was homogeneous along the barrier, despite the fact that the section of the drift where Heater #1 was emplaced included a metabasic dyke and several other more conductive geological features such as fissures or dykes. The effect of the heater was barely noticeable, since the average water content for all the sections, both in cold and in hot areas, spanned only a narrow range between 22.6 and 23.1%.

This suggests roughly uniform water uptake from the geosphere along the dismantled section. Within the buffer around the heater, there was a significant redistribution of moisture from the blocks nearest the heater towards the rock.

After 13 additional years of operation the average overall water content increased from 22% to 25.5%, which reflects the slowing down of the hydration rate over time. Furthermore, in this case, the hot and cold sections had very different water contents that clearly increased away from the heater towards the plug and back of the tunnel. The average water contents of the different sections spanned between 24.9% around the middle part of Heater #2 to 32.4% at the back of the

gallery. These results indicate that the effect of the thermal gradient on the overall water intake was negligible in the first stages of saturation, but was very relevant as hydration proceeded, delaying saturation in the areas around the heater.

The comparison between the initial and final dry densities shows that the latter were lower, despite the fact that no bentonite mass or overall volume changes took place during operation. As shown in Chapter 4 and Section 5.2, decompression during dismantling and sampling mostly accounted for this decrease, since the samples used to determine dry density suffered some expansion with respect to their state in the barrier. This effect was more significant during the final dismantling, when the higher bentonite water content induced more expansion upon pressure release. Concerning the density longitudinal changes, the part of the barrier dismantled after five years of operation had average dry densities in vertical sections that did not change much along the gallery axis, with an average value of 1.58 g/cm^3. Only two of the sections around the heater had dry densities slightly lower. These sections coincided with the area of the metabasic dyke where, due to irregularities of the drift, many blocks had to be trimmed, causing lower installation density. In contrast, the part of the barrier dismantled after 18 years of operation showed important longitudinal changes in dry density. As discussed in Section 5.2, these differences were partly inherited from installation, in particular the lower dry density at the back of the gallery, which made the barrier swell preferentially towards this area with larger construction gaps. The decrease in dry density with respect to the installation as observed at the front of Heater #2 could have resulted from processes occurring at two different times: 1) in 2002, when the preparation of the bentonite surface that was to be in contact with the shotcrete plug involved some mass loss, and again after the plug installation, because the additional supply of water coming from the shotcrete (reflected in the higher water content of the bentonite in this area) would have made the bentonite swell, pushing towards the back of the gallery, and 2) during dismantling in 2015, because the pressure release upon the concrete plug removal made the bentonite barrier move forwards (see Section 5.2.5 and Chapter 4).

Therefore, a barrier with an initially homogeneous dry density ended up having important inhomogeneities in terms of dry density and water content (Villar et al. 2018d). This could indicate that the volume changes induced during the initial saturation were irreversible. Lloret & Villar (2007) stated that, according to laboratory tests with untreated samples interpreted using generalised plasticity models (Lloret et al. 2003) and provided that the net stresses in the barrier do not exceed the bentonite swelling pressure, these macroscopic changes would be irreversible and the density heterogeneity throughout the barrier would remain.

These gradients have not impaired the performance of the barrier, but imply that the bentonite barrier may be inhomogeneous, which can influence its thermo-hydro-mechanical properties, since most of these (thermal conductivity, swelling pressure, permeability, water retention, etc.) depend greatly on the density and water content of the bentonite, as shown in Section 5.3.3 and discussed below.

10.1.2 Bentonite properties

The FEBEX-DP studies undertaken by several laboratories in order to characterise the retrieved bentonite confirmed the good performance and stability of the bentonite barrier over a time period of 18 years (see Section 5.3). The previous section explained that the bentonite provided a continuous barrier, in which, once saturated, the interfaces between blocks did not play any role in the water content and density distribution or fluid transport. Additionally, the comparison with the laboratory results obtained after the first dismantling in 2002 (Villar et al. 2006) allows some conclusions to be drawn about the evolution of the barrier and the changes in the bentonite properties over time.

Within the accuracy limits of the techniques used, no relevant changes were observed in the mineralogy of the bentonite, its physico-chemical and surface properties (such as charge location), water adsorption capacity or montmorillonite crystal chemistry. This was also the conclusion of the analyses performed after the first dismantling. However, there was a decrease in the bentonite specific surface area in the zones subjected to the highest temperature that had also been observed after five years of operation. This is consistent with the quick drying that took place around the heater in the first stages of operation (see Chapter 2).

Due to the inward groundwater movement and the thermal gradient caused by the heater, changes in the porewater chemistry and the cation exchange complex were observed. When extrapolating these results to other repository concepts, the particularities of the FEBEX bentonite porewater and of the availability and composition of the groundwater have to be taken into account. The porewater of the FEBEX bentonite was initially of Na-Mg-Cl^-(SO_4)-type (I ~ 0.3 M), reflecting its marine origin (Fernández 2004), whereas there was an abundance of groundwater at the drift location and this was quite dilute (Garralón et al. 2018); for this reason the contribution of external ionic species can be considered negligible.

The hydration of the bentonite blocks in contact with the granite gave place to dilution and consequently to dissolution of the more soluble minerals in the bentonite (sulphates, carbonates and chlorides) that were transported towards the inner part of the barrier. This caused the salinity of the bentonite porewater in the external part of the barrier to quickly decrease (in less than 5 years) and remain low over time (for at least up to 18 years). The movement of the dissolved species was affected primarily by the thermal gradient, which conditioned the hydration rate and hence their advective transport, and then by the particular solubility and size of the ions and by their participation in other processes, such as exchange reactions and dissolution/precipitation. In this sense, chloride, being a conservative ion, moved steadily towards the core of the barrier and showed concentration maxima at about 20 cm from the heater after five years of operation and at the heater surface after 18 years of operation (Fig. 10-6, left). The trends of sodium, calcium and magnesium were similar to that of chloride, but the maxima were not as pronounced because these ions were also involved in exchange reactions and dissolution/precipitation of other species. However, sulphate mobilisation was significantly retarded with respect to the mentioned ions, with maxima in intermediate parts of the barrier that also progressed over time (Fig. 10-6, right). In the cooler parts of the barrier, the inward movement of ionic species was much delayed with respect to that under thermal gradient.

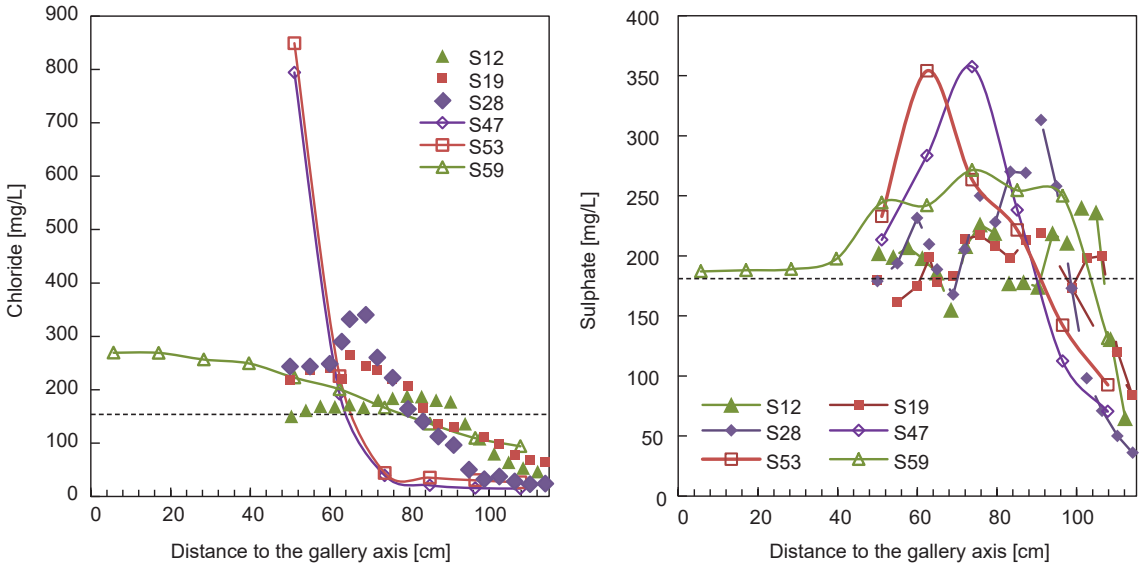


Fig. 10-6: Concentration of ionic species measured in 1:4 aqueous extracts of bentonite samples taken in 2002 (S12 to S28) and 2015 (S47 to S59)

Sections S12 and S59 were cool sections (see Fig. 10-1 for locations of sections).

With respect to the changes in the exchangeable cation complex, these were mostly triggered by the thermal gradient, as, in the cooler areas, the changes with respect to the reference bentonite were minimal. The clearer features, observed after both 5 and after 18 years of operation, were a decrease in exchangeable sodium towards the heater and an overall increase in exchangeable potassium, which was also observed in the cool areas. The increase in exchangeable magnesium towards the heater observed after 18 years was not observed after 5 years of operation.

The thermal, hydraulic and mechanical properties analysed depended on the dry density and water content of the bentonite and were consistent with the range expected for the reference bentonite. Due to the dry density gradients generated in the barrier, these properties were not homogeneous across the barrier.

The hydraulic conductivity measured in the samples retrieved in 2002 and 2015 remained very low ($< 10^{-13}$ m/s for all the samples with a dry density above 1.5 g/cm^3), but the variability with respect to the expected values was high and without a clear trend (Fig. 10-7).

There was no irreversible change in the swelling capacity of the FEBEX bentonite – determined as deformation upon saturation and swelling pressure –after five years of being subjected to repository conditions, nor after 18 years. The results of the tests performed in samples retrieved in 2015 showed that prolonged drying did not impair the bentonite swelling capacity.

The apparent pre-consolidation pressure of the samples retrieved both in 2002 and in 2015 tended to be lower as the initial void ratio was higher and suction was lower, with values in all cases below 15 MPa (Fig. 10-8). This means an important decrease with respect to the initial pre-consolidation pressure (around 40 MPa), which is explained by the microstructural changes associated with the volume increase experienced during hydration.

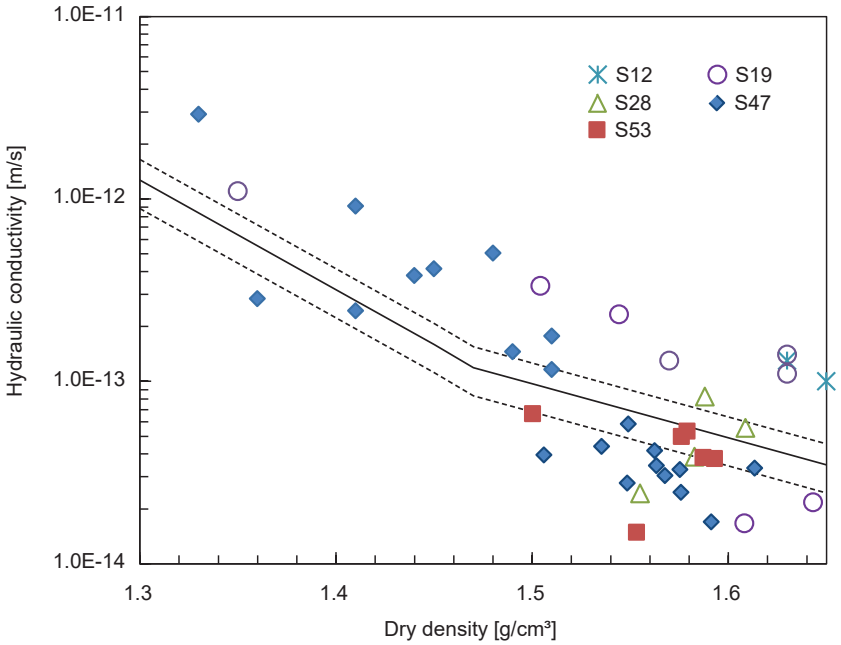


Fig. 10-7: Hydraulic conductivity of samples trimmed from blocks retrieved from different sampling sections in 2002 (S12 to S28) and 2015 (S47 and S53) as determined by different laboratories

The lines indicate the empirical correlation for untreated FEBEX material.

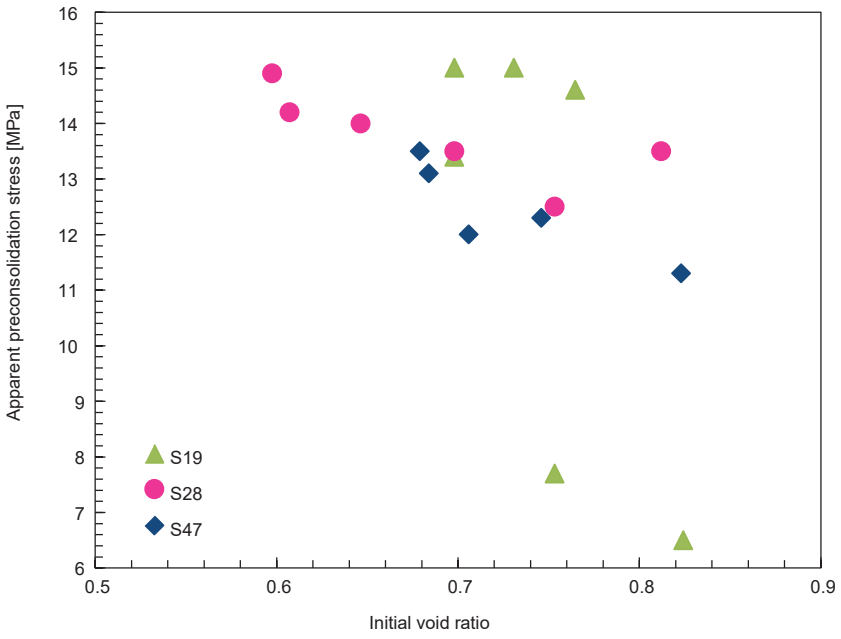


Fig. 10-8: Apparent pre-consolidation stresses estimated from oedometer tests for samples trimmed from blocks retrieved from different sections in 2002 (S19 and S28) and 2015 (S47)

The experiments performed on samples retrieved during 2002, remoulded and prepared with artificial joints parallel and perpendicular to the percolation flow, showed that, upon saturation, the medium became homogeneous and the joints completely sealed. The hydro-mechanical properties of the material depended only on its dry density. However, in unsaturated samples, the hydrodynamic properties of the clay were modified by the existence of joints parallel to the infiltration flow. This was confirmed by the gas permeability measurements performed in non-remoulded samples with interfaces along them retrieved in 2015, which were tested maintaining the same dry density and water content conditions in the barrier (Villar et al. 2018c). The samples from the intermediate and outer rings of the barrier (which had a very low accessible void ratio because of their high saturation) had permeabilities closer to those corresponding to the same accessible void ratio in the reference bentonite, indicating the complete sealing and healing of the interface. However, samples drilled between two blocks from the inner ring of the barrier had a higher permeability than samples of similar accessible void ratio in the reference bentonite.

Finally, it has to be pointed out that the modifications observed in the chemical and mineralogical composition of the bentonite and its porewater could not be clearly correlated with any important variation in the macroscopic thermo-hydro-mechanical properties, which is a conclusion of the first and the final dismantling.

10.1.3 Implications for long term performance

The detailed investigations in the FEBEX in-situ test have shown that:

- There was no significant influence of particular features of the geosphere on the buffer during the 18 years of heating and saturation.
- Swelling pressure close to the rock wall developed quickly due to saturation from the geosphere and redistribution of moisture from the buffer close to the heater.
- The gaps between the rock wall and the bentonite buffer closed within five years. Gaps between the blocks near the wall also closed during this period.
- Gaps between the blocks closed across the whole buffer after 18 years.
- Heterogeneity in buffer dry density due to saturation, swelling and heating developed within five years and was largely unaltered after 18 years as the buffer approached full saturation.
- Properties of the bentonite, after accounting for dry density changes, were largely unaltered, with no significant impairment of swelling capacity after 18 years of heating.
- The hydraulic conductivity of the buffer material remained low.

11 Assessment of the FEBEX experiment

Requirements related to the performance and design specifications of the bentonite buffer have developed with the evolution of specific repository design and boundary conditions over the last 25 years since the initiation of the FEBEX project in the early 1990s. Due to a more detailed understanding of the processes and phenomena related to repository-induced effects, requirements today can generally be formulated with less conservatism. However, the overriding safety functions of the bentonite buffer have not significantly changed during this period.

Uncertainties related to the bentonite performance have evolved over time and the questions asked when FEBEX was planned could be more specific or less relevant today, but other questions are being asked (e.g. interaction of bentonite and Fe-corrosion, microbiology, etc.). In the following assessment of the performance of the bentonite, initial questions posed at the planning stage of FEBEX as well as more recent topics are discussed.

For high-level waste/spent fuel (HLW/SF) disposal concepts with a clay-based buffer and sealing materials, the respective safety functions have been summarised by Sellin & Leupin (2013) as:

- limiting transport in the near-field: primarily limiting advective transport (determined by the hydraulic properties), but also retardation or attenuation (determined by the chemical retention properties)
- resisting mineralogical transformations (to retain the favourable properties on the short and long term)
- reducing microbial activity (to protect the canister)
- damping rock shear movements and preventing canister sinking (to protect the canister)
- limiting pressure on canister and rock (to protect the canister or the overlying bedding structure in the case of sedimentary host rocks), and
- no harmful effects on the other barriers, i.e. the buffer should not contribute to increased corrosion of the canister/container or have a lasting detrimental effect on the host rock

Some of these safety functions are less of a concern for a repository in clay rock (e.g. damping rock shear movements). In a repository in crystalline rock, the requirements on the bentonite buffer are generally more stringent. However, this does not affect the discussion of the bentonite performance below.

An inherent difficulty with assessing the performance of a bentonite buffer is that most of the requirements can only be met when the bentonite is largely saturated. Most, but not all, of the buffer of the FEBEX in-situ test reached full saturation in almost 20 years (see Section 5.2.6). This must be considered when discussing the performance of the EBS.

11.1 Performance of the EBS in the FEBEX experiment

11.1.1 Limiting transport in the near-field

Limited transport in the near-field is primarily controlled by diffusion-dominated transport processes (determined by the hydraulic properties), but also by retardation or attenuation processes (determined by the chemical retention properties).

When using blocks of bentonite, a major concern are the joints between these blocks and their effect on transport properties. The on-site bentonite analysis revealed that the gaps between the blocks disappeared between 1997 and 2015 and that the blocks were tightly sealed (Villar et al. 2017, Section 5.2). This is also the case for the bentonite-rock interface. However, the interfaces were found to influence gas permeability (which increased) close to the heater. The effect on gas permeability is less visible in the more saturated samples in the cold sections and closer to the tunnel wall.

The overall water content distribution increased over time (Villar et al. 2017 and Sections 5.2 and 10.1). As expected, a lower water content was found where the temperatures were the highest. In the colder sections, the entire barrier was saturated homogeneously to a high degree. The dry density profiles in the radial and axial direction are presented in Sections 5.2.3 and 5.2.5. Dry density gradients developed and remained in both the radial and axial directions, and they are similar to those in the first partial dismantling. This can be seen in Fig. 10-4, which indicates that homogenisation did not progress significantly during 13 years of further saturation.

Dueck et al. (in Villar et al. 2017) conducted swelling pressure tests with ground and remoulded FEBEX blocks and intact FEBEX block sample material. They could not find any large deviation in swelling pressure. The largest deviation in swelling pressure was a reduction found in the order of the ones at ground and recompacted samples from the innermost part. This is in line with results from other field tests at the Äspö Hard Rock Laboratory. Next to the concrete interface, the swelling strain was found to be lower by 1%. Dueck et al. (2011) concluded from the retention curves that no large deviation in the main part of the water retention curve was found. At the highest relative humidity values, higher water contents were measured. However, a larger deviation in hydraulic conductivity was observed, which was probably due to sample preparation as no trend could be found.

In summary:

- The overall water content of the buffer increased over time, indicating ongoing saturation.
- Swelling pressure developed rapidly to values close to those expected for full saturation near the tunnel wall and resulted in closure of the gaps between the blocks. The gaps only showed an influence on gas permeability in the lower saturation samples nearest the heater.
- Only minor differences in the permeability-dry density relationship were found between the reference material and the sample material.
- Heterogeneity in dry density distribution developed within the first five years and was still present after 18 years of saturation. However, the minimum dry density measured was still above 1.5 g/cm^3 (average 1.59 g/cm^3) for all but the buffer section at the back of the tunnel where difficulties were encountered during emplacement (low emplacement densities). Overall, the heterogeneity induced by emplacement processes appears to be relatively small (1.55 – 1.65 g/cm^3). However, since the relevant bentonite properties (hydraulic and thermal conductivities, swelling strain, etc.) are within the required targets the achieved homogeneity will be sufficient for safety.

There were inevitably some "artefacts" associated with buffer dismantling which should be borne in mind when interpreting the data from the buffer:

- The effects of the partial dismantling may have resulted in a general "loosening" of the buffer around the dummy canister, resulting in lower density.
- Small deformations of the buffer (outwards into the tunnel, at the front of the buffer and towards the end of the tunnel at the rear).

- Reduction in the thermal gradient due to switching off the heater. This is likely to have resulted in some increased transport of moisture towards the heater, which in turn would result in an overestimation of water content and saturation around the heater (this effect was considered in the modelling of the dismantling process).

However, the effects of these artefacts appear to have been small and to not have significantly hindered the interpretation of the results. Where "undisturbed" buffer samples were needed, the coring and preservation techniques developed during the partial and final dismantling helped to minimise the inevitable disturbance due to the dismantling processes.

None of the observations in FEBEX contradict the prediction that a bentonite barrier will limit advective transport in the near-field. There will be a sufficiently high swelling pressure to ensure tightness towards the rock or a liner and a sufficiently low hydraulic conductivity to ensure that diffusion is the dominant transport mechanism.

11.1.2 Resisting mineralogical transformations

Mineralogical interactions occurring over time due to elevated temperatures and chemical interactions with other components of the disposal system should not lead to significant alteration and/or loss of the buffer functions. Losing the beneficial properties of the swelling mineral smectite in the bentonite could lead to not fully satisfying buffer safety functions to "attenuate releases" and "protect the canister".

Fernández et al. (2018a) reported on the evolution of mineralogy and porewater geochemistry with a focus on the alteration of smectite (see also Section 5.3.2.3). They found no differences in the smectite content between samples from around Heaters #1 and #2 that could be distinguishable by XRD. Smectite content was constantly above 92 wt.-%. The same was true for the fraction smaller than 2 μm.

Also, Fernández et al. (2018b) also reported that, at the interfaces with the rock and the heater, smectite was enriched in magnesium. Other authors (ETH and UAM, see Sections 5.1.5 and 5.3.2) observed illite at the granite interface. As in many other heater tests, FTIR analyses revealed an increase of Mg in smectite at the heater interface (and a decrease in Ca). As expected, the salinity of the porewater increased towards the heater. Fernández et al. (2018b) found an increase in Ca in the exchange position at the cement interface. Na was found to be slightly depleted in the cool parts.

Turrero and Cloet (2017) found no morphological changes in smectite observed at the cement interface. However, Na and Ca decreased towards, and K increased in, the bentonite (2 mm). Soluble Mg^{2+} was accumulated in the first 2 mm from the concrete interface. In bentonite, however, Mg^{2+} measured in aqueous extracts was negligible, as precipitation of Mg silicates occurred, favoured by the solution chemistry at the interface. Most studies agree that the bentonite chemistry reflects the bulk bentonite chemistry 4 – 5 mm from the interface.

Fernández et al. (2018a) reported that no significant changes were found in adsorption isotherms, the surface area and CEC. The BET however, decreased slightly towards the heater.

As stated in Section 5.1.6, after 13 years of interaction no safety-relevant properties of the bentonite were affected and the concrete-bentonite interaction thus has no safety-relevant impact. However, some mineralogical changes in the bentonite did occur, such as limited smectite dissolution and the change of cations at the exchange sites.

The hydrogeochemical composition of the groundwater in the FEBEX gallery should favour the stability of smectite colloids, since the cation content is low (< 10 mM, Chapter 9 and Garralón et al. 2017). Waters from different intervals of various boreholes at different distances from the bentonite surfaces were analysed to verify the existence of colloidal particles and to identify their nature. The maximum concentration of bentonite colloids (considering that the entire aluminium signal comes from the bentonite) was around 0.8 ppm, but these data are not sufficient to demonstrate the presence of bentonite colloids (Section 3.4).

The in-situ experiment was of limited duration and was still in a hydrological and geochemical transient prior to final dismantling, which made it difficult to extrapolate to the time frame relevant to the safety case. There was, however, no significant mineralogical alteration of the bentonite barrier in FEBEX during this initial period.

If advective flow occurs in a repository, the buffer will be most vulnerable to erosion during transients associated with early saturation or, in the case of initially saline groundwaters, intrusion of fresh water (e.g. during glacial retreat). In FEBEX, there was no evidence of bentonite erosion or clay colloid generation despite the greater part of the bentonite having become saturated and significant swelling pressure having developed at the rock interface. Given the low salinity of the Grimsel groundwater, a significant loss of buffer mass would have been noticed, and the observations support the stability of the bentonite barrier in a repository in low-permeability rock.

11.1.3 Canister protection

The development of swelling pressure and low hydraulic conductivity upon saturation of bentonite buffers contribute to the protection of the canister. Diffusion-dominated hydraulic transport properties, absence of microbially induced corrosion and buffering of rock movement are the most relevant results from the saturation of bentonite in this respect.

Bengtsson et al. (2017a) reported that bacteria were mainly found in Section 60 (cold-saturated), while other sections were bacteria-free. Bacteria in Section 60 could have been active, however, none could be cultivated from the bentonite where microbially induced corrosion was suspected. The results are also consistent with corrosion data in that area which did not indicate any signs of microbially induced corrosion, such as sulphide-related corrosion. Haynes et al. (2018) reported that the biomass in FEBEX remained relatively low and the microbial population remained small.

Despite a fairly high dry density (> 1.5 g/cm^3), numerous bacteria could be cultivated after 18 years Section 60. Consequently, there does not appear to be a threshold density or pressure at which the microorganisms in the highly compacted FEBEX bentonite would be completely eradicated. Cultivability is, however, a poor indicator for microbial activity. As stated in the previous paragraph, no indications of sulphide-related corrosion have been found, which supports the hypothesis of a limit on microbial activity.

11.1.4 Limiting pressure on canister and rock

Total pressure measurements (stress, Section 2.4) show that a significant swelling pressure develops with time. Since FEBEX was excavated before full saturation of the entire buffer, some uncertainty regarding the final stress at the rock-bentonite interface remains. However, the measured total pressures are consistent with the expected final swelling pressure, and the recorded stresses indicate that the safety functions regarding swelling pressure will be fulfilled.

Dueck et al. (in Villar et al. 2017) conducted unconfined compression tests on the recovered bentonite. They did not observe any large deviations in maximum deviator stress. A reduced strain at failure was found at all positions, which is probably due to a higher brittleness of the bentonite due to the thermal gradient. The shear resistance is, however, not affected by the reduced strain at failure.

The final position of the heater was not assessed further as it was controlled by the stiff but perforated liner. However, the dry density distribution reported in Section 5.2.3 for a cross-section indicates no significant compression of the bentonite by the heater/liner assembly.

11.1.5 Corrosion

FEBEX was not designed to allow for corrosion studies, even though a few corrosion coupons were installed close to the heater. The construction focused on engineering aspects with a liner for sliding in the heater, and the non-airtight plug just allowed too many experimental artefacts. The corrosion studies described in Section 5.4, however, concluded that smectite was not altered by the corrosion close to the liner.

11.2 Assessment of the performance of the FEBEX bentonite with regard to disposal systems

Although the buffer did not achieve complete saturation, and despite experimental artefacts, the bentonite proved to perform as expected. The bulk of the bentonite reached a saturation above 97%, with only the bentonite closest to the heater remaining below 85%. The available data do not indicate any trends that bentonite cannot meet long-term target safety requirements.

11.3 Assessment of the instrumentation and monitoring system

The excellent performance of the monitoring system, even after 18 years of operation and beyond the expected lifetime of sensors, allowed continuous control of the heating system and generated a large experimental monitoring database of the buffer and geosphere evolution. Post-mortem recalibration of sensors further supports the quality of the initial design and implementation of the in-situ test. Sensor recalibration has in some cases provided an improvement in data quality and has been retrospectively applied to data (see Chapter 6). The monitoring data, together with the laboratory-based sample analysis, have been of great importance in improving the understanding of THM processes (Papafotiou et al. 2017) and on validating and refining several existing modelling codes. The latter has been ongoing in diverse modelling efforts (DECOVALEX, EBS Task Force).

11.4 Assessment of modelling performance and developments

THM and THC modelling were continued throughout the course of the experiment from design to post-mortem. The modelling proved to be an invaluable tool for achieving a proper understanding and interpretation of test observations and results. No unexplained patterns of THM observations arose during the experiment, indicating that no significant processes were ignored (at least in the early saturation phase) in the model formulations.

While the temperature field has generally been well reproduced, there have been larger discrepancies in the relative humidity within the buffer, which is probably due to the high sensitivity of the hydration process to small changes in hydraulic properties. Quantitative discrepancies concerning observed stresses in the barrier probably relate to uncertainties in the measurements and/

or to shortcomings of the mechanical constitutive models. The state of the buffer at both partial dismantling (after five years) and final dismantling was relatively well described, although the predicted water content was slightly lower than measured. Differences between modelling groups are probably due to different assumptions regarding the mechanical constitutive behaviour and may be related to the need to incorporate irreversible/stress path-dependent features of behaviour (ongoing work within the BEACON project). The inclusion of more sophisticated formulations or the incorporation of additional phenomena (e.g. thermo-osmosis, water retention hysteresis, double structure and fabric evolution) did not lead to significantly improved results.

The OBC (operational base case) model framework including constitutive models and relevant parameter values based on the extensive laboratory programme was established at the start of the in-situ test and has remained essentially unchanged over the course of the 18 years of operation. Changes to experimental boundary conditions related to partial and final dismantling have been implemented together with a revision of the numerical grid to support the simulation of dismantling. Aside from this, the model defined in 1997 has been able to adequately predict the performance of the buffer over 18 years of operation. The OBC and similar models did not consider:

- the initial heterogeneity within the buffer (block joints and other gaps around the blocks)
- the heterogeneity of the rock mass

The success of the OBC model framework demonstrates that these features did not have a significant impact on the early saturation phase.

THC simulations require knowledge of thermal and hydraulic conditions at every point of the domain and, therefore, the performance of associated TH calculations requires the incorporation of mechanical effects (especially bentonite swelling). This is also crucial to achieve a good representation of the chemical observations from the test. Consequently, a proper representation of the experiment requires the performance of THMC analyses. Fortunately, all the indications suggest that the coupling from chemical variables towards THM phenomena are minor.

A large proportion of the chemical modelling work performed during the FEBEX experiment has been devoted to the development of conceptual formulations and codes capable of accounting for the observed and expected features of the test. As a result, there have been very considerable advances involving conceptual approaches, numerical methodologies and code development.

Although the availability of comparisons with the observations from the final dismantling is limited, some discrepancies with the observations from the partial dismantling suggest that relevant geochemical processes can exist that are not yet included in the model formulations.

The very complete database from the FEBEX in-situ experiment offers an exceptional opportunity to conduct a systematic study of the THM modelling of a complex large-scale system in order to identify key processes and critical parameters as well as to evaluate uncertainties. However, when the goal is to identify and characterise specific processes, additional dedicated small-scale experiments are bound to be necessary. A large amount of geochemical data (as well as associated THM variables) exist that may provide key information concerning the necessary improvements of the models with a particular focus on potentially missing processes in the formulations. Again, dedicated small-scale experiments are likely to be required to identify and unambiguously characterise specific phenomena.

12 Conclusions & lessons learned

12.1 FEBEX – have the objectives been met?

The original aims of FEBEX (ENRESA 2000) were:

- demonstration of the practicality of the concept and its engineering soundness and construction of an EBS with the Spanish reference concept for crystalline rock (AGP Granito)
- monitoring the early evolution of the THM and THC processes within the buffer and the geosphere under natural conditions
- validation, calibrate and improvement of THM and THC models and predictions

These aims were at least partly successfully accomplished after the first five years, and the partial dismantling in 2002 (ENRESA, 2006a) showing that:

hydration progressed homogeneously from the outer part in contact with rock to the inner and hotter part, and the hydration process closed the construction gaps and joints existing after the installation.

the state of the instrumentation system allowed the continuous monitoring of the THM evolution of the buffer and geosphere and was evaluated during the partial dismantling by laboratory inspection and re-calibration of the instruments.

laboratory and in-situ tests as well as THM modelling indicated that there is no significant EDZ around the FEBEX drift.

the original hydraulic properties of the rock did not undergo any major modification as a result of either the excavation or the test itself.

12.2 FEBEX-DP – have the objectives been met?

The FEBEX-DP objectives were an advanced and complementary development of the FEBEX objectives, predominantly taking advantage of the prolonged saturation time that led to a close to full saturation state by using the information gathered from the partial dismantling and having two observation windows in the early evolution of an EBS. This provided information and input on:

- the physical, physico-chemical, mineralogical, chemical and textural changes that occurred in the near-field, EBS and interfaces due to continuous heating and hydration over 18 years and the assessment of the potential changes with respect to the reference bentonite. The focus was on interfaces of blocks and the various materials which revealed local phenomena (Chapters 5 and 10).
- monitoring, analysis and modelling of the first 18 years of THM and THC processes
- studying microbial and corrosion processes in greater detail, despite limitations in the design of the original FEBEX (Sections 5.4 and 5.5)
- evaluation of the capability of numerical codes (THM and THC). However, further efforts in modelling are currently ongoing and not yet complete.

The information derived from the FEBEX-DP investigations has led to:

- confirmation of a significantly increased, though not complete, saturation of the buffer, with an ongoing but slowing increase in overall water content

- evidence for a saturation-induced spatial heterogeneity in dry density that has remained stable over the 13 years since partial dismantling
- additional characterisation of corrosion processes and iron-bentonite interactions active over the 18 years of heating, and comparison with the state after five years to identify their limited impact on the buffer
- the finding that the shotcrete plug performed well as a mechanical closure of an EBS in a granitic environment and the interfaces remained limited into the buffer, being restricted to a few centimetres at most
- The FEBEX-DP objectives were met and the project has provided valuable data on EBS evolution but also data to be further explored in terms of the ongoing transient saturation and homogenisation of a clay-based buffer.
- The quality and comprehensive nature of the investigations together with the duration of the in-situ test (resulting in a high level of saturation) make the final dataset of particular value for understanding the early transient phase of the disposal system

12.3 Lessons learned

12.3.1 Lessons learned from the FEBEX partial dismantling

The analysis of the FEBEX partial dismantling in 2002 provided insights into the construction of an EBS that were informative for the disposal concept (ENRESA 2006a):

- The drift diameter considered in the Spanish disposal concept (2.40 metres compared to the FEBEX gallery) was regarded as too small to accommodate the equipment required for the emplacement of canisters in a real case.
- The ambient relative humidity in the gallery during installation will strongly control the integrity of the blocks, and this has to be carefully monitored.

Air gaps were unavoidable because of the requirements for the emplacement of bentonite blocks and their manufacturing tolerances. ln a repository with horizontal drifts, these gaps are accumulated at the roof and may play a fundamental role, at least during the unsaturated period. Similarly, additional air gaps were unavoidable due to the liner concept. Construction gaps in the buffer were not regarded as a problem as long as they were kept at the same level as in the FEBEX experiment. Under test conditions, these gaps closed very quickly, preventing the creation of preferential flow paths for water. However, the presence of water in the drift during the emplacement operation can pose a serious problem and even make the construction of the buffer impossible. The experience in FEBEX has shown that a small amount of water is manageable, but the upper limits were not inverstigated.

Heater #1 was retrieved without any complications, especially considering the low degree of saturation of the inner part of the buffer. Therefore, it was not regarded as a fully representative retrieval operation. Under advanced or complete buffer saturation, the situation could differ substantially, and it would probably be necessary to adopt a different approach, possibly requiring the removal of all the bentonite in the top part to free the canister. As has been demonstrated, after 18 years of continued hydration, still no complications were encountered during the dismantling activities.

Handling of the bentonite blocks requires special precautions in relation to potential mechanical damage and absorption of humidity from the air. Handling of larger blocks with a robotized or teleoperated manipulator will require specific considerations related to the gripping system and positioning references, which however may become possibly available in the future.

The progress made in modelling (THM and THG) the FEBEX in-situ test but also the large-scale mock-up test, together with the large number of laboratory tests being performed elsewhere, allowed the development of an understanding of the near-field behaviour of the in-situ test and the derivation of parameters needed for the long-term performance assessment of a repository.

Some of these conclusions have led to adjustments or improvements and some features are no longer considered in repository designs. For instance, the liner concept used in the AGP Granito concept will no longer be used, which will result in a significant reduction in the amount of corrodible iron. Furthermore, density variations caused due to the perforation of the liner and constructional gaps are no longer an issue. Full-block concepts in horizontal drifts are currently not being considered and have been replaced with granular bentonite material (GBM) concepts with block pedestals supporting the canister (e.g. Nagra 2019). As a consequence, construction gaps are no longer a severe problem. However, lower buffer dry densities will be achieved using GBM which must be evaluated in in terms of their minimum requirements in the overall performance assessment. Furthermore, gallery shape is important for block emplacement, which will not be the case for all host rocks or gallery construction procedures.

12.3.2 Lessons learned from the FEBEX-DP – final dismantling

A number of lessons learned can be concluded from FEBEX-DP that can be beneficial for further experiments.

Gas sampling:

- While ceramic filter tubes are preferable for gas and water sampling because they are less reactive to chemical and mineral species from the rock and pore water and are more suitable for redox measurements, they are not recommended in a saturated, compacted bentonite barrier because of their low resistance to swelling pressures, which may be less relevant when surrounded by GBM
- After gas collection, a carrier gas was used for flushing the gas/water sampling lines from the pipes to extract additional porewater samples. Nitrogen gas was used in most of the sampling campaigns, with helium gas used in the last two (2014 and 2015). The drawback of nitrogen is that it is the main gas dissolved in granitic waters and is generated and/or consumed in different bio-geochemical reactions. For this reason, the use of non-reactive gases such as argon or helium is recommended.

Dismantling of the buffer:

- The use of a demolition robot proved effective and provided the required accuracy and care to avoid damaging the cables, sensors and gas pipes. However, the concrete had to be wetted to avoid dust emission, while the vibration of the robot affected and loosened the concrete/rock interface/contact, which was planned to be sampled intact.
- The successful shotcrete/bentonite overcoring provided valuable intact interfaces that were analysed in great detail by multiple laboratories. These techniques should be considered in the future to provide "in-state" samples. However, the success of these techniques will be limited in case of much higher buffer temperatures (in the FEBEX-DP case in the order of 30 °C) or in case of unsaturated, uncompacted GBM.

- Many laboratories with specific requirements caused some delays during dismantling from a practical point of view, which required some compromises in the aims and objectives of the dismantling. However, CIEMAT (and AITEMIN) were able to provide the core data mostly used in this report. Shipping to too many organisations was regarded as complicating dismantling activities. However, conclusions drawn from data for the same or similar parameters strengthened the conclusions drawn from FEBEX-DP. A key-contractor for the main data set is thus to be preferred.
- The shutting down of the heater and the resulting re-arrangement of gradients in saturation, etc. cannot be avoided with the current sampling techniques. In particular, rear parts of Heater #2 were equilibrated for around three months. However, the majority of monitoring and sampling data suggest that the buffer evolution can still be sufficiently characterised.
- The retrieval of Heater #2 was executed without complications, despite this being anticipated as the dummy canister was stuck fully in the liner due to bentonite intrusion through the perforated liner. However, the dummy canister and the surroundings experienced variable conditions which are not representative for a repository. Nevertheless, the higher degree of saturation of the inner part of the buffer as well as the protrusions of the bentonite through the liner provide evidence that retrieval can become more difficult with time.
- An on-site QA procedure for the dismantling activities facilitated a sampling procedure that provided high-quality samples, a record of dismantling activities for sampling data interpretation and sampling circumstances as well as ensuring safe and efficient dismantling procedures and management of activities.
- A graphical user interface alongside the dismantling activities and daily dismantling reports enabled a timely dissemination of information of the dismantling progress and activities. It also allowed focused sampling as well as functioning as a long-term archive of the activities.

Characterisation of corrosion processes:

- Corrosion processes and microbiological effects were limited and consistent with the fact that the experiment was not designed for these investigations as it was not air-tight. One zone that was unusually strongly affected by corrosion at dismantling Section 42 (front part of Heater #2) should not be regarded as a common phenomenon as it was affected by the partial dismantling. Nevertheless, information gathered proofed useful for assessing the system behaviour.
- Since the corrosion coupons were exposed to conditions of low humidity throughout the experiment, the findings deduced are of limited significance. A comparison with the same type of coupons in the wetter parts (i.e., outer parts) of the experiment would have helped in the interpretation. Moreover, it would have been advantageous to analyse the surface of the coupons (as well as the liner and heater) before their emplacement, which is commonplace by now.

Characterisation of interface evolution:

- The evolution of porosity in both concrete and bentonite needs to be understood in more detail in order to predict how far the interaction front will progress at a given time. Reliable analysis and evaluation of the long-term safety of the repository also requires the implementation of reactive transport models, which are tested and calibrated using relevant experiments. This work is in progress.

Monitoring of long-term tests:

- The FEBEX-DP experiment benefitted from a monitoring system where the numerous sensors provided data for significantly longer time than their manufacturer-guaranteed lifetime. Based on this experience and ongoingly new developed techniques, long-term monitoring can be successful if carefully planned and selected.
- The use of high-TRL (technological readiness level) sensors using passive measuring methods (such as the vibrating wire technique) proved to be the best choice. The failure rate for the low-TRL sensors could be minimised for future applications by improving their mechanical protection, using corrosion-resistant metals and avoiding weak plastic parts.
- The cables, if not avoided altogether (i.e., by using wireless devices), should be armored, built with long-lasting materials and routed to provide flexibility so that pulling forces due to bentonite swelling/movements can be avoided.
- In case of the usage of blocks, sensor bodies should not be too long and joints between the bentonite blocks/layers should be avoided to the greatest degree possible to minimise mechanical deformations (see Fig. 6-4), largely resulting from shearing, which could lead to fatal damage to the sensor functionality.

12.4 Relevance of the project over the last 20 years and for the future

The great benefit of the FEBEX experiment is the wealth of monitoring and laboratory data collected from two dismantling activities performed at different times during the early transient evolution of an EBS under natural conditions and at a 1:1 scale. This information can be used in a variety of ways in safety and performance assessment analysis, if the context of the FEBEX set-up is considered. It also provides a valuable database for comparison with other ongoing or completed experiments, as well as a basis for the planning of future experiments. The data have also helped to continuously test models and develop new or dedicated numerical codes. While experiments may not always be easily or completely comparable due to differing objectives and set-ups, the information collected by FEBEX still provides benchmark values and an understanding and confirmation of developing phenomena and processes.

FEBEX can be compared with other large-scale, in-situ, 1:1 scale non-isothermal heater experiments such as the Prototype Repository experiment at the Äspö Hard Rock Laboratory. The outer section of the Prototype Repository experiment was dismantled in 2010/2011 after seven years of hydration, while the four modules/heaters of the inner section have remained in place under ambient conditions since 2001 (Svemar et al. 2016). These experiments with different configurations and boundary conditions also confirm the feasibility and capability of constructing and predicting the evolution of an EBS. Given the experience from these experiments and ongoing RD&D efforts, current concepts have been adjusted and refined as necessary.

The information gathered from these experiments has provided input for follow-up concept-specific or generic experiments, such as the FE experiment at the Mont Terri Rock Laboratory (Müller et al. 2017), running since 2014, or the HotBENT experiment started in 2020 (Kober et al. 2018, Nagra et al. 2020).

The establishment of a well-defined THM model very early in the project and its continued application throughout the experiment lifetime provided a demonstration of the understanding of the significant processes and coupling during the early saturation of a clay-based buffer. A formal validation of such a model would require a careful definition of performance measures and relevant metrics but would be a valuable contribution for future experiments.

12.5 Future and outlook based on FEBEX/FEBEX-DP

The synthesis provided here gives a summary of the different aspects of the individual datasets (see Tab. 1-7), together with an appraisal of buffer evolution over 18 years of heating and an assessment of the project itself.

The final dataset as well as additional samples has been part of further work, in particular regarding the integration of THMC processes, interface properties and the influence of microbiology which have been used in a range of international projects. However, reporting on these is outside the scope of this synthesis report:

- MIND (Microbiology in Nuclear Waste Disposal – http://www.mind15.eu/) – was completed in 2019 and used FEBEX-DP material to study whether there are viable microbes after almost two decades in the clay/bentonite and also to develop methods to extract DNA from clay particles. Of particular interest were microorganisms that can accelerate canister corrosion in the near-field either by hydrogen scavenging or by sulphide and/or acetate production.
- CEBAMA (Cement-based Materials, Properties, Evolution, Barrier Functions – https://igdtp.eu/activity/cebama-cement-based-materials-properties-evolution-barrier-functions/) was completed in 2019 and focused on studies of interface processes between cement-based materials and host rocks or bentonite. This was accomplished by (i) assessing the specific impact on transport properties, (ii) quantifying radionuclide retention under high-pH cement conditions, and (iii) developing comprehensive modelling approaches. FEBEX-DP provided a large dataset for investigation of e.g., intact interface concrete-bentonite samples.
- BEACON (Bentonite Mechanical Evolution - http://www.beacon-h2020.eu/) – focused on the homogenisation of buffers under continuous heating and saturation processes and the developing gradients and how these material property distributions comply with safety requirements. The dense sampling and analysis programme of FEBEX provided a valuable database for the investigation of in-situ, large scale phenomena.
- Modelling in the EBS Task Force (Task 9: "FEBEX in-situ test" Stage 2) and DECOVALEX 2019 (Task D – https://decovalex.org/D-2019/task-d.html) has been using FEBEX/FEBEX-DP data.

In addition to the dataset, FEBEX has provided a unique focus for the development of conceptual and numerical models of EBS evolution and a "training ground" for many researchers.

13 References

AITEMIN (2012): Sensors Data Report (In-situ Experiment). Special Report after 15 Years of Heating Phase. FEBEX Data Report No. 6.

Alonso, E.E. & Alcoverro, J. (2005): DECOVALEX III PROJECT: Modelling of FEBEX In-situ Test. SKI Report 2005:20. SKI, Stockholm, Sweden.

Alonso, E.E., Gens, A. & Josa, A. (1990): A constitutive model for partially saturated soils. Géotechnique 40/3, 405-430, doi:10.1680/geot.1990.40.3.405.

Alonso, E., Alcoverro, J., Coste, F., Malinsky, L., Merriensoukatchoff, V., Kadiri, I., Nowak, T., Shao, H., Nguyen, T. & Selvadurai, A. (2005): The FEBEX Benchmark Test: Case Definition and Comparison of Modelling Approaches. International Journal of Rock Mechanics and Mining Sciences 42/5-6, 611-638.

Andersson, J. (2005): Research DECOVALEX III PROJECT Thermal-Hydro-Mechanical Coupled Processes in Safety Assessments. SKI Report 2005:29. SKI, Stockholm, Sweden

Bárcena, I., García-Siñeriz J.L. & Alonso. J. (2007): Deliverable D3.3.2.4. Sensors Data Report of the FEBEX "in-situ" test. EU Project NF-PRO, RTD C3 WP3.3.

Bárcena, I. & García-Siñeriz, J.L. (2015a): FEBEX-DP (GTS) Full Dismantling Test Plan. Nagra Arbeitsbericht NAB 15-15.

Bárcena, I. & García-Siñeriz J.L. (2015b): FEBEX-DP (GTS) Full Dismantling Sampling Plan. Nagra Arbeitsbericht NAB 15-14.

Bárcena, I., Fuentes-Cantillana, J.L. & García-Siñeriz, J.L. (2003): Dismantling of the Heater #1 at the FEBEX "in-situ" test. Description of operations, ENRESA Technical Report 9/2003

Bengtsson, A., Blom, A., Taborowski, T., Schippers, A., Edlund, J., Kalinowski, B. & Pedersen, K. (2017a): FEBEX-DP: Microbiological. Nagra Arbeitsbericht NAB 16-15.

Bengtsson, A., Blom, A., Hallbeck, B., Heed, C., Johansson, L., Stahlén, J. & Pedersen, K. (2017b): Microbial sulphide-producing activity in water saturated MX-80, Asha and Calcigel bentonite at wet densities from 1500 to 2000 kg m^{-3}. TR-16-09, SKB, Stockholm, Sweden.

Birgersson, M., Zheng, L., Samper, J., Mon, A. & Montenegro, L. (2018): FEBEX-DP: Predismantling THC Modelling. Nagra Arbeitsbericht NAB 16-23.

Buil, B., Gómez, P., Peña, J., Garralón, A., Turrero, M.J., Escribano, A. & Durán, J.M. (2010): Modelling of bentonite–granite solutes transfer from an in-situ full-scale experiment to simulate a deep geological repository (Grimsel Test Site, Switzerland). Applied geochemistry, 25(12), 1797-1804.

Campos, G. & Villar, M.V. (2018): Water Retention Curves of Bentonite Samples of the Febex Dismantling Project (FEBEX-DP). Informes Técnicos CIEMAT 1432. Madrid, 44 pp.

Carbonell, B., Villar, M.V., Martín, P.L., & Gutiérrez-Álvarez, C. (2019): Gas transport in compacted bentonite after 18 years under barrier conditions. Geomechanics for Energy and the Environment, 17, 66-74.

Charlier, R., Radu, J.-P. & Collin, F (2001): Numerical modelling of coupled transient phenomena. Revue Française de Génie Civil 5/6, 719-741.

Dai, Z. & Samper, J. (2004): Inverse problem of multicomponent reactive chemical transport in porous media: Formulation and Applications. Water Resources Res. 40, W07407. doi:10.1029/2004WR003248.

Dixon, D., Chandler, N., Graham, J. & Gray, M.N. (2002): Two Large-scale Sealing Tests Conducted at Atomic Energy of Canada's Underground Research Laboratory: The Buffer-container Experiment and the Isothermal Test. Canadian Geotechnical Journal 39/3, 503518.

Daucousse, D. & Lloret, A. (2003): Results of in-situ measurements of water content and dry density. FEBEX-II internal Report 70-UPC-L-5-012, 103 pp.

Dueck, A., Johannesson L.-E., Kristensson O. & Olsson S. (2011): Report on hydro-mechanical and chemical-mineralogical analyses of the bentonite buffer in Canister Retrieval Test. SKB Technical Report TR-11-07. Svensk Kärnbränslehantering, Sweden.

Dupray, F., François, B. & Laloui, L. (2013): Analysis of the FEBEX Multi-barrier System Including Thermoplasticity of Unsaturated Bentonite. International Journal for Numerical and Analytical Methods in Geomechanics 37/4, 399-422.

ENRESA (1995): Almacenamiento Geológico Profundo de Residuos Radiactivos de Alta Actividad (AGP). Diseños Conceptuales Genéricos. Publicaciones Técnicas 11/95. ENRESA, Madrid, Spain.

ENRESA (1998a): FEBEX. Bentonite: origin, properties, and fabrication of blocks. Publicación Técnica ENRESA 5/98. 146 pp, Madrid, Spain.

ENRESA (1998b): FEBEX Full-scale Engineered Barriers Experiment in Crystalline Host Rock. Final Design and Installation of the "in-situ" Test at Grimsel. December 1998. ENRESA Technical Report 12/98, Madrid, Spain.

ENRESA (1998c): Preoperational thermo-hydro-mechanical (THM) modelling of the "in-situ" test. Publicación Técnica 09/98, ENRESA, Madrid, Spain.

ENRESA (2000): FEBEX Project. Full-scale Engineered Barriers Experiment for a Deep Geological Repository for High Level Radioactive Waste in Crystalline Host Rock. Final Report. ENRESA Report 1/2000, ENRESA, Madrid, Spain.

ENRESA (2004a): FEBEX II Project – Post-mortem analysis; EDZ assessment. Publicación Técnica 11/2004, ENRESA, Madrid, Spain.

ENRESA (2004b): FEBEX project Post-mortem Analysis: Corrosion Study. ENRESA PT 082004, ENRESA, Madrid, Spain.

ENRESA (2006a): Full-scale Engineered Barriers Experiment. Updated Final Report 1994 – 2004. ENRESA PT Report 05-0/2006. ENRESA, Madrid, Spain.

ENRESA (2006b): FEBEX Project final report. Addendum sensors data report. *In-situ* experiment. PT Report 05-5/2006, ENRESA, Madrid, Spain.

ENRESA (2006c): FEBEX Project final report. Post-mortem bentonite analysis. ENRESA Report 05-1/2006. ENRESA, Madrid, Spain.

ENRESA (2006d): FEBEX Project final report. Final report on the thermo-hydro-mechanical modelling. ENRESA Report 05-2/2006. ENRESA, Madrid, Spain.

Fernández, A.M. & Rivas, P. (2005): Analysis and distribution of waters in the compacted FEBEX bentonite: Pore water chemistry and adsorbed water properties. *In:* Alonso, E.E., Ledesma, A. (eds.): Advances in Understanding Engineered Clay Barriers. A.A. Balkema Publishers, Leiden, 257-275.

Fernández, A.M., Sánchez-Ledesma, D.M., Melón, A., Robredo, L. M., Rey, J.J., Labajo, M., Clavero, M.A., Carretero, S. & González, A.E. (2018a): Thermo-hydro-chemical (THC) behaviour of a Spanish bentonite after dismantling Heater #1 and Heater #2 of the FEBEX *in-situ* test at the Grimsel Test Site. Technical report CIEMAT/DMA/2G216/03/16. Nagra Technical Report NAB 16-25.

Fernández, A.M., Kaufhold, S., Sánchez-Ledesma, D. M., Rey, J. J., Melón, A., Robredo, L. M., & Clavero, M. A. (2018b): Evolution of the THC conditions in the FEBEX in-situ test after 18 years of experiment: Smectite crystallochemical modifications after interactions of the bentonite with a C-steel heater at 100° C. Applied Geochemistry, 98, 152-171.

Fernández A.M. (2019): Gas and water sampling from the FEBEX *in-situ* test. Nagra Arbeitsbericht NAB 16-13.

Foct, F. & Gras, J.M. (2003): Semi-empirical model for carbon steel corrosion in long term geological nuclear waste disposal. In Prediction of Long Term Corrosion Behaviour in Nuclear Waste Systems. Proceedings of an International Workshop, Cadarache, France. Eurpean Federation of Corrosion Publications Nr. 36, 91-102.

Frieg, B., Blaser, P., Adams, J., Albert, W., Dollinger, H., Kuhlmann, U. & Lanyon G.W. (2012): Grimsel Test Site Excavation Disturbed Zone Experiment (EDZ). Nagra Technical Report NTB 98-01.

García-Siñeriz J.L., Martínez V., Rey M. & Abós H. (2016a): Results of laboratory investigations in preparation of the dismantling of the FEBEX-e/FEBEX-DP in-situ test and on-site experiments during the dismantling. Nagra Arbeitsbericht NAB 16-09.

García-Siñeriz, J.L., Abós, H., Martínez L.V., De la Rosa, C., Mäder, U. & Kober, F. (2016b): FEBEX DP: Dismantling of Heater #2 at the FEBEX in-situ test: Description of operations. Nagra Arbeitsbericht NAB 16-11.

García-Siñeriz, J.L., Mazón, M.R., Kober, F. & Sakaki, T. (2019): Performance of THM monitoring instrumentation in FEBEX bentonite barrier after 18 years of operation under repository-like conditions. Geomechanics for Energy and the Environment, 17, 75-89.

Garralon, A., Gomez P., Turrero M.J., Torres E., Bui B., Sanchez L. & Pena J. (2017): Hydrogeochemical characterisation of the groundwater in the FEBEX gallery. Nagra Arbeitsbericht NAB 16-14.

Gaus, I., Wieczorek, K., Schuster, K., Garitte, B., Senger, R., Vasconcelos, R. & Mayor, J.-C. (2014): EBS behaviour immediately after repository closure in a clay host rock: HE-E experiment (Mont Terri URL). Clays in Natural and Engineered Barriers for Radioactive Waste Confinement, 5th international meeting, Montpellier, October 22-25, 2012, Geological Society, London, Special Publications 400, 71-91.

Gens, A., García-Molina, A.J., Olivella, S., Alonso, E.E. & Huertas, F. (1998): Analysis of A Full Scale In-situ Test Simulating Repository Conditions. International Journal for Numerical and Analytical Methods in Geomechanics 22/7, 515-548.

Gens, A., Guimarães, L.D.N. & García-Molina, A. (2002): Factors Controlling Rock–clay Buffer Interaction in a Radioactive Waste Repository. Engineering Geology 64/2-3, 297-308.

Gens, A., Sánchez, M., Guimarães, L.D.N., Alonso, E.E., Lloret, A., Olivella, S., Villar, M.V. & Huertas, F. (2009): A Full-scale in-situ Heating Test for High-level Nuclear Waste Disposal: Observations, Analysis and Interpretation. Géotechnique 59/4, 377-399, doi:10.1680/geot.2009.59.4.377.

Giroud, N. (2014): FEBEX – Assessment of Redox Conditions in Phase 2 before Dismantling. Nagra Arbeitsbericht NAB 14-55.

Giroud, N., Tomonaga, Y., Wersin, P., Briggs, S., King, F., Vogt, T. & Diomidis, N. (2018): On the fate of oxygen in a spent fuel emplacement drift in Opalinus Clay. Applied geochemistry, 97, 270-278.

Graham, J., Chandler, N.A., Dixon, D.A., Roach, P.J. To, T. & Wan A.W.L. (1997): The Buffer/Container Experiment: Results, Synthesis, Issues, Atomic Energy of Canada Limited Report, AECL-11746, COG-97-46-I, Chalk River.

Guimerà, J., Ortuño, F., Vázquez, E., Ruiz, B., Martínez, L., Carrera, J. & Meier, P. (1996): Pulse tests at "in drift" boreholes. Performance and evaluation. UPC, 70-UPC-L-0-1001.

Guimerà, J., Carrera, J., Martínez, L., Vázquez, E., Ortuño, F., Fierz, T., Bülher, C., Vives, L., Meier, P., Medina, A., Saaltink, M., Ruiz, B. & Pardillo, J. (1998): FEBEX Hydrological characterisation and modelling. UPC, 70-UPC-M-0-1001, Jan. 1998.

Guimarães LN. (2002): Análisis multi-componente no isotermo en medio poroso deformable no saturado. Ph.D. Thesis, Geotechnical Engineering Department, Technical University of Catalunya (in Spanish).

Guimarães, J. do N., Gens, A., Sánchez, M. & Olivella, S. (2006): THM and reactive transport analysis of expansive clay barrier in radioactive waste isolation. Communications in numerical methods in engineering. 22/8, 849-859. DOI: 10.1002/cnm.

Haynes, H., Pearce, C., Boothman, C. & Lloyd J. (2018): Response of Bentonite Microbial Communities to Stresses Relevant to Geodisposal of Radioactive Waste. Chemical Geology 501, 58-67. https://doi.org/10.1016/j.chemgeo.2018.10.004.

Juncosa, R. (2001): Modelos de fujo multifásico no isotermo y de transporte reactivo multicomponente en medios porosos. PhD dissertation, UPC, Madrid, 287 pp.

Keusen, H.R., Ganguin, J., Schuler, P., & Buletti, M. (1989): Felslabor Grimsel: Geologie. Nagra Technical Report NTB 87-14.

King, F., Lilja, C., Pedersen, K., Pitkänen, P. & Vähänen, M. (2012): An update of the state-of-the-art report on the corrosion of copper under expected conditions in a deep geologic repository. POSIVA 2011-01. 246 p. ISBN 978-951-652-178-0, Posiva Oy, Eurajoki, Finland and Swedish Nuclear Fuel and Waste Management Co. (SKB). Technical Report SKB TR-10-67, Stockholm, Sweden.

Kober, F., & Van Meir, N. (2017): FEBEX-DP – Dismantling related supplementary documents. Nagra Arbeitsbericht NAB 16-68.

Kober, F., Vomvoris, S. & Finsterle, S. (2018): HotBENT: Preliminary Design Study - Overview of Results. Nagra Arbeitsbericht NAB 17-29.

Laloui, L. & François, B. (2009): ACMEG-T: soil thermoplasticity model. Journal of engineering mechanics, 135(9), 932-944.

Lanyon G.W. & Gaus I. (2016): Grimsel Test Site Investigation Phase VI: Main outcomes and review of the FEBEX In-situ Test (GTS) and Mock-up after 15 years of operation. Nagra Technical Report NTB 15-04.

Lloret, A. & Alonso, E.E. (1985): State surfaces for partially saturated soils. Proc. of the 11th International Conference on Soils Mechanics and Foundation Engineering, San Francisco, USA. Balkema, 557-562.

Lloret, A. & Villar, M.V. (2007): Advances on the Knowledge of the Thermo-hydro-mechanical Behaviour of Heavily Compacted 'FEBEX' Bentonite. Physics and Chemistry of the Earth, Parts A/B/C 32/8-14, 701-715.

Lloret, A., Villar, M.V, Sánchez, M., Gens, A., Pintado, X. & Alonso, E.E. (2003): Mechanical Behaviour of Heavily Compacted Bentonite Under High Suction Changes. Géotechnique 53/1, 27-40.

Mäder, U., Detzner, K., Kober, F., Abplanalp, H., Baer, T. & Cloet, V. (2016): FEBEX-DP – Plug Overcoring and Concrete-Bentonite Interface Sampling prior to Dismantling. Nagra Arbeitsbericht NAB 16-10.

Martín, P.L., Barcala, J.M. & Huertas, F. (2006): Large-scale and Long-term Coupled Thermo-hydro-mechanic Experiments with Bentonite: the FEBEX Mock-up Test. Journal of Iberian Geology 32/2, 259-282.

Martínez V., Abós H. & García-Siñeriz J.L. (2016): FEBEXe: Final Sensor Data Report (FEBEX in-situ Experiment). Nagra Arbeitsbericht NAB 16-19.

Martínez-Landa, L. & Carrera, J. (2005): An analysis of hydraulic conductivity scale effects in granite (Full-scale Engineered Barrier Experiment (FEBEX), Grimsel, Switzerland). Water Resour. Res. 41/3, W03006, doi:10.1029/2004WR003458.

Masurat, P., Eriksson, S. & Pedersen, K. (2010): Microbial sulphide production in compacted Wyoming bentonite MX-80 under in-situ conditions relevant to a repository for high-level radioactive waste. Applied Clay Science 47, 58-64.

Mayor, J.C., García-Siñeriz, J.L., Alonso, E., Alheid, H.J. & Blümling, P. (2007): Engineered barrier emplacement experiment in Opalinus clay for the disposal of radioactive waste in underground repositories. *In:* Bossart, P., Nussbaum, C., (eds). Mont Terri project e heater experiment, engineered barriers emplacement and ventilation tests. Swiss Geological Survey; 115179.

Meier, P., Fernández, P., Carrera, J. & Guimerà, J. (1995): FEBEX – PHASE 1. Results of hydraulic testing in boreholes FBX 95.001, FBX 95.002, BOUS 85.001 and BOUS 85.002. UPC, Dec. 1995.

Meyer, M. & Kircher, M. (2010): Illumina sequencing library preparation for highly multiplexed target capture and sequencing. Cold Spring Harbor Protocols, 2010(6), pdb-prot5448.

Missana T., Alonso U., Albarran N., García-Gutierrez M. & Cormenzana J.L. (2011): Analysis of colloids erosion from the bentonite barrier of a high level radioactive waste repository and implications in safety assessment. Physics and Chemistry of the Earth, Parts A/B/C Volume 36, Issues 17-18, 1607-1615.

Missana, T., Alonso, U., García-Gutiérrez, M., López, T. (2018): Analysis of bentonite colloid generation in the FEBEX gallery at the Grimsel Test Site (Switzerland): global evaluation of the experimental data obtained from 2006 to 2014. CIEMAT report.

Müller, H.R., Garitte, B., Vogt, T., Köhler, S., Sakaki, T., Weber, H. & Cloet, V. (2017): Implementation of the full-scale emplacement (FE) experiment at the Mont Terri rock laboratory. Swiss Journal of Geosciences, 110(1), 287-306.

Nagra (2019): Implementation of the Full-scale emplacement Experiment at Mont Terri: Design, Construction and Preliminary Results. Nagra Technical Report NTB 15-02.

Nagra (2020): HotBENT – Experiment plan. Nagra Arbeitsbericht NAB 19-43.

Olivella, S., Gens, A., Carrera, J. & Alonso, E.E. (1996): Numerical formulation for a simulator (CODE_BRIGHT) for the coupled analysis of saline media. Engineering Computations 13/7, 87-112, doi:10.1108/02644409610151575.

Papafotiou, A., Li, C., Kober, F., Qiao, Y.F., Ferrari, A., Laloui, L., Sánchez, M., Gens, A. & Åkesson, M. (2017): Pre-dismantling THM modelling of the FEBEX in-situ experiment. Nagra Arbeitsbericht NAB 16-22.

Pérez-Estaún, A., Carbonell R., Martínez L., Dentz M., Suso J., Carretero G. & Bueno J. (2006): "New boreholes to investigate the bentonite/crystalline rock interface in the FEBEX tunnel (Grimsel, Switzerland)." In 1st Annual Workshop Proceedings of Integrated Project FUNMIG. CEA Report CEA, pp. 157-162. 2006.

Rey, M., Bárcena, I. & García-Siñeriz, J.L. (2015): Full Dismantling Sampling Plan. Rev. 5. AITEMIN.

Rey, M., Sanz, F-J. & García-Siñeriz, J.L. (2016): FEBEX-DP Post-mortem analysis: Sensors. Nagra Arbeitsbericht NAB 16-20.

Rodríguez-Dono, A., Olivella, S. & Mokni, M. (2018): Assessment of high-level spent nuclear fuel disposal model. Environmental Geotechnics. https://doi.org/10.1680/jenge.18.00017 (published online ahead of print). 2020 7/1, 42-58.

Sakaki, T., Kober, F. & Schlaeger, S. (2017): FEBEX-DP: Bentonite TDR probe inspection and data verification report. Nagra Arbeitsbericht NAB 16-21.

Samper, J.R., Juncosa, J., Molinero, L., Montenegro, L. & Vázquez, A. (2001): Update of the Thermo-hydro-geochemical Model of the Mock-up Test. Technical Report. FEBEX Project 70-ULC-L-5-022. University of La Coruña, Spain.

Samper, J., Yang, C. & Montenegro, L. (2003): CORE2D version 4 – a code for groundwater flow and reactive solute transport. User Manual. University of La Coruña, Spain.

Samper, J., Vázquez, A. & Montenegro, L. (2005): Inverse hydrochemical modelling of aqueous extracts experiments for the estimation of FEBEX bentonite porewater chemistry. *In:* Alonso, E.E. & Ledesma, A. (eds.): Advances in Understanding Engineered Clay Barriers. Proceedings of the International Symposium on Large Scale Field Tests in Granite, Sitges, Barcelona (Spain), 12-14 November, 553-563. A.A. Balkema Publ. Leiden, The Netherlands.

Samper, J., Zheng, L., Montenegro, L., Fernández, A.M. & Rivas, P. (2008): Coupled thermo-hydro-chemical models of compacted bentonite after FEBEX *in-situ* test. Applied Geochemistry 23/5, 1186-1201, doi:10.1016/j.apgeochem.2007.11.010.

Samper, J., Yang, C., Zheng, L., Montenegro, L., Xu, T., Dai, Z., Zhang, G., Lu, C. & Moreira, S. (2012): CORE2D V4: A Code for Water Flow, Heat and Solute Transport, Geochemical Reactions, and Microbial Processes. Groundwater Reactive Transport Models, 160-186.

Sánchez, M., Gens, A., Guimarães, L.D.N. & Olivella, S. (2005): A double structure generalized plasticity model for expansive materials. International Journal for Numerical and Analytical Methods in Geomechanics 29/8, 751-787, doi:10.1002/nag.434.

Sánchez, M. & Gens, A. (2007): Progress report on comparison of existing predictions with ongoing measurements. Deliverable 3.3.4. EU project NF-PRO (FI6W-CT-2002-02389). Technical Report CIMNE/DETCG.

Sánchez, M. & Gens, A. (2008): Final activity report of CIMNE for RTDC3, WP3.3. Deliverable 3.3.10. EU project NF-PRO (FI6W-CT-2002-02389). Technical Report CIMNE/DETCG.

Sánchez, M., Villar, M.V., Lloret, A. & Gens, A. (2007): Analysis of the Expansive Clay Hydration Under Low Hydraulic Gradient. *In:* Experimental Unsaturated Soil Mechanics. Springer Proceedings in Physics. Springer, Berlin 112, 309-318.

Sánchez, M., Gens, A. & Olivella, S. (2010): Effect of thermo-coupled processes on the behaviour of a clay barrier submitted to heating and hydration. Anais da Academia Brasileira de Ciências 82/1, 153-168.

Sánchez, M., Gens, A. & Olivella, S. (2012a): THM Analysis of a Large-scale Heating Test Incorporating Material Fabric Changes. International Journal for Numerical and Analytical Methods in Geomechanics 36/4, 391-421, doi:10.1002/nag.1011.

Sánchez, M., Gens, A. & Guimarães, L. (2012b): Thermal–hydraulic–mechanical (THM) Behaviour of a Large-scale *in-situ* Heating Experiment During Cooling and Dismantling. Canadian Geotechnical Journal 49/10, 1169-1195.

Schneeberger, R., Kober, F., Lanyon, G.W., Spillmann, T. & Blechschmidt, I. (2019): Grimsel Test Site: Revisiting the site-specific geoscientific knowledge. Nagra Technical Report NTB 19-01.

Sellin, P. & Leupin, O. (2013): The use of clay as an engineered barrier in radioactive waste management – a review. Clays and Clay Minerals. 61(6):477-498. DOI: 10.1346/CCMN.2013.0610601.

SKB (2011): Long-term safety for the final repository for spent nuclear fuel at Forsmark. Main report of the SR-Site project. SKB Technical Report TR-11-01, Stockholm, Sweden.

Stroes-Gascoyne, S., Hamon, C.J. & Maak, P. (2010): The effects of the physical properties of highly compacted smectitic clay (bentonite) on the culturability of indigenous microorganisms. Applied Clay Science 47, 155-162.

Svemar, C., & Huertas, F. (2004): Experience in EBS engineering development and handling feasibility. In EURADWASTE'04 Conference Proceedings. 271-280.

Svemar, C., Johannesson, L.-E., Grahm, P., Svensson, D., Kristensson, O., Lönnqvist, M. & Nilsson, U. (2016): Prototype Repository: Opening and Retrieval of Outer Section of Prototype Respository at Äspö Hard Rock Laboratory: Summary Report. SKB TR-13-22, Svensk Kärnbränslehantering AB, Stockholm, Sweden.

Svensson, D. (2015): The bentonite barrier – Swelling properties, redox chemistry and mineral evolution. Ph. D. thesis. ISBN 978-91-7422-385-9, Lund, 184 pp.

Svensson, D. & Hansen, S. (2013): Redox chemistry in two iron-bentonite field experiments at Äspö Hard Rock Laboratory, Sweden: an XRD and Fe k-edge XANES study. Clays and Clay Minerals 61, 566-579.

Tsang, C.F., Jing, L., Stephansson, O. & Kautsky, F. (2005): The DECOVALEX III Project: A Summary of Activities and Lessons Learned. International Journal of Rock Mechanics and Mining Sciences 42/5-6, 593-610.

Turrero, M. & Cloet, V. (2017): FEBEX-DP Concrete ageing, concrete/bentonite and concrete/rock interaction analysis. Nagra Arbeitsbericht NAB 16-18.

Villar, M.V. (2002): Thermo-hydro-mechanical characterisation of a bentonite from Cabo de Gata. A study applied to the use of bentonite as sealing material in high level radioactive waste repositories. Publicación Técnica ENRESA, Madrid, 258 pp.

Villar, M.V., & Lloret, A. (2004): Temperature influence on the mechanical behaviour of a compacted bentonite. In Elsevier Geo-Engineering Book Series, Vol. 2, pp. 305-310.

Villar, M.V., García-Siñeriz, J.L., Bárcena, I. & Lloret, A. (2005): State of the bentonite barrier after five years operation of an *in-situ* test simulating a high level radiactive waste repository. Engineering Geology 80: 175-198. doi:10.1016/j.enggeo.2005.05.001.

Villar, M.V., Sánchez, M. & Gens, A. (2008): Behaviour of a Bentonite Barrier in the Laboratory: Experimental Results up to 8 years and Numerical Simulation. Physics and Chemistry of the Earth, Parts A/B/C 33, S476-S485.

Villar, M.V., Gómez-Espina, R. & Lloret, A. (2010): Experimental Investigation into Temperature Effect on Hydro-mechanical Behaviours of Bentonite. Journal of Rock Mechanics and Geotechnical Engineering 2/1, 71-78

Villar, M.V., Iglesias, R.J., Abós, H., Martínez, V., de la Rosa, C. & Manchón, M.A. (2016): FEBEX-DP on-site analyses report. Nagra Arbeitsbericht NAB 16-12.

Villar, M.V. (2017): FEBEX-DP Postmortem THM/THG Analysis Report. Nagra Arbeitsbericht NAB 16-17 Rev. 1.

Villar, M.V., Iglesias, R.J., Gutiérrez-Alvarez, C., Carbonell, B., Campos, R., Campos, G., Martín, P.L. & Castro, B. (2018a): FEBEX-DP: Thermo-hydro-mechanical post-mortem analysis of bentonite performed at CIEMAT. Technical report CIEMAT/DMA/2G216/2/16. Nagra Arbeitsbericht NAB 16-24.

Villar, M.V., Iglesias, R.J., Gutiérrez-Álvarez, C. & Carbonell, B. (2018b): Hydraulic and mechanical properties of compacted bentonite after 18 years in barrier conditions. Applied Clay Science 160: 49-57.

Villar, M.V., Carbonell, B., Martín, P.L. Gutiérrez-Álvarez, C. & Barcala, J.M. (2018c): Gas Permeability of Bentonite Samples of the FEBEX Dismantling Project (FEBEX-DP). Informes Técnicos CIEMAT 1431. Madrid, 89 pp.

Villar, M.V., Iglesias, R.J. & García-Siñeriz, J.L. (2018d): State of the in-situ FEBEX test (GTS, Switzerland) after 18 years: a heterogeneous bentonite barrier. Environmental Geotechnics 7/2 147-159. https://doi.org/10.1680/jenge.17.00093.

Villar, M.V., Iglesias, R.J., García-Siñeriz, J.L., Lloret, A. & Huertas, F. (2020): Physical evolution of a bentonite buffer during 18 years of heating and hydration. Engineering Geology, 264, 105408.

Wersin, P., Jenni, A. & Mäder, U. (2015): Interaction of corroding iron with bentonite in the ABM1 experiment at Äspö, Sweden: a microscopic approach. Clays and Clay Minerals, 63(1): 51-68.

Wersin, P. & Kober, F. (2017): FEBEX-DP. Metal Corrosion and Iron-bentonite Interaction Studies. Nagra Arbeitsbericht NAB 16-16.

Wieczorek, K., Gaus, I., Mayor, J.C., Schuster, K., García-Siñeriz, J.L. & Sakaki, T. (2017): In-situ experiments on bentonite-based buffer and sealing materials at the Mont Terri rock laboratory (Switzerland). Swiss Journal of Geosciences, 110(1), 253-268.

Zheng, L. & Samper, J. (2004): Formulation of the inverse problem of non-isothermal multiphase flow and reactive transport in porous media. *In:* Miller, C.T., Farthing, M.W., Gray, W.G., Pinder, G.F. (eds.): Computational Methods in Water Resources. Vol. 2. Elsevier, 13171327.

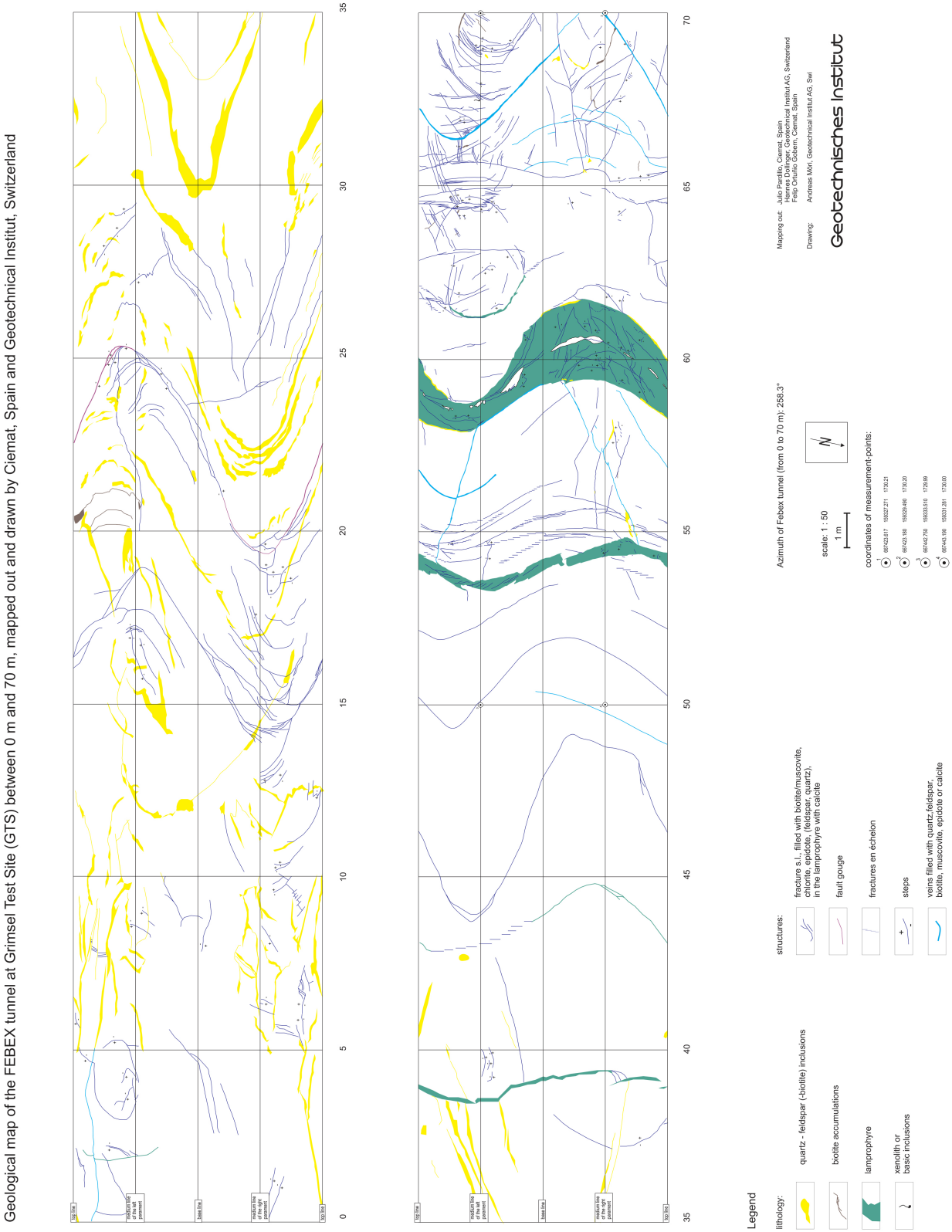
Zheng, L. & Samper, J. (2005): Inverse problem of non-isothermal multiphase flow and reactive transport in deformable porous media. *In:* Samper, J., Paz González, A. (eds.): VII Jornadas de Investigación en la Zona no Saturada de Suelo. ZNS'05, La Coruña, Spain, 307-313.

Zheng, L. & Samper, J. (2008). A coupled THMC model of FEBEX mock-up test. Physics and Chemistry of the Earth, Parts A/B/C, 33, S486-S498.

Zheng, L. Samper, J. & Montenegro, L. (2011): A Coupled THC Model of the FEBEX in-situ Test with Bentonite Swelling and Chemical and Thermal Osmosis. Journal of Contaminant Hydrology 126/1-2, 45-60, doi:10.1016/j.jconhyd. 2011.06.003.

Appendix A:

A.1 MAP 1 Geology FEBEX Gallery – Geotechnisches Institut



A.2 MAP 2 Geology FEBEX Gallery – Geologisches Institut

